Report No. KS-26-01 ▪ FINAL REPORT ▪ January 2026

Computational Fluid Dynamics Investigation of High Mast Illumination Poles: Influence of Light Fixtures

Briceson Junge
Caroline Bennett, Ph.D., P.E.
William Collins, Ph.D., P.E.
Jian Li, Ph.D., P.E.
Mark Ewing, Ph.D.

The University of Kansas

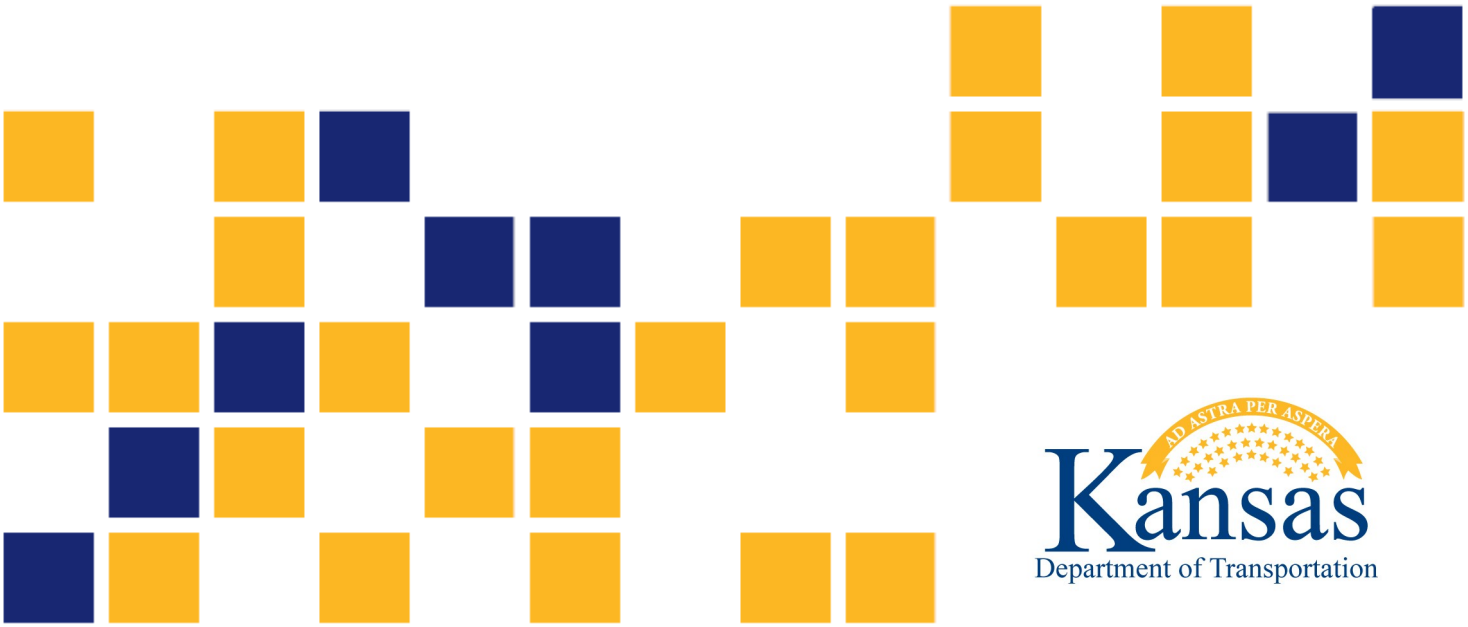

Kansas Department of Transportation

1 Report No. KS-26-01	**2 Government Accession No.**	**3 Recipient Catalog No.**
4 Title and Subtitle Computational Fluid Dynamics Investigation of High Mast Illumination Poles: Influence of Light Fixtures		**5 Report Date** January 2026 **6 Performing Organization Code**
7 Author(s) Briceson Junge; Caroline Bennett, Ph.D., P.E.; William Collins, Ph.D., P.E.; Jian Li, Ph.D., P.E.; Mark Ewing, Ph.D.		**8 Performing Organization Report No.**
9 Performing Organization Name and Address The University of Kansas Department of Civil, Environmental & Architectural Engineering 1530 West 15th St Lawrence, Kansas 66045-7609		**10 Work Unit No. (TRAIS)** **11 Contract or Grant No.** C2153
12 Sponsoring Agency Name and Address Kansas Department of Transportation Bureau of Research 2300 SW Van Buren Topeka, Kansas 66611-1195		**13 Type of Report and Period Covered** Final Report September 2019 – August 2022 **14 Sponsoring Agency Code** RE-0797-01
15 Supplementary Notes For more information write to address in block 9.		

16 Abstract

High Mast Illumination Poles (HMIPs) are lighting towers that are taller than 55 ft (16.8 m) and are typically located along highways and rest stops. In March 2019, a wind event, referred to as a "bomb cyclone," caused several HMIPs in Kansas to excite and experience large-amplitude deflections on the order of several feet called "lock-in" behavior. Lock-in behavior is when the frequency of vibration matches a natural frequency of the structure and excess deformations will be observed. Pole vibrations can be caused by multiple wind actions and wind-structure interactions, including aeroelastic phenomenon like vortex shedding. Following the bomb cyclone event in 2019, the poles were inspected, and cracks were identified around the handhole openings in several of the structures. These poles were taken out of service having only been in service for approximately one year. Their premature failure caused significant concern. New, LED luminaires had been implemented with the construction of these poles. The Kansas Department of Transportation (KDOT) sought to learn if selection of LED luminaires (rather than older-style incandescent fixtures) had any influence on the behavior observed during this event.

The goal of this research project was to examine and compare the behavior of wind flow past LED and incandescent luminaires used in Kansas using computational fluid dynamics (CFD) modeling. Two-dimensional models were developed in Abaqus/CFD 2016 representing a projection of the full lighting assembly at the top of an HMIP. Simulations were created for each luminaire type on assemblies including three and four fixtures. The angle of wind relative to the light fixture and wind speed were varied throughout the simulations. Three-fixture simulations used wind angles of attack of 0, 30, and 60 degrees and four-fixture simulations used wind angles of attack of 0, 22.5, and 45 degrees. All assemblies and wind angles of attack were simulated for wind speeds of 15 (6.7), 25 (11.2), 30 (13.4), 35 (15.6), and 45 mph (20.1 mps). Time histories of the resulting forces on the lighting assemblies in the along-wind and cross-wind directions were extracted from the models. Power spectral density (PSD) curves were developed, identifying the dominant frequencies in the time-history data. The peaks in the PSD curves were extracted and compared with the first three natural frequencies of four representative HMIP archetypes used in the state. Natural frequencies of those four HMIP archetypes were determined using structural models of the poles using Abaqus/CAE 2017. To account for uncertainties in the analyses, ±10% bounds around each natural frequency were used when comparing the peaks in the PSD data with structural natural frequencies. When a peak fell within these bounds, it was treated as a "hit," having potential to excite that natural frequency mode and produce lock-in behavior. Hit counts were used to evaluate the data and compare each fixture type, angle of wind attack, and wind speed.

17 Key Words Lighting, Lighting equipment, Luminaires, Aerodynamic force, Fluid dynamics		**18 Distribution Statement** No restrictions. This document is available to the public through the National Technical Information Service www.ntis.gov.	
19 Security Classification (of this report) Unclassified	**20 Security Classification (of this page)** Unclassified	**21 No. of pages** 206	**22 Price**

Form DOT F 1700.7 (8-72)

This page intentionally left blank.

Computational Fluid Dynamics Investigation of High Mast Illumination Poles: Influence of Light Fixtures

Final Report

Prepared by

Briceson Junge
Caroline Bennett, Ph.D., P.E.
William Collins, Ph.D., P.E.
Jian Li, Ph.D., P.E.
Mark Ewing, Ph.D.

The University of Kansas

A Report on Research Sponsored by

THE KANSAS DEPARTMENT OF TRANSPORTATION
TOPEKA, KANSAS

and

THE UNIVERSITY OF KANSAS
LAWRENCE, KANSAS

January 2026

NOTICE

The authors and the state of Kansas do not endorse products or manufacturers. Trade and manufacturers names appear herein solely because they are considered essential to the object of this report.

This information is available in alternative accessible formats. To obtain an alternative format, contact the Office of Public Affairs, Kansas Department of Transportation, 700 SW Harrison, 2nd Floor – West Wing, Topeka, Kansas 66603-3745 or phone (785) 296-3585 (Voice) (TDD).

DISCLAIMER

The contents of this report reflect the views of the authors who are responsible for the facts and accuracy of the data presented herein. The contents do not necessarily reflect the views or the policies of the state of Kansas. This report does not constitute a standard, specification or regulation.

Abstract

High Mast Illumination Poles (HMIPs) are lighting towers that are taller than 55 ft (16.8 m) and are typically located along highways and rest stops. In March 2019, a wind event, referred to as a "bomb cyclone," caused several HMIPs in Kansas to excite and experience large-amplitude deflections on the order of several feet called "lock-in" behavior. Lock-in behavior is when the frequency of vibration matches a natural frequency of the structure and excess deformations will be observed. Pole vibrations can be caused by multiple wind actions and wind-structure interactions, including aeroelastic phenomenon like vortex shedding. Following the bomb cyclone event in 2019, the poles were inspected, and cracks were identified around the handhole openings in several of the structures. These poles were taken out of service having only been in service for approximately one year. Their premature failure caused significant concern. New LED luminaires had been implemented with the construction of these poles. The Kansas Department of Transportation (KDOT) sought to learn if selection of LED luminaires (rather than older-style incandescent fixtures) had any influence on the behavior observed during this event.

The goal of this research project was to examine and compare the behavior of wind flow past LED and incandescent luminaires used in Kansas using computational fluid dynamics (CFD) modeling. Two-dimensional models were developed in Abaqus/CFD 2016 representing a projection of the full lighting assembly at the top of an HMIP. Simulations were created for each luminaire type on assemblies including three and four fixtures. The angle of wind relative to the light fixture and wind speed were varied throughout the simulations. Three-fixture simulations used wind angles of attack of 0, 30, and 60 degrees and four-fixture simulations used wind angles of attack of 0, 22.5, and 45 degrees. All assemblies and wind angles of attack were simulated for wind speeds of 15 (6.7), 25 (11.2), 30 (13.4), 35 (15.6), and 45 mph (20.1 mps). Time histories of the resulting forces on the lighting assemblies in the along-wind and cross-wind directions were extracted from the models. Power spectral density (PSD) curves were developed, identifying the dominant frequencies in the time-history data. The peaks in the PSD curves were extracted and compared with the first three natural frequencies of four representative HMIP archetypes used in the state. Natural frequencies of those four HMIP archetypes were determined using structural

models of the poles using Abaqus/CAE 2017. To account for uncertainties in the analyses, ±10% bounds around each natural frequency were used when comparing the peaks in the PSD data with structural natural frequencies. When a peak fell within these bounds, it was treated as a "hit," having potential to excite that natural frequency mode and produce lock-in behavior. Hit counts were used to evaluate the data and compare each fixture type, angle of wind attack, and wind speed.

The results of the simulations showed the following: 1) both luminaire types were susceptible to vibrations that could lead to lock-in behavior across the first three natural frequencies of the poles, 2) the number of peaks in the PSD curves developed from each simulation that fell within a natural frequency range increased as the wind speed increased, 3) more peaks fell within the mode 1 range for the incandescent luminaires than for the LED luminaires, and 4) there was no clear indication that LED luminaires might incite a greater response than incandescent luminaires in the first mode.

Recommendations for future work include a continuation of this work for a broader spectrum of wind speeds, development of three-dimensional models to capture the influence of changes in geometry through the depth of the luminaire on the flow behavior, and instrumentation of existing HMIP structures with different luminaire types to determine real responses and compare with the numerical predictions presented in this document.

Acknowledgments

The authors gratefully acknowledge funding from the Kansas Department of Transportation under project RE-0797-01, enabling this work to be completed.

Table of Contents

List of Tables

List of Figures

Chapter 1: Introduction & Background

High mast illumination poles (HMIPs) are light towers taller than 55 ft (16.8 m). They are ubiquitous throughout Kansas and other states and are typically located along freeways, at interchanges, and rest stops. The poles typically consist of tapered, long hollow steel sections with a lighting assembly attached to the top, as shown in Figure 1.1. Wind loading is the primary loading considered in the design and analysis of lighting and sign structures. Despite their widespread use, the industry's understanding of wind loading and the susceptibility of HMIPs to wind-induced aeroelastic phenomena, like vortex shedding and buffeting, remains significantly underdeveloped.

There have been numerous documented failures of HMIP structures throughout the United States. In February 2003, a winter storm led to the collapse of approximately 140 tapered aluminum light poles in western Illinois thought to be due to wind-induced vibrations (Caracoglia & Jones, 2004). The Wisconsin Department of Transportation reported cracking and failures of high mast luminaire support structures and other support structures across the state (Foley et al., 2004). On November 12, 2003, a high mast light pole fell along I-29, near Sioux City, Iowa (Dexter, 2004). On April 11, 2004, two high mast lighting structures failed near Denver International Airport during a wind event (Goode & van de Lindt, 2007).

In March 2019, a Kansas wind event referred to as a "bomb cyclone" caused several HMIPs to excite and experience large-amplitude deflections on the order of several feet. Following this event, the poles were inspected, and cracks were identified around the handhole openings in several of the structures, as shown in Figure 1.2. These poles were taken out of service. The poles taken out of service had only been in service for approximately one year; therefore, their premature failure caused significant concern. The University of Kansas was retained to conduct a forensics investigation on the failed poles, and in parallel, engaged in an effort described in this report to develop an improved understanding of the response of HMIPs to wind loading.

Figure 1.1: High Mast Illumination Pole Lighting Assembly with LED Luminaires (K. Peterson [KDOT], personal communication, March 13, 2019)

Figure 1.2: Cracking Observed at the Handhole Weld (K. Peterson [KDOT], personal communication, March 13, 2019)

Previous research into interactive effects between wind and HMIP response has typically focused on instrumentation of existing poles and theoretical analysis of flow past the pole body, neglecting the lighting assembly. Ahearn and Puckett (2010) instrumented in-service HMIPs with anemometers and accelerometers to analyze how the poles responded to wind loading. Data were also gathered for poles retrofitted with helical strakes and perforated shrouds to characterize

effectiveness of retrofits at reducing dynamic responses. It was found that poles experienced lock-in behavior, mainly in the third natural frequency mode (Ahearn & Puckett, 2010). Giosan (2006) used an analytical approach to incrementally calculate susceptibility to vortex shedding near a natural frequency along the height of an HMIP. For the pole considered, it was found that shedding near the first four natural frequency modes at some points along the pole was possible within a practical wind speed range (Giosan, 2006). Peavy (2018) performed instrumentation of existing poles, computational fluid dynamics (CFD) modeling, and fluid-structure interaction (FSI) modeling of HMIPs. The 3D FSI model included the lighting assembly modeled as a thin projection of the shape attached to the top of the pole. Force and deflection data along the height of the pole were studied. Slower wind speeds around 5 mph (2.2 m/sec) were explored in the FSI model resulting in low deflections. The results showed it was difficult to predict the conditions at which excess vibrations will occur (Peavy, 2018).

1.1 Wind-Induced Vibrations

1.1.1 Vortex Shedding

Vortex shedding is an aeroelastic phenomenon that occurs when vortices form in the wake of a body and begin to interact and oscillate. This interaction results in forces on the body perpendicular to the direction of flow. A diagram of the phenomenon is shown in Figure 1.3. A "lock-in" phenomenon can occur when the vortex shedding frequency nears the natural frequency of the structure; under lock in, the structure begins to excite and can experience excess deformations and stresses. Vortex shedding typically develops at sustained wind speeds between 10 mph (4.47 m/s) and 45 mph (20.1 m/s) and produces structural vibrations in the direction perpendicular to the flow. Turbulence tends to be too high at wind speeds greater than 45 mph (20.1 m/s) for the phenomenon to occur. Wind speeds below 10 mph (4.47 m/s) are considered not significant enough to produce vortex shedding (AASHTO, 2001).

The Reynolds Number is defined as the ratio of inertia forces to viscous forces for fluid flow around an object or surface (NASA, 2009). Vortices begin to develop when the Reynolds number is between 5 and 40. Vortex shedding develops and is laminar when the Reynolds Number is above 40, then becomes turbulent between 300 to 300,000. Above this range, turbulence breaks

up vortex formation (Lienhard, 1966). Currently, the American Association of State Highway and Transportation Officials (AASHTO) specifications include design for wind loading on all components. Provisions are made conservative enough to aim to prevent possible damages due to fatigue from vortex shedding induced loading (AASHTO, 2013).

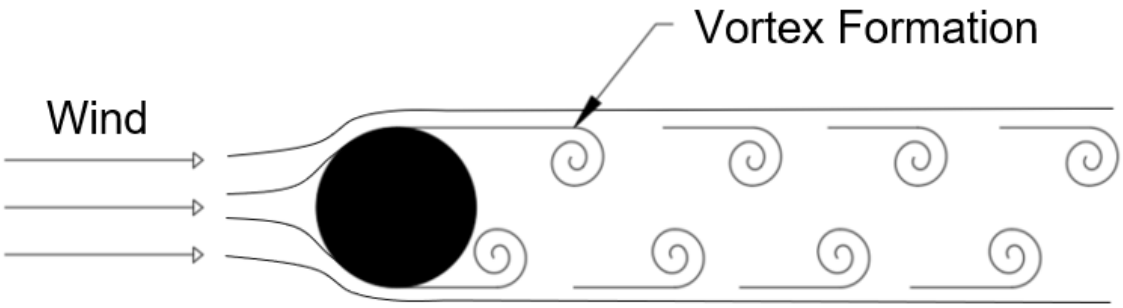

Figure 1.3: Formation of Vortex on Leeward Side of Body Causing Forces Perpendicular to Flow Direction

1.1.2 Buffeting

Buffeting is an irregular motion of a structure or parts of a structure in a flow, excited by turbulence in the flow. This turbulence can be caused by increased flow velocity or separation of flow around a body upstream. The result of buffeting can be damaging to the structure (Fung, 1955). Vortex shedding and buffeting can be captured through a CFD model by analyzing a time history of the pressure at a point on the leeward side of the object.

1.2 Objective and Scope

The objective of this study was to determine the influence of luminaire type on the susceptibility of HMIPs to vortex shedding using a computational fluid dynamics (CFD) modeling approach. Two types of luminaires were considered: LED and incandescent fixtures. The number of light fixtures was varied, along with orientation of the fixtures with respect to wind flow and wind velocity. Time histories of wind force on the lighting assembly projection were used to determine dominant frequencies produced by the wind flow and were compared with the first three natural frequency modes of poles commonly used in Kansas. This approach can provide insights

for wind behavior as it flows across the assemblies, and which, if any, structural modes it may excite. This approach isolates the lighting assembly; therefore, it does not provide insight as to how the lighting assembly and pole respond together.

Chapter 2: Methodology and Modeling Approach

The modeling approach adopted in this research was focused on characterizing wind flow past the lighting assembly, specifically comparing different light fixture types, number of fixtures, orientations with respect to the wind, and wind speed. A two-dimensional CFD modeling approach for the lighting assemblies was selected, reducing computational demands in comparison with those required by a three-dimensional analysis. Therefore, this approach considers a geometrically projected section through the luminaires that neglects small geometric details.

Pressure data was extracted from the models at points on or near the surface on the leeward side of the body in the CFD model. Similarly, the total force components on the surface of the body could be extracted. A time history of these force components was used for analysis to characterize how interactions in the wind with the body create forces acting on the body. Further, this data was analyzed to examine the frequency of oscillation of these forces. These data can be analyzed considering features such as magnitude of force or pressure, as well as through power spectral density (PSD) analysis. PSD curves reveal the dominant frequencies that the time-history record exhibits, which is a useful feature because the frequencies identified in each dataset could then be compared to the natural frequencies of a given HMIP to judge its likelihood of experiencing vortex induced vibrations (VIV).

2.1 Pole and Luminaire Geometry

The Kansas Department of Transportation (KDOT) provided drawings for HMIPs that are commonly used throughout Kansas. KDOT HMIPs consist of a tapered, round pole constructed in either two or three sections. The bottom pole section is welded to a baseplate, which is bolted into the foundation. The two-section pole considered in this study is 100-ft (30.5-m) tall, while the three-section poles considered have heights of 100 ft, 110 ft, and 120 ft (30.5 m, 33.5 m, and 36.6 m). The three-section pole is a newer design and provides an extra section of greater thickness near the base. The sections are connected with slip joint splices. An access hole (handhole) is located near the base of the pole to allow for lifting and lowering of the lighting fixture. The four HMIP archetypes are shown in Figure 2.1.

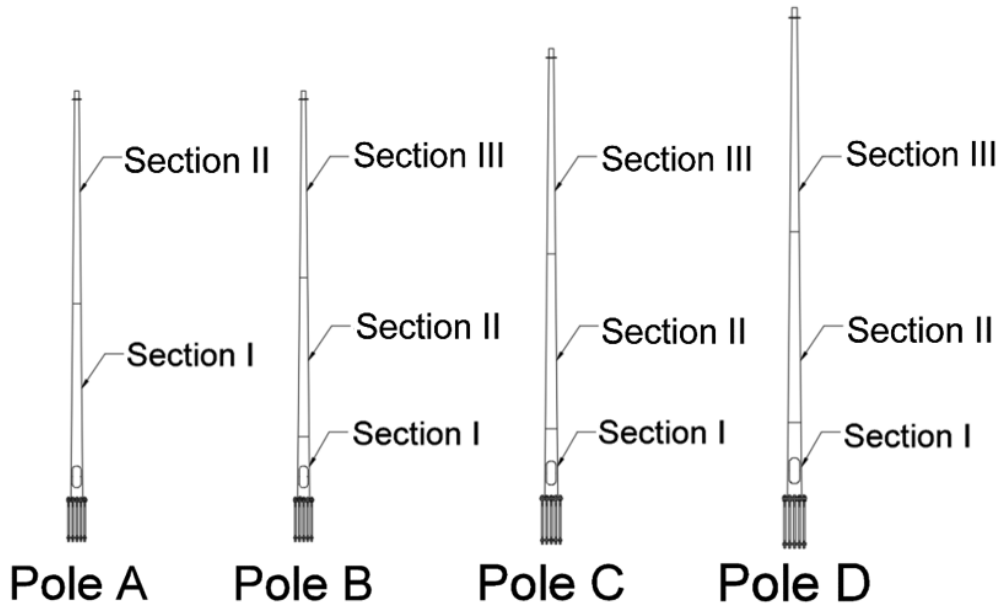

Figure 2.1: High Mast Illumination Pole Geometry

The lighting assembly located at the top of the pole includes luminaires attached to a lowering ring assembly (Figure 2.2). Movement of the lowering device is accomplished using an internal cable and pulley system. The number of luminaires attached to the lowering device depends on the amount of light required at that pole, with three to four luminaires commonly used on a single pole.

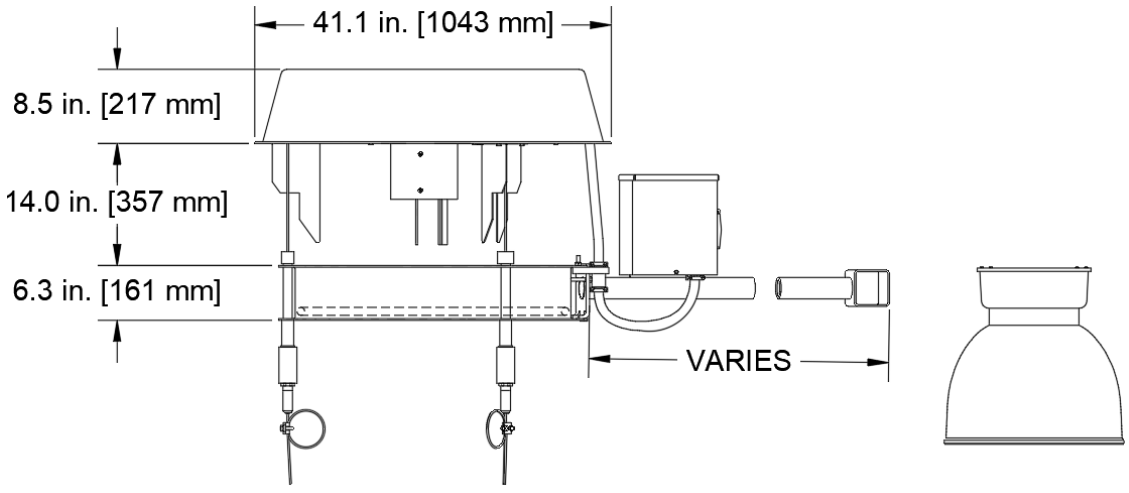

Figure 2.2: Lowering Ring Assembly

Two different types of luminaires were considered in this study—incandescent and LED. Until recently, KDOT used incandescent luminaires in all HMIP structures. However, newer structures utilize Holophane HMLED3 LED luminaires, which have a significantly slimmer profile and are brighter and more efficient than incandescent options. The LED luminaire is shown in Figure 2.3. The most common incandescent luminaire used in the KDOT lighting inventory is the Holophane HMSC High Mast Cutoff Series Luminaire, shown in Figure 2.3.

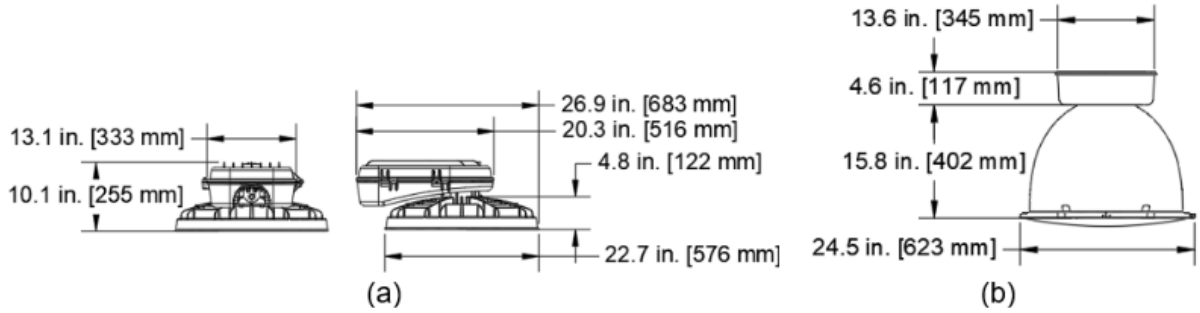

Figure 2.3: Luminaire Geometry (a) LED Luminaire (b) Incandescent Luminaire

2.2 Natural Frequency Analysis

The commercially available finite element analysis (FEA) software Abaqus/CAE (DSS, 2017) was used to calculate the first three modes of natural vibration of the HMIP archetypes. A three-dimensional structural model of each pole was developed based on the provided drawings. The lighting assembly was modeled as a lump mass at the top of the pole for simplicity in the natural frequency analysis.

Natural frequencies were determined for the four different archetype poles, as presented in Figure 2.1: a 100-ft (30.5-m) pole comprised of two tapered sections (Pole A), and 100-ft, 110-ft, and 120-ft (30.5-m, 33.5-m, and 36.6-m) poles comprised of three tapered sections (Poles B, C, and D, respectively). Pole geometries are presented in Table 2.1, with slip distance defined as the overlap between a pole section and the section below it. The poles are made of grade A572 steel, galvanized in the fabricated condition; material properties adopted in the models are listed in Table 2.2.

A linear perturbation frequency analysis step was created in Abaqus to compute the natural frequencies of the structure using Equations 2.1 and 2.2. The default settings for the step were used, and the first three dominant mode shapes were extracted. Torsional modes were disregarded in this analysis.

$$M^{NM}\ddot{u}^{M} + F^{N}(u^{M}) = 0$$

Equation 2.1

$$(-\omega^{2}M^{MN} + K^{MN})\varphi^{N} = 0$$

Equation 2.2

Where M^{MN} is the mass matrix, K^{MN} is the stiffness matrix, and φ^{N} is the eigenvectors or modes.

Table 2.1: High Mast Illumination Pole Tapered Section Measurements

Pole Label	Total Height, ft (m)	Section	Base Diameter, in. (mm)	Top Diameter, in. (mm)	Length ft (m)	Thickness, in. (mm)	Slip Distance, ft (m)
A	30.48 (100)	I	25.50 (647.7)	18.39 (467.1)	50.80 (15.48)	0.2500 (6.350)	N/A
		II	19.25 (491.6)	11.87 (301.5)	52.68 (5.867)	0.1880 (4.775)	28.31 (8.629)
B	30.48 (100)	I	26.00 (660.4)	23.42 (594.9)	18.40 (5.608)	0.5000 (12.70)	N/A
		II	24.50 (622.3)	18.63 (473.2)	41.90 (12.77)	0.2500 (6.350)	36.00 (10.97)
		III	19.50 (495.3)	12.88 (327.2)	47.32 (14.42)	0.1875 (4.763)	28.69 (8.745)
C	33.53 (110)	I	26.00 (660.4)	22.93 (582.4)	21.91 (6.678)	0.5000 (12.70)	N/A
		II	24.00 (609.6)	17.16 (435.9)	48.85 (14.89)	0.2500 (6.350)	35.25 (10.74)
		III	18.00 (457.2)	11.47 (291.3)	46.61 (14.21)	0.1875 (4.763)	26.44 (8.059)
D	36.58 (120)	I	26.00 (660.4)	21.95 (557.5)	28.93 (8.818)	0.5000 (12.70)	N/A
		II	23.00 (584.2)	16.18 (411.0)	48.73 (14.85)	0.2500 (6.350)	33.75 (10.29)
		III	17.00 (431.8)	10.08 (256.0)	49.46 (15.08)	0.1875 (4.763)	24.94 (7.602)

Table 2.2: Material Properties for A572 Steel

Material	Density (ρ)	Modulus of Elasticity (E)	Poisson's Ratio (v)
	lb/ft^3 (kg/m^3)	ksi (GPa)	-
A572 Steel	490 (7849)	29,000 (200)	0.30

2.3 CFD Modeling

Commercially available finite element modeling (FEM) software programs, Abaqus/CFD 2016 (DSS, 2016), were used to create computational fluid dynamics models of air flowing around the different lighting assemblies; different wind velocities and angles of attack were included in the modeling effort. The models were used to analyze the behavior of the wind force parallel and perpendicular to the flow direction, and to characterize the influence of specific luminaire details (incandescent versus LED, and number of light fixtures) on aerodynamic response. To model flow, the lighting assembly geometry was "cut out" of a large, rectangular fluid domain.

The air domain and lighting assembly were modeled in two dimensions rather than three to simplify model construction and improve computational efficiency. It should be noted that this approach sacrifices the inclusion of small details on the luminaires and lowering ring, and neglects changes in luminaire shape through depth. However, the two-dimensional approach has been successfully applied in numerous aerodynamic studies and is expected to represent global aerodynamic behavior for the lighting assemblies with reasonable accuracy, enabling comparison between incandescent and LED luminaires.

The modeled geometries are projections of the luminaire shapes and lowering ring in the lighting assembly configurations, as shown in Figure 2.4. The luminaires are spaced from the housing based on an 18-inch arm stretching from the lowering ring to the attachment point on the luminaire. Both fixtures attach to the arms on the back of their respective housings. Due to the placement of the LED fixture housings on the lowering ring, LED assemblies produce a larger total projected diameter than the equivalent incandescent assemblies. For both fixture types, the arms were omitted from the simulation geometry.

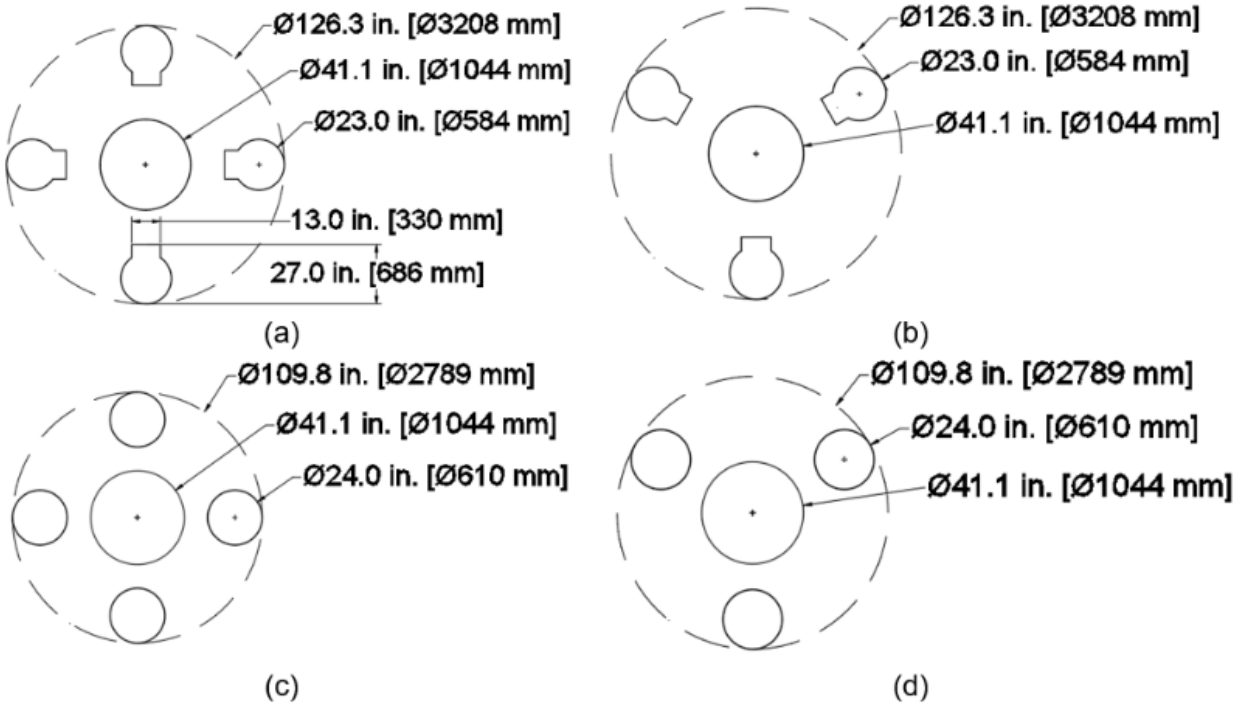

Figure 2.4: CFD Lighting Assembly Two-Dimensional Geometry for (a) 4 LED Luminaires, (b) 3 LED Luminaires, (c) 4 Incandescent Luminaires, and (d) 3 Incandescent Luminaires

2.3.1 Abaqus/CFD Modeling

Abaqus/CFD 2016 was chosen to perform CFD simulations for this study. A pseudo two-dimensional modeling approach that used a fluid domain with a one-element thickness was adopted. This approach precludes any changes in velocity or pressure over the depth normal to the plane, thus modeling two-dimensional behavior. The lighting assembly was modeled as a void in the fluid domain. The fluid domain is shown in Figure 2.5. The fluid inlet was modeled as a velocity inlet, positioned five diameters from the nearest point of the center circle representing the housing of the lighting assembly. A diameter was defined as the diameter of the center circle of the geometry equal to 41 in. (1.04 m). The pressure outlet was positioned 15 diameters to the edge of the center circle. The initial pressure at the outlet was set at 0 psi. Far field boundaries (walls) were modeled as velocity inlets with velocity equal in magnitude and direction to the front inlet. These were also positioned five diameters to the edge of the center circle. The lighting assembly geometry was defined to have no-slip boundaries where velocity is zero.

The fluid domain was carefully partitioned as shown in Figure 2.5 to allow for structured refinement of the mesh around the luminaire geometry. Partitions were offset 3 in. (76.2 mm) from each lighting assembly component. A seeding bias was placed normal to the boundaries to create inflation layers with a first element height of 0.01 in. (0.254 mm) which increased to 0.50 in. (12.7 mm). The mesh was unstructured within the box partition surrounding the full assembly to allow the mesh to conform around the geometry as different assemblies and rotations were modeled. The outsides of this box were seeded at 2 in. (50.8 mm), and the mesh increased to a 5-in. (127-mm) seed dimension in the region outside the interior box partition.

A dense mesh was necessitated near the wall boundaries to properly develop the boundary layer. The Spalart-Allmaras turbulence model works best with a y-plus value of approximately 1.0, where y-plus is a relative measurement of the first mesh element size against a boundary in a CFD model. Inflation layers in the mesh were created around the geometry where the first cell height was 0.01 in. (0.254 mm) and increased at a growth rate of 10% of the previous layer's height. The first layer height of 0.01 in. (0.254 mm) corresponded to a y-plus value greater than 1, but this was the smallest mesh size that Abaqus allowed for.

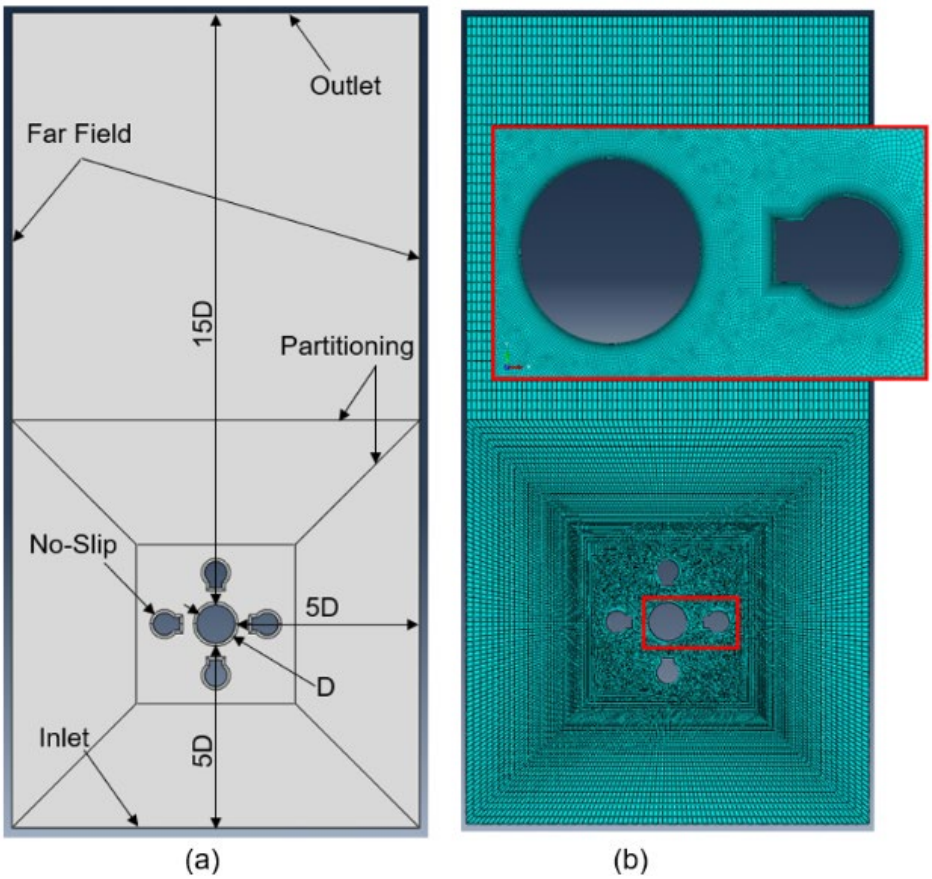

Figure 2.5: Abaqus/CFD Fluid Domain

Fluid properties were defined as having the density and viscosity of standard air, as presented in Table 2.3. These properties correlate to air at sea level at a temperature of 59 °F (15 °C).

Table 2.3: Fluid Properties for Air

Material	ρ	μ
	lb/ft^3 (kg/m^3)	lbf·s/ft^2 (Pa·s)
Air	2.37×10^{-3} (1.225)	3.740×10^{-7} (1.789×10^{-5})

The Reynolds Number can be calculated using Equation 2.3. The main factor influencing the Reynolds Number is air velocity, but air properties also have an effect. Notably, air properties change based on elevation and temperature. Density and pressure decrease as elevation above sea level increases, corresponding with decreases in the Reynolds Number. The density of air also

decreases as temperature increases. Due to these factors, air properties can vary significantly based on location and weather. Over a temperature range of 0 °F to 100 °F (-17.8 °C to 37.8 °C), the Reynolds Number will differ by approximately 30 percent. Increasing altitude from sea level to 5,000 ft (1524 m) corresponds with a decrease in the Reynolds Number of approximately 9 percent.

$$Re = \frac{\rho V L}{\mu}$$

Equation 2.3

The Spalart-Allmaras turbulence solver was utilized in all CFD models created and executed using Abaqus 2016 CFD software (DSS, 2016). The Spalart-Allmaras solver is a one-equation Reynolds-averaged Navier-Stokes (RANS) turbulence model approach. Default constants for the equation are listed in Table 2.4. In the solver controls, kinematic eddy viscosity was set to 0.01 in.^{2}/s (6.45×10-6 m^2/s) in all areas.

Table 2.4: Spalart-Allmaras Turbulence Modeling Constants (DSS, 2016)

Constant	Value
C_{b1}	0.1355
C_{b2}	0.622
C_{v1}	7.1
C_{v2}	5
C_{w1}	3.2391
C_{w2}	0.3
C_{w3}	2
σ	0.6667
K	0.41

Simulations were executed for 12 seconds of flow time with a fixed step size of 0.01 seconds, allowing for enough data points for post processing of the data. Solver limitation settings chosen are listed in Table 2.5.

Table 2.5: Abaqus CFD Solver Settings

Solver	Momentum Equation	Pressure Equation	Transport Equation
Iteration Limit	600	1200	600
Convergence Checking Frequency	1	10	1
Linear Convergence Limit	1×10^{-12}	1×10^{-14}	1×10^{-12}

The Strouhal Number is a useful dimensionless quantity for describing vortex shedding frequency. The relationship between the Strouhal Number and the Reynolds Number is shown in Figure 2.6. A range of Strouhal Numbers is shown because different conditions can produce slightly different results at the same Reynolds Number, such as the shape of the body the fluid is moving across or the roughness of the surface. The relationship is defined by an equation from Re = 250 to Re = 200,000. The Strouhal Number remains nearly constant with a magnitude of approximately 0.20 within this range. Above this value, the relationship is vague due to turbulent instabilities. This region is denoted with dashed lines in Figure 2.6. The Strouhal Number can be approximated while in the non-turbulent realm using Equation 2.4:

$$S = 0.198(1 - \frac{19.7}{Re})$$

Equation 2.4

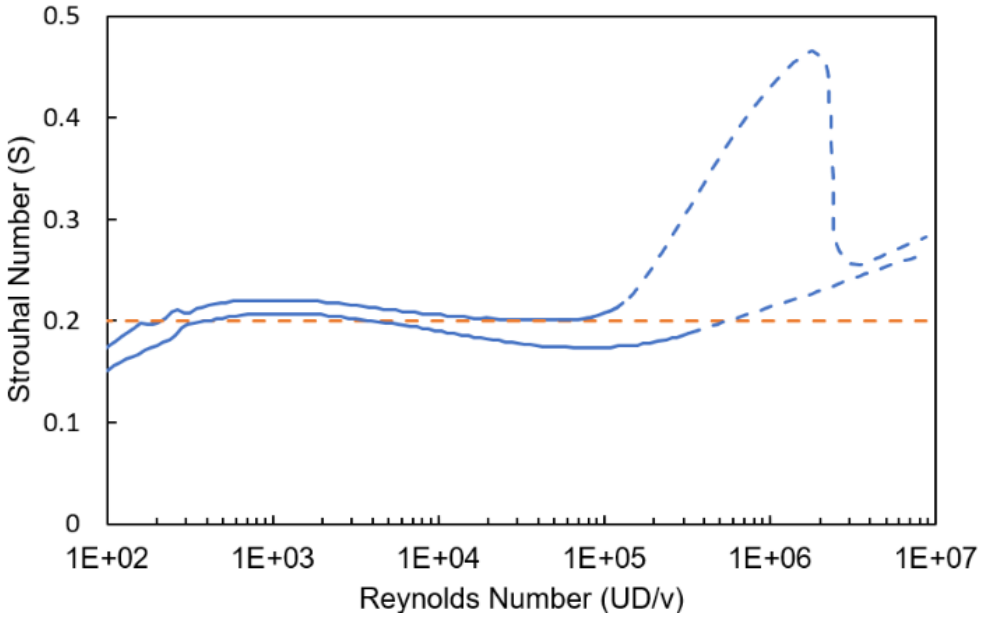

Figure 2.6: Relationship between Reynolds Number and Strouhal Number (Blevins, 1990)

The Strouhal Number can be calculated from experimental data using Equation 2.5, where f is the shedding frequency, D is the object diameter, and U is the free stream velocity.

$$S = \frac{fD}{U}$$

Equation 2.5

2.4 Model Matrix

Table 2.6 shows the modeling matrix, developed to capture common configurations with the luminaires in consideration. It was determined that three and four luminaire assemblies were the most common used in Kansas. The orientation of each luminaire assembly was defined with respect to the inlet. Orientations for each model begin at 0 degrees with one of the luminaires pointing towards the inlet. Then the models were rotated to capture the effects of orientation to fluid flow direction. Figure 2.7 shows the rotations considered, which served to vary the angle of attack of the wind. Four-luminaire fixture assemblies were explored with wind angles of attack of 0, 22.5, and 45 degrees. Three-luminaire assemblies were modeled with wind angles of attack at 0, 30, and 60 degrees. Velocity was initially based on wind velocity observed during the weather event causing the vibrations seen in the field. The wind speed measured at the nearest weather station was 35 mph (15.6 m/s) with gusts at 40 to 61 mph (17.9 to 27.3 m/s).

The data extracted from the CFD models includes the time history of the lift and drag coefficients and forces on the lighting assemblies. Lift is defined as force in the direction perpendicular to flow, and drag is the force that develops parallel to flow. The lift and drag coefficients were calculated based on a reference length defined as the width of the geometry perpendicular to the flow direction.

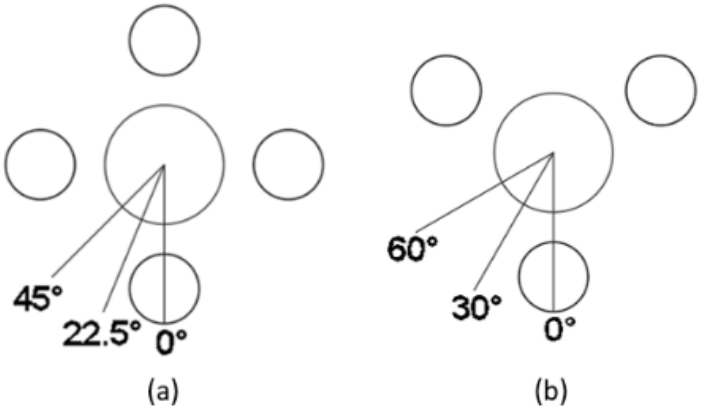

Figure 2.7: Lighting Assembly Model Rotations

Table 2.6: CFD Model Matrix

Luminaire Type	Number of Fixtures	Rotation (degrees)
Incandescent	3	0
		30
		60
	4	0
		22.5
		45
LED	3	0
		30
		60
	4	0
		22.5
		45

2.5 Power Spectral Density

After obtaining the results from the CFD simulation, MATLAB was utilized to determine the power spectral density of the time-history data. Power spectral density (PSD) is a representation of the signal power over frequencies (Stoica & Moses, 2005). The resulting curve shows the dominant frequencies present in the force data obtained in the CFD analysis. Figure 2.8 shows a PSD curve. Before finding the PSD, the average value of the data was subtracted out of each point to remove any static component. Also, a short portion at the beginning of the simulation was disregarded to neglect behavior where the flow was initiating and the model was not

experiencing a full response. Due to varying amplitudes and for clarity, the PSD curves were each normalized respective to their own maximum values. In each PSD curve, the first three natural frequencies of a given HMIP geometry were superimposed to provide practical context for the frequency response data. The natural frequencies are presented with a ±10% range in recognition of practical variations in stiffness. With these pieces of information present, the dominant frequencies in the PSD curves could then be compared to the natural frequency ranges for a given pole.

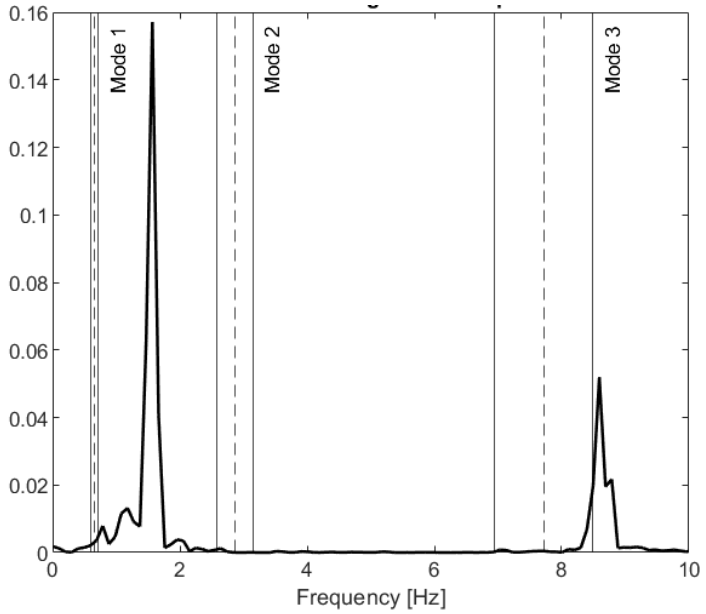

Figure 2.8: Power Spectral Density with Overlaid Natural Frequency Modes

Chapter 3: Results & Discussion

3.1 Natural Frequency Analysis Results

The natural frequencies computed for the first three modes for each pole type are shown in Table 3.1, based on the results from a structural dynamic model created using Abaqus. Frequencies were computed for the four lighting assembly configurations and four different pole geometries. Natural frequency varied slightly with changes in mass between the different lighting assembly configurations; however, they differed noticeably between pole geometries. The range of natural frequencies for the four pole geometries and various light fixture arrangements included in the study varied from 0.53–0.77 Hz for Mode 1, 2.13–3.33 Hz for Mode 2, and 5.35–8.62 Hz for Mode 3. Table 3.5 through Table 3.8 shows frequency bands 10% above and below each natural frequency. These ranges were plotted with the power spectral density results of their respective configuration.

Table 3.1: HMIP Natural Frequencies with 3 Incandescent Fixtures

Incandescent 3 Fixtures	Natural Frequency (Hz)			
Mode	**Pole 1**	**Pole 2**	**Pole 3**	**Pole 4**
1	0.65	0.76	0.64	0.55
2	2.85	3.31	2.65	2.16
3	7.72	8.62	6.81	5.39

Table 3.2: HMIP Natural Frequencies with 4 Incandescent Fixtures

Incandescent 4 Fixtures	Natural Frequency (Hz)			
Mode	**Pole 1**	**Pole 2**	**Pole 3**	**Pole 4**
1	0.63	0.74	0.62	0.53
2	2.82	3.27	2.61	2.13
3	7.66	7.19	6.76	5.35

Table 3.3: HMIP Natural Frequencies with 3 LED Fixtures

	Natural Frequency (Hz)			
LED 3 Fixtures	**Mode**	**Pole 1**	**Pole 2**	**Pole 3**	**Pole 4**
	1	0.66	0.77	0.64	0.55
	2	2.87	3.33	2.66	2.18
	3	7.75	7.78	6.83	5.40

Table 3.4: HMIP Natural Frequencies with 4 LED Fixtures

	Natural Frequency (Hz)			
LED 4 Fixtures	**Mode**	**Pole 1**	**Pole 2**	**Pole 3**	**Pole 4**
	1	0.64	0.75	0.63	0.54
	2	2.84	3.29	2.63	2.15
	3	7.72	8.59	6.79	5.37

Table 3.5: HMIP Natural Frequencies with 3-Incandescent Fixtures

	Mode	Pole 1		Pole 2		Pole 3		Pole 4	
Incandescent-3 Fixtures		**-10%**	**+10%**	**-10%**	**+10%**	**-10%**	**+10%**	**-10%**	**+10%**
	1	0.59	0.72	0.69	0.84	0.57	0.70	0.49	0.60
	2	2.57	3.14	2.98	3.64	2.38	2.91	1.95	2.38
	3	6.94	8.49	7.76	9.48	6.13	7.49	4.85	5.93

Table 3.6: HMIP Natural Frequency Ranges with 4-Incandescent Fixtures

	Mode	Pole 1		Pole 2		Pole 3		Pole 4	
Incandescent-4 Fixtures		**-10%**	**+10%**	**-10%**	**+10%**	**-10%**	**+10%**	**-10%**	**+10%**
	1	0.57	0.70	0.67	0.82	0.56	0.68	0.48	0.59
	2	2.54	3.10	2.94	3.60	2.35	2.88	1.92	2.35
	3	6.90	8.43	6.47	7.91	6.09	7.44	4.82	5.89

Table 3.7: HMIP Natural Frequency Ranges with 3-LED Fixtures

LED-3 Fixtures	Mode	Pole 1		Pole 2		Pole 3		Pole 4	
		-10%	+10%	-10%	+10%	-10%	+10%	-10%	+10%
	1	0.59	0.72	0.70	0.85	0.58	0.71	0.50	0.61
	2	2.58	3.16	3.00	3.66	2.40	2.93	1.96	2.39
	3	6.97	8.52	7.00	8.56	6.14	7.51	4.86	5.94

Table 3.8: HMIP Natural Frequency Ranges with 4-LED Fixtures

LED-4 Fixtures	Mode	Pole 1		Pole 2		Pole 3		Pole 4	
		-10%	+10%	-10%	+10%	-10%	+10%	-10%	+10%
	1	0.58	0.71	0.68	0.83	0.56	0.69	0.49	0.59
	2	2.55	3.12	2.96	3.62	2.37	2.90	1.93	2.36
	3	6.95	8.50	7.74	9.45	6.11	7.46	4.83	5.91

3.2 CFD Simulation Results

3.2.1 Abaqus/CFD Results

As previously described, time histories of lift and drag forces acting on the light fixtures were extracted from the simulations. It was observed that the variation and amplitude of lift force tended to far exceed that of the drag force, as illustrated in Figure 3.1. For this reason, responses in the lift, or crosswind, direction were focused on. Time-history plots for all simulations are provided in Appendix A. Generally, force tended to ramp up at the beginning of the simulations while the response was developing. This ramp portion of the data was disregarded in post processing. The lift force typically oscillated around 0 force, while drag force tended to oscillate around a positive value. This value is the constant force component on the geometry. Before developing the PSD curves, the average force value was subtracted out of the data to remove this constant force component.

Figure 3.2 shows the power spectral density curves for an LED configuration with three fixtures oriented at a 0-degree rotation relative to the wind direction, subjected to wind velocity of 30 mph (13.4 m/s). PSD curves for all simulations are presented in Appendix B. The spikes in the PSD represent dominant frequencies present in the time-history data. Four separate plots were

created to overlay the natural frequency ranges for each pole type. Each plot uses the same PSD curve. The natural frequency ranges for the respective pole presented in Table 3.1 through Table 3.4 were overlaid on the plots, allowing consideration of the dominant frequencies from the time-history responses in the context of the natural frequencies of the different pole geometries considered. For the cases presented in Figure 3.2, the response was greatest for frequencies less than 5 Hz, with the largest response at 1.17 Hz and next largest at 1.86 Hz. These two spikes did not occur within any of the natural frequency ranges, implying that resonance should not occur. However, smaller peaks were present that intersected mode 1 and mode 2 natural frequencies for all pole types, implying that resonance could still be possible at lower amplitude responses.

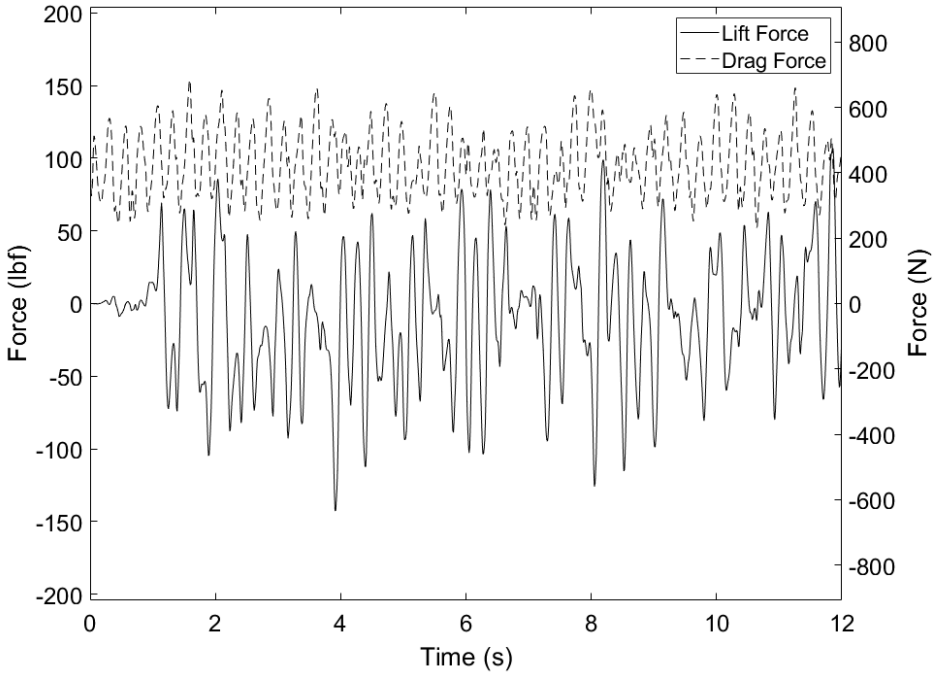

Figure 3.1: Time History of Lift and Drag Force for the 3 LED Light Fixture Configuration with 0-Degree Rotation at 30 mph (13.4 m/s)

When considering the PSD data, a *peak* was defined as occurring when a local maximum existed that was greater than 5% of the maximum peak prominence of a given PSD curve. *Prominence* was defined as the height of a local maximum measured from the valley in the curve separating it from the next highest peak. Because the PSD curves were normalized, the maximum

possible prominence was 1.0. Adding a prominence requirement allowed for numerous small local maxima that were effectively noise in the data to be filtered out and not be counted as peaks.

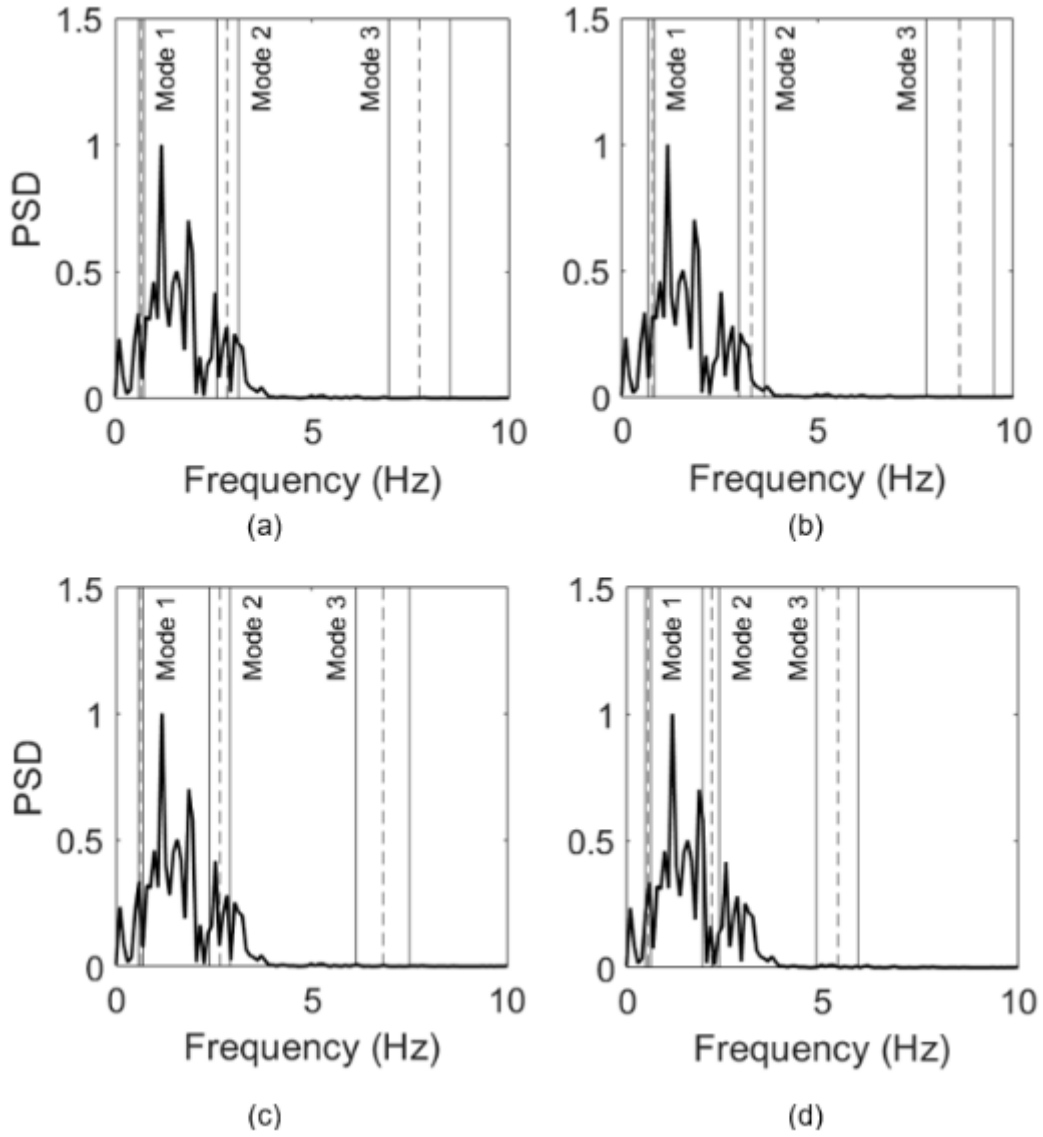

Figure 3.2: Power Spectral Density Curve of the Time History of Crosswind Force on the Lighting Assembly for the 3 LED Configuration at a 0-Degree Rotation at 15 mph: (a) Pole A, (b) Pole B, (c) Pole C, (d) Pole D

Additional methods for defining peaks were explored. These alternative methods included considering minimum spacing between peaks and a minimum peak height, rather than minimum prominence. The requirement of a minimum spacing between peaks would come into effect when

two peaks occurred within a specified tolerance. The peak with higher prominence would be counted and the other would be neglected. This approach was found to not sufficiently filter the data and neglected important peaks. A minimum height requirement would specify a minimum value that a local maximum must exceed to be counted. On the normalized scale, this value was set to 0.10–0.30. The advantage to this approach is that peaks would not be omitted if they were characterized by high values but relatively low prominences. This approach was not selected because small peaks creating noise in the curve would not be filtered out when they were above the threshold value, resulting in a large number of peaks in some instances.

Peaks were determined relative to the data of a single simulation. This is flawed because a peak in a dataset at a higher wind speed could be excluded when it has a higher amplitude than one that is not excluded at a lower wind speed when compared. To further identify the peaks in the data and compare them to peaks in other simulations, a series of color band comparison charts were created, as discussed in the following.

Figure 3.3 shows a color band comparison chart for the 3-LED light fixture configuration oriented at a 0-degree position relative to the wind direction, with data represented for all wind speeds considered. The colors represent amplitude of the PSD curves. These data were not normalized as was done in the PSD plots, so that changes in amplitude between variables could be considered. Translating the PSD curves to color bands allowed for multiple curves to be placed adjacent to one another for comparison. Peaks in the data are identified with an ‘X’. Like the individual PSD curves, a chart was created for each HMIP type and its respective natural frequency ranges were overlaid on the chart across all the bands. These ranges were not labeled for clarity. The mode 1 range is the lowest range, with modes 2 and 3 ordered above it on the plots.

These plots were used to compare the light assembly configurations over the various wind speed and rotation ranges considered. For the configuration presented in Figure 3.3 (3 LEDs), peaks in the response data tended to shift to higher frequencies with increasing wind speed. The amplitude of the data also increased with wind speed. Color band charts for all simulations are presented in Appendix C.

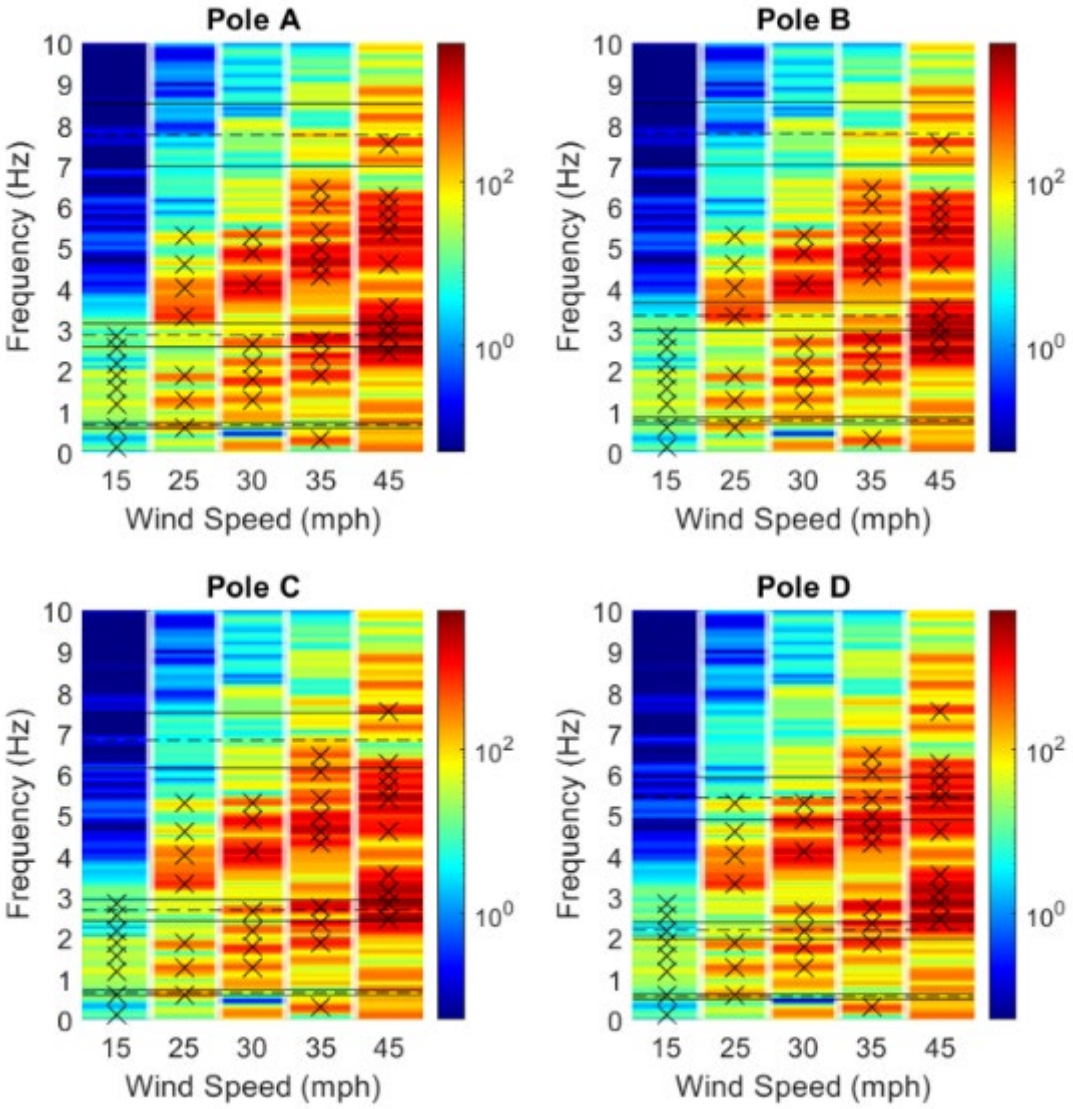

Figure 3.3: Color Band Comparison Chart of PSD Curves for 3-LED Fixture Configuration at 0-Degree Rotation

To analyze broad patterns in the overall dataset, a series of bubble plots were created, indicating the number of times a dominant frequency in the PSD data fell within a natural frequency band for a given pole (Figure 3.4). The size of each bubble denotes the number of 'hits' occurring for a given assembly rotation and wind speed. Each hit count is denoted with numbers overlaid on the bubbles. The mode 1 hits are indicated on the upper half of the bubbles with the number of hits proceeded by "M1." Modes 2 and 3 are labeled in similar fashion with mode 2 hits located in the center, and mode 3 on the lower half of the bubbles. Frequency bands were taken as

10% above and below the natural frequency for a given mode for each HMIP type (Table 3.5 through Table 3.8).

Hits were counted when a peak fell within the frequency range of a given mode. The ranges were applied two ways: 10% above and below the frequency of a given mode, and 10% of a single mode applied across all three modes. When a 10% boundary was applied to each mode respectively, the result was ranges that increased in size as the mode increased. Figure 3.5 shows bubble plots developed with 10% bounds on each respective natural frequency. Applying 10% bounds of one of the modes across all of them resulted in a fixed size for all modes. This was done to try to address any bias in the data based on the size of a given range. The mode 1 range will naturally result in fewer hits than modes 2 and 3 due to the tighter range and vice versa. Figure 3.6 shows three bubble plots for the 4-incandescent fixture configuration where the range associated with a single mode was applied to all modes. Figure 3.6(a) is the bubble plot where hits for each mode were counted with a range 10% above and below the first mode.

Generally, the data showed that more hits occurred with increasing wind speed. Lower wind speeds tended to result in less excitations and excitation of lower frequencies. As wind speed increased, more excitation was seen in the PSD curves which encompassed a broader range of frequencies. This led to more hits across all modes as wind speed increased. Also, the most hits were found to occur when the lighting assemblies were oriented at a 0-degree rotation.

Between the two luminaire types, more mode 1 range hits were seen with the incandescent luminaires for the instance of using mode 2 frequency bands. This would indicate the incandescent fixtures would be more likely to incite a mode 1 response. It is not indicative that either luminaire type would excite any HMIP type in any mode. Mode 1 excitation involves larger deformations resulting in larger stresses in the pole, and as the mode increases, vibrations are associated with lower deformations and stresses. Larger stresses can lead to fatigue cracking at fatigue prone details, such as the handhole at the base of the poles. Therefore, it is beneficial to limit excitations in lower modes, specifically mode 1.

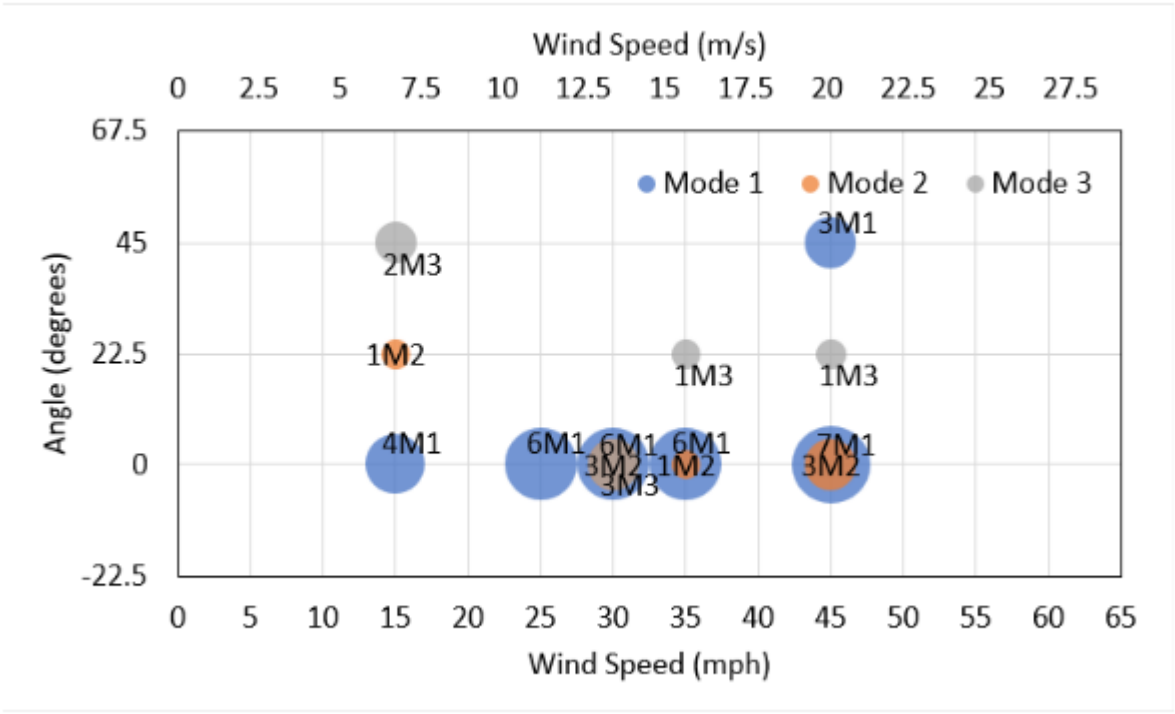

(a)

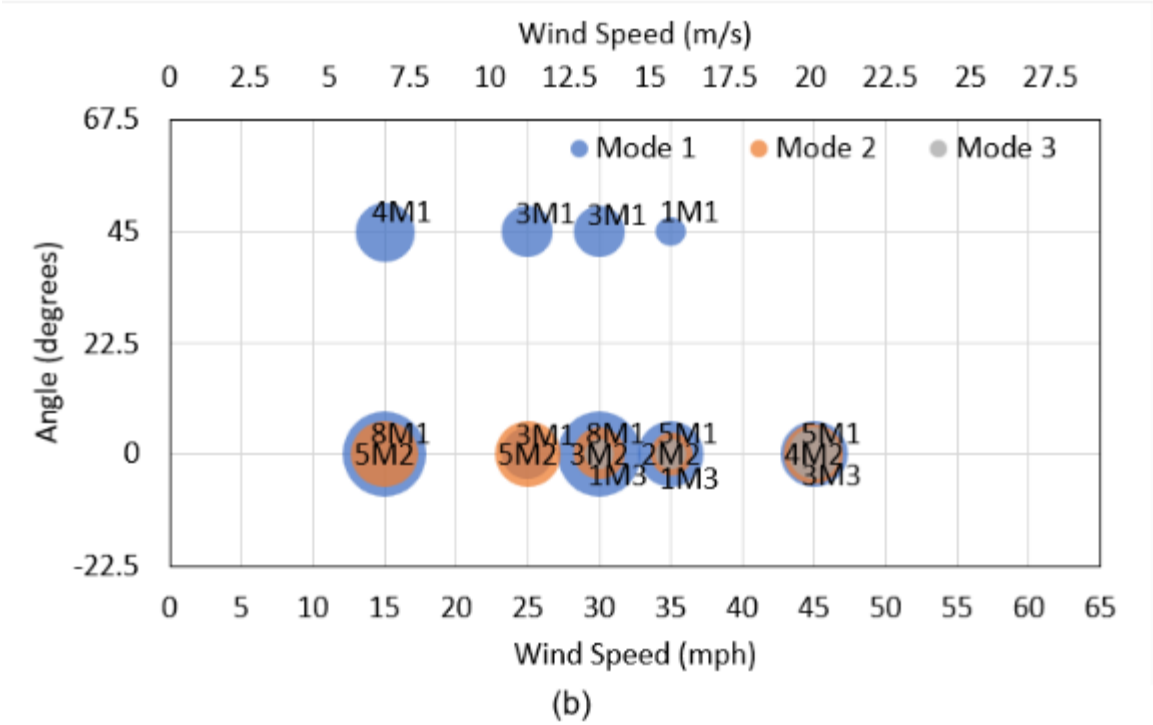

(b)

Figure 3.4: Peak Hit Comparison Bubble Charts: (a) 4 Incandescent (Mode 2 Fixed Range), (b) 3 Incandescent (Mode 2 Fixed Range), (c) 4 LED (Mode 2 Fixed Range), (d) 3 LED (Mode 2 Fixed Range)

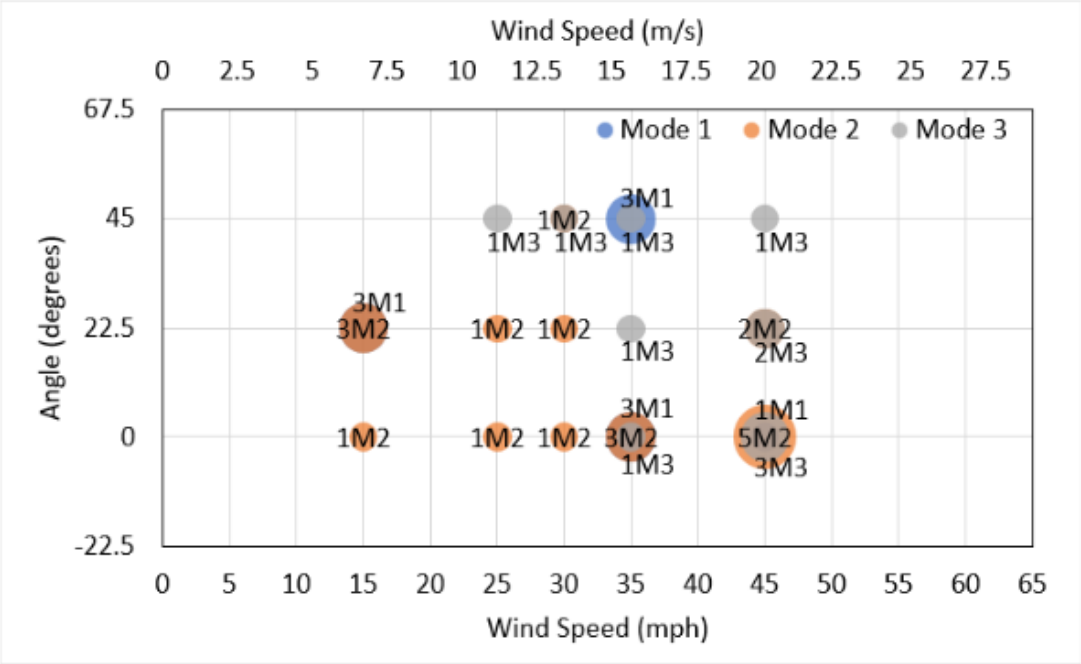

(c)

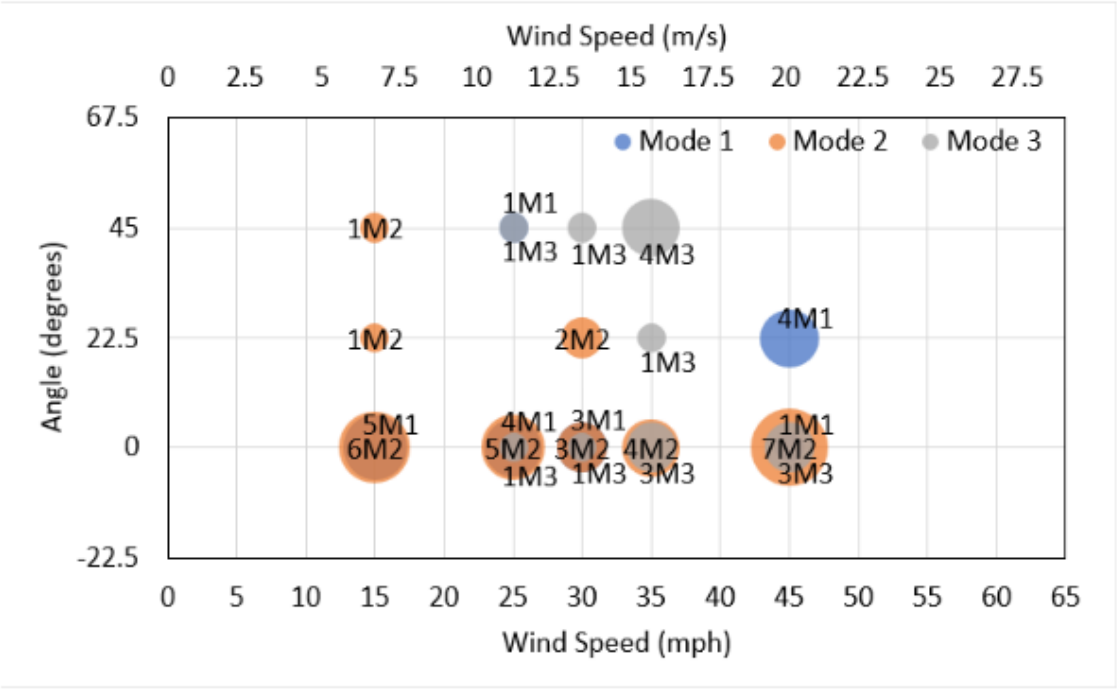

(d)

Figure 3.4: Peak Hit Comparison Bubble Charts: (a) 4 Incandescent (Mode 2 Fixed Range), (b) 3 Incandescent (Mode 2 Fixed Range), (c) 4 LED (Mode 2 Fixed Range), (d) 3 LED (Mode 2 Fixed Range) (continued)

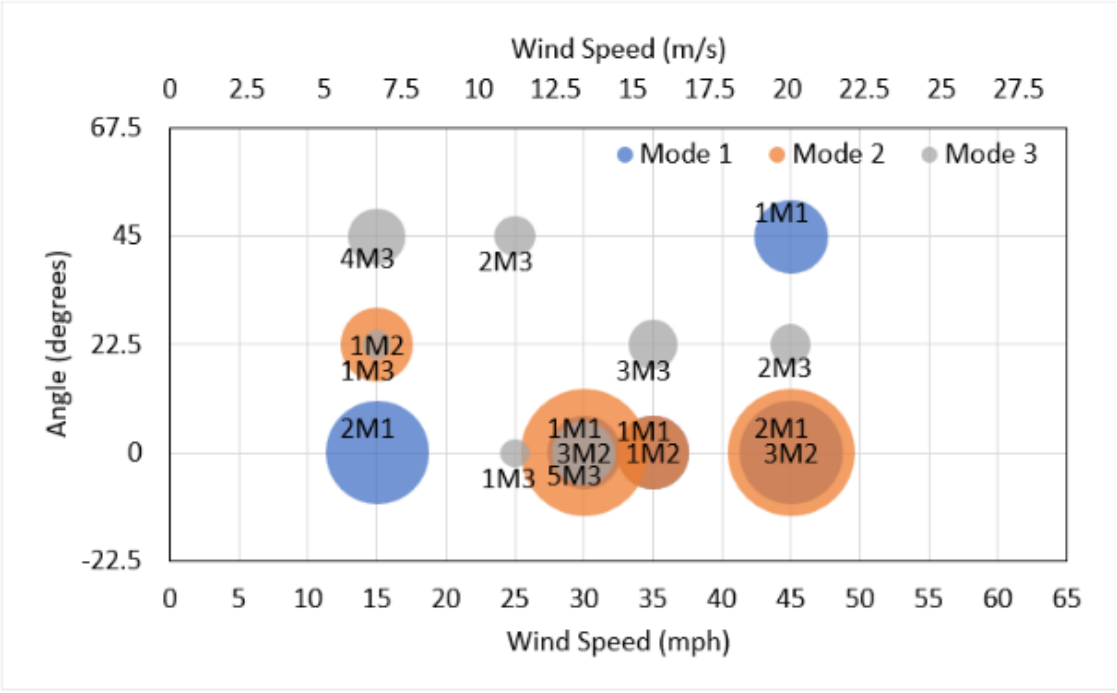

(a)

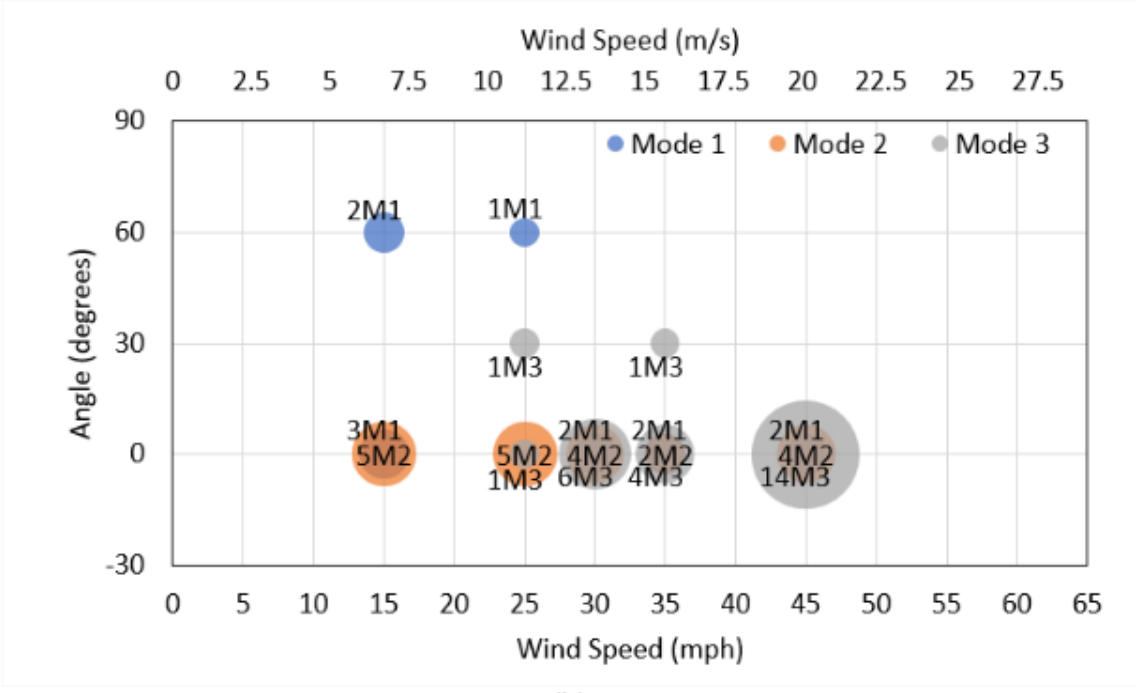

(b)

Figure 3.5: Peak Hit Comparison Bubble Charts Using ±10% of Each Natural Frequency: (a) 4 Incandescent, (b) 3 Incandescent, (c) 4 LED, (d) 3 LED

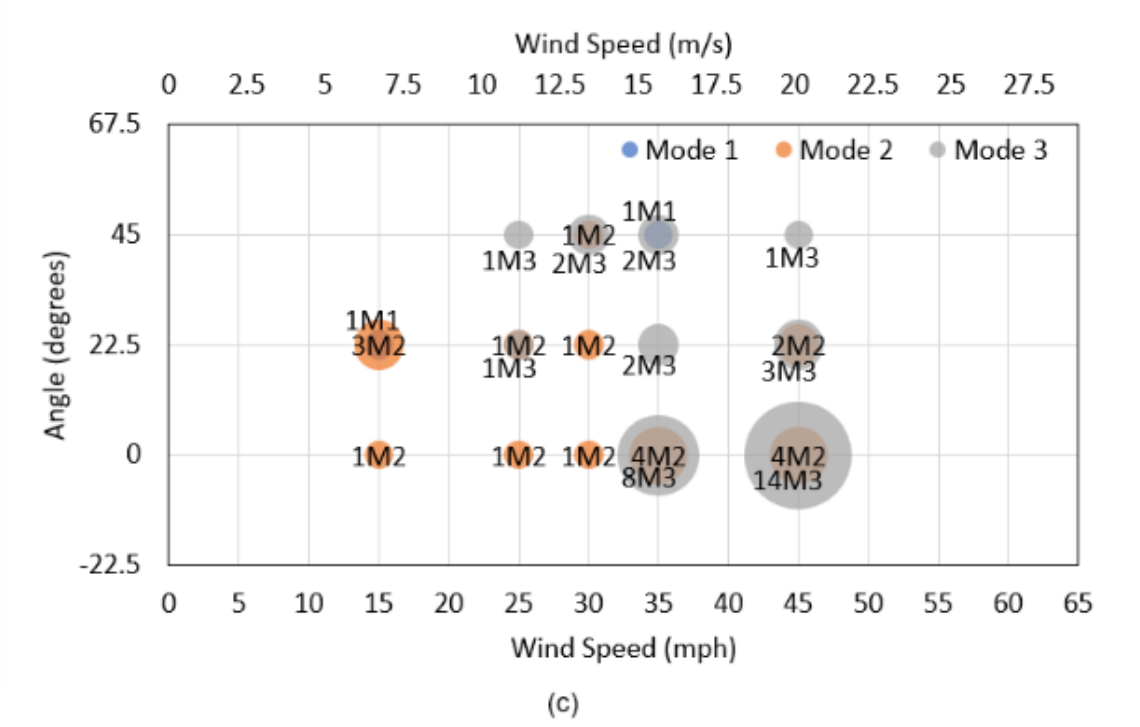

(c)

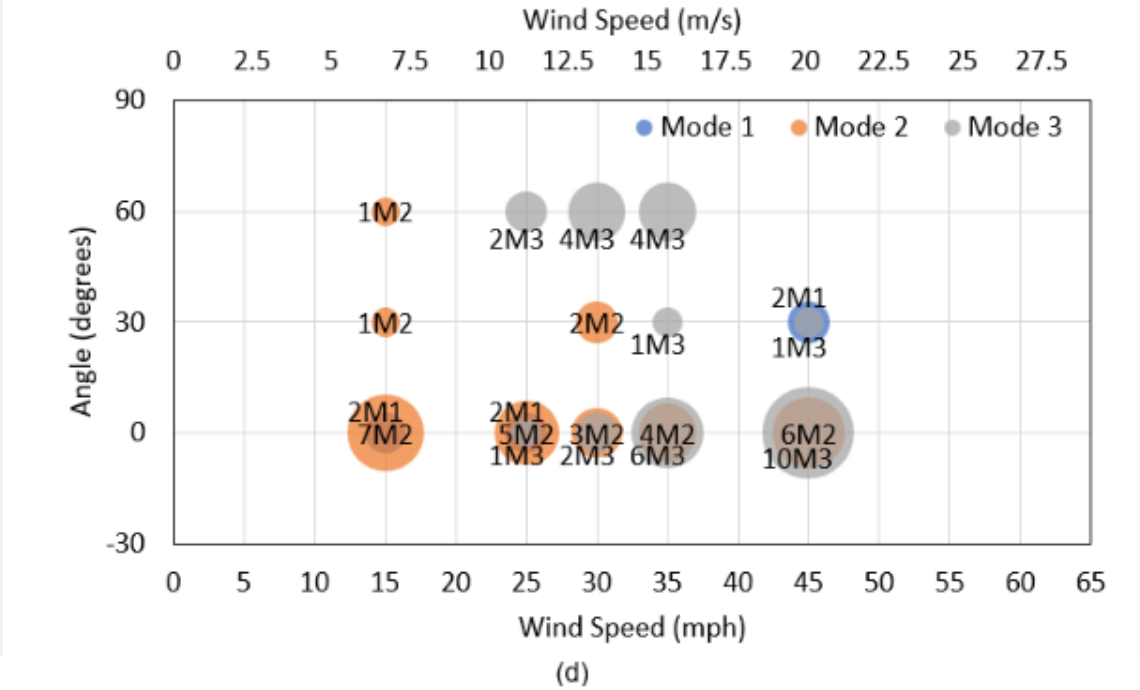

(d)

Figure 3.5: Peak Hit Comparison Bubble Charts Using ±10% of Each Natural Frequency: (a) 4 Incandescent, (b) 3 Incandescent, (c) 4 LED, (d) 3 LED (continued)

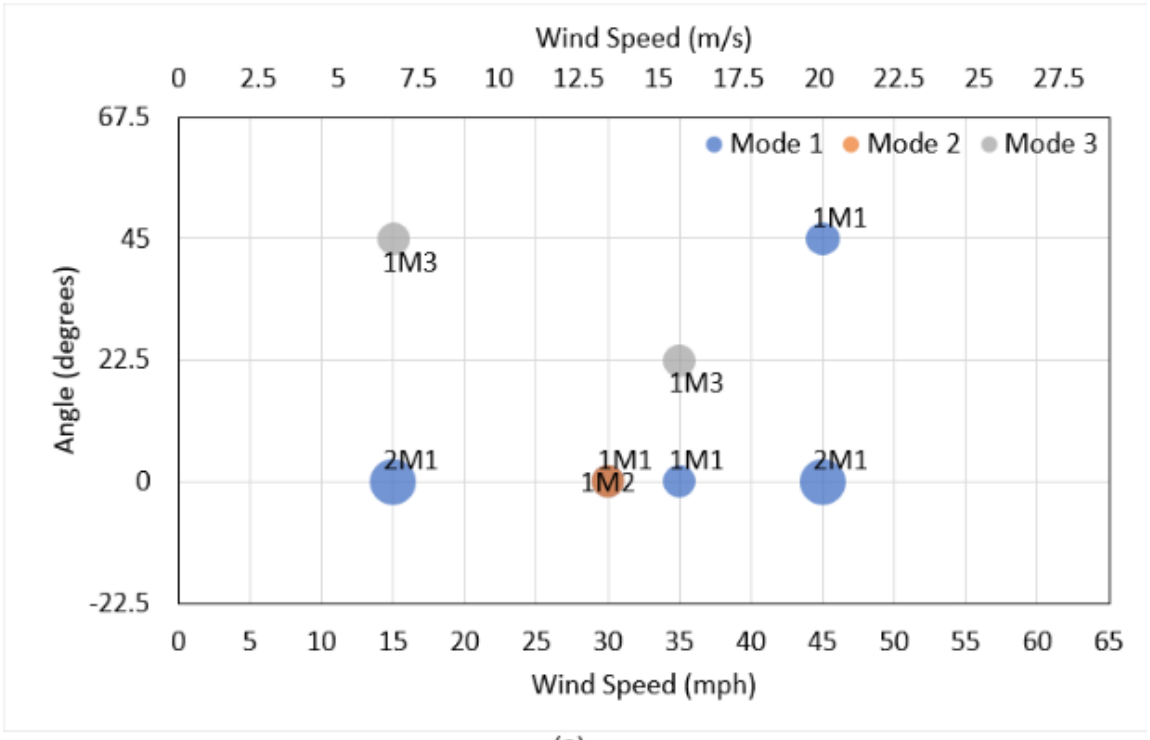

(a)

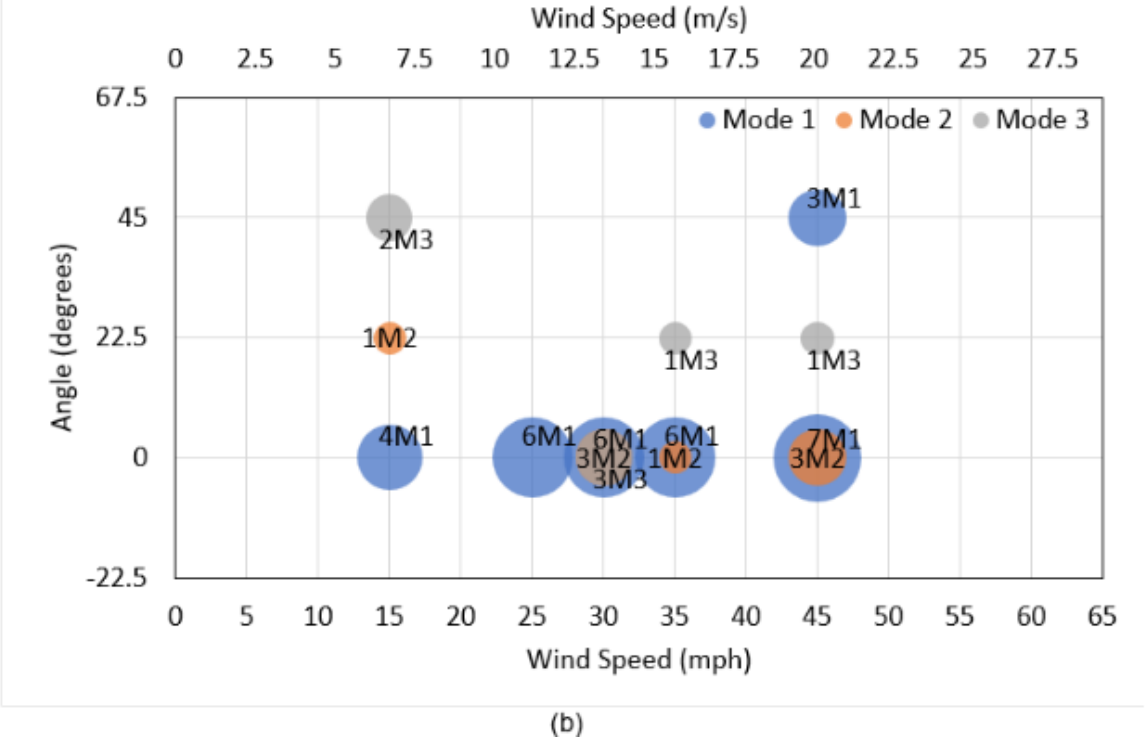

(b)

Figure 3.6: Peak Hit Comparison Bubble Charts for 4 Incandescent Fixture Configurations Using (a) ±10% of Mode 1, (b) ±10% of Mode 2, (c) ±10% of Mode 3

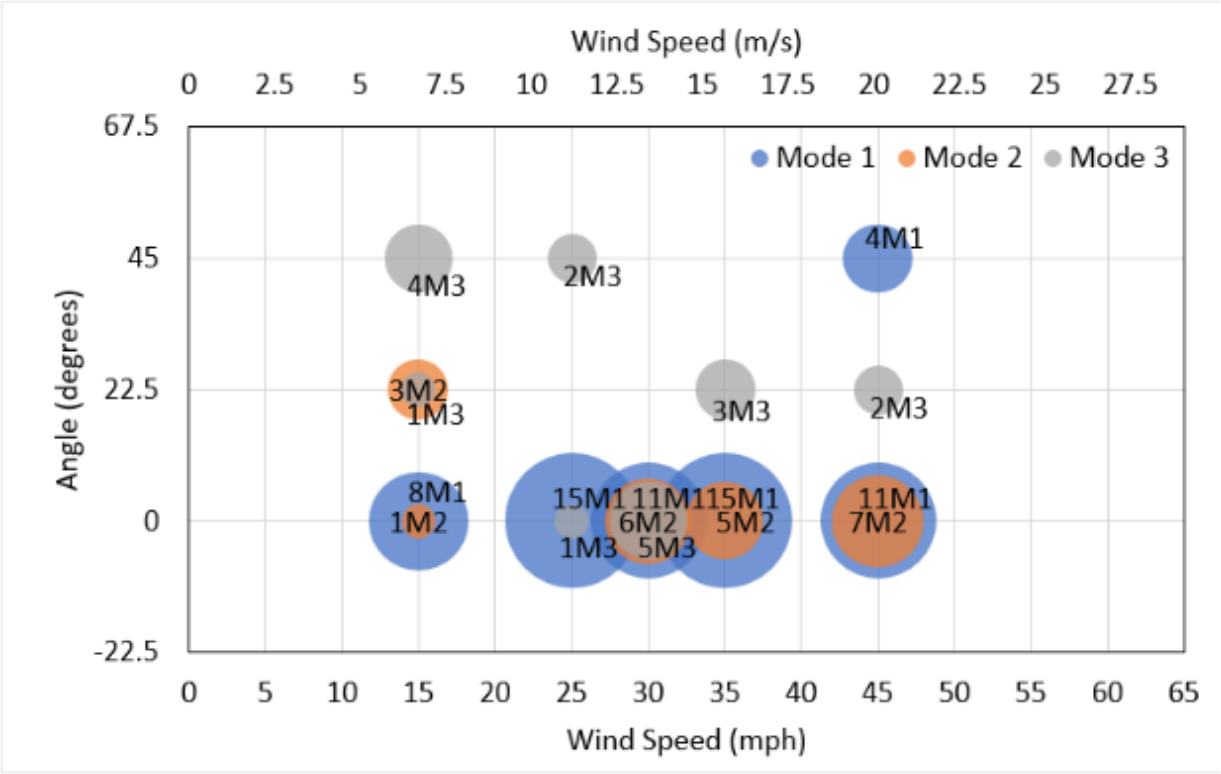

(c)

Figure 3.6: Peak Hit Comparison Bubble Charts for 4 Incandescent Fixture Configurations Using (a) ±10% of Mode 1, (b) ±10% of Mode 2, (c) ±10% of Mode 3 (continued)

Chapter 4: Conclusions & Future Work

4.1 Conclusions

This report describes a study focused on the susceptibility of high mast poles with various light fixture configurations to vortex shedding (lock-in behavior) under various wind speeds and directions. The study utilized a computation fluid dynamics (CFD) modeling approach, in which force time histories were extracted to determine the frequency of the wind loading on the light fixture assemblies, and compared with the natural frequency of HMIP structures used in Kansas. This comparison facilitated a "hit count" for vortex shedding susceptibility for different light fixture combinations (3 LEDs, 4 LEDs, 3 incandescent, and 4 incandescent). The study has led to the following conclusions:

1. There was no clear indication that LED luminaires might incite a greater response than incandescent luminaires in the first mode. This finding is in contrast to a hypothesis that arose after observations of high-amplitude deformations observed in the wind event of February 2019, which appeared to largely affect structures with LED fixtures.
2. A greater number of Mode 1 hits were observed in models with incandescent luminaires than for LED luminaires when the ±10% natural frequency bandwidth was based on the Mode 2 natural frequency. This finding indicates that incandescent fixtures are more likely to correspond with a Mode 1 response.
3. The number of hits in any frequency range generally increased with wind speed, indicating greater potential for lock-in behavior under vortex shedding with increasing wind speed.
4. Cases in which the wind direction was straight on (0-degree angle with the fixture) corresponded with more frequency range hits than the other wind directions for the three and four fixture configurations. Overall, the results were found to be dependent on wind direction.

The results showed susceptibility of both light fixture types to vortex shedding lock-in behavior across the first three natural modes. There was no identifiable trend that selecting one luminaire type over another could decrease susceptibility to lock-in behavior.

4.2 Future Work

The following recommendations for future work are provided:

1. Models should be created and analyzed for a larger range of wind speeds, particularly higher speeds.
2. Additional common luminaire geometries should be considered and included in a suite of models.
3. Three-dimensional models of the luminaires and lowering ring assemblies should be developed to capture the influence of geometry changes along the depth.
4. Fluid-structure interaction models should be developed such that realistic influence of structural deformations in the lowering ring and pole can be considered in tandem with the CFD analysis.
5. Existing HMIP structures with different luminaire types should be instrumented to determine real responses and compared with the numerical predictions presented in this document.
6. Establish a connection between the PSD magnitude, level of force, and "hits" identified in the data to gauge the likelihood of large deformations due to vortex shedding.
7. Explore the use of vibration dampening devices on HMIPs to mitigate the effects of wind-induced vibrations from a phenomenon like vortex shedding. This could be done through field testing. CFD modeling could also be utilized, more specifically for geometry altering methods.

Overall, this research has advanced the state-of-the-art data surrounding the behavior of high mast illumination poles under wind loading and specifically considered: the influence of light fixture selection, orientation with respect to wind direction, and wind speed. This constitutes a

novel and important contribution to the field. Additionally, the techniques used for analysis of the data are considered to be novel and have not been applied to this problem before—to our knowledge.

Given that the research did not reveal clear differences in susceptibility to vortex shedding between the light fixtures studied: we recommend that solutions for damping high-amplitude responses in HMIP structures be developed and implemented.

References

Ahearn, E. B., & Puckett, J. A. (2010). *Reduction of wind-induced vibrations in high-mast light poles* (Report No. FHWA-WY-10/02F). Wyoming Department of Transportation. https://rosap.ntl.bts.gov/view/dot/23968

American Association of State Highway and Transportation Officials (AASHTO). (2001). *Standard specifications for structural supports for highway signs, luminaires, and traffic signals* (4th ed.).

American Association of State Highway and Transportation Officials (AASHTO). (2013). *Standard specifications for structural supports for highway signs, luminaires, and traffic signals* (6th ed.).

Blevins, R. D. (1990). *Flow-induced vibration* (2nd ed.). Van Nostrand Reinhold.

Caracoglia, L., & Jones, N. P. (2004). *Analysis of light pole failures in Illinois* (Report No. 635).

Dassault Systèmes Simulia (DSS). (2016). *Abaqus/CAE user's guide.* Dassault Systèmes Simulia Corp.

Dassault Systèmes Simulia (DSS). (2017). *Abaqus/CAE user's guide*. Dassault Systèmes Simulia Corp.

Dexter, R. J. (2004). *Investigation of cracking of high-mast lighting towers*. Iowa Department of Transportation.

Foley, C. M., Ginal, S. J., Peronto, J. L., & Fournelle, R. A. (2004). *Structural analysis of sign bridge structures and luminaire supports* (Report No. WHRP 04-03). Wisconsin Department of Transportation, Wisconsin Highway Research Program. https://www.wistatedocuments.org/digital/collection/p267601coll4/id/16732/rec/1

Fung, Y. C. (1955). *An introduction to the theory of aeroelasticity*.

Giosan, I. (2006). *Vortex shedding induced loads on free standing structures*. Structural Vortex Shedding Response Estimation Methodology and Finite Element Simulation. https://www.academia.edu/download/39020061/vortex_shedding.pdf

Goode, J. S., & van de Lindt, J. W. (2007). Development of a semiprescriptive selection procedure for reliability-based fatigue design of high-mast lighting structural supports. *Journal of Performance of Constructed Facilities*, *21*(3), 193-206. https://doi.org/10.1061/(ASCE)0887-3828(2007)21:3(193)

Lienhard, J. H. (1966). *Synopsis of lift, drag, and vortex frequency data for rigid circular cylinders* (College of Engineering, Research Division, Bulletin 300). Washington State University, Technical Extension Service.

National Aeronautics and Space Administration (NASA). (2009). *Reynolds Number*. Retrieved from https://www.grc.nasa.gov/www/BGH/reynolds.html

Peavy, M. D. (2018). *An aeroelastic investigation of wind induced vibrations of high-mast poles* (Doctoral dissertation). Universite Libre de Bruxelles. https://hdl.handle.net/2013/ULB-DIPOT:oai:dipot.ulb.ac.be:2013/274208

Stoica, P., & Moses, R. L. (2005). *Spectral analysis of signals*.

Appendix A

A.1 Time History of Directional Forces on the Surface in the CFD Simulations

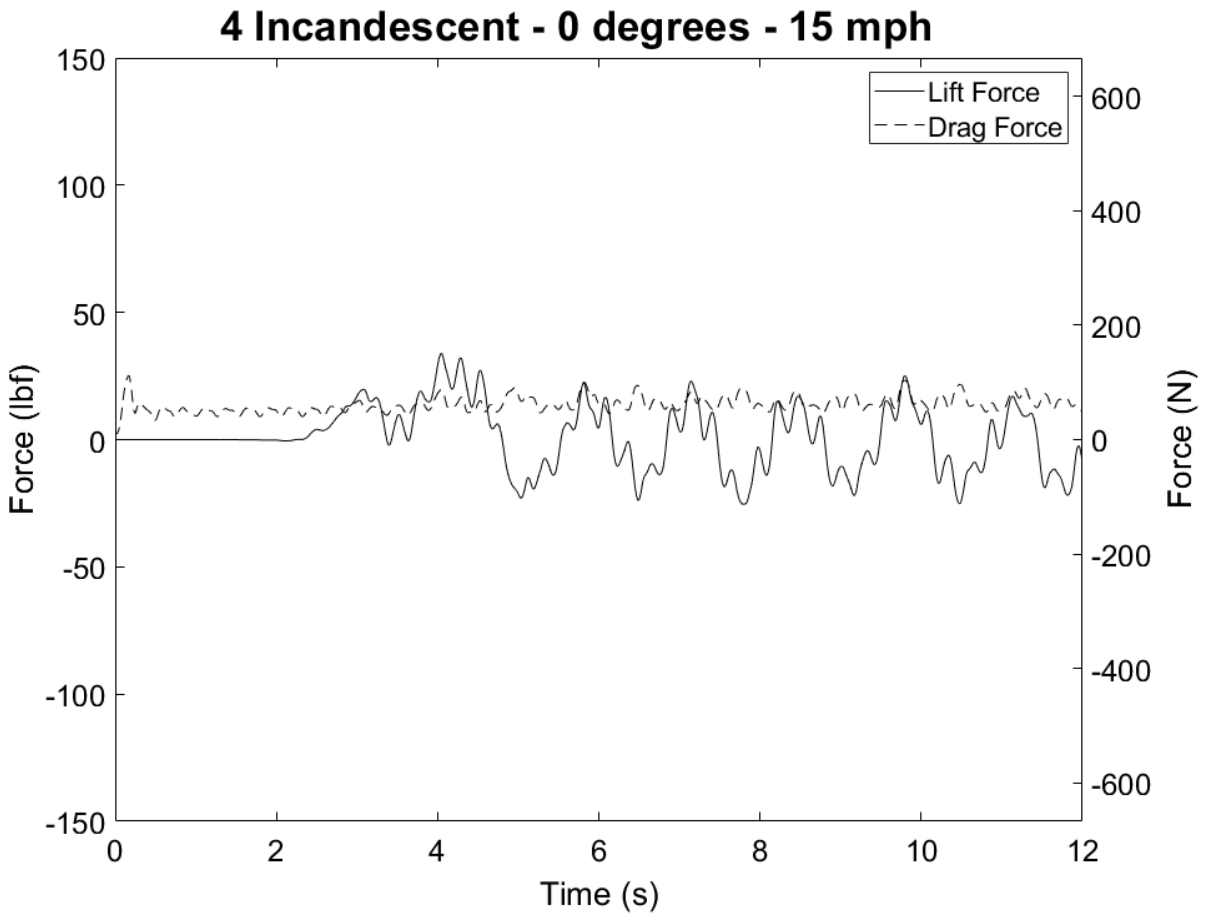

Figure A.1: Force-Time Relationship for 4-Indandescent Light Fixture Subjected to 15 mph Wind at an Angle of 0 Degrees

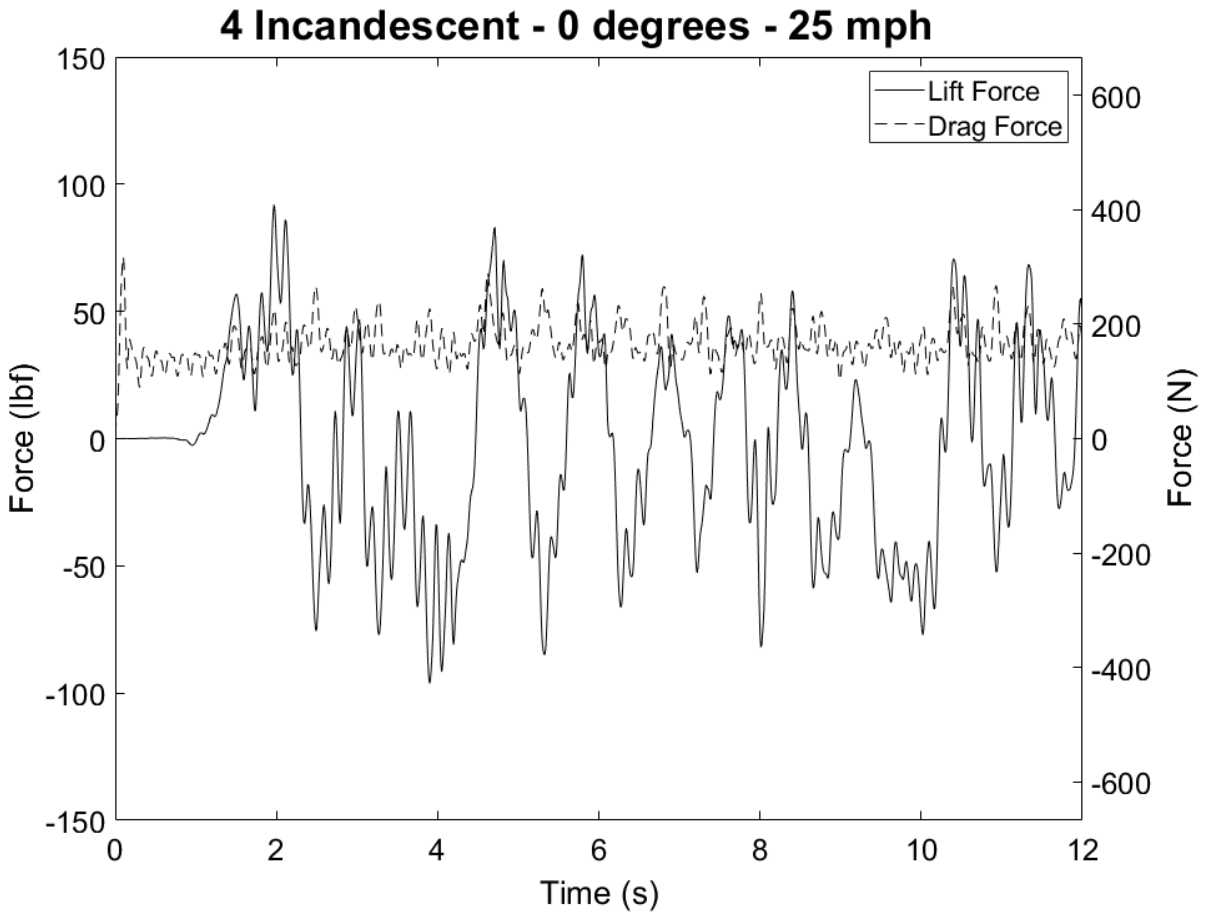

Figure A.2: Force-Time Relationship for 4-Indandescent Light Fixture Subjected to 25 mph Wind at an Angle of 0 Degrees

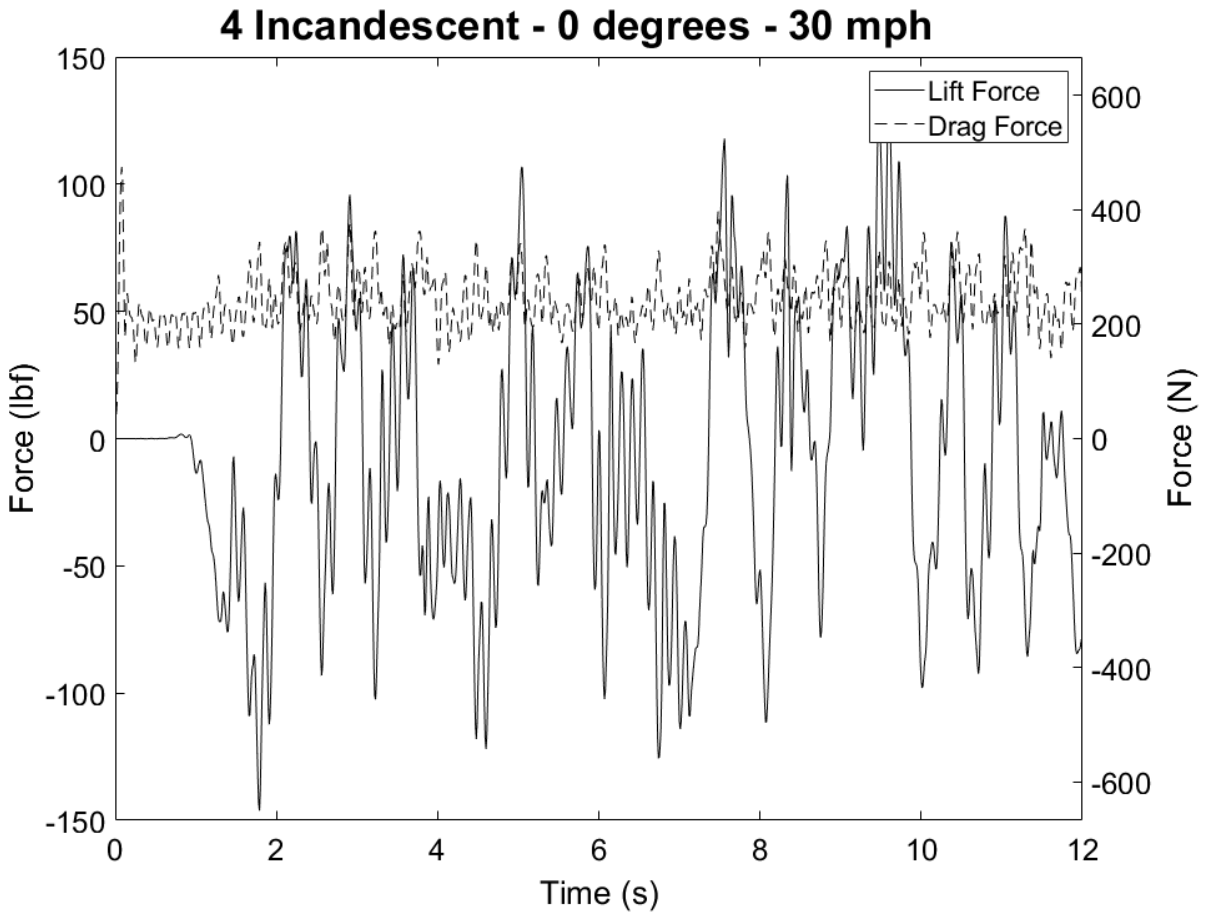

Figure A.3: Force-Time Relationship for 4-Indandescent Light Fixture Subjected to 30 mph Wind at an Angle of 0 Degrees

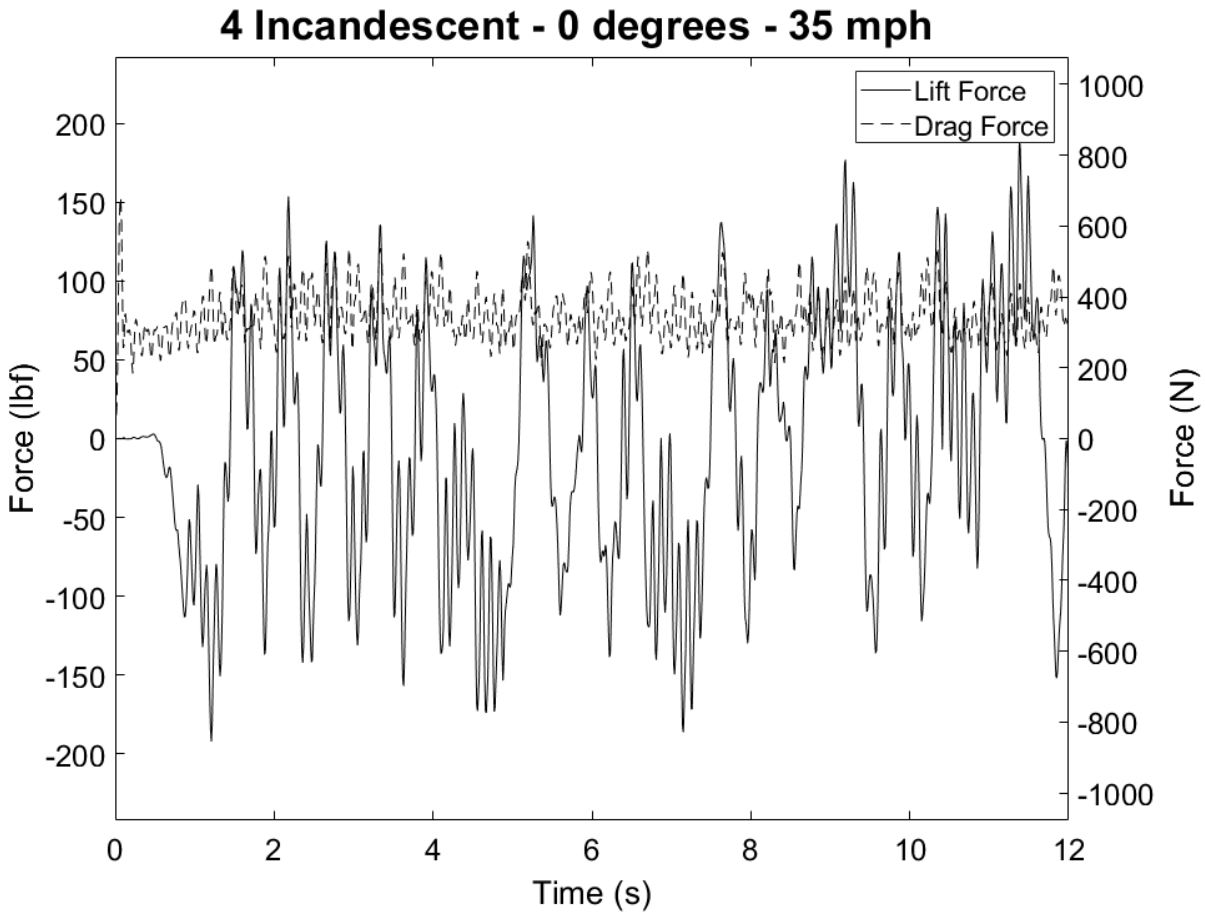

Figure A.4: Force-Time Relationship for 4-Indandescent Light Fixture Subjected to 35 mph Wind at an Angle of 0 Degrees

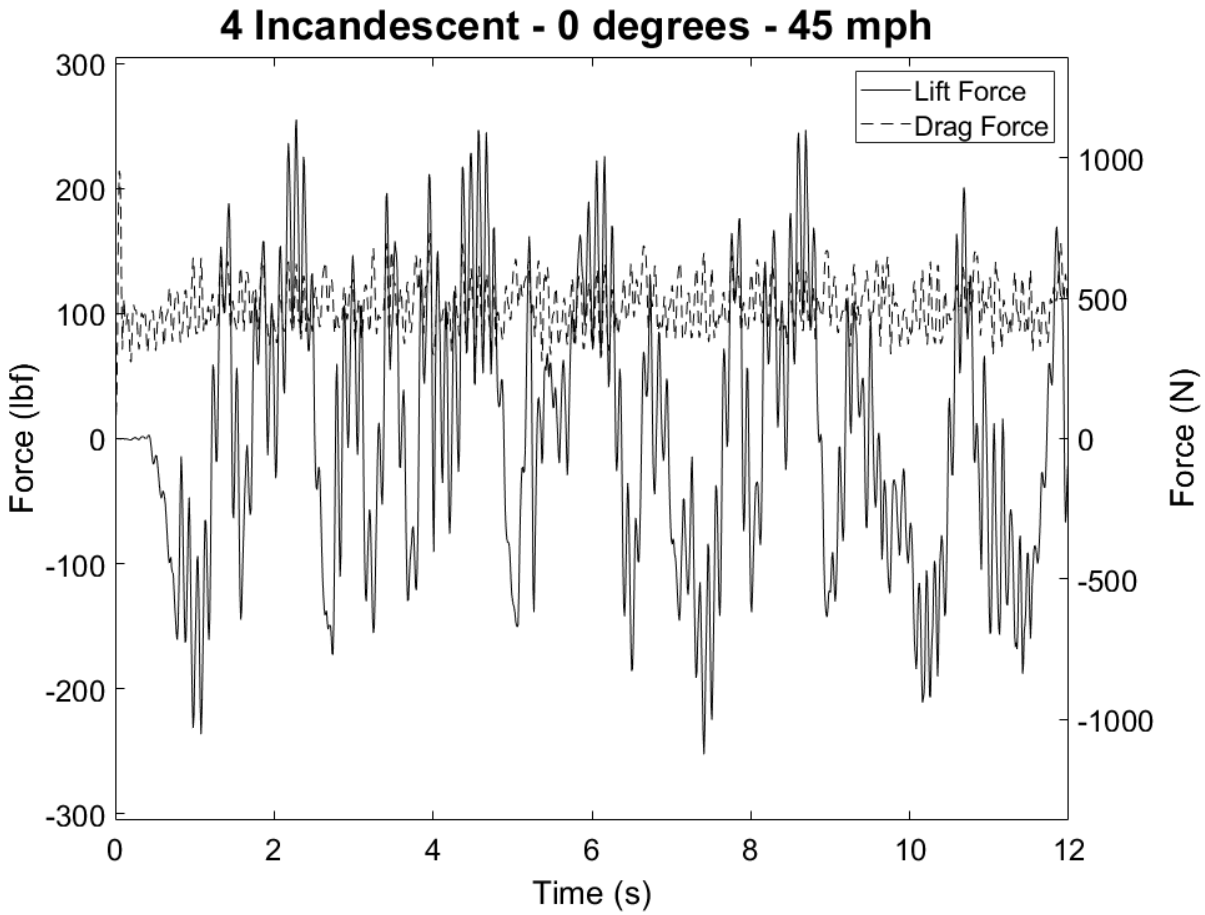

Figure A.5: Force-Time Relationship for 4-Indandescent Light Fixture Subjected to 45 mph Wind at an Angle of 0 Degrees

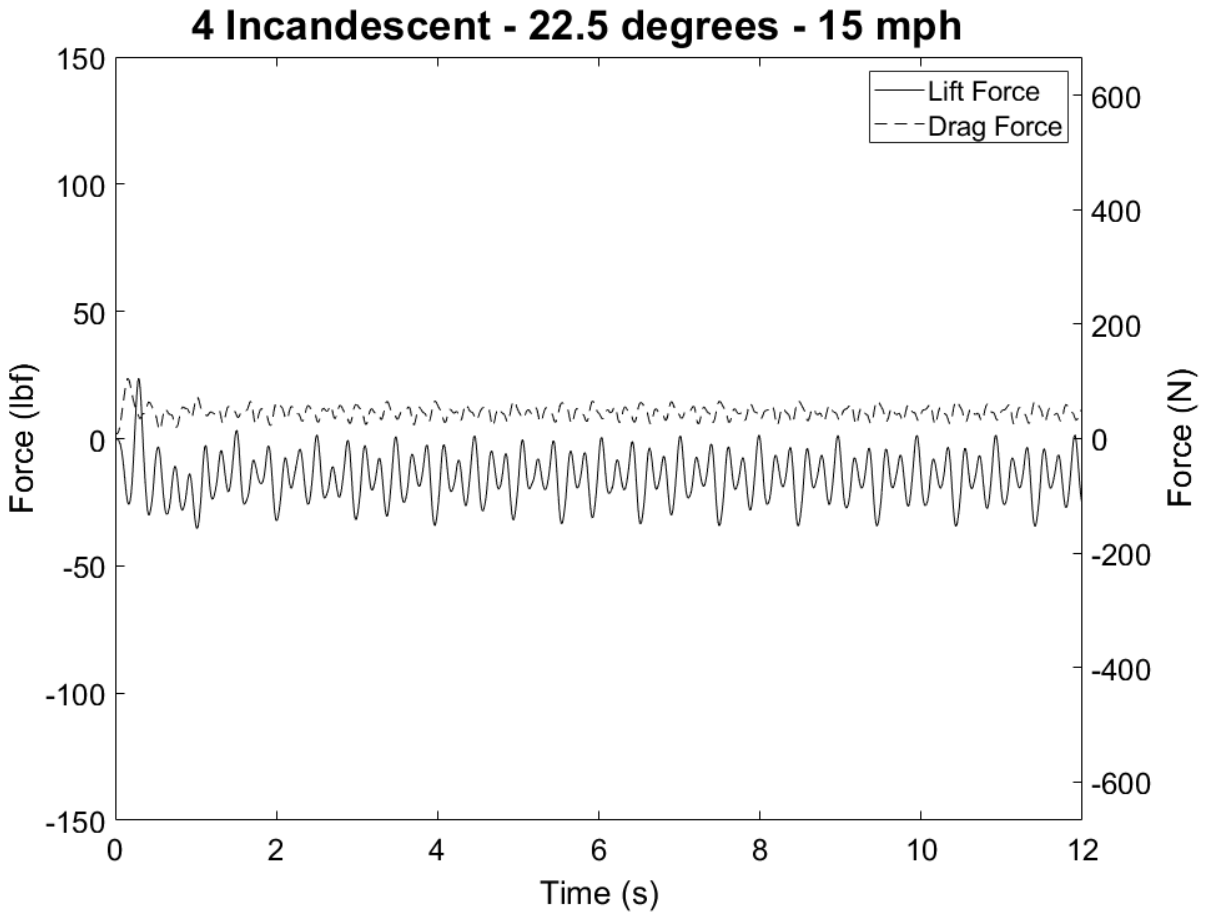

Figure A.6: Force-Time Relationship for 4-Indandescent Light Fixture Subjected to 15 mph Wind at an Angle of 22.5 Degrees

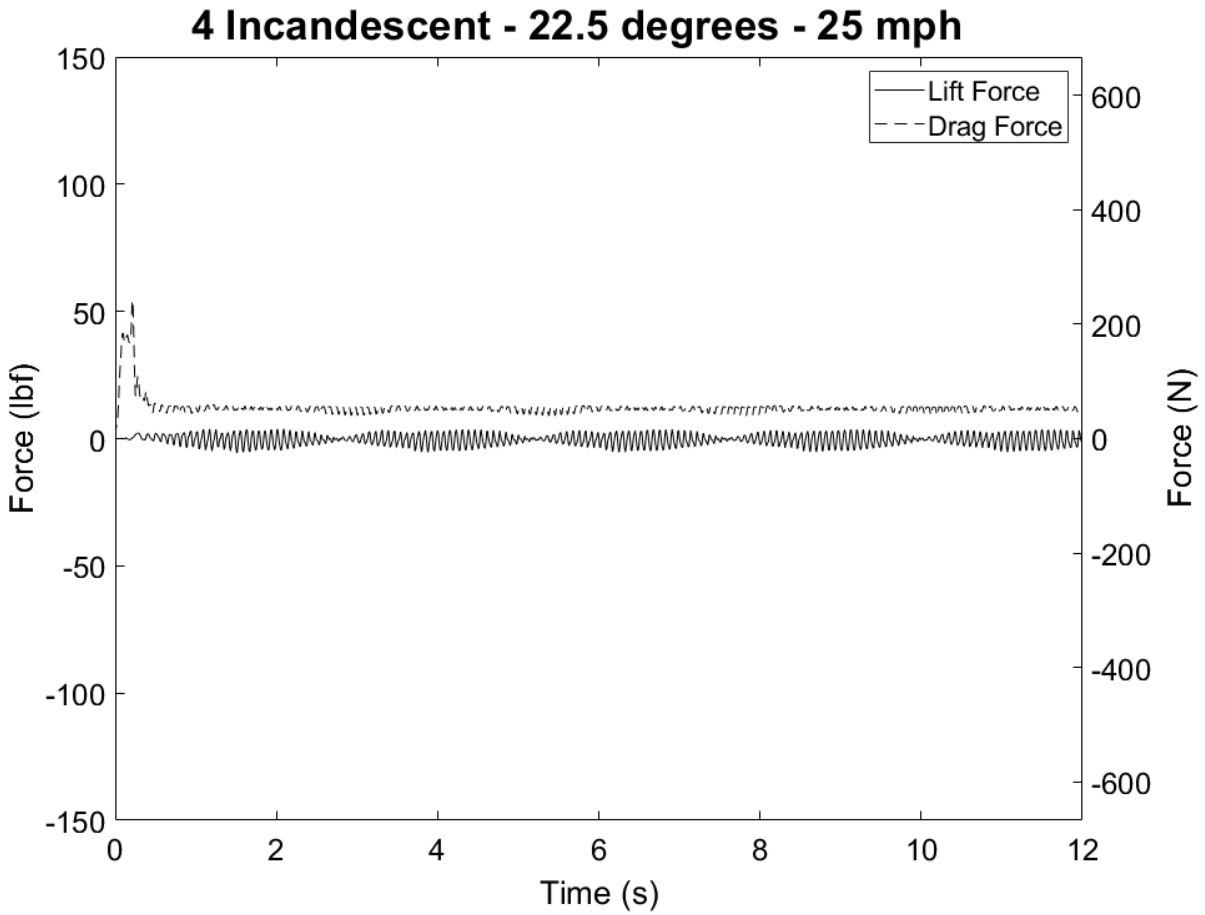

Figure A.7: Force-Time Relationship for 4-Indandescent Light Fixture Subjected to 25 mph Wind at an Angle of 22.5 Degrees

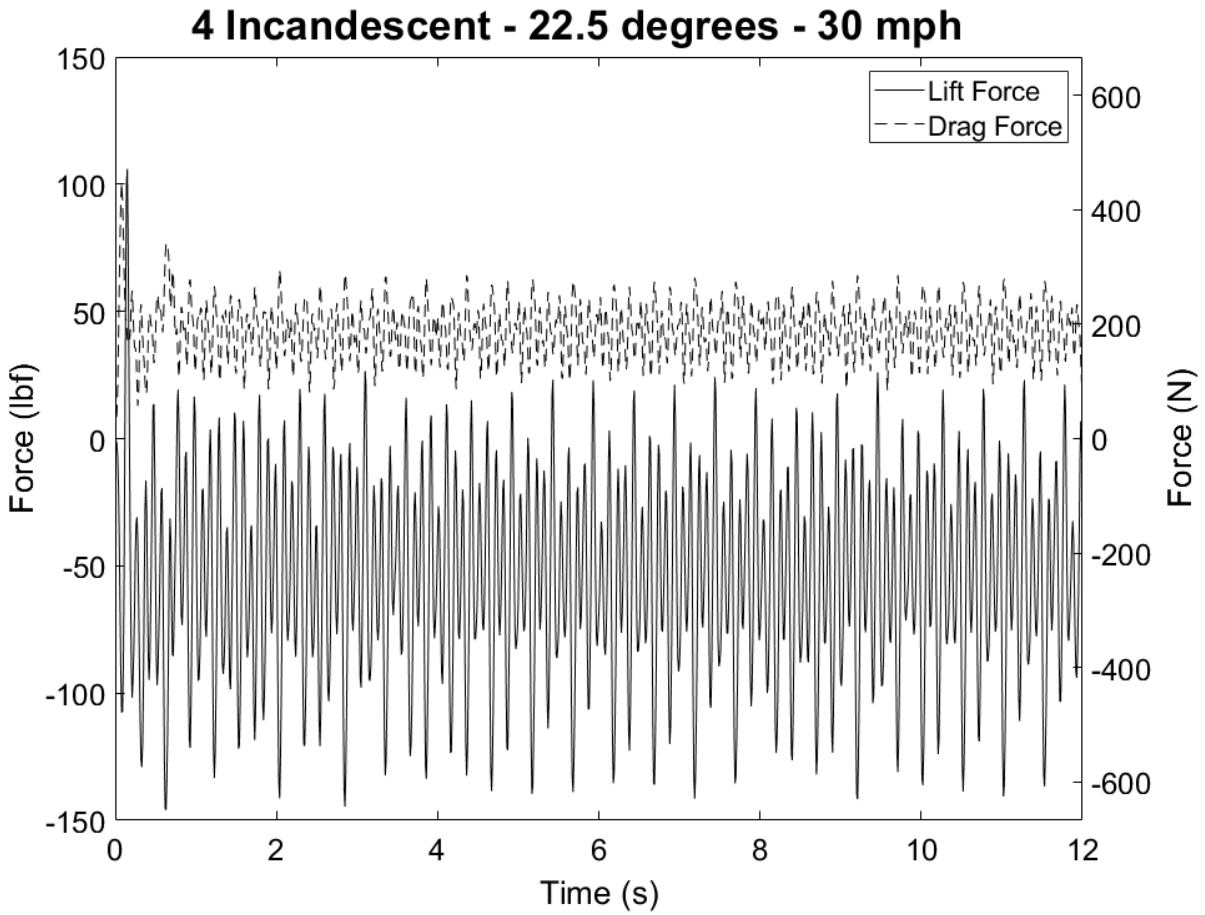

Figure A.8: Force-Time relationship for 4-Indandescent Light Fixture Subjected to 30 mph Wind at an Angle of 22.5 Degrees

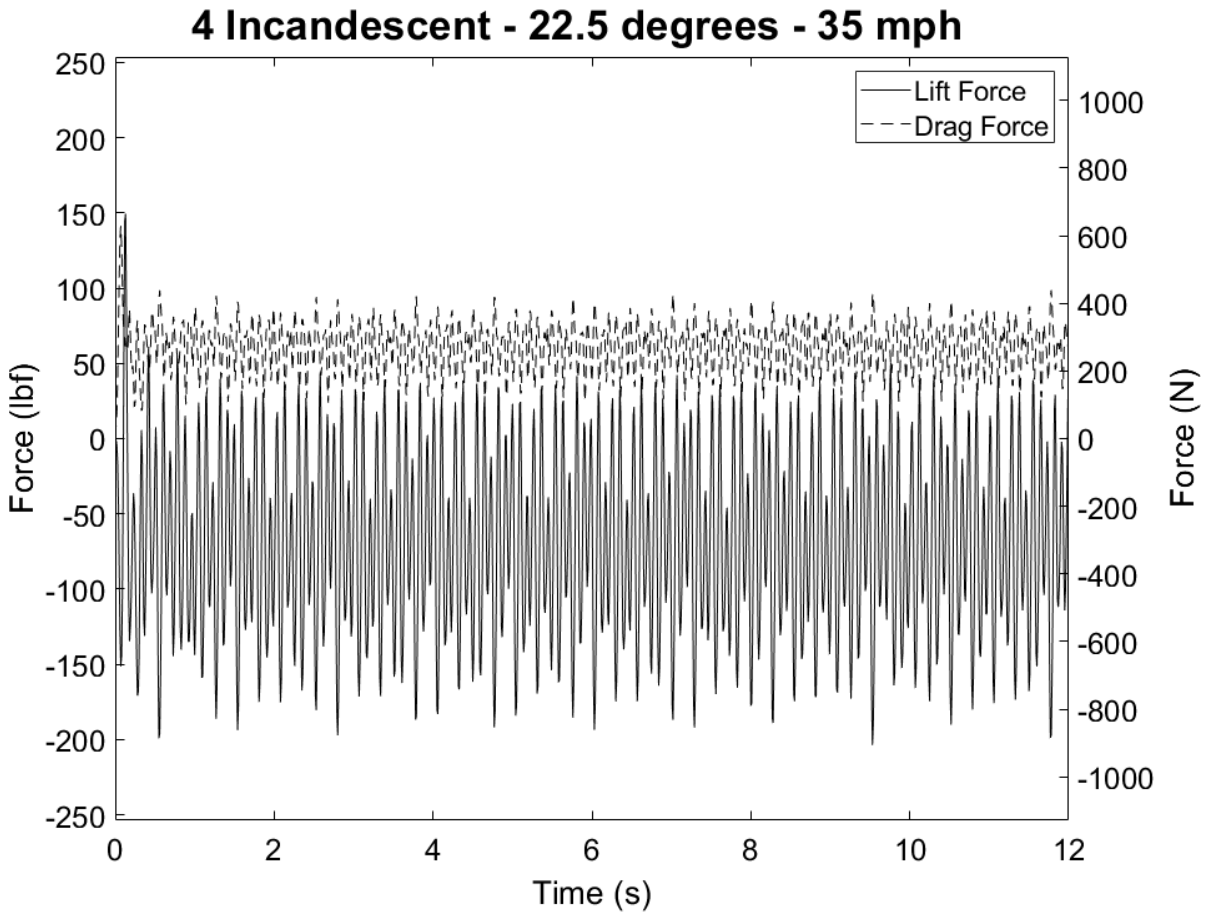

Figure A.9: Force-Time Relationship for 4-Indandescent Light Fixture Subjected to 35 mph Wind at an Angle of 22.5 Degrees

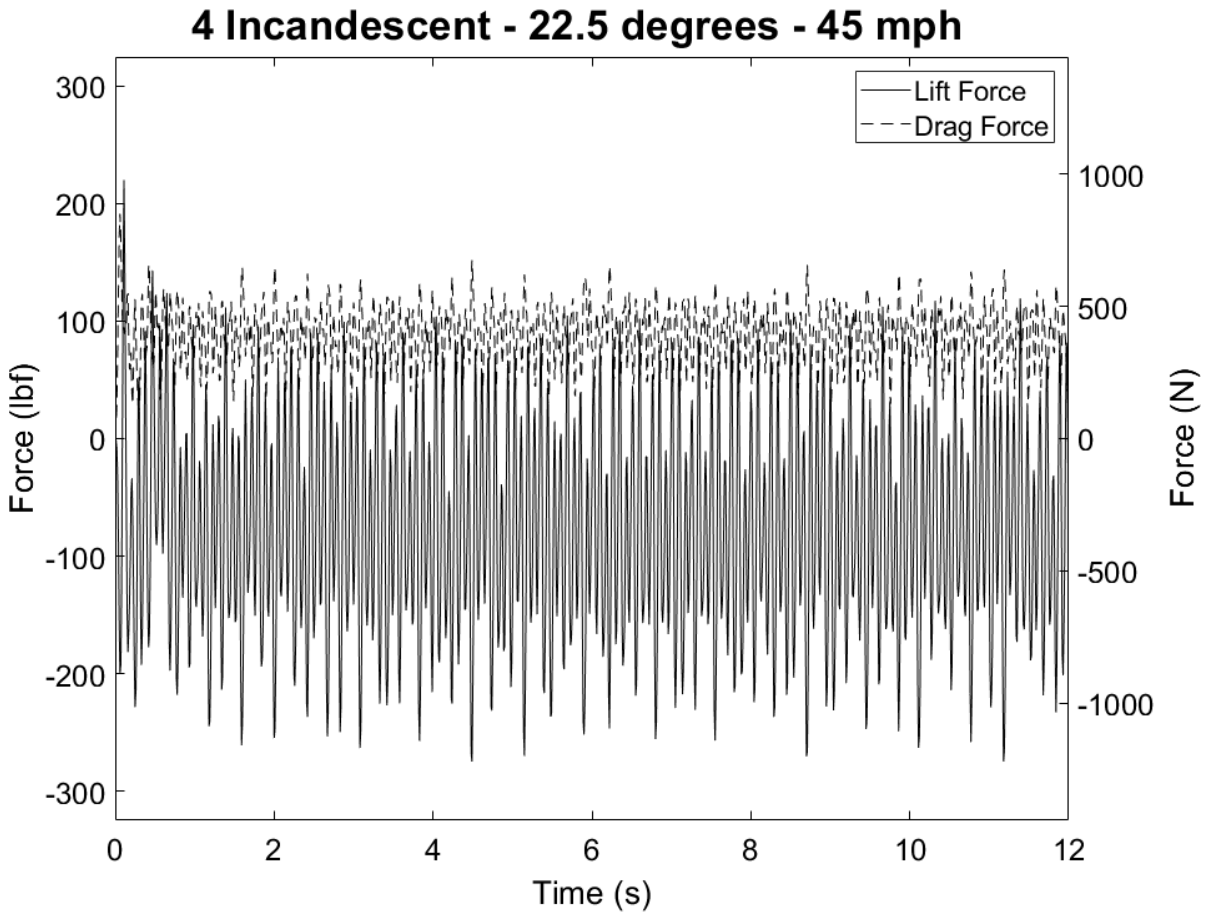

Figure A.10: Force-Time Relationship for 4-Indandescent Light Fixture Subjected to 45 mph Wind at an Angle of 22.5 Degrees

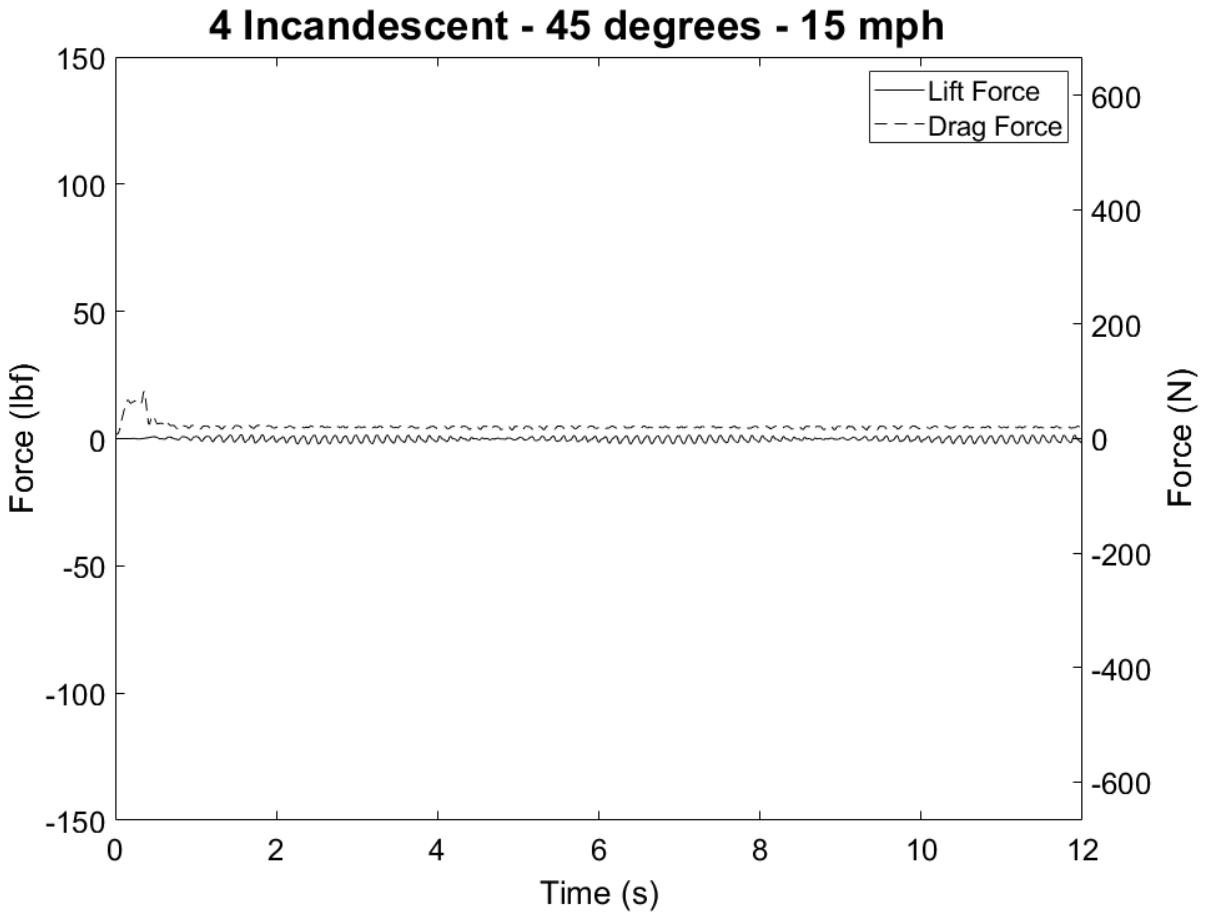

Figure A.11: Force-Time Relationship for 4-Indandescent Light Fixture Subjected to 15 mph Wind at an Angle of 45 Degrees

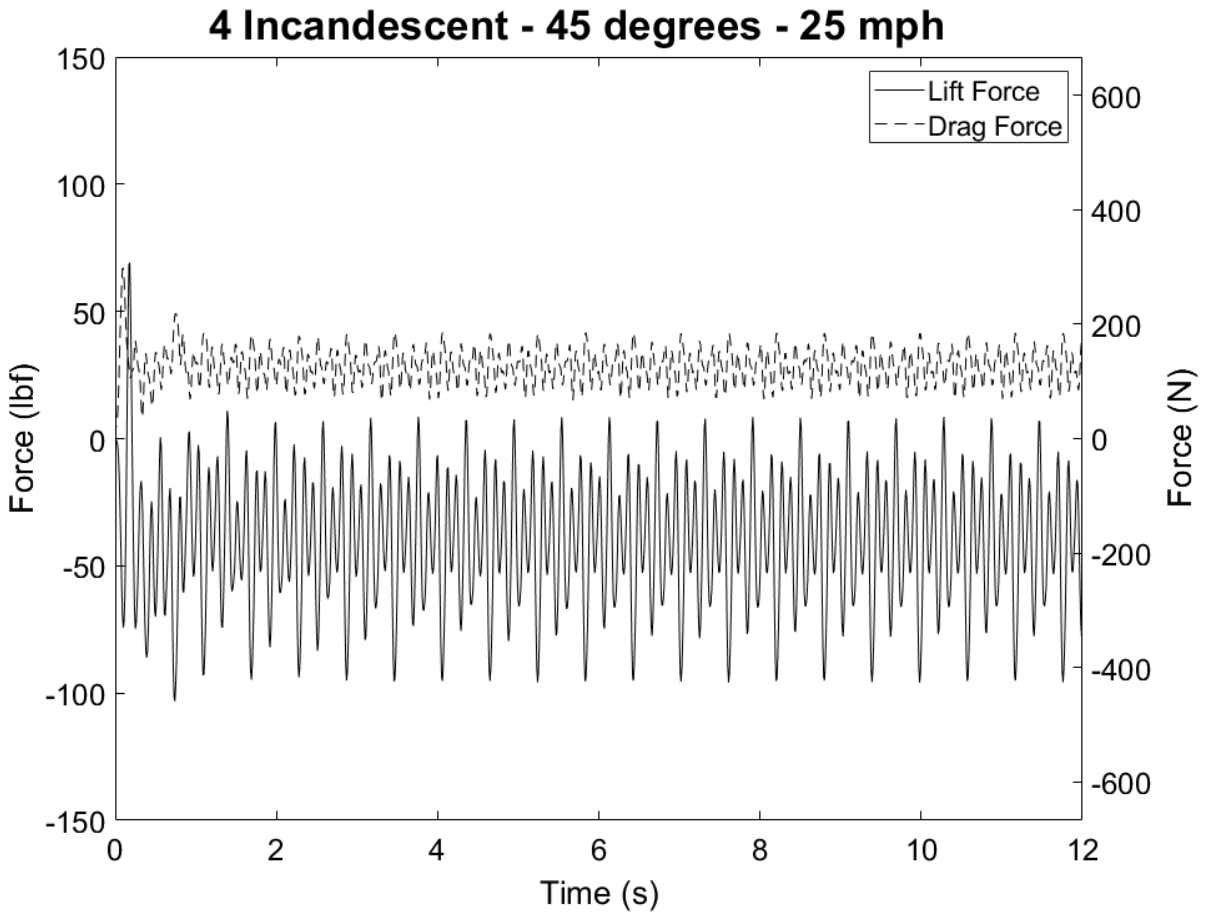

Figure A.12: Force-Time Relationship for 4-Indandescent Light Fixture Subjected to 25 mph Wind at an Angle of 45 Degrees

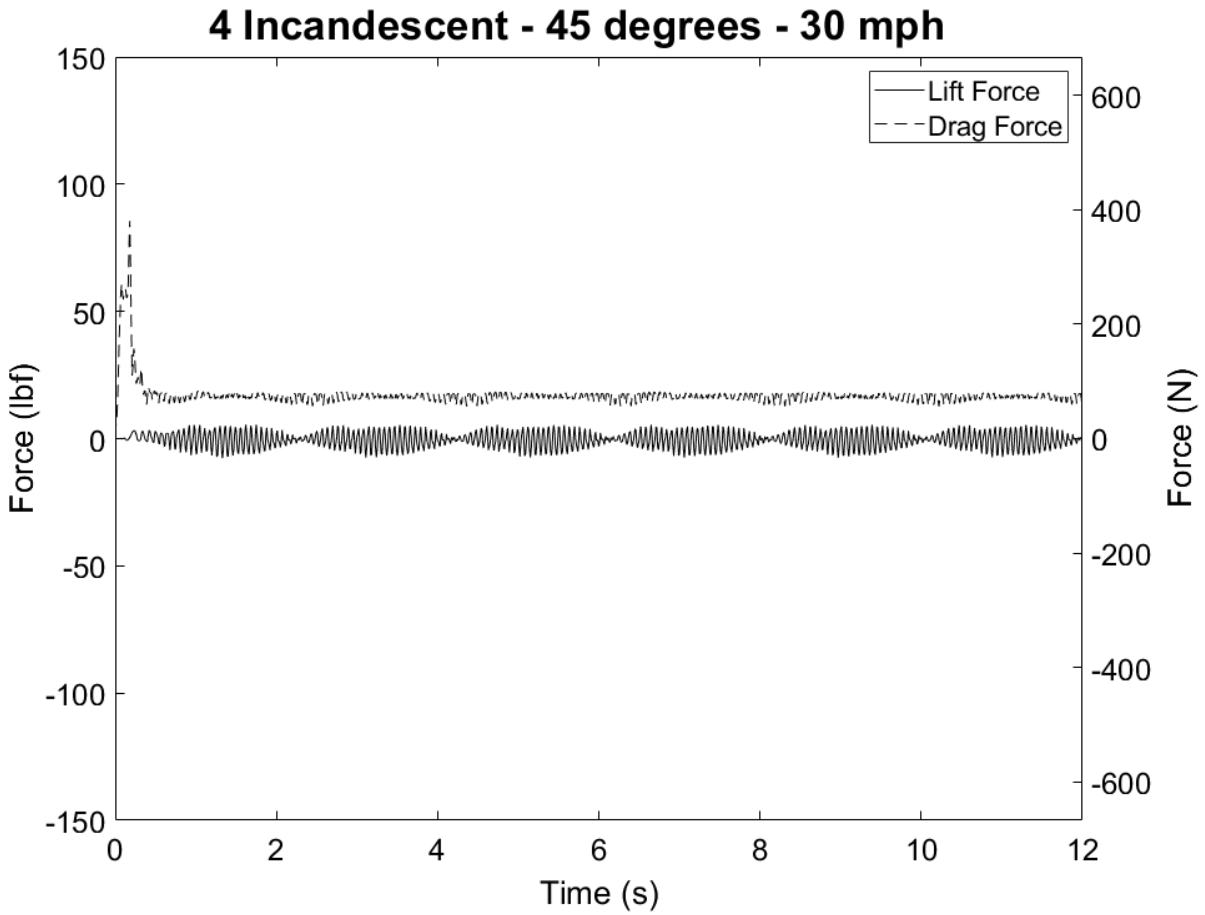

Figure A.13: Force-Time Relationship for 4-Indandescent Light Fixture Subjected to 30 mph Wind at an Angle of 45 Degrees

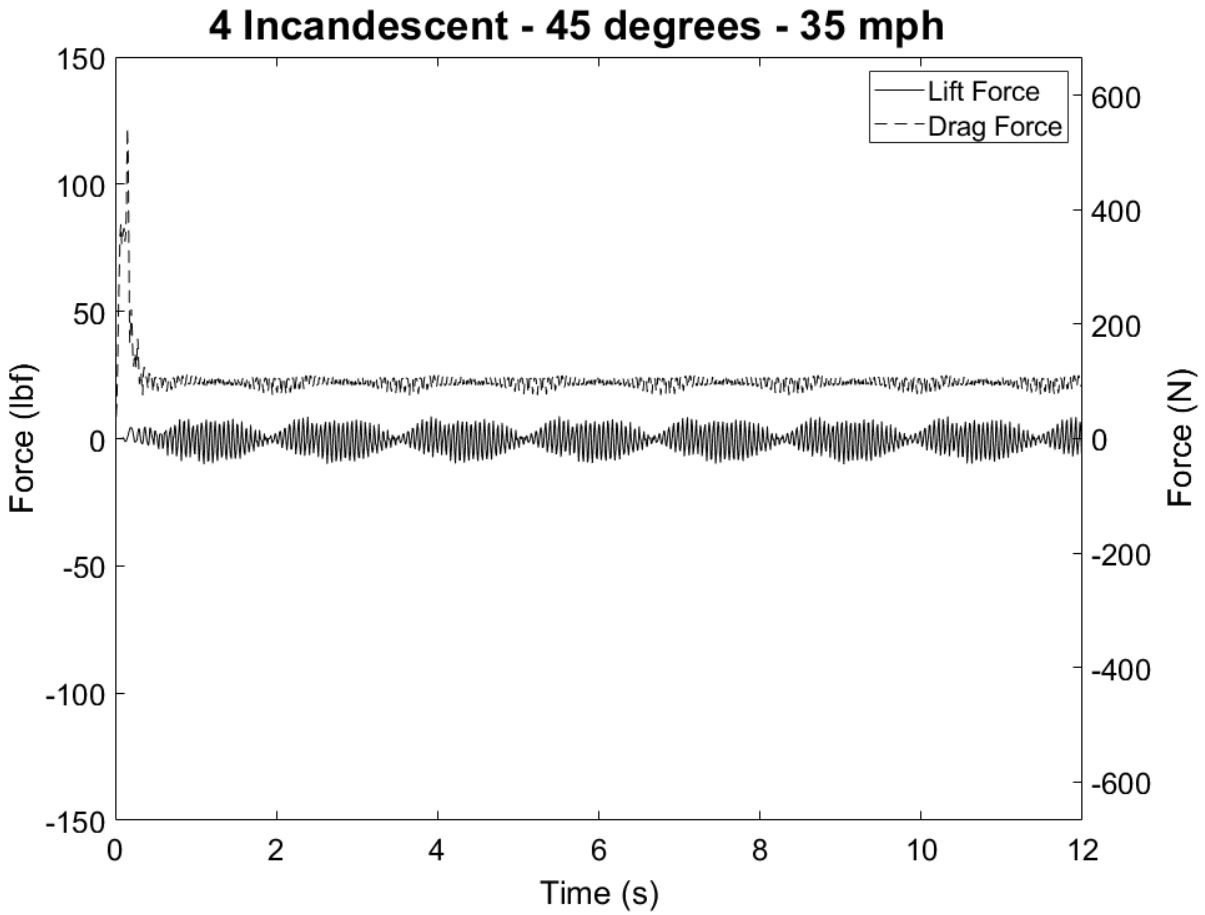

Figure A.14: Force-Time Relationship for 4-Indandescent Light Fixture Subjected to 35 mph Wind at an Angle of 45 Degrees

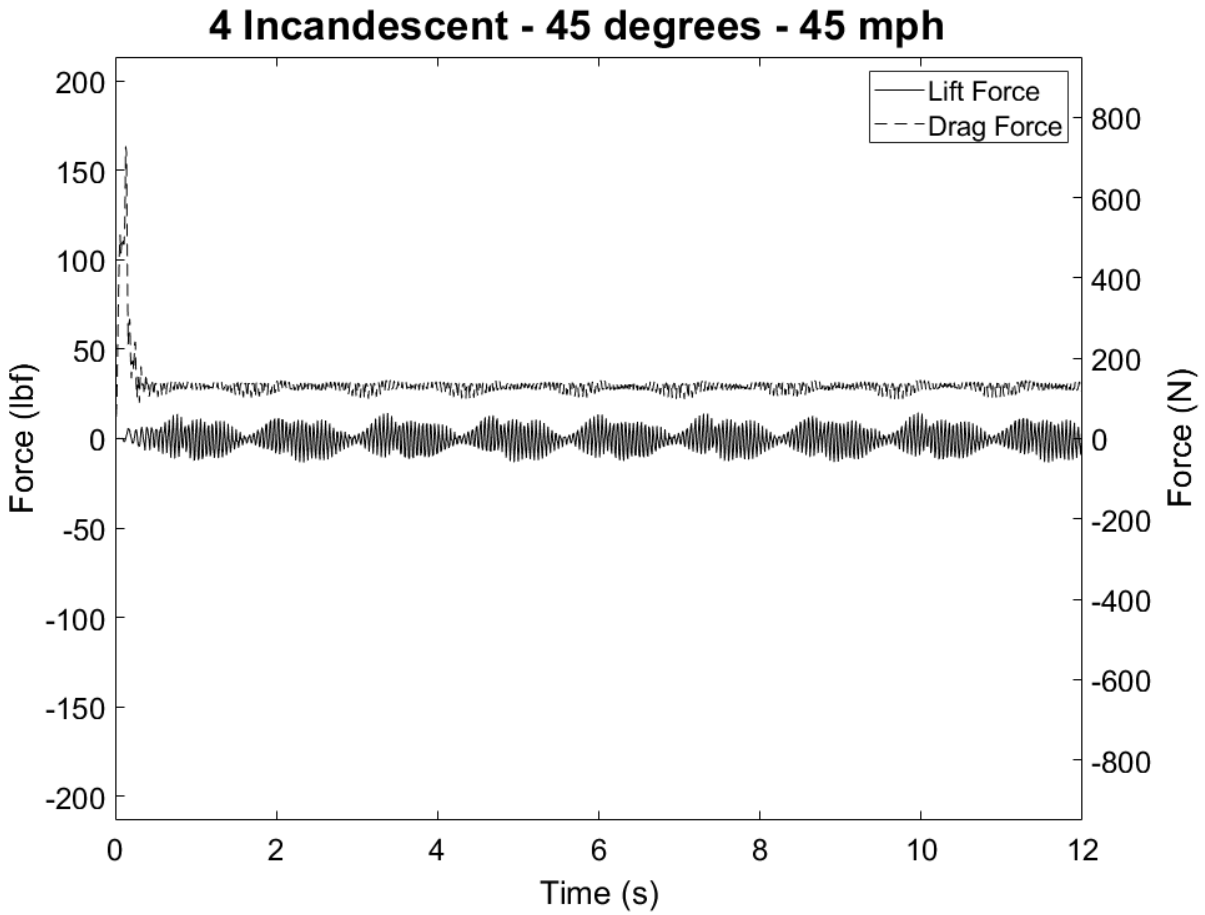

Figure A.15: Force-Time Relationship for 4-Indandescent Light Fixture Subjected to 45 mph Wind at an Angle of 45 Degrees

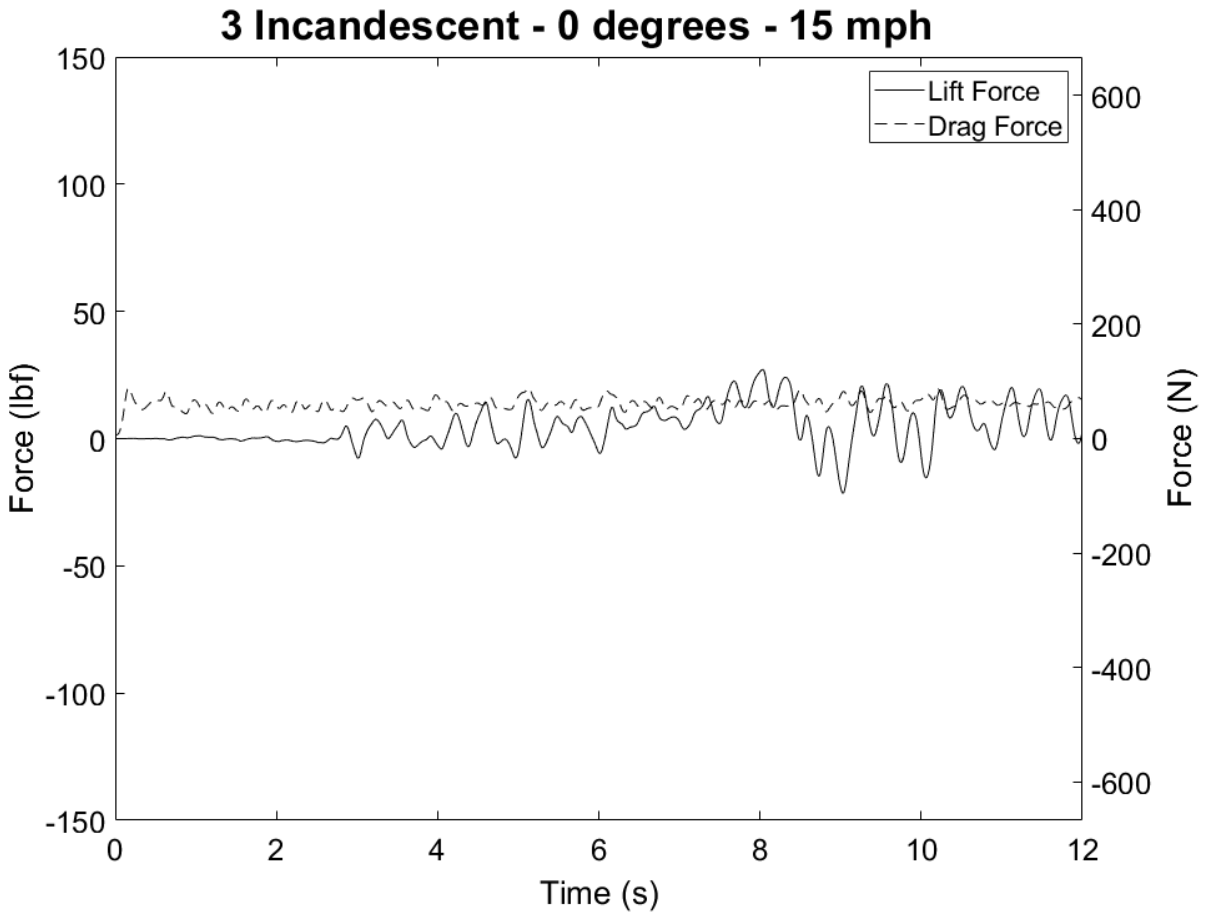

Figure A.16: Force-Time Relationship for 3-Indandescent Light Fixture Subjected to 15 mph Wind at an Angle of 0 Degrees

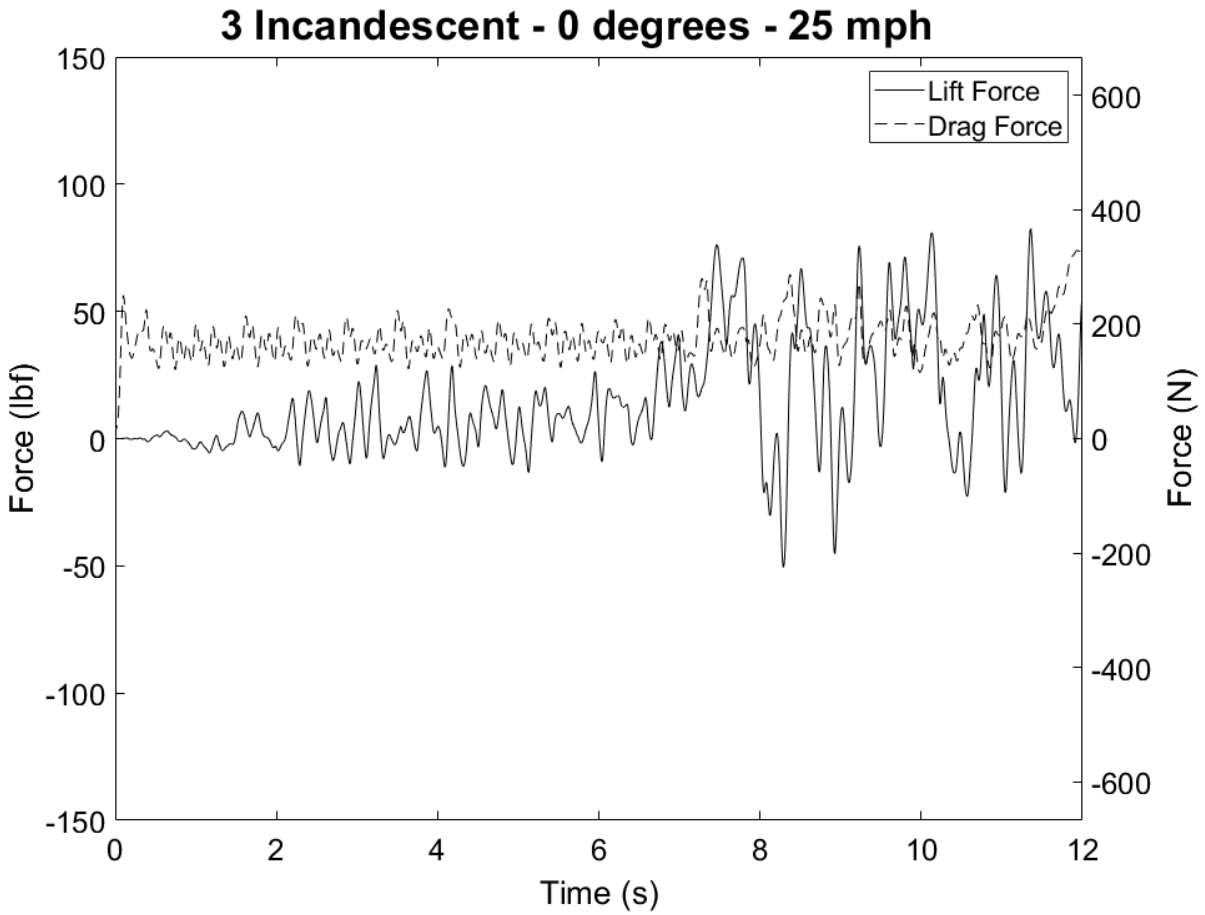

Figure A.17: Force-Time Relationship for 3-Indandescent Light Fixture Subjected to 25 mph Wind at an Angle of 0 Degrees

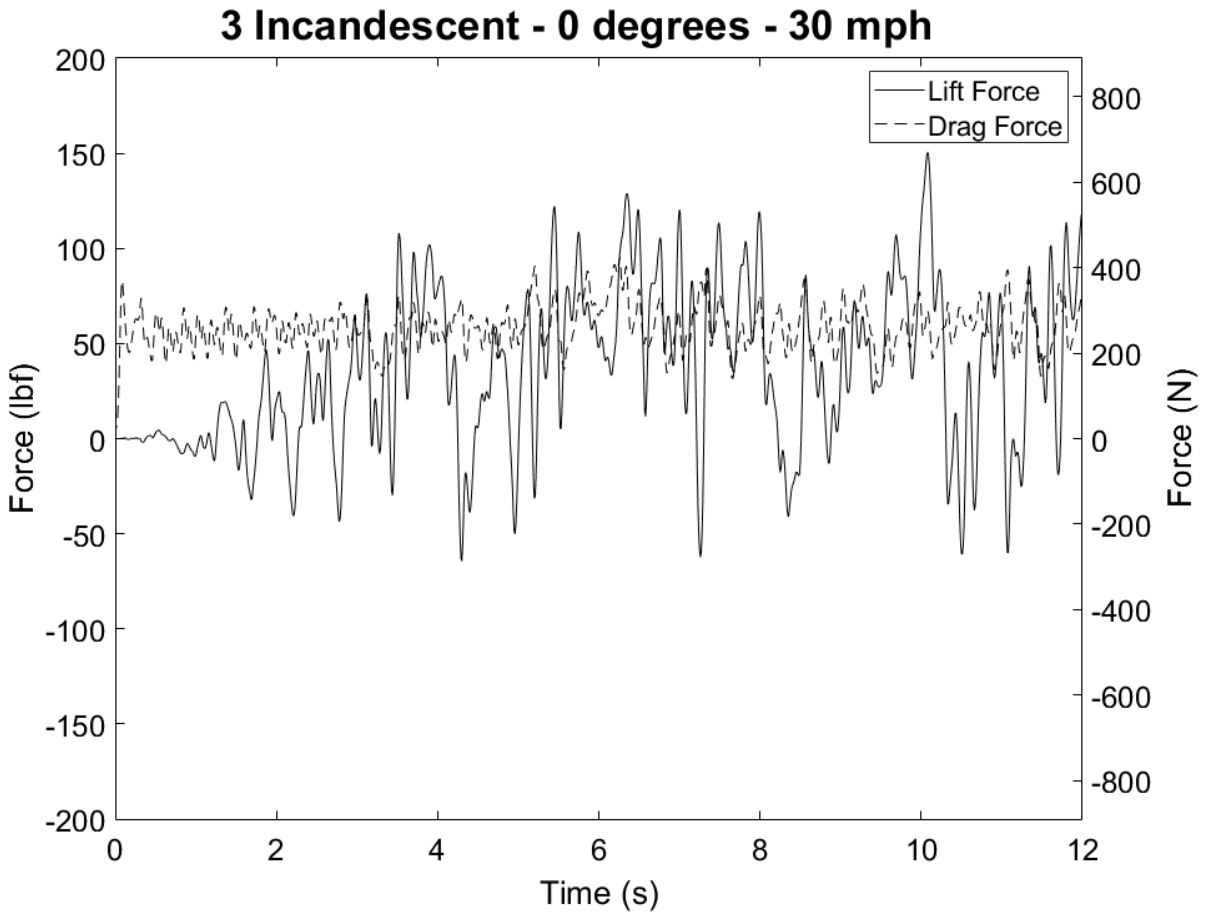

Figure A.18: Force-Time Relationship for 3-Indandescent Light Fixture Subjected to 30 mph Wind at an Angle of 0 Degrees

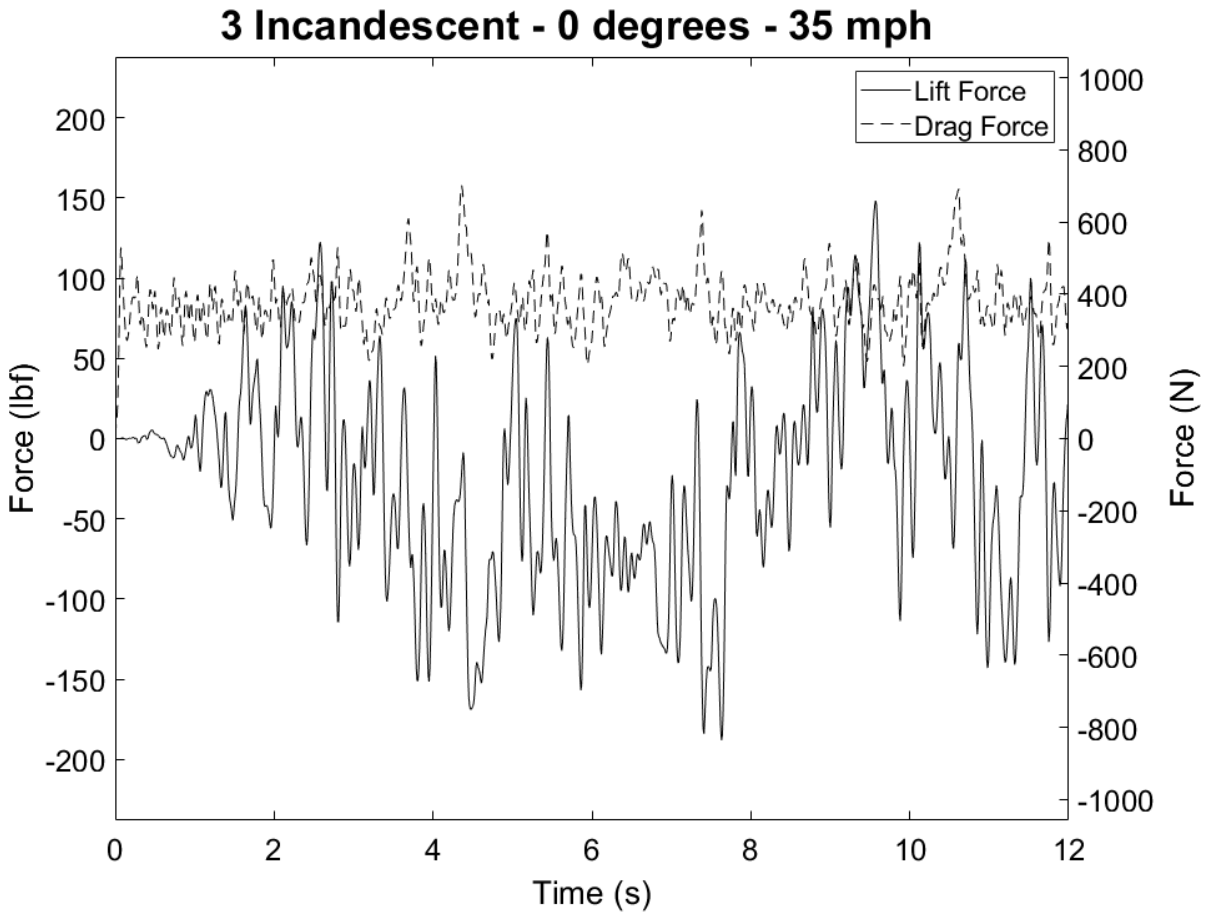

Figure A.19: Force-Time Relationship for 3-Indandescent Light Fixture Subjected to 35 mph Wind at an Angle of 0 Degrees

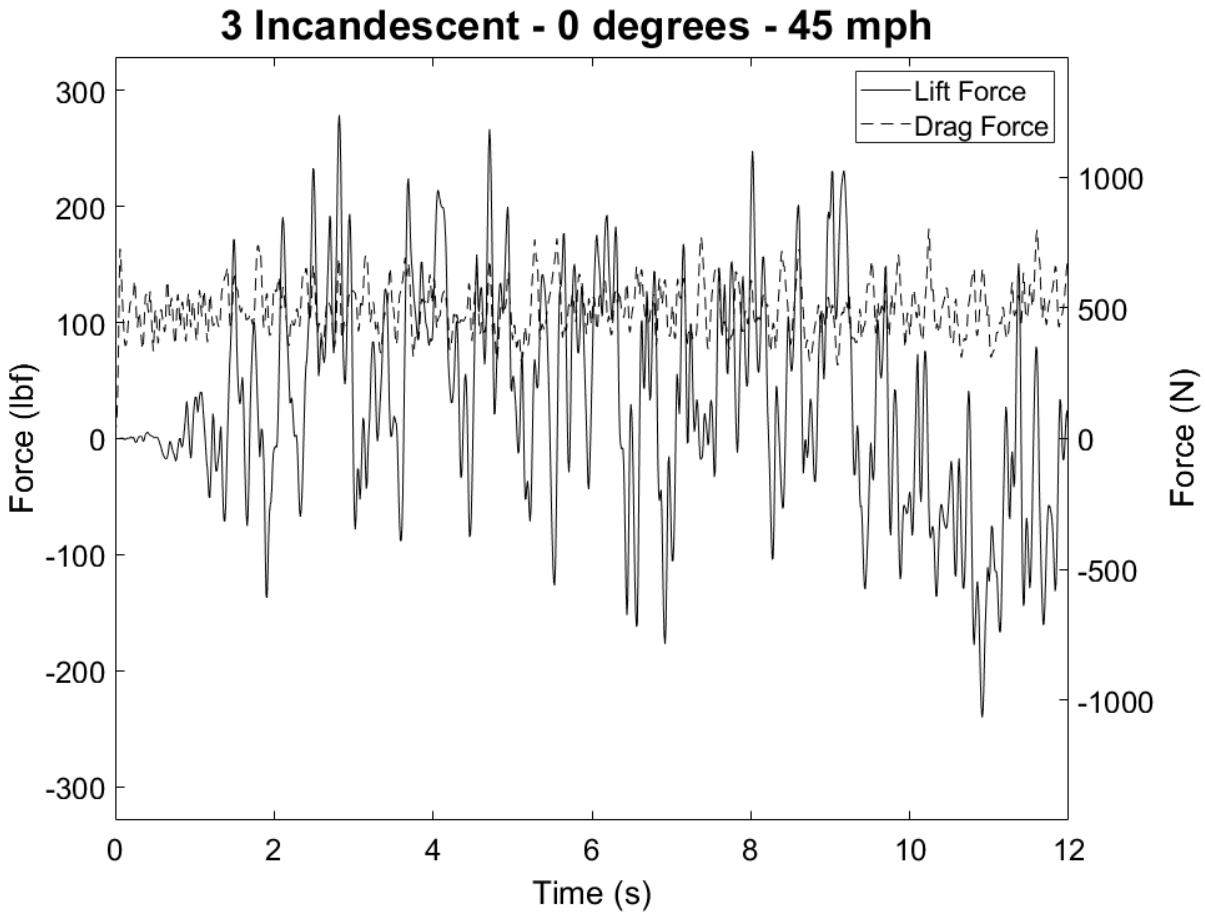

Figure A.20: Force-Time Relationship for 3-Indandescent Light Fixture Subjected to 45 mph Wind at an Angle of 0 Degrees

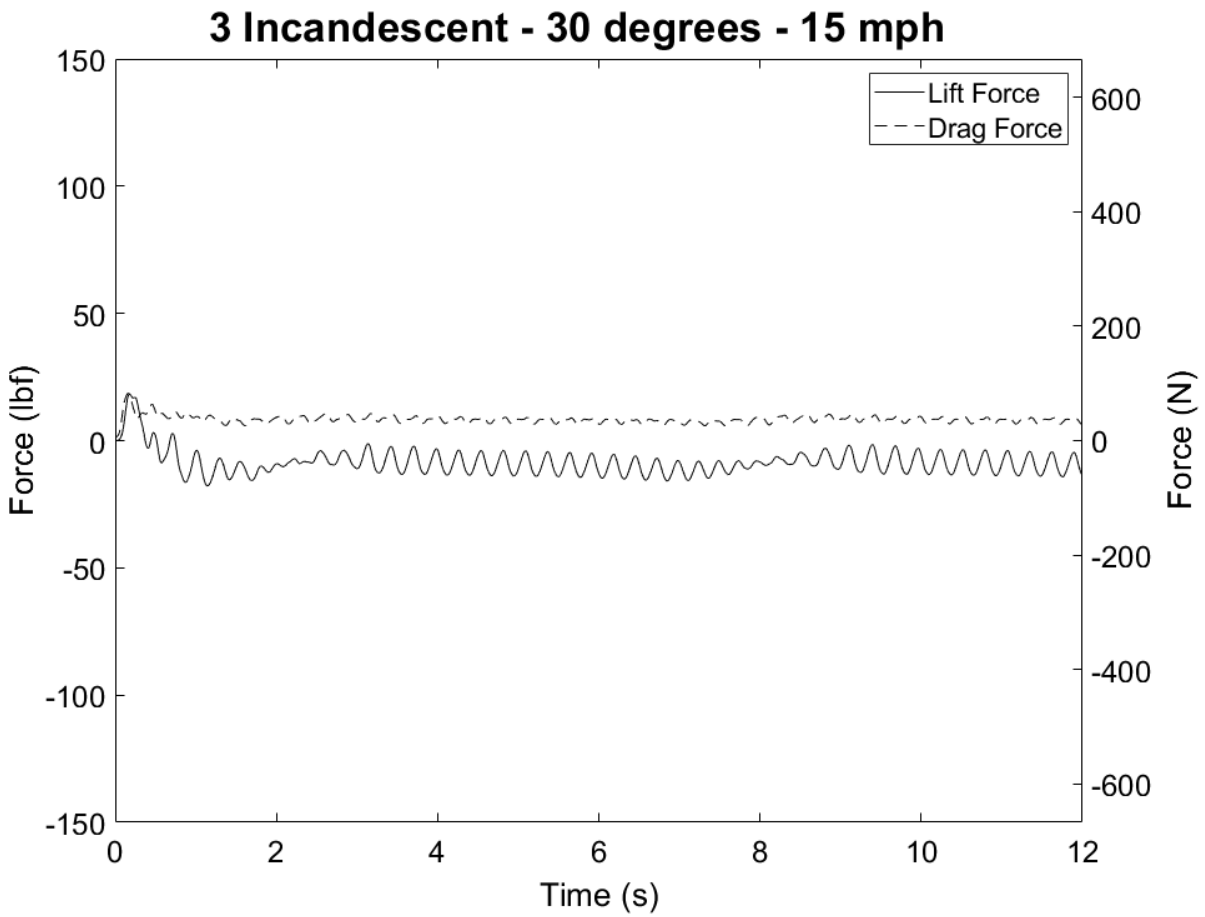

Figure A.21: Force-Time Relationship for 3-Indandescent Light Fixture Subjected to 15 mph Wind at an Angle of 30 Degrees

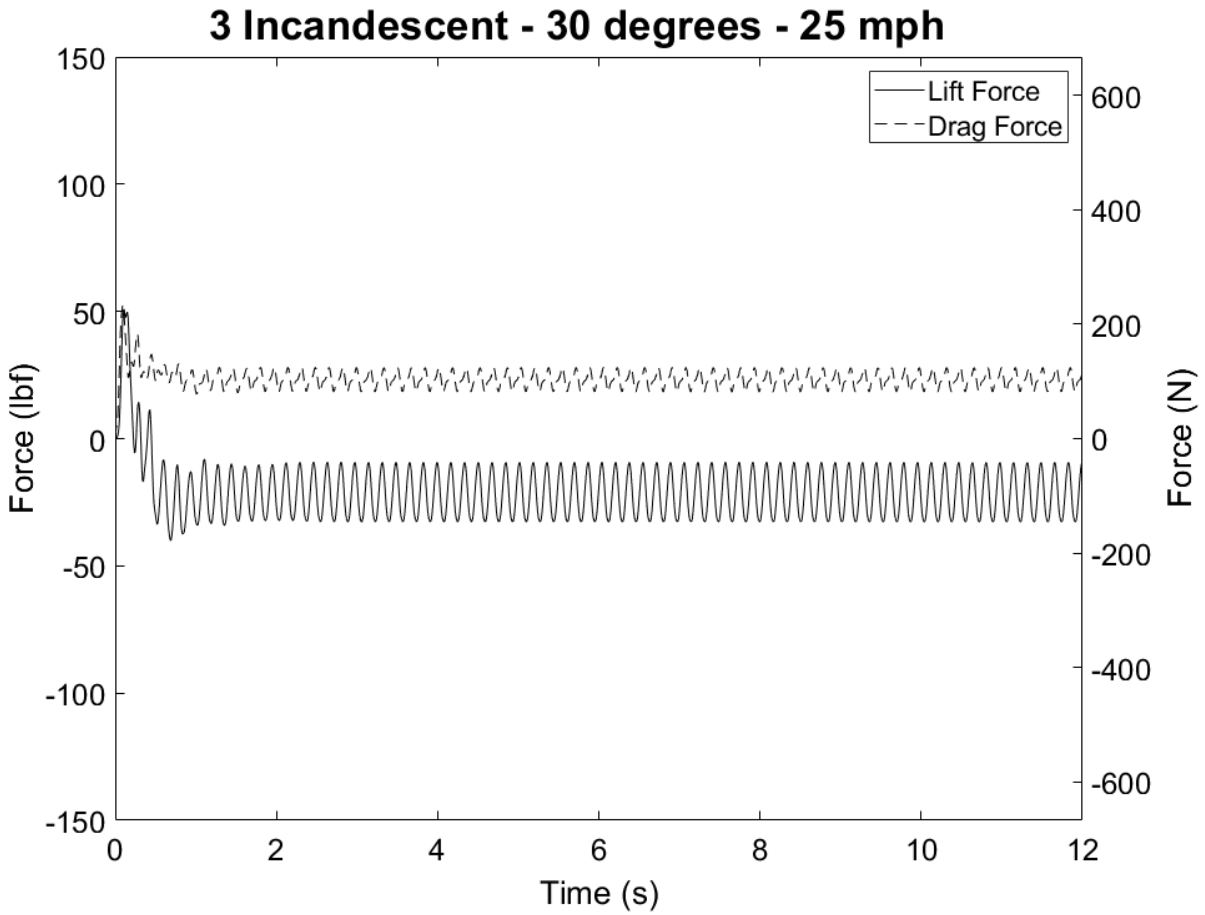

Figure A.22: Force-Time Relationship for 3-Indandescent Light Fixture Subjected to 25 mph Wind at an Angle of 30 Degrees

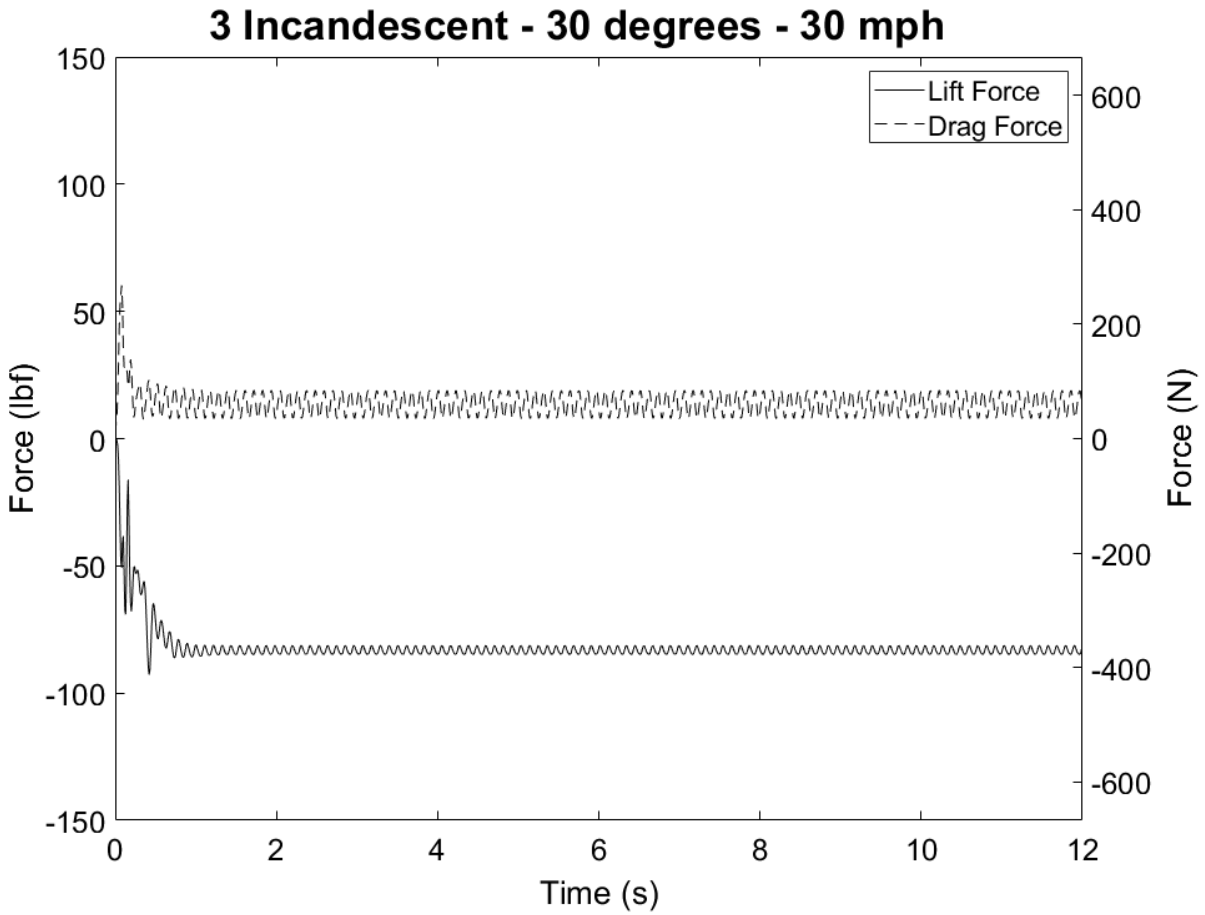

Figure A.23: Force-Time relationship for 3-Indandescent Light Fixture Subjected to 30 mph Wind at an Angle of 30 Degrees

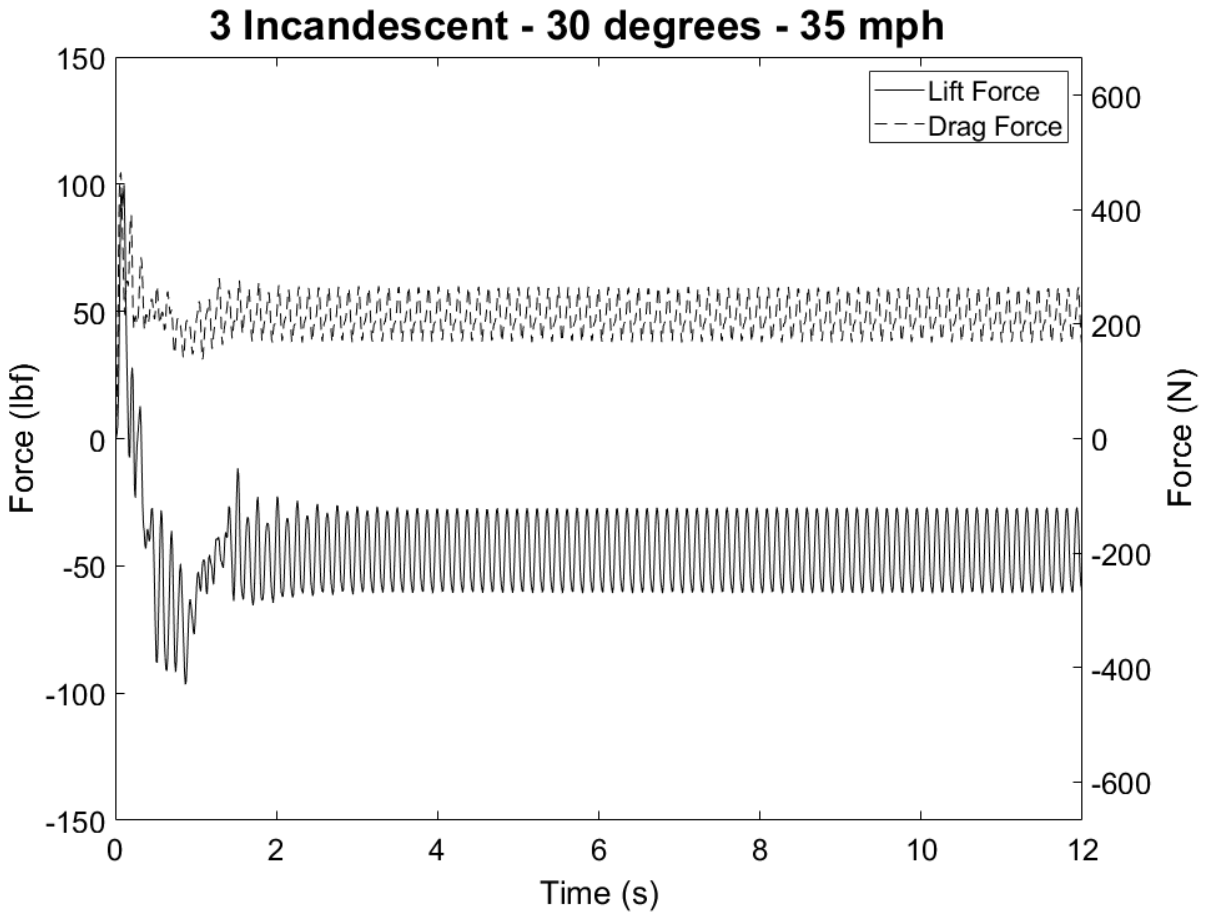

Figure A.24: Force-Time Relationship for 3-Indandescent Light Fixture Subjected to 35 mph Wind at an Angle of 30 Degrees

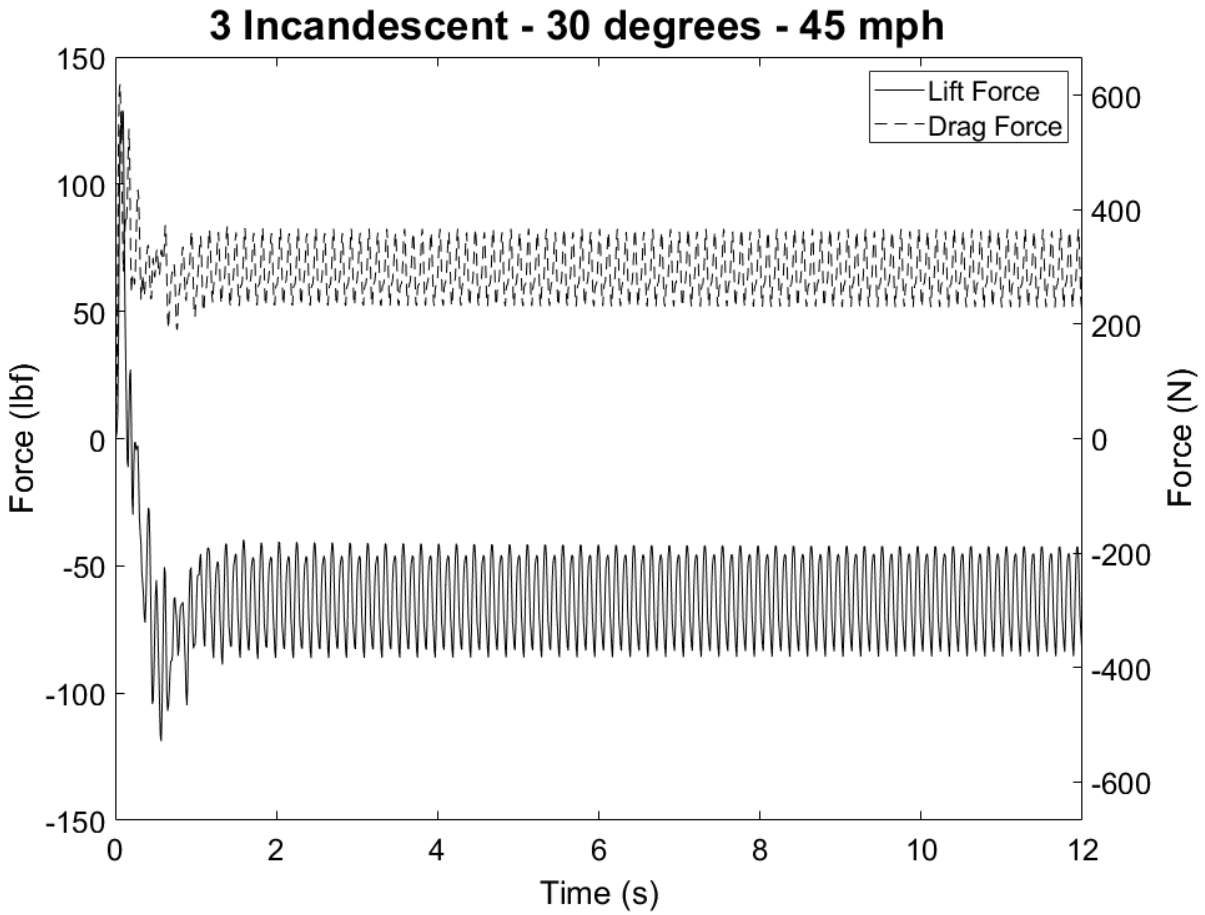

Figure A.25: Force-Time Relationship for 3-Indandescent Light Fixture Subjected to 45 mph Wind at an Angle of 30 Degrees

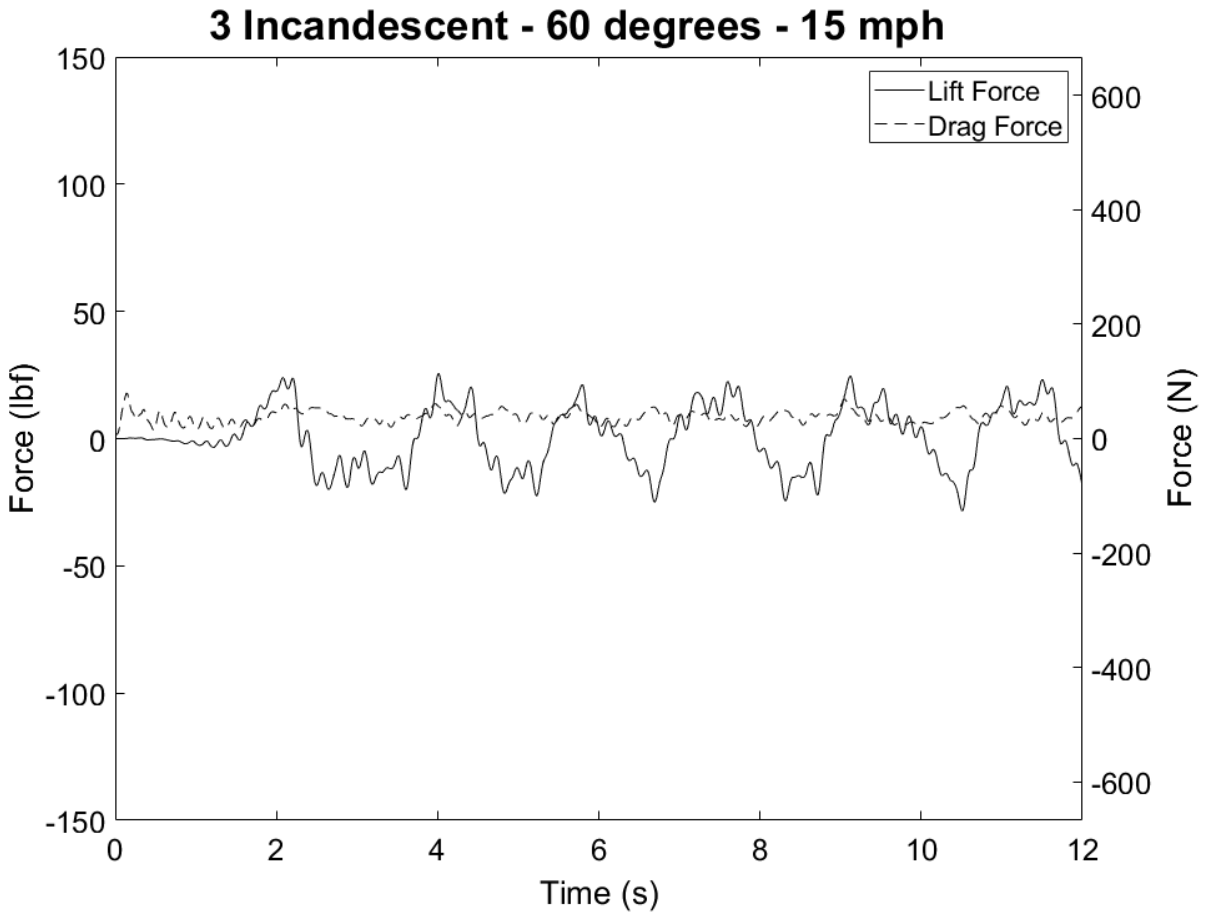

Figure A.26: Force-Time Relationship for 3-Indandescent Light Fixture Subjected to 15 mph Wind at an Angle of 60 Degrees

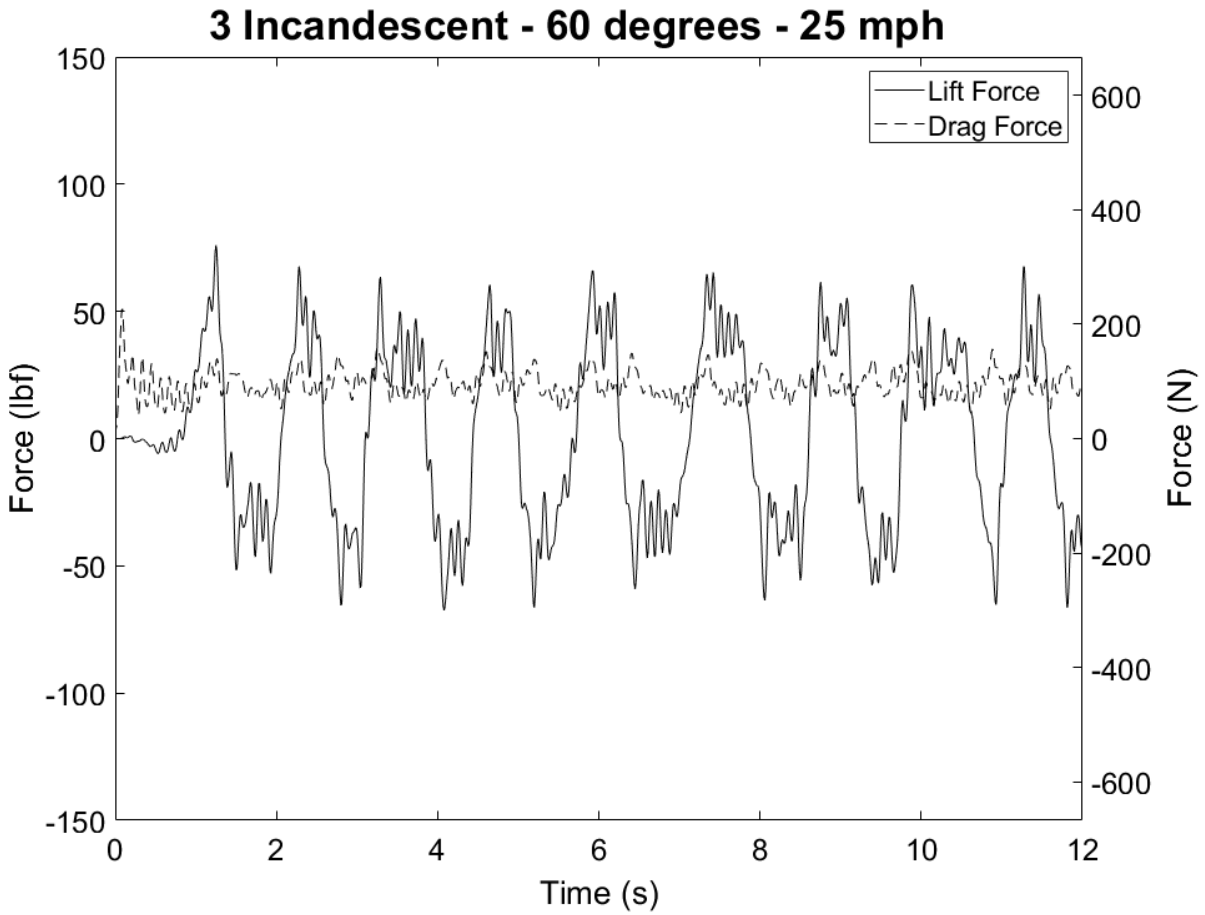

Figure A.27: Force-Time Relationship for 3-Indandescent Light Fixture Subjected to 25 mph Wind at an Angle of 60 Degrees

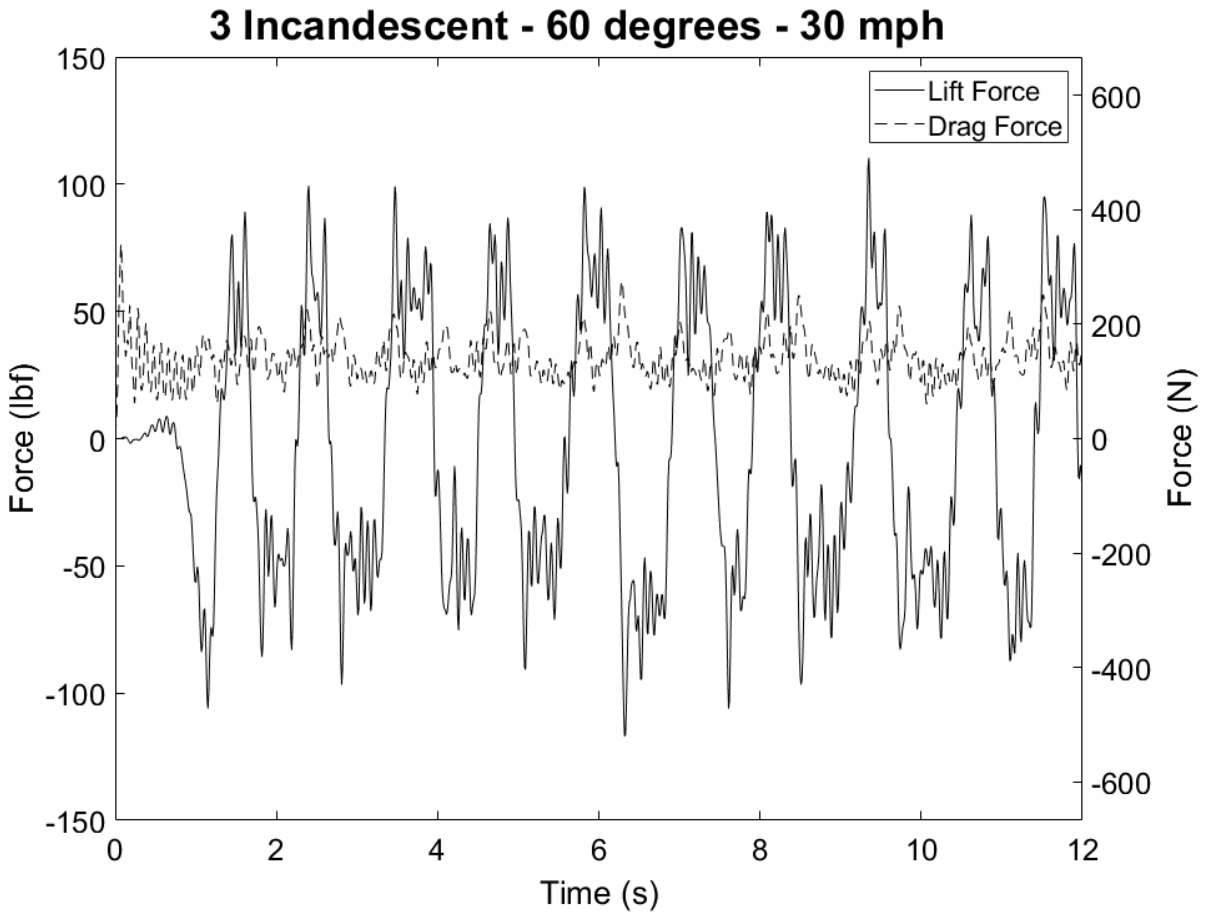

Figure A.28: Force-Time Relationship for 3-Indandescent Light Fixture Subjected to 30 mph Wind at an Angle of 60 Degrees

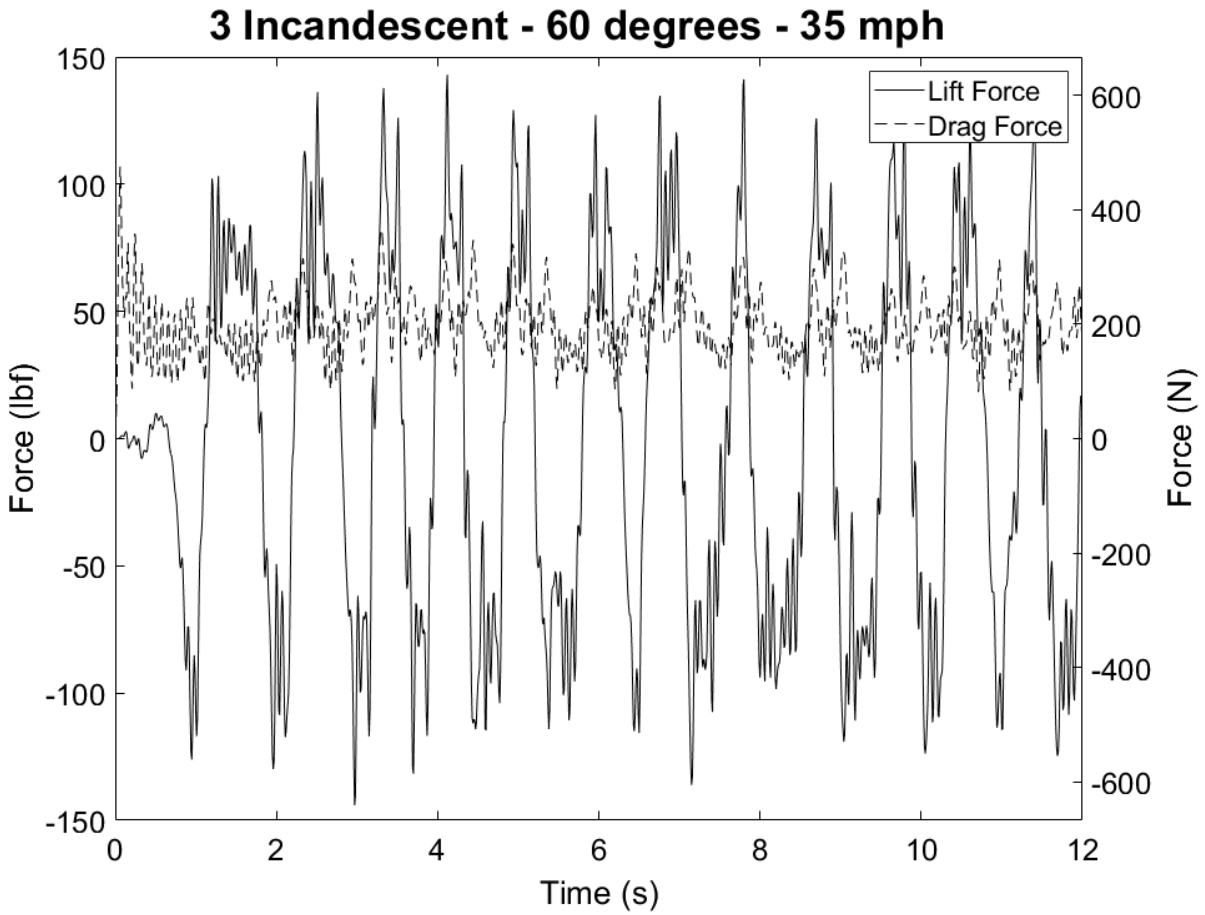

Figure A.29: Force-Time Relationship for 3-Indandescent Light Fixture Subjected to 35 mph Wind at an Angle of 60 Degrees

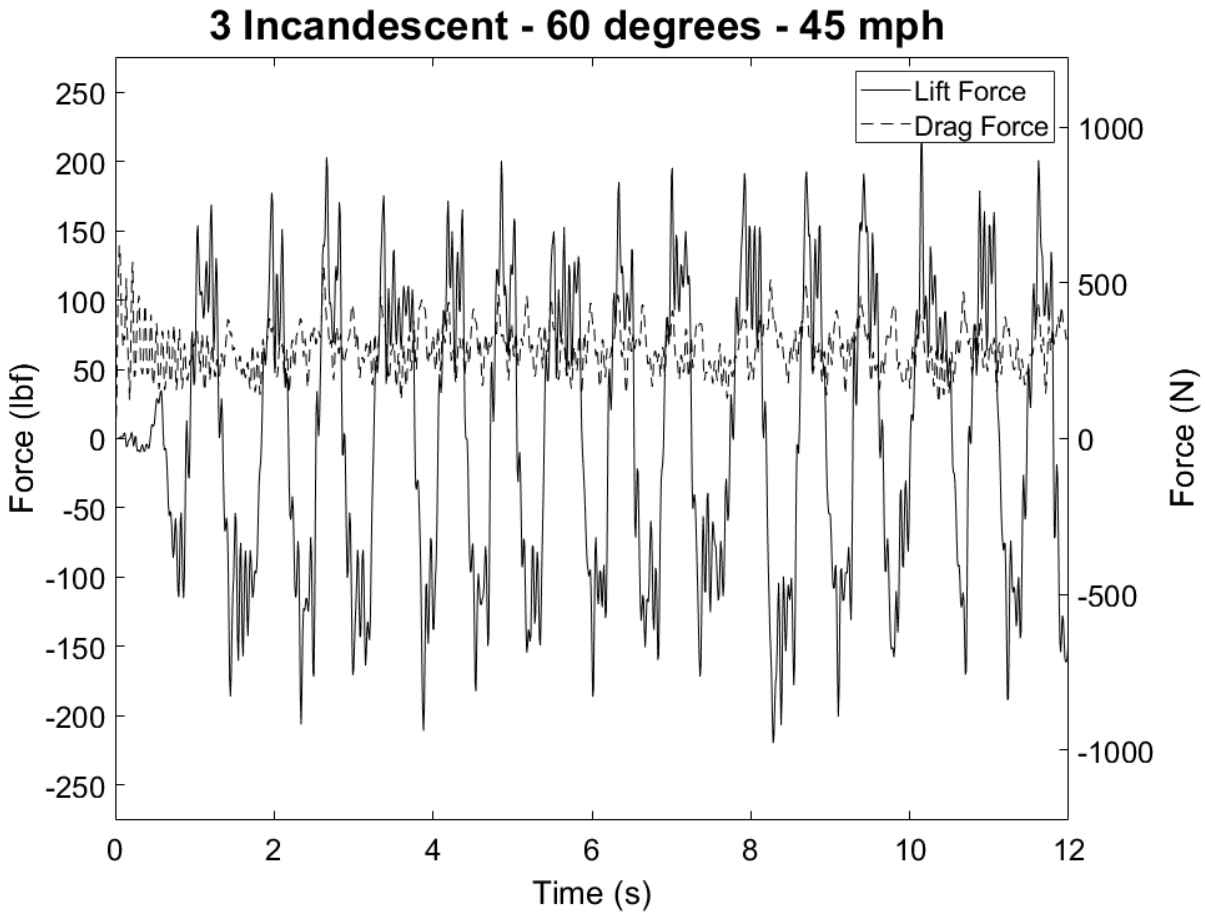

Figure A.30: Force-Time Relationship for 3-Indandescent Light Fixture Subjected to 45 mph Wind at an Angle of 60 Degrees

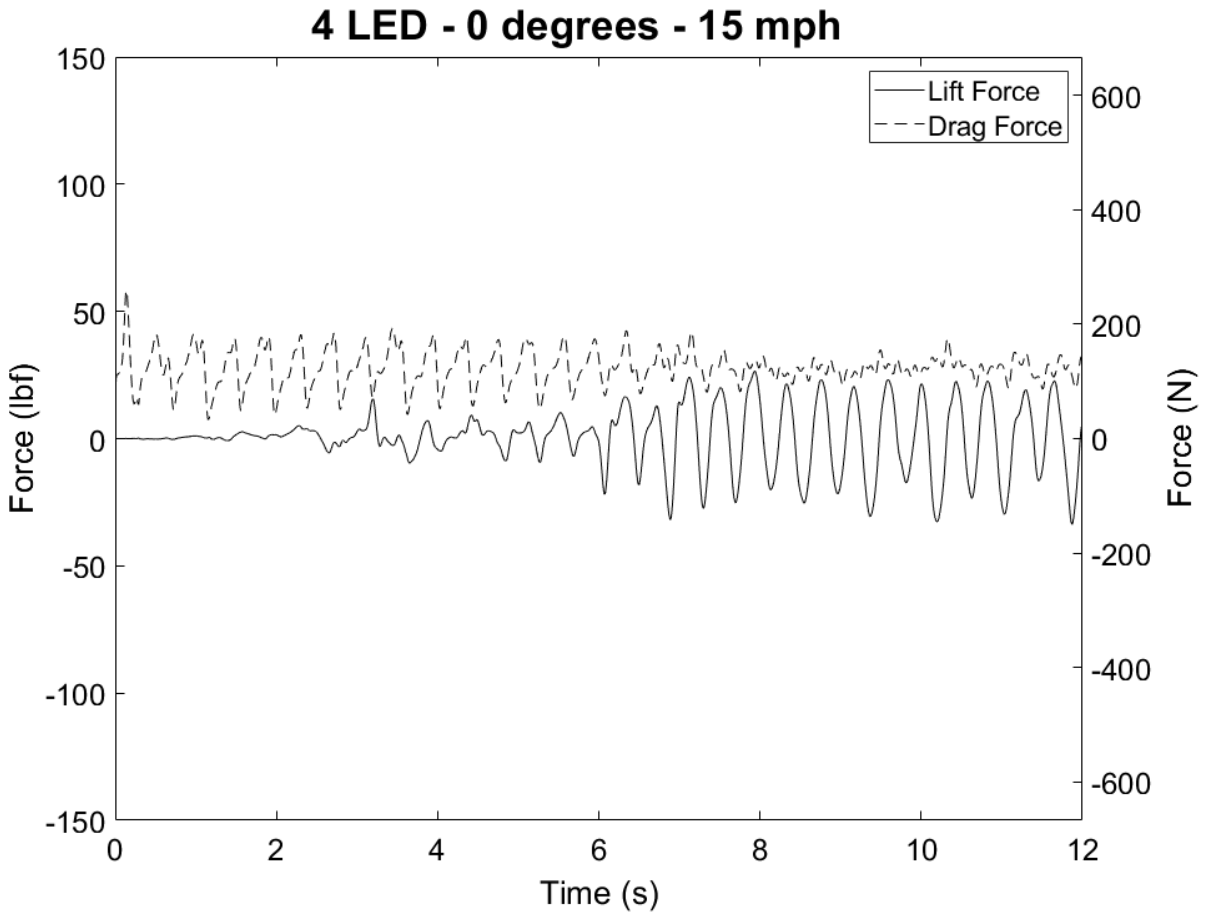

Figure A.31: Force-Time Relationship for 4-LED Light Fixture Subjected to 15 mph Wind at an Angle of 0 Degrees

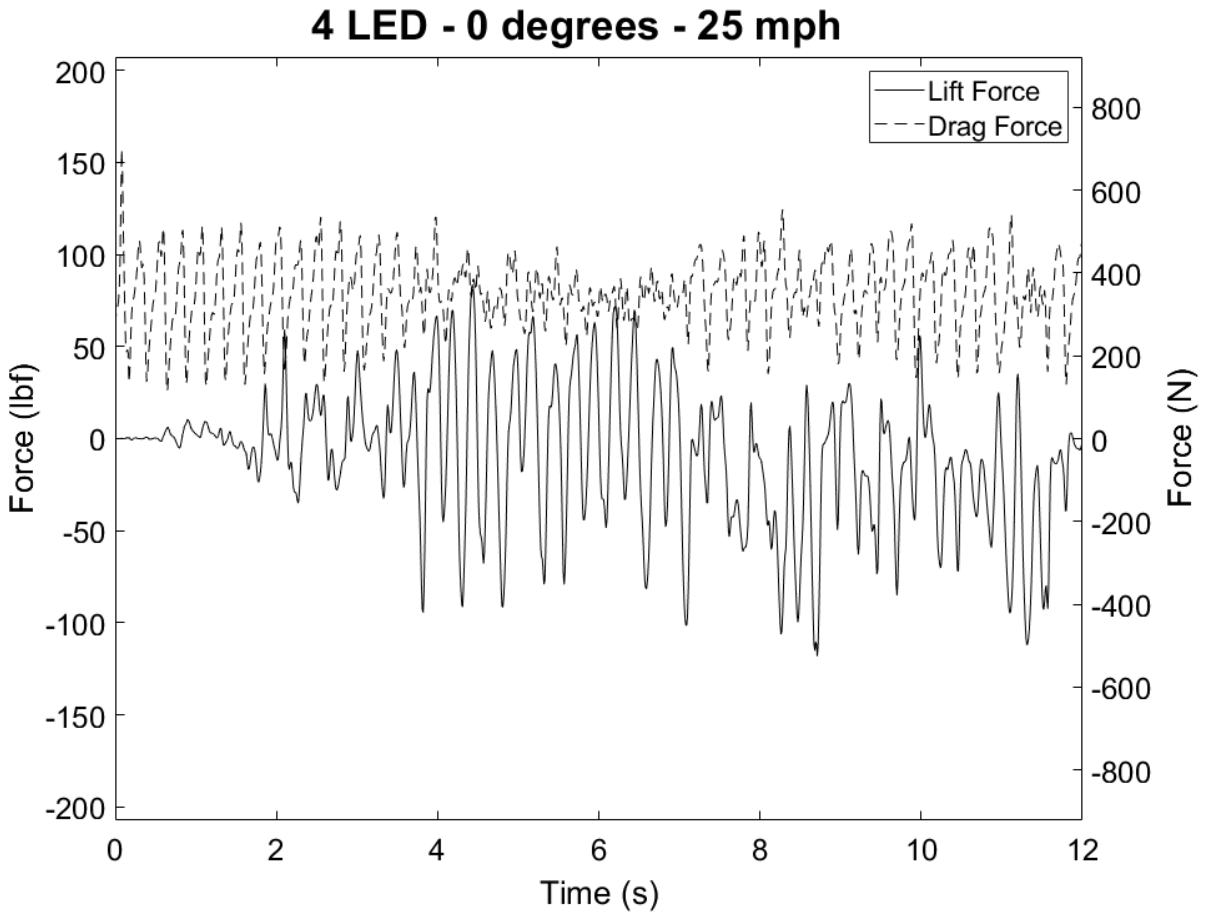

Figure A.32: Force-Time Relationship for 4-LED Light Fixture Subjected to 25 mph Wind at an Angle of 0 Degrees

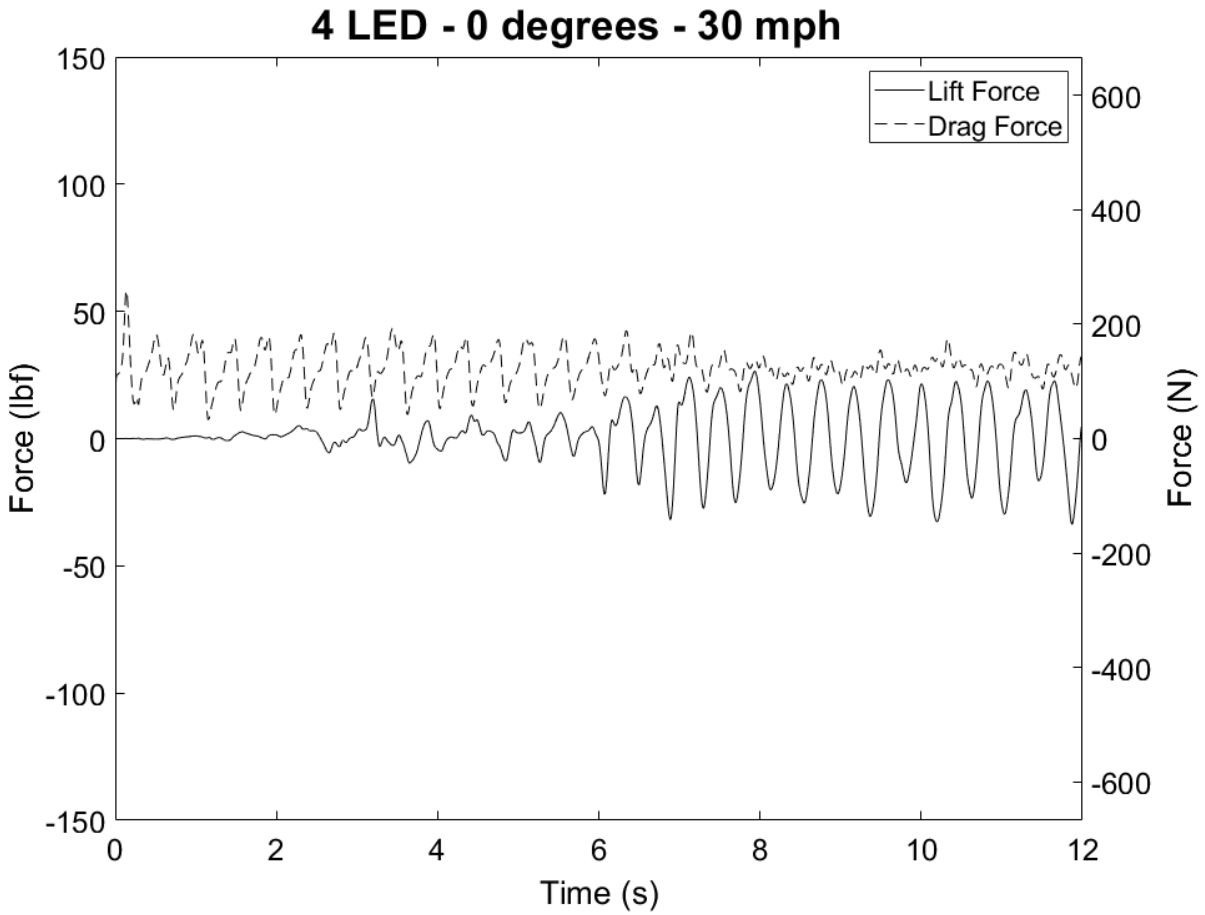

Figure A.33: Force-Time Relationship for 4-LED Light Fixture Subjected to 30 mph Wind at an Angle of 0 Degrees

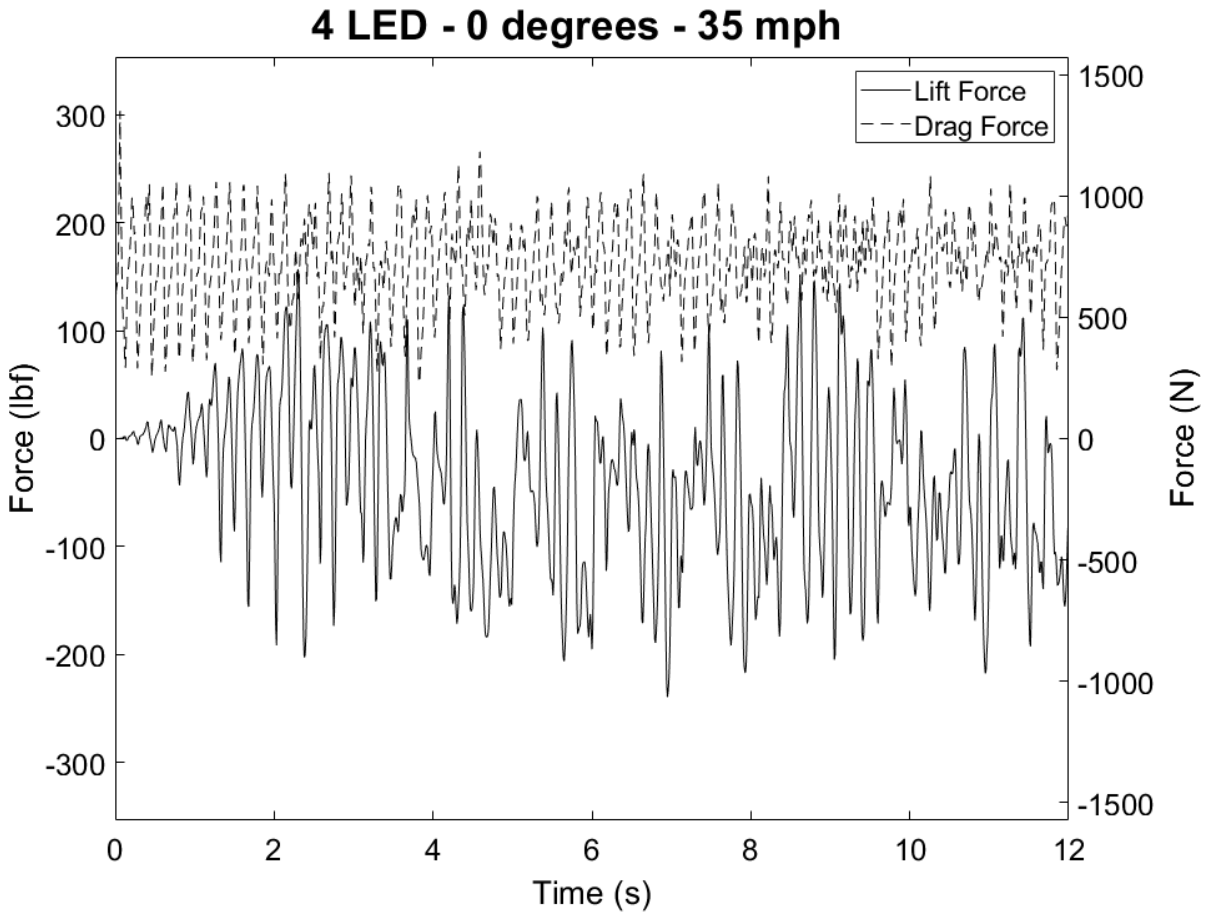

Figure A.34: Force-Time relationship for 4-LED Light Fixture Subjected to 35 mph Wind at an Angle of 0 Degrees

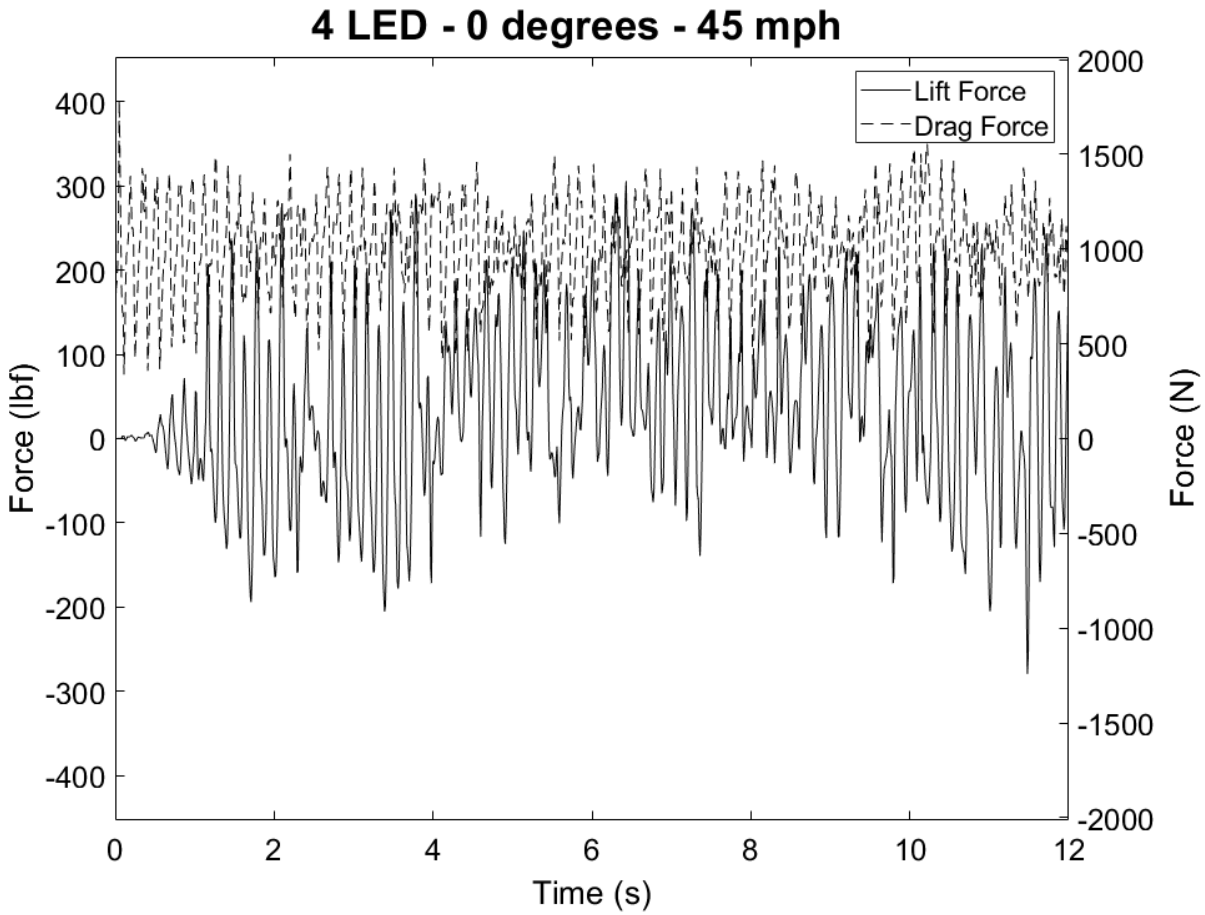

Figure A.35: Force-Time Relationship for 4-LED Light Fixture Subjected to 45 mph Wind at an Angle of 0 Degrees

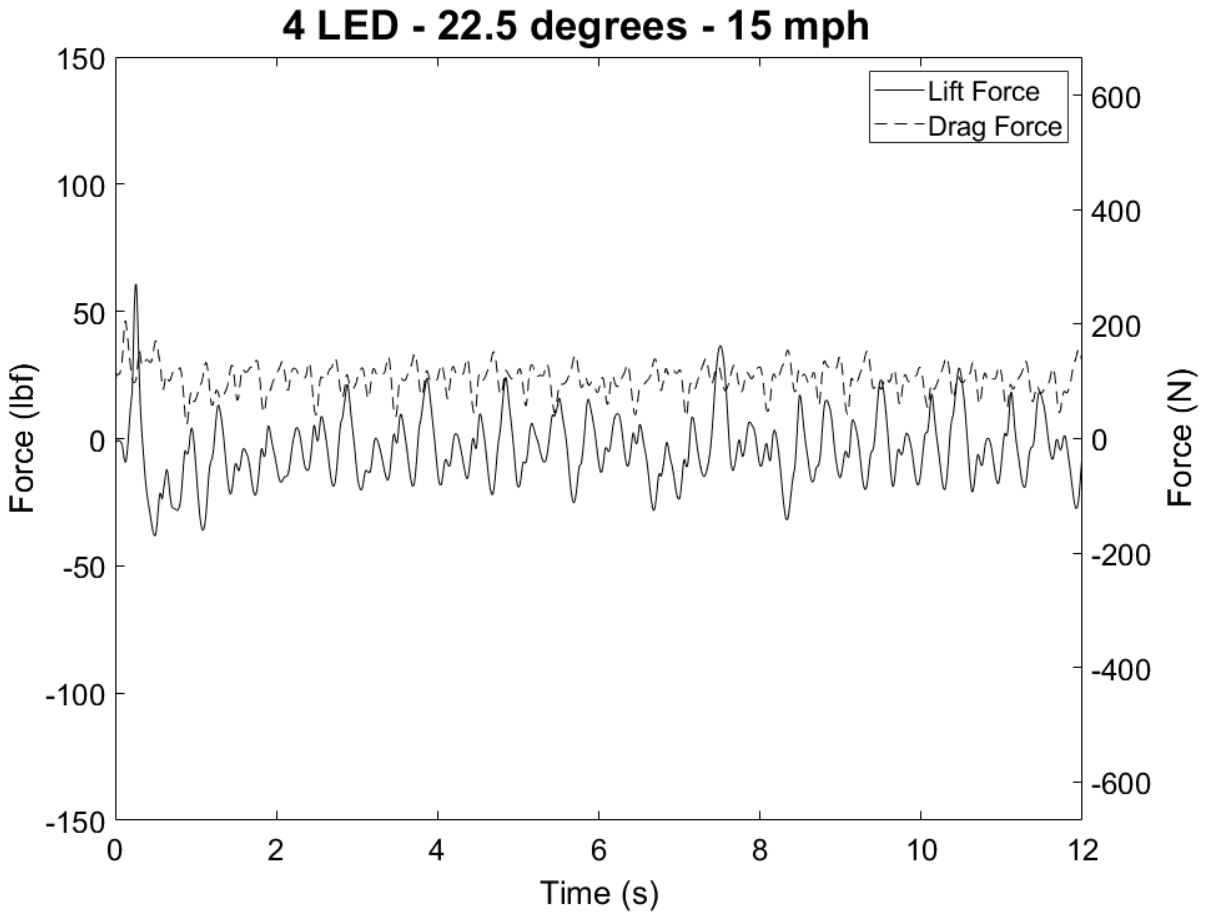

Figure A.36: Force-Time Relationship for 4-LED Light Fixture Subjected to 15 mph Wind at an Angle of 22.5 Degrees

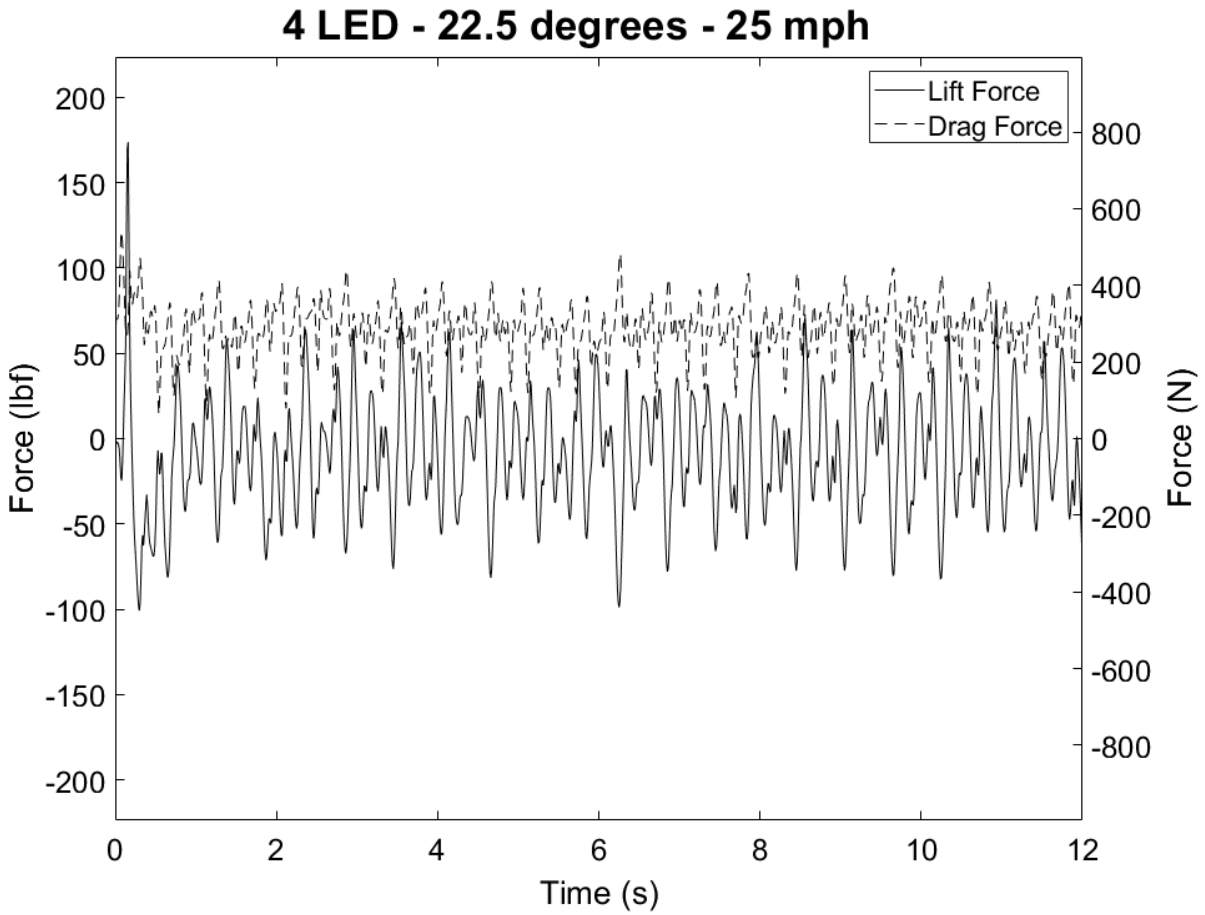

Figure A.37: Force-Time Relationship for 4-LED Light Fixture Subjected to 25 mph Wind at an Angle of 22.5 Degrees

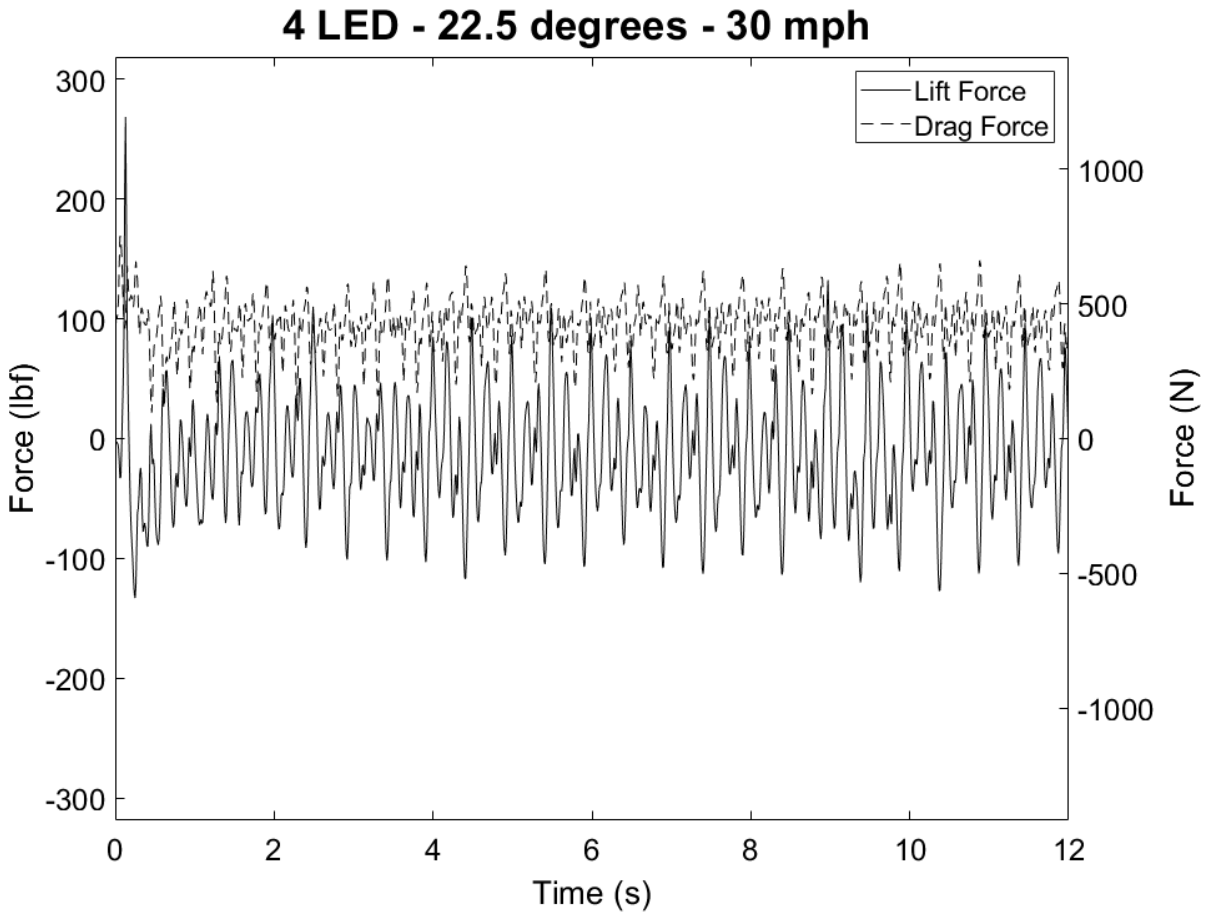

Figure A.38: Force-Time Relationship for 4-LED Light Fixture Subjected to 30 mph Wind at an Angle of 22.5 Degrees

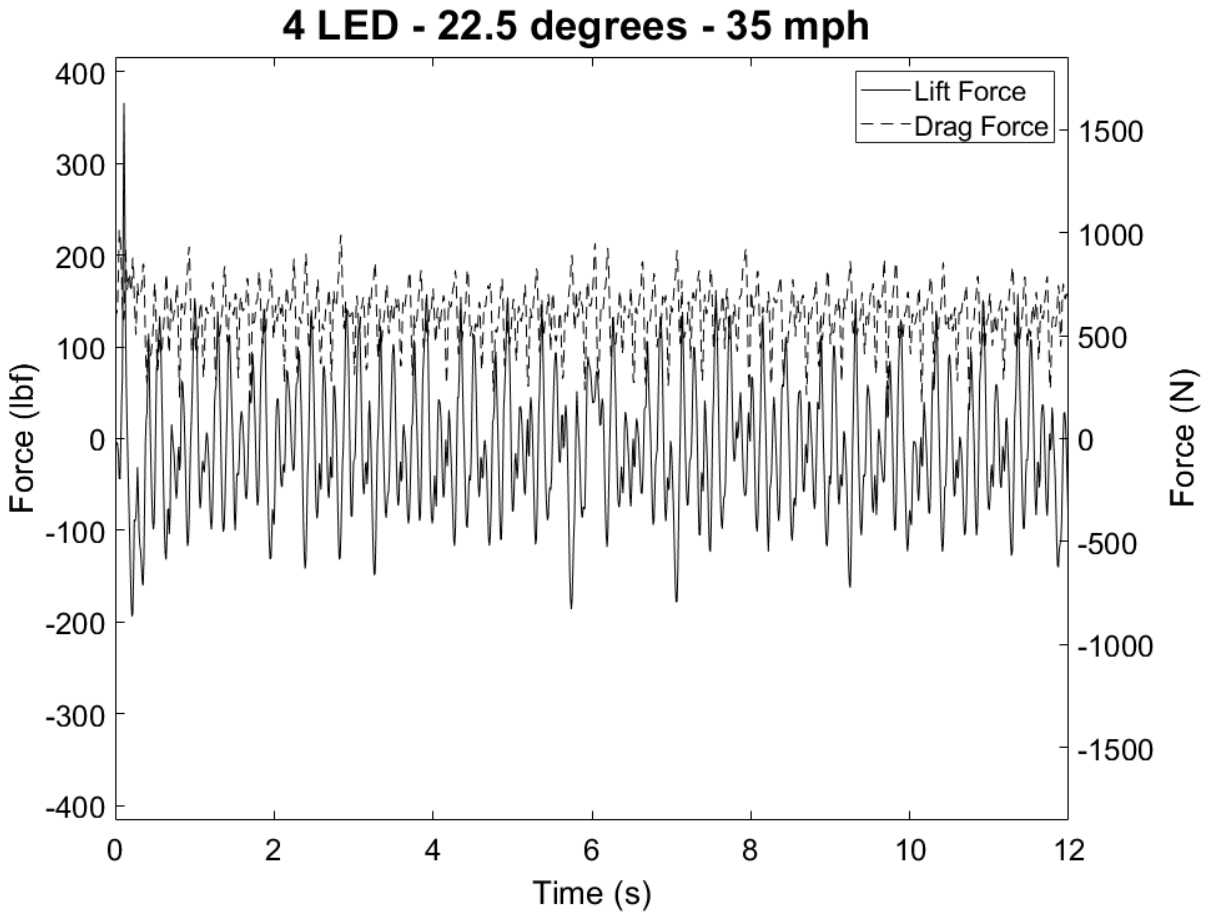

Figure A.39: Force-Time Relationship for 4-LED Light Fixture Subjected to 35 mph Wind at an Angle of 22.5 Degrees

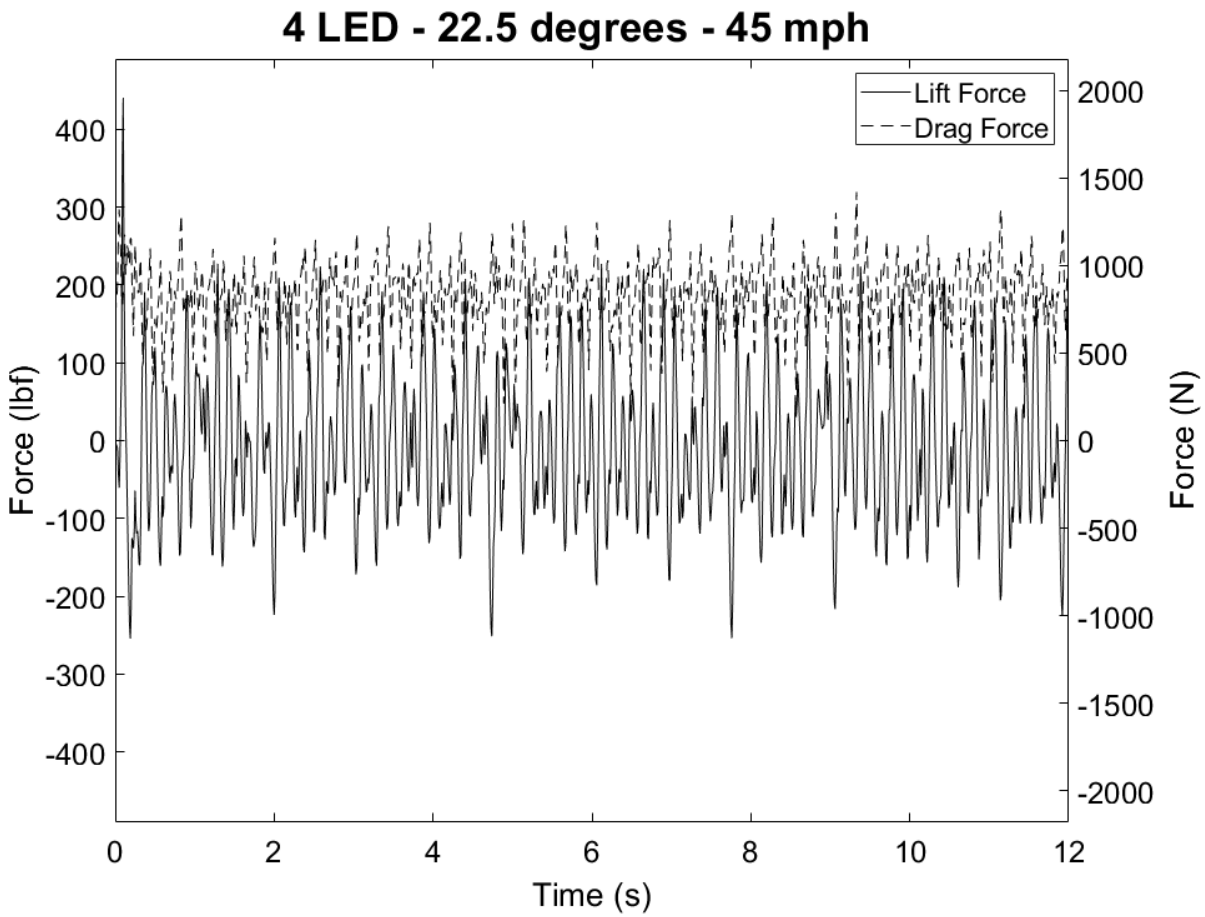

Figure A.40: Force-Time Relationship for 4-LED Light Fixture Subjected to 45 mph Wind at an Angle of 22.5 Degrees

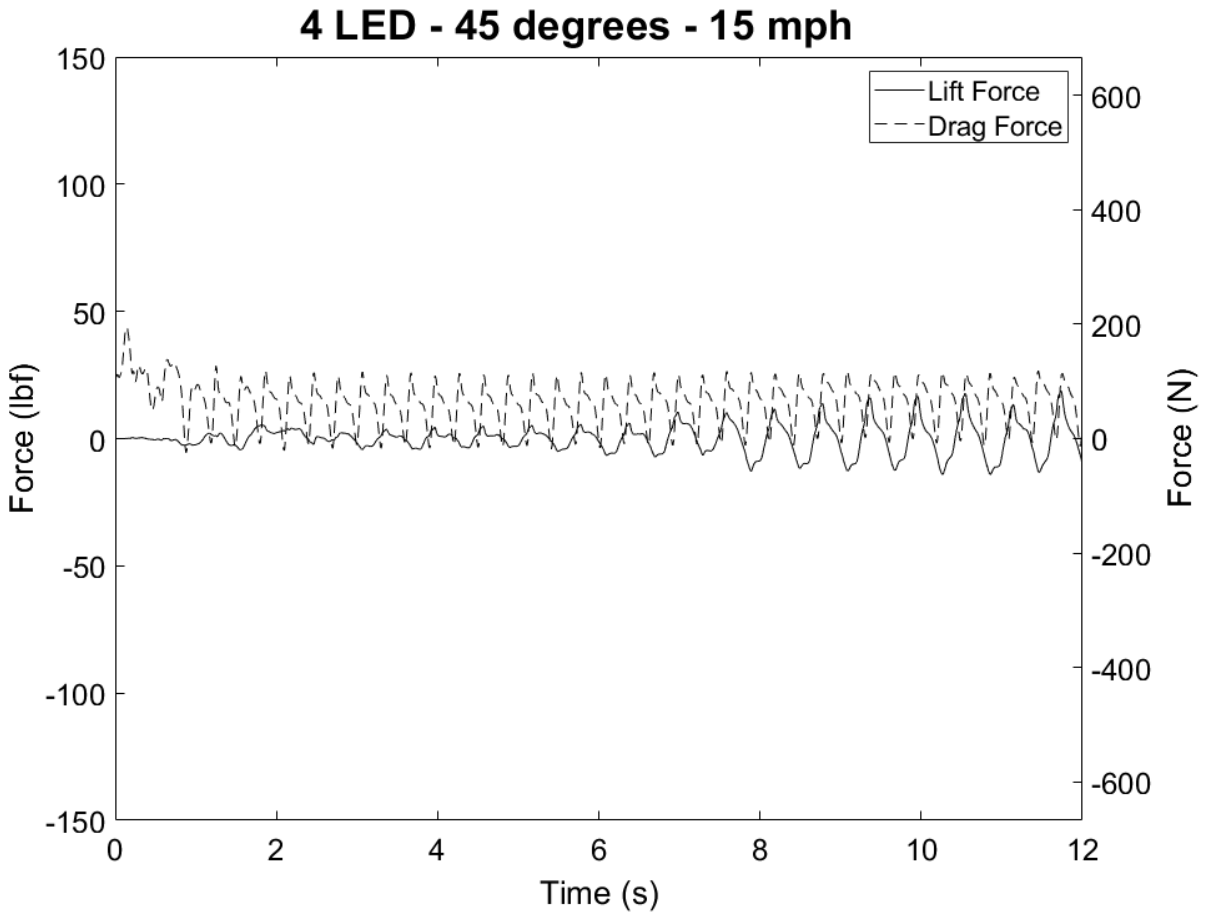

Figure A.41: Force-Time Relationship for 4-LED Light Fixture Subjected to 15 mph Wind at an Angle of 45 Degrees

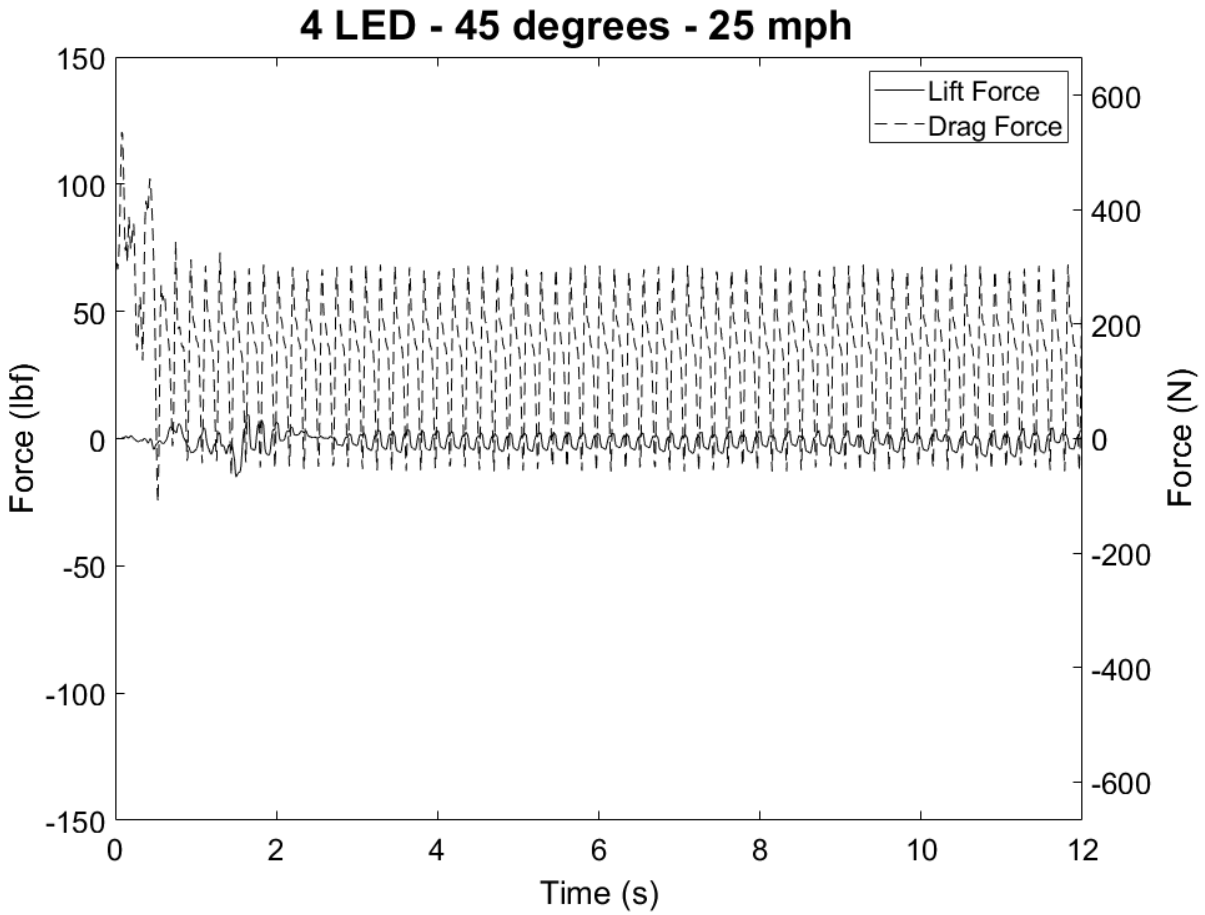

Figure A.42: Force-Time Relationship for 4-LED Light Fixture Subjected to 25 mph Wind at an Angle of 45 Degrees

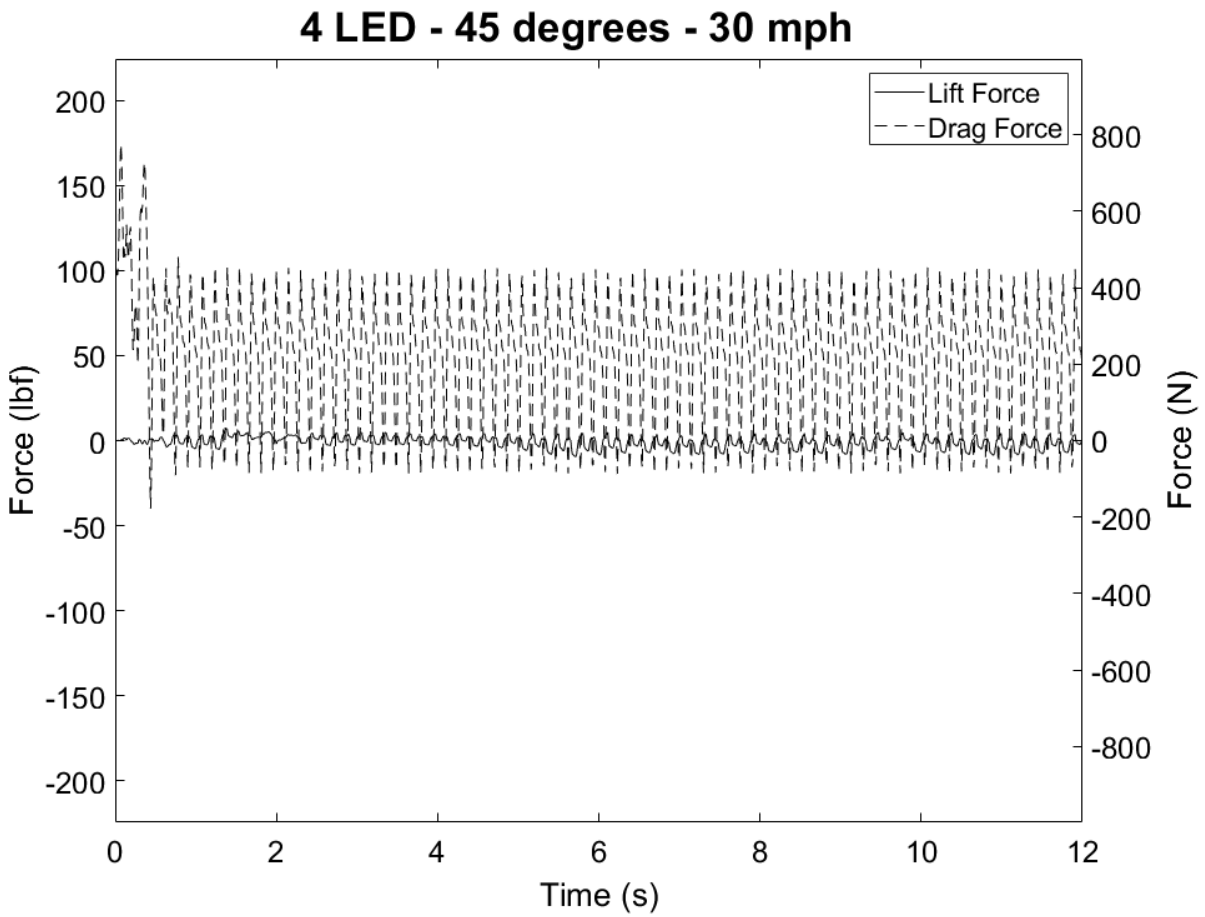

Figure A.43: Force-Time Relationship for 4-LED Light Fixture Subjected to 30 mph Wind at an Angle of 45 Degrees

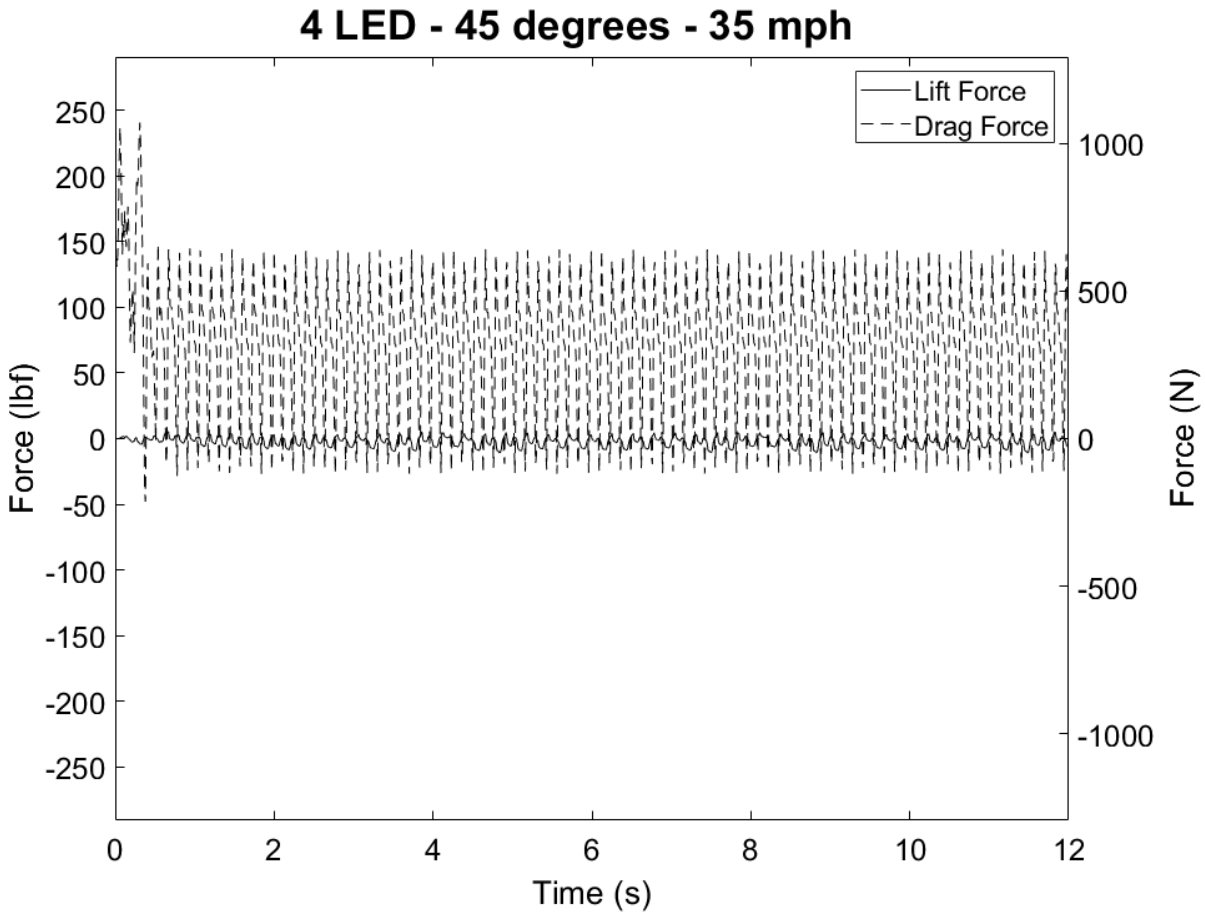

Figure A.44: Force-Time Relationship for 4-LED Light Fixture Subjected to 35 mph Wind at an Angle of 45 Degrees

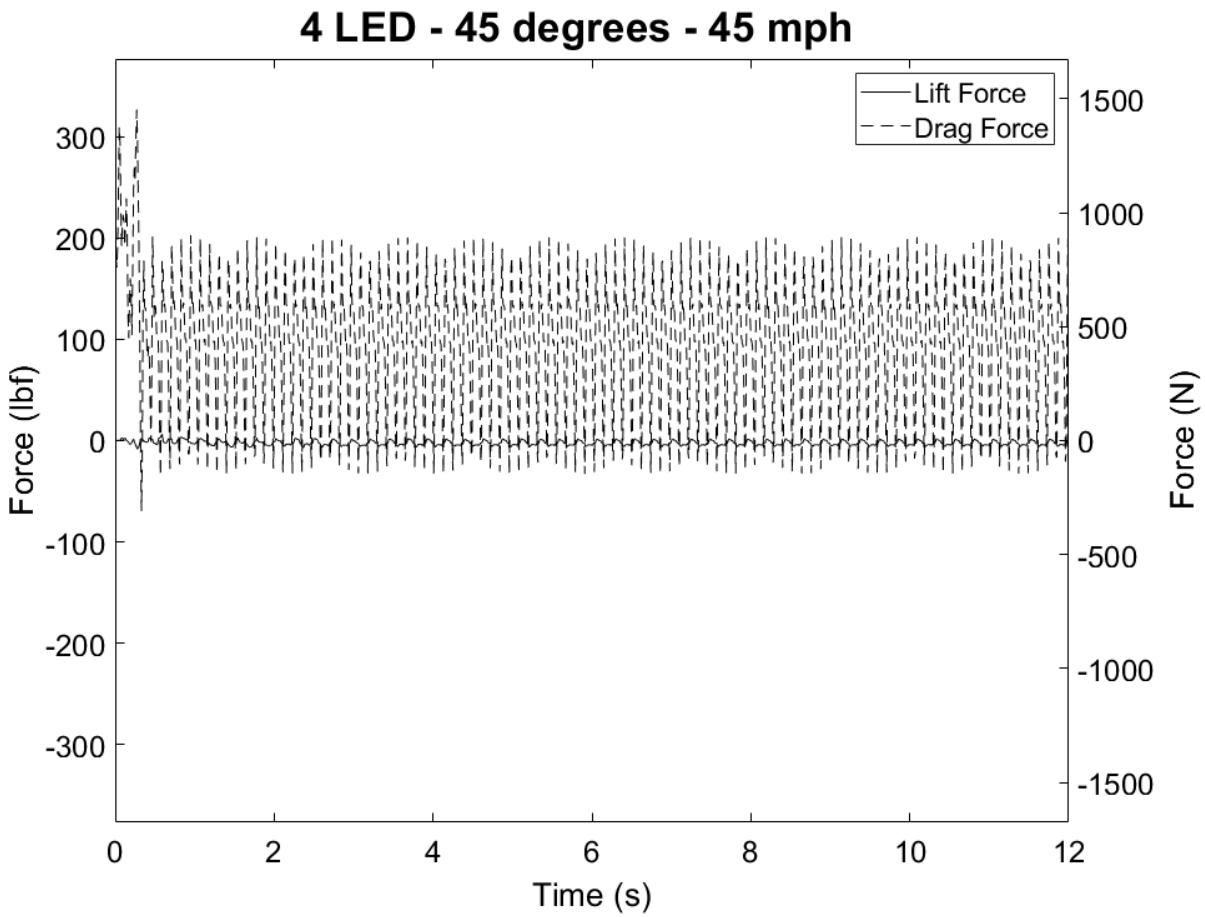

Figure A.45: Force-Time Relationship for 4-LED Light Fixture Subjected to 45 mph Wind at an Angle of 45 Degrees

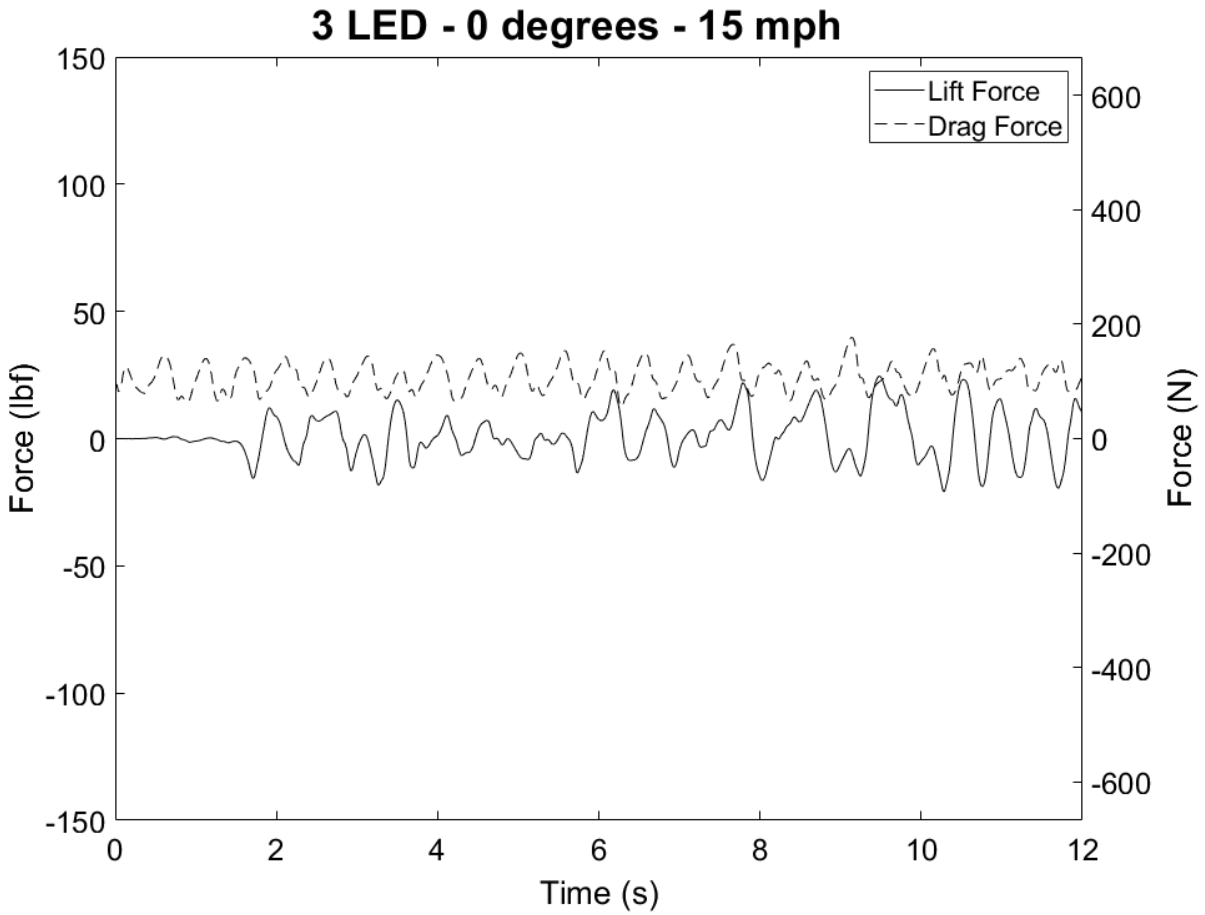

Figure A.46: Force-Time Relationship for 3-LED Light Fixture Subjected to 15 mph Wind at an Angle of 0 Degrees

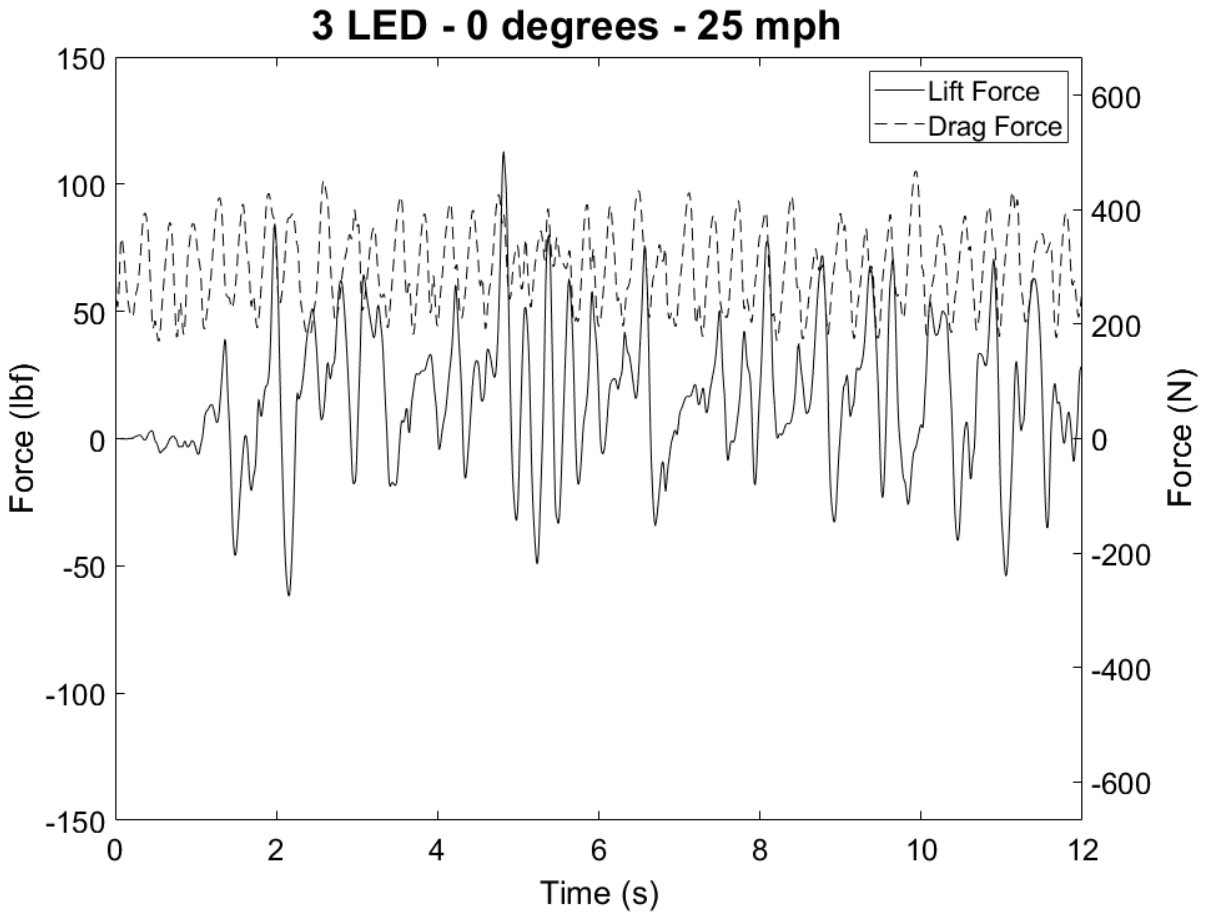

Figure A.47: Force-Time Relationship for 3-LED Light Fixture Subjected to 25 mph Wind at an Angle of 0 Degrees

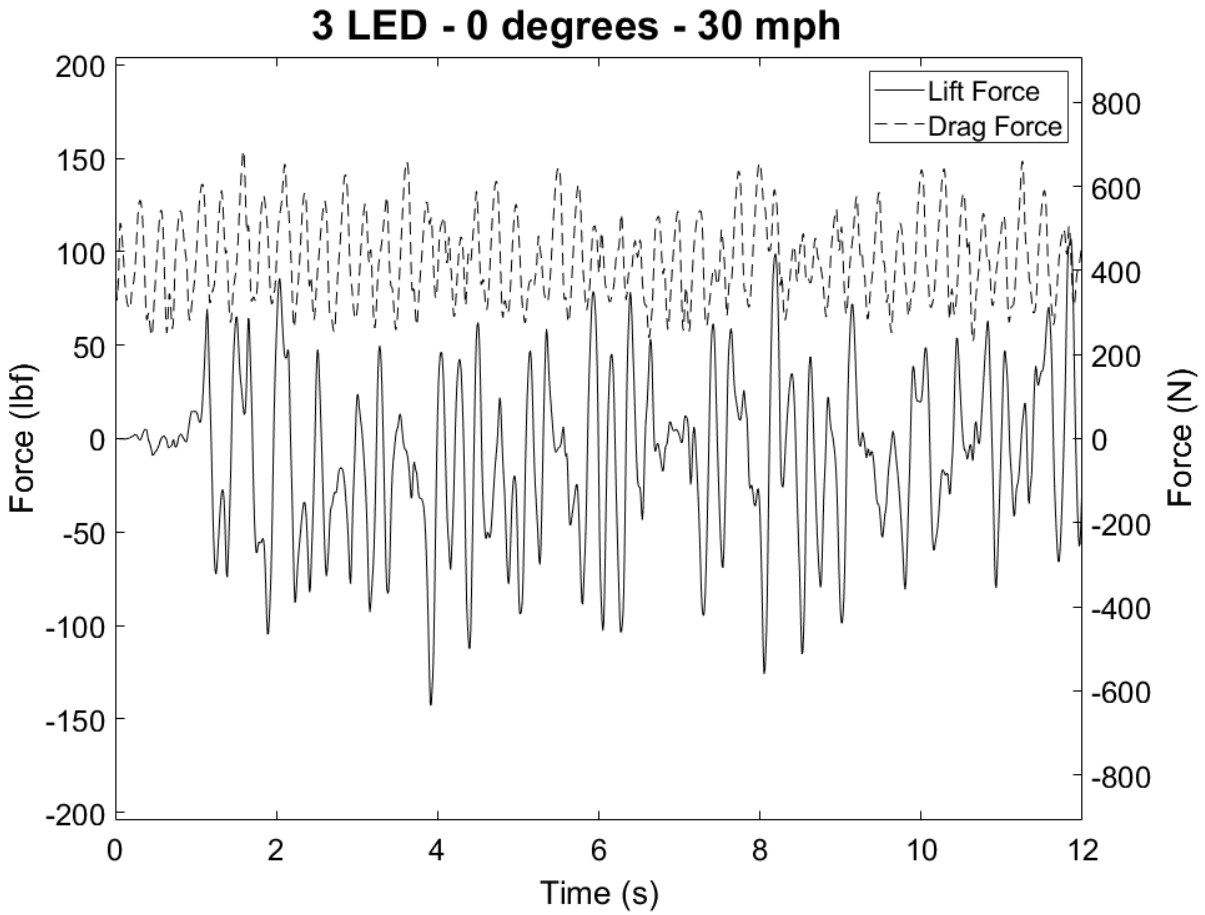

Figure A.48: Force-Time Relationship for 3-LED Light Fixture Subjected to 30 mph Wind at an Angle of 0 Degrees

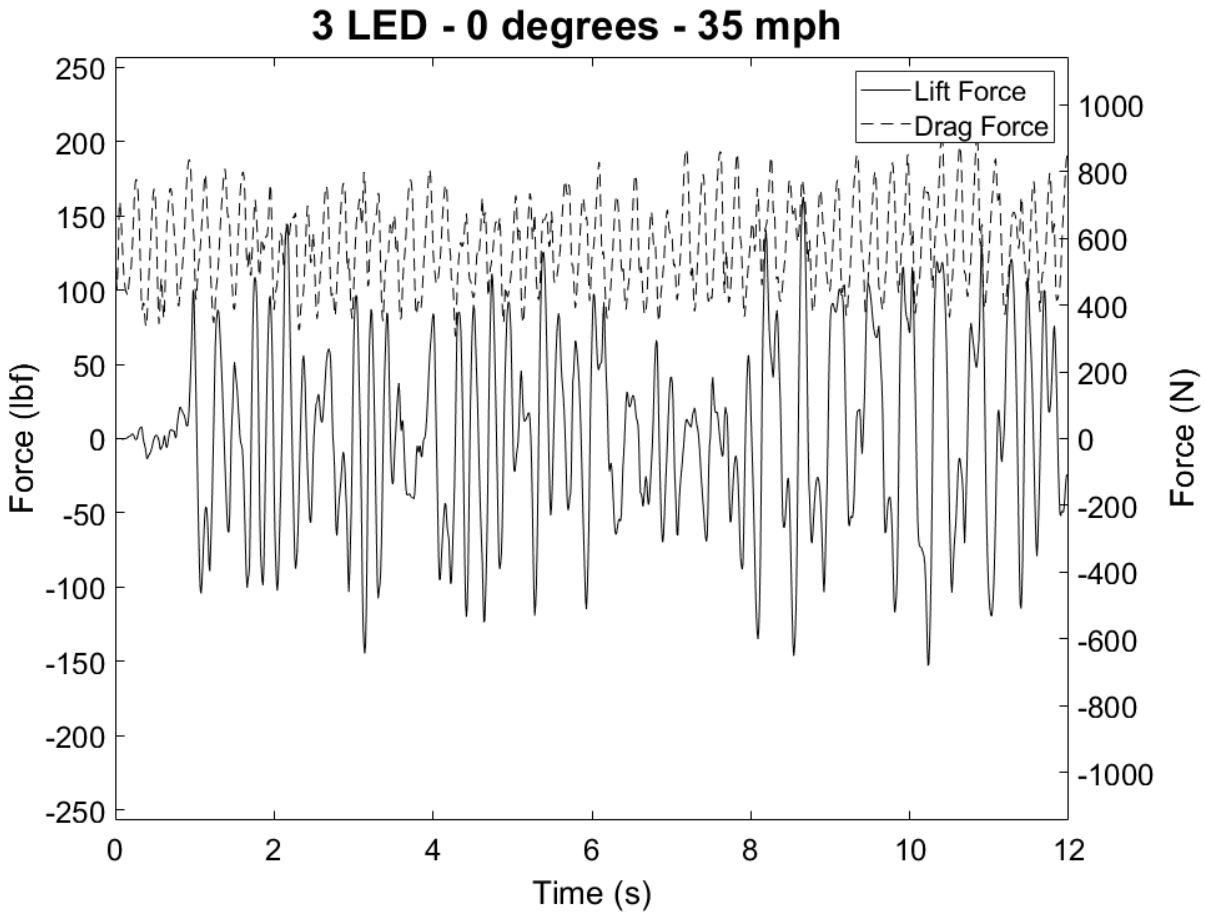

Figure A.49: Force-Time Relationship for 3-LED Light Fixture Subjected to 35 mph Wind at an Angle of 0 Degrees

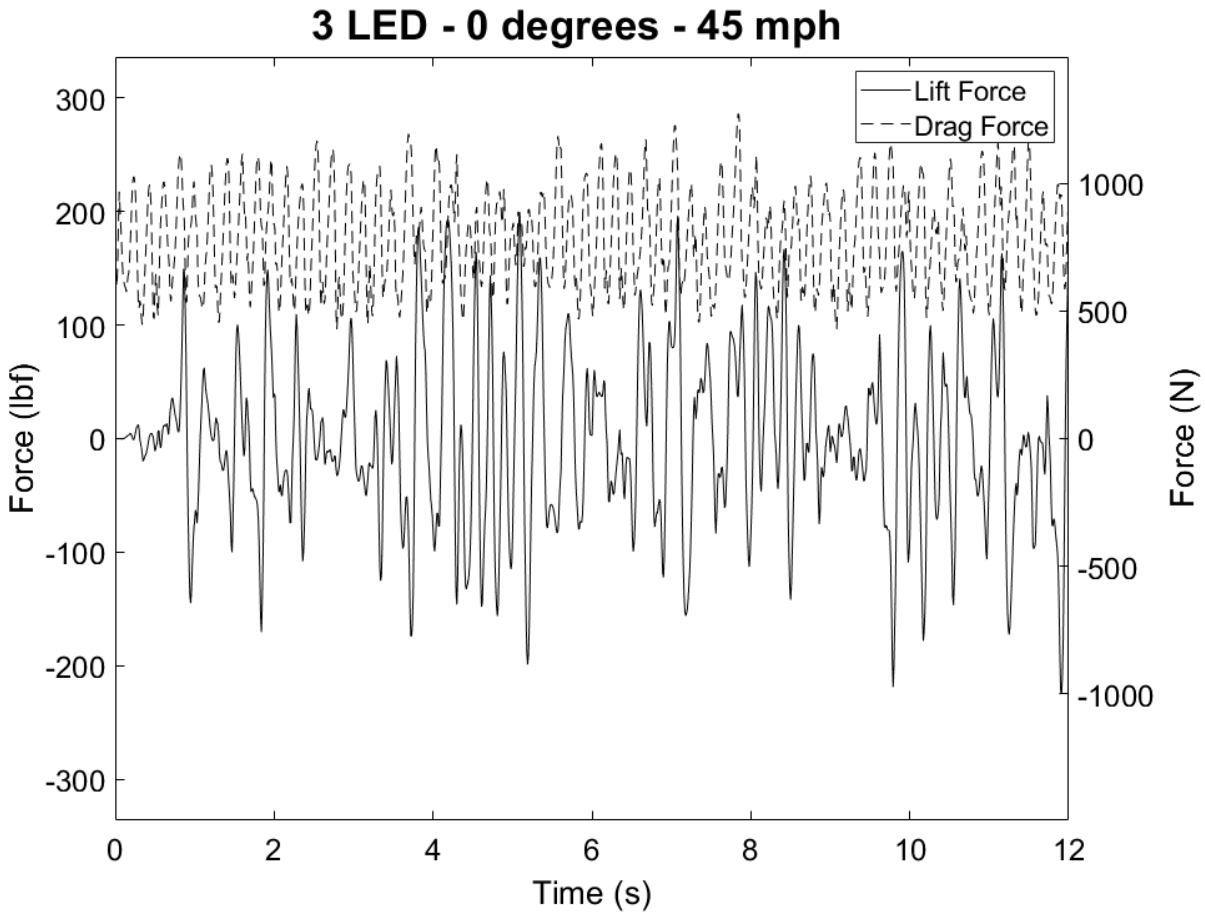

Figure A.50: Force-Time Relationship for 3-LED Light Fixture Subjected to 45 mph Wind at an Angle of 0 Degrees

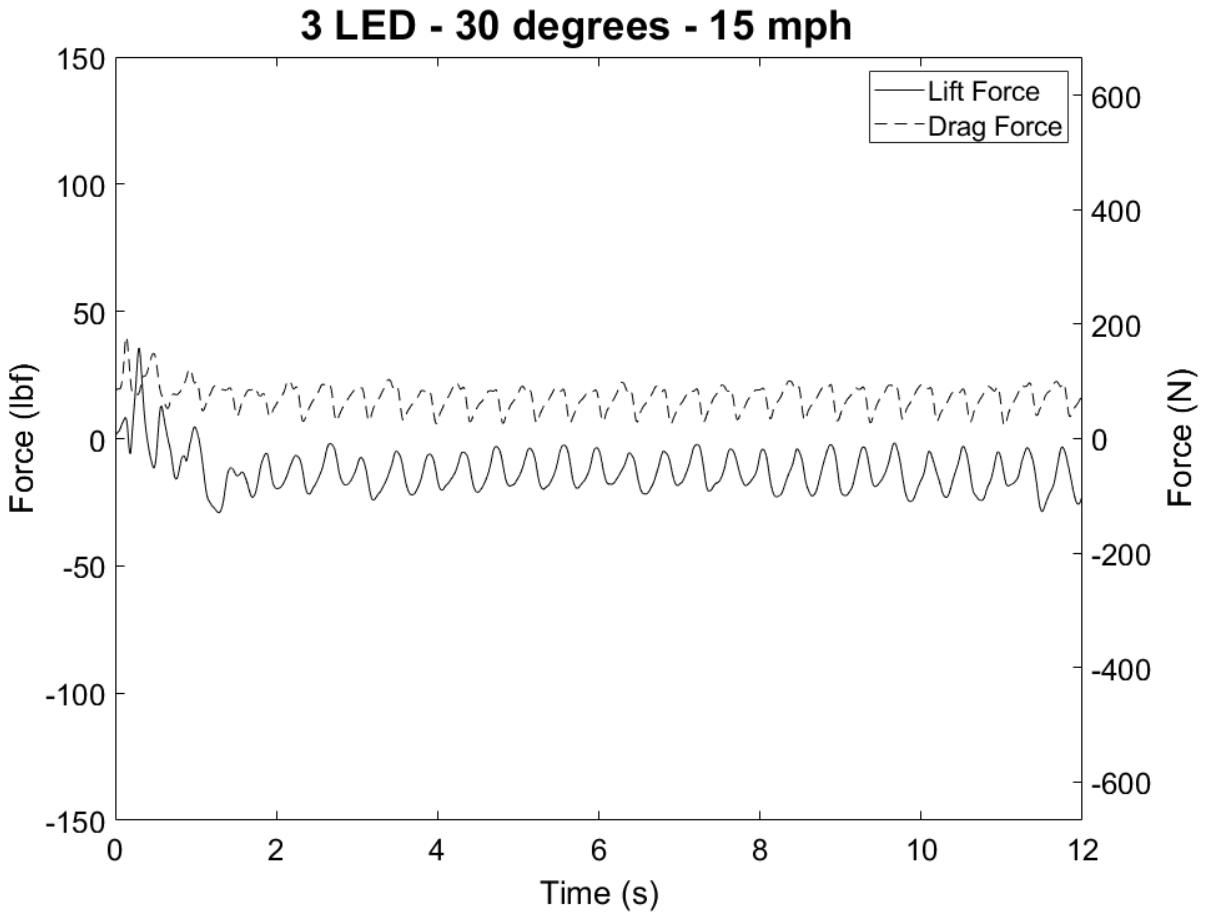

Figure A.51: Force-Time Relationship for 3-LED Light Fixture Subjected to 15 mph Wind at an Angle of 30 Degrees

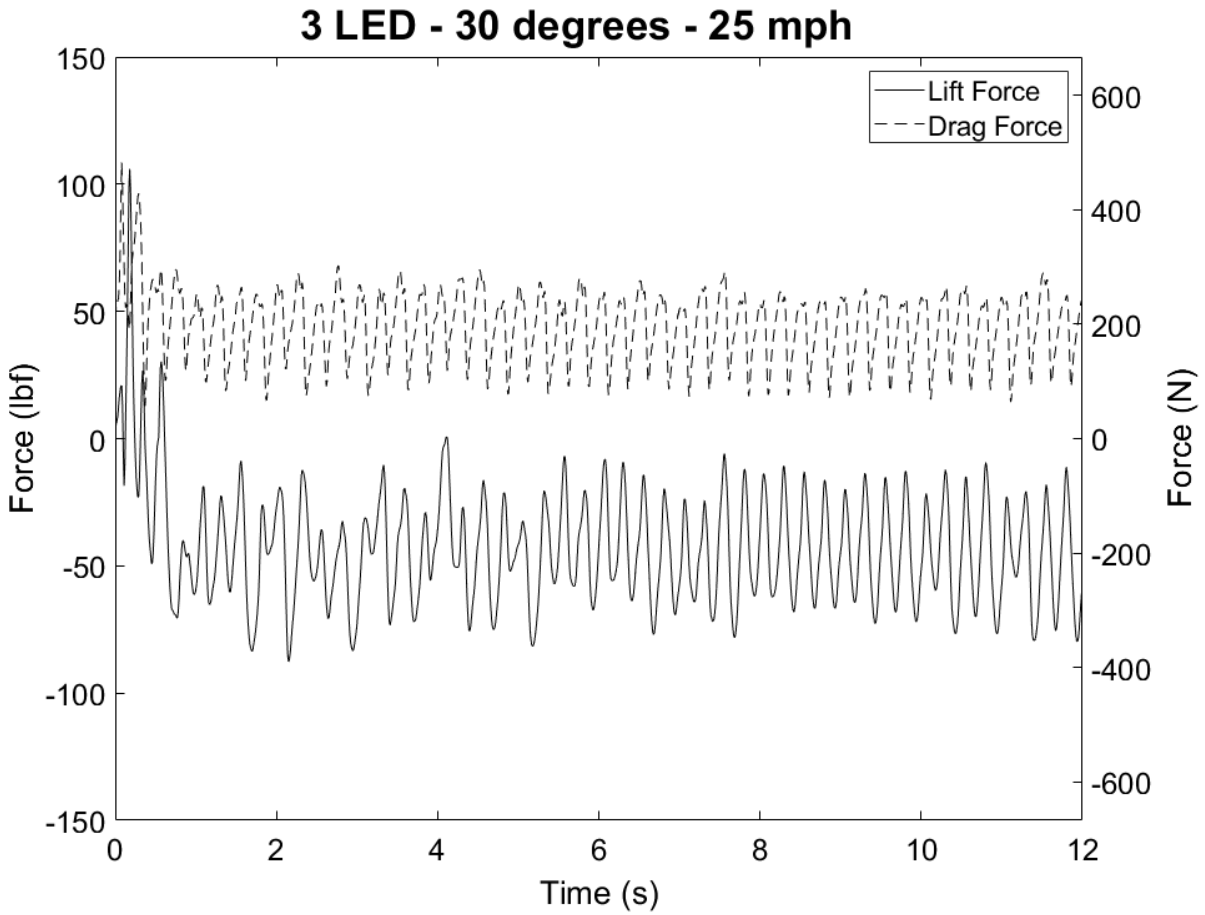

Figure A.52: Force-Time Relationship for 3-LED Light Fixture Subjected to 25 mph Wind at an Angle of 30 Degrees

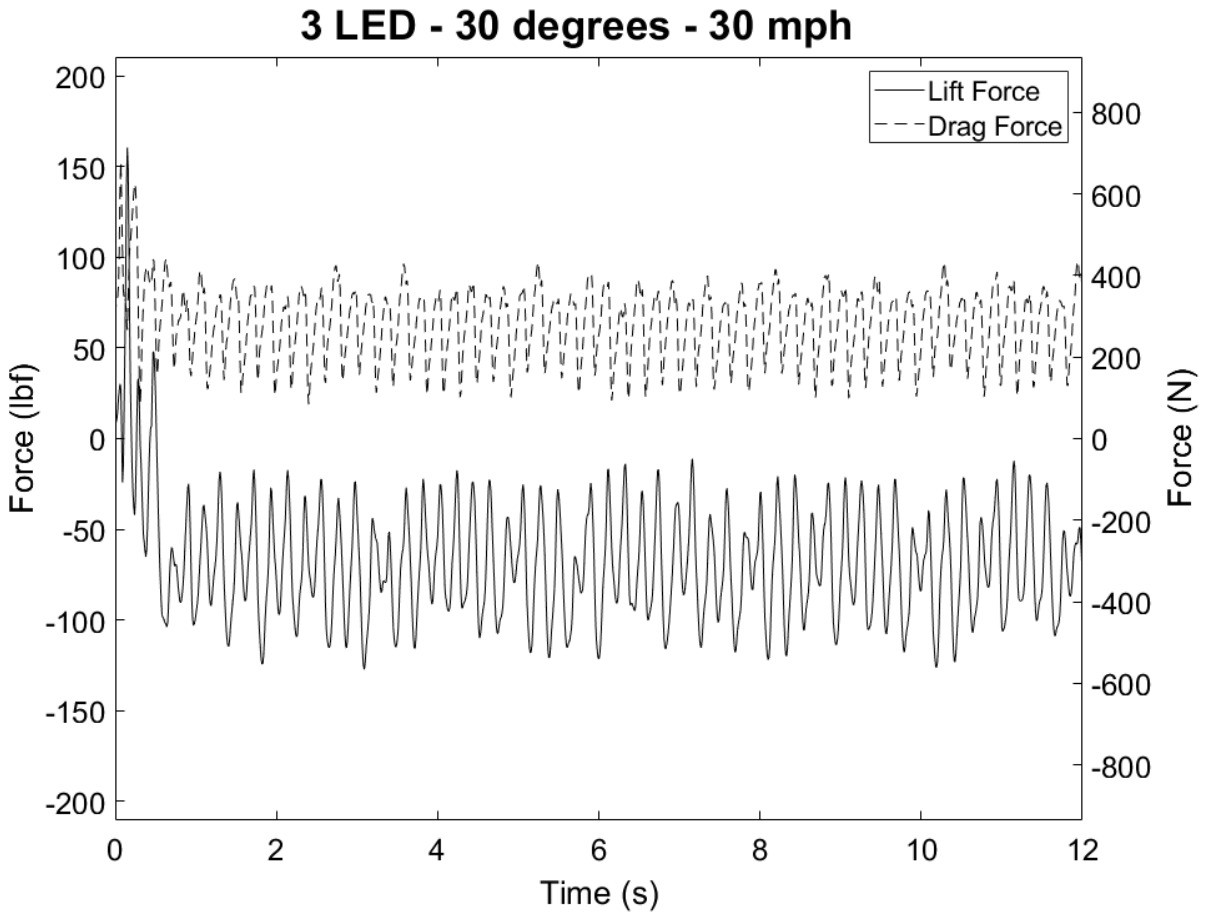

Figure A.53: Force-Time Relationship for 3-LED Light Fixture Subjected to 30 mph Wind at an Angle of 30 Degrees

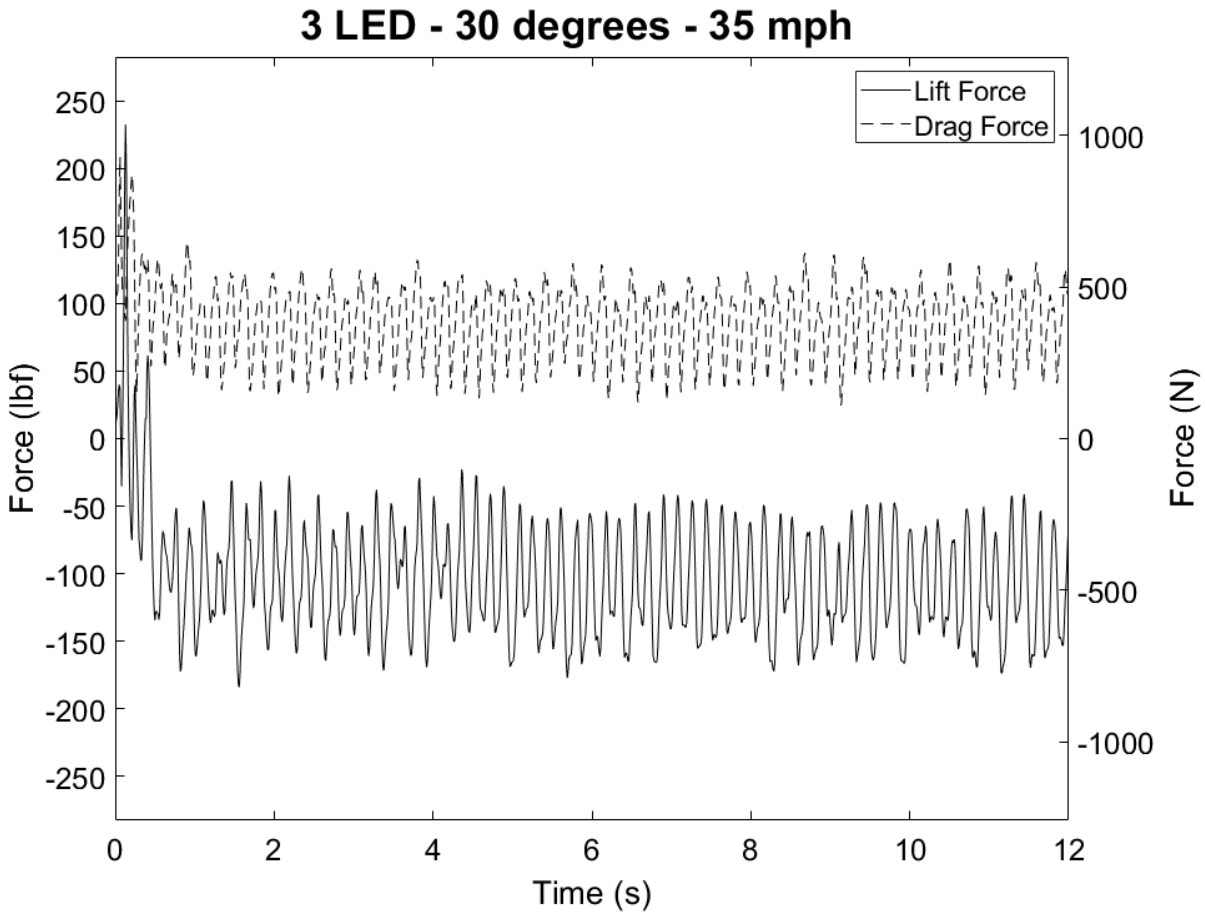

Figure A.54: Force-Time Relationship for 3-LED Light Fixture Subjected to 35 mph Wind at an Angle of 30 Degrees

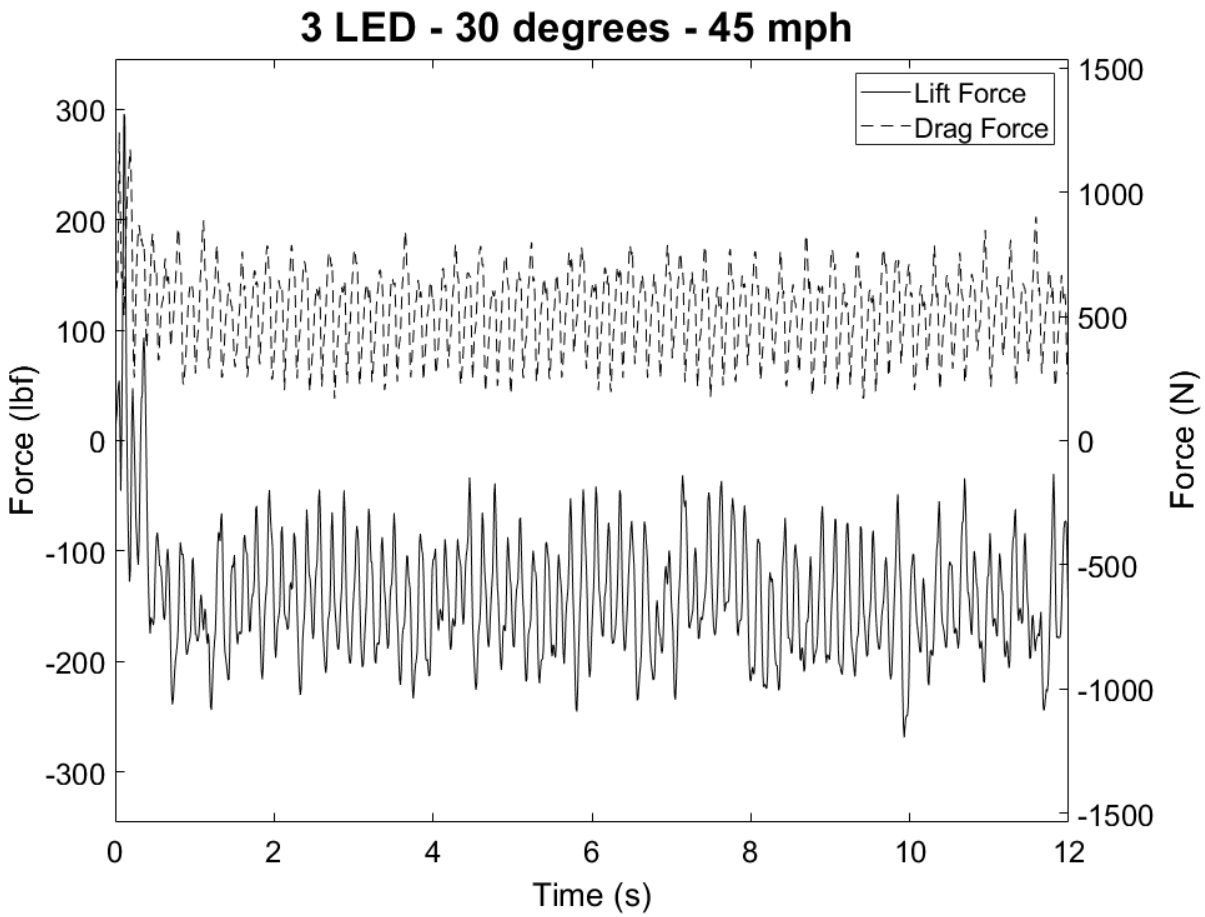

Figure A.55: Force-Time Relationship for 3-LED Light Fixture Subjected to 45 mph Wind at an Angle of 30 Degrees

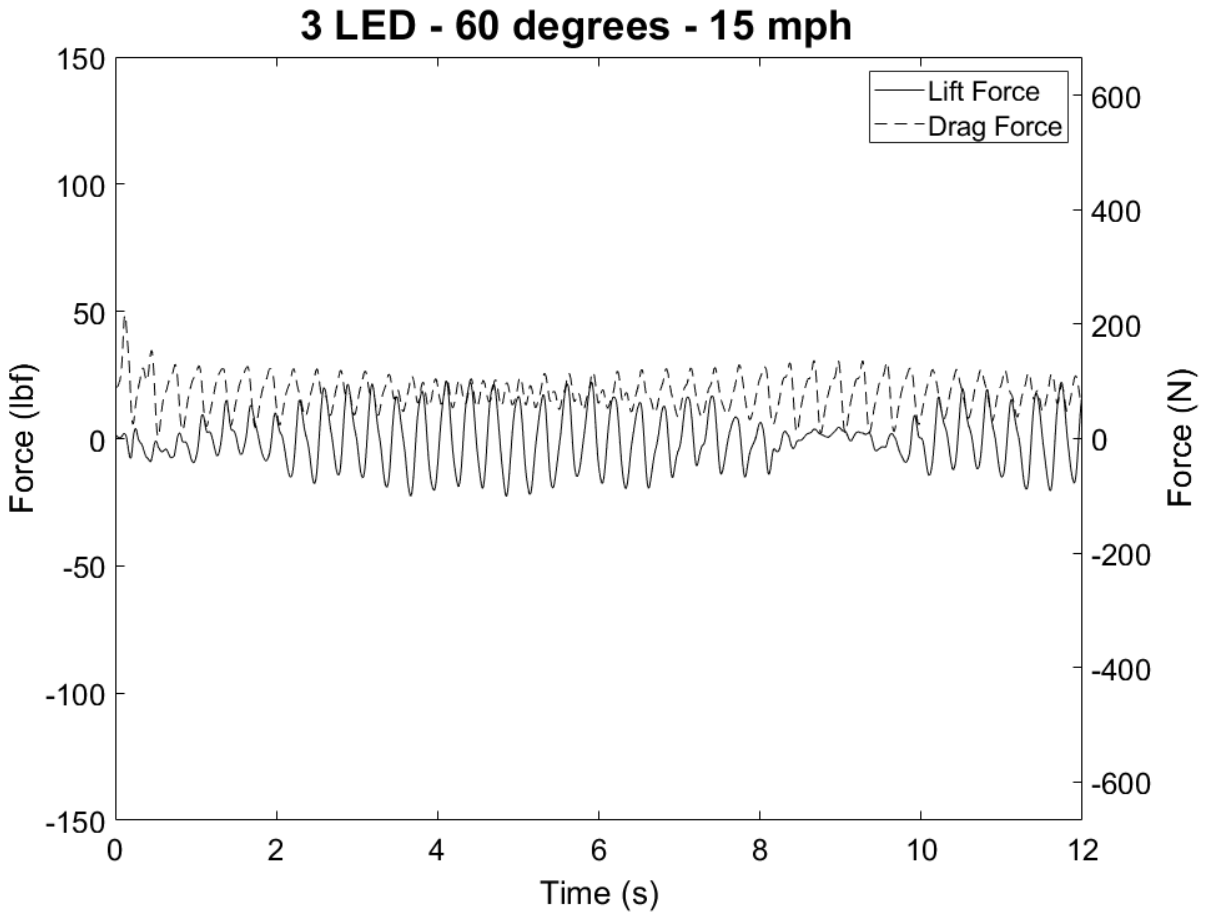

Figure A.56: Force-Time Relationship for 3-LED Light Fixture Subjected to 15 mph Wind at an Angle of 60 Degrees

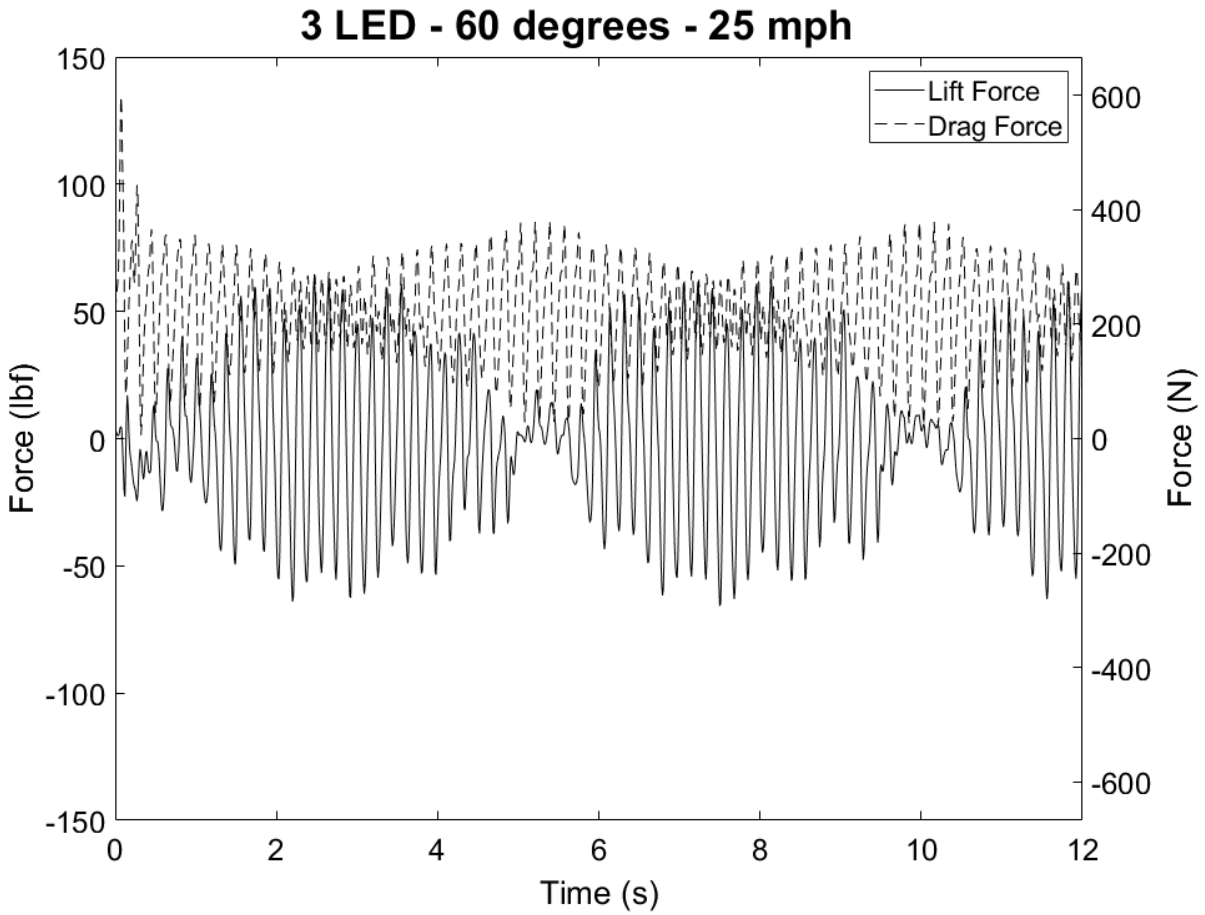

Figure A.57: Force-Time Relationship for 3-LED Light Fixture Subjected to 25 mph Wind at an Angle of 60 Degrees

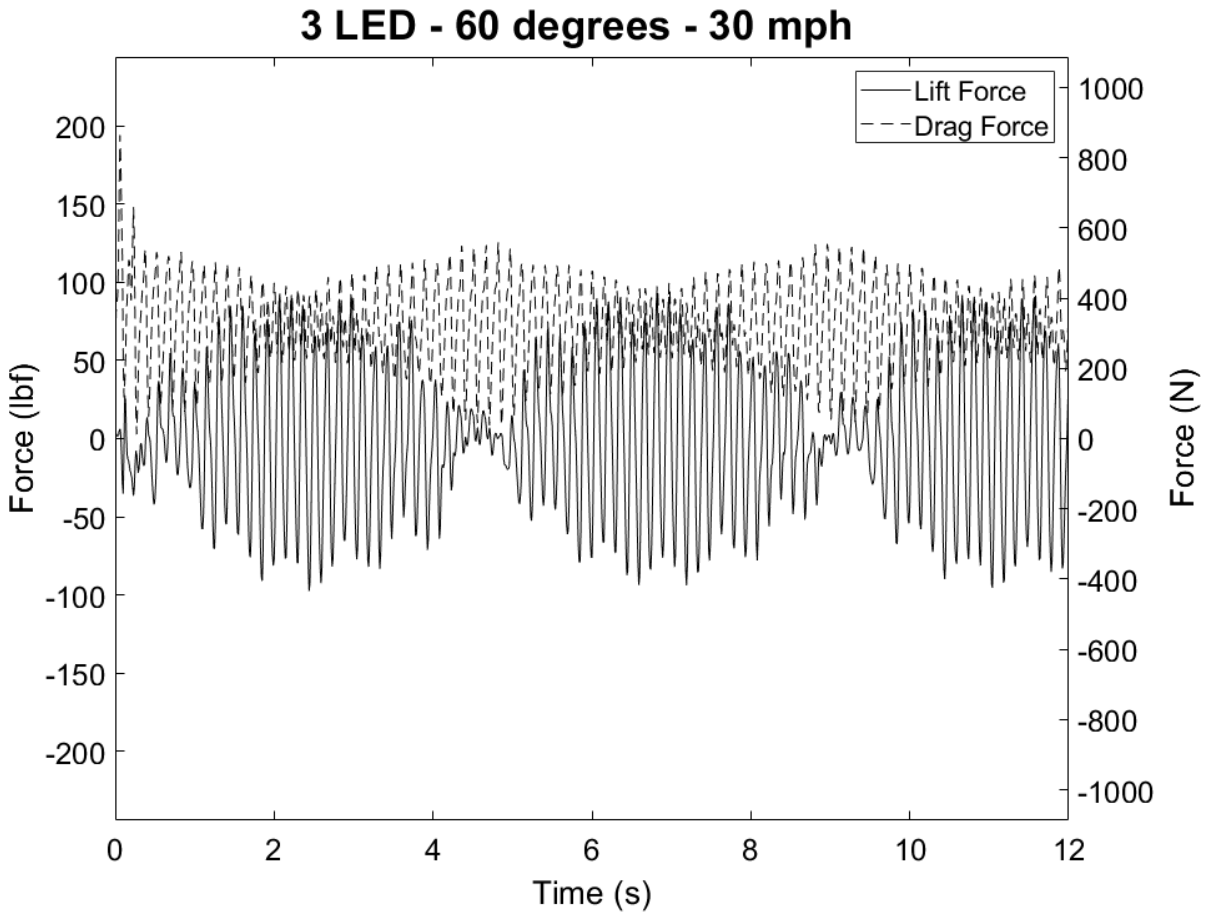

Figure A.58: Force-Time Relationship for 3-LED Light Fixture Subjected to 30 mph Wind at an Angle of 60 Degrees

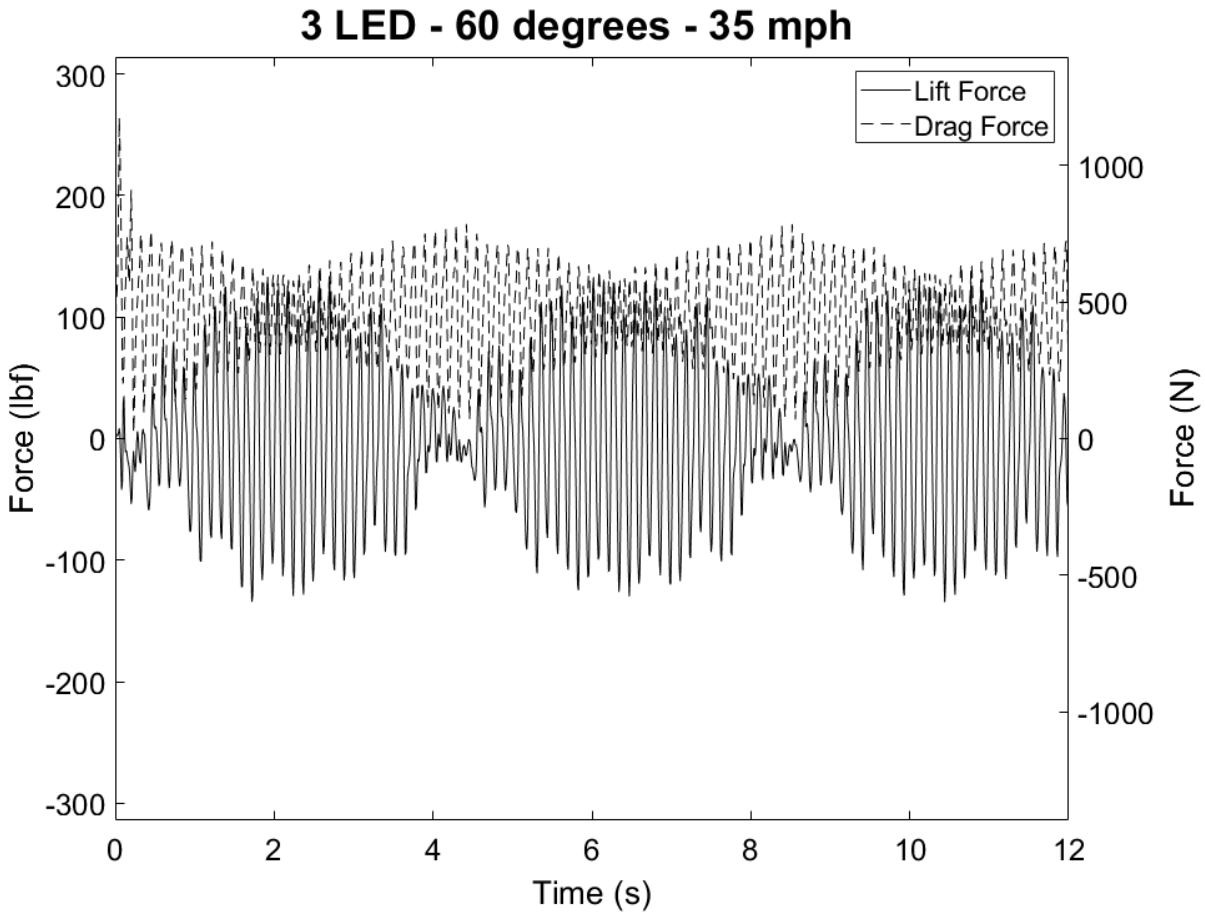

Figure A.59: Force-Time Relationship for 3-LED Light Fixture Subjected to 35 mph Wind at an Angle of 60 Degrees

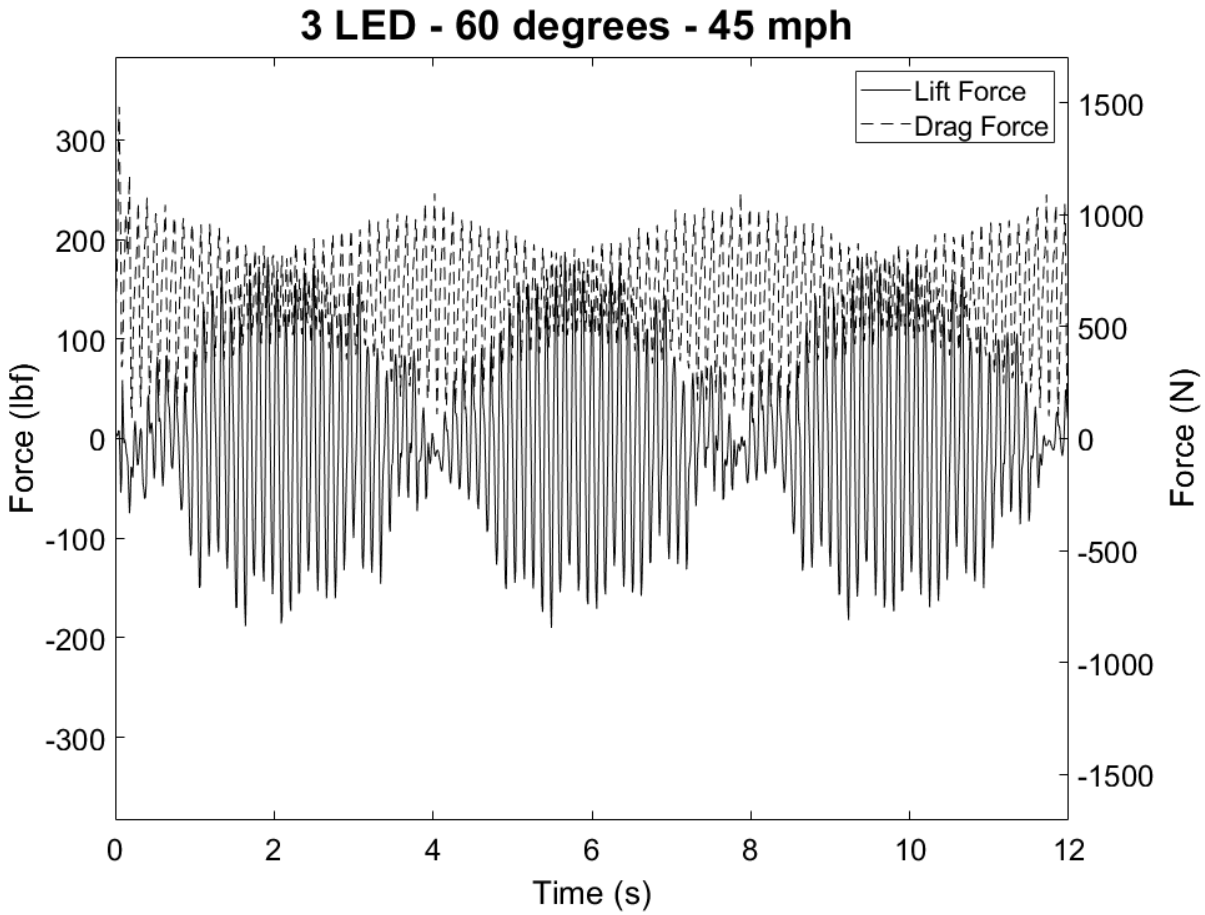

Figure A.60: Force-Time Relationship for 3-LED Light Fixture Subjected to 45 mph Wind at an Angle of 60 Degrees

Appendix B

B.1 Power Spectral Density Plots for Abaqus Simulations

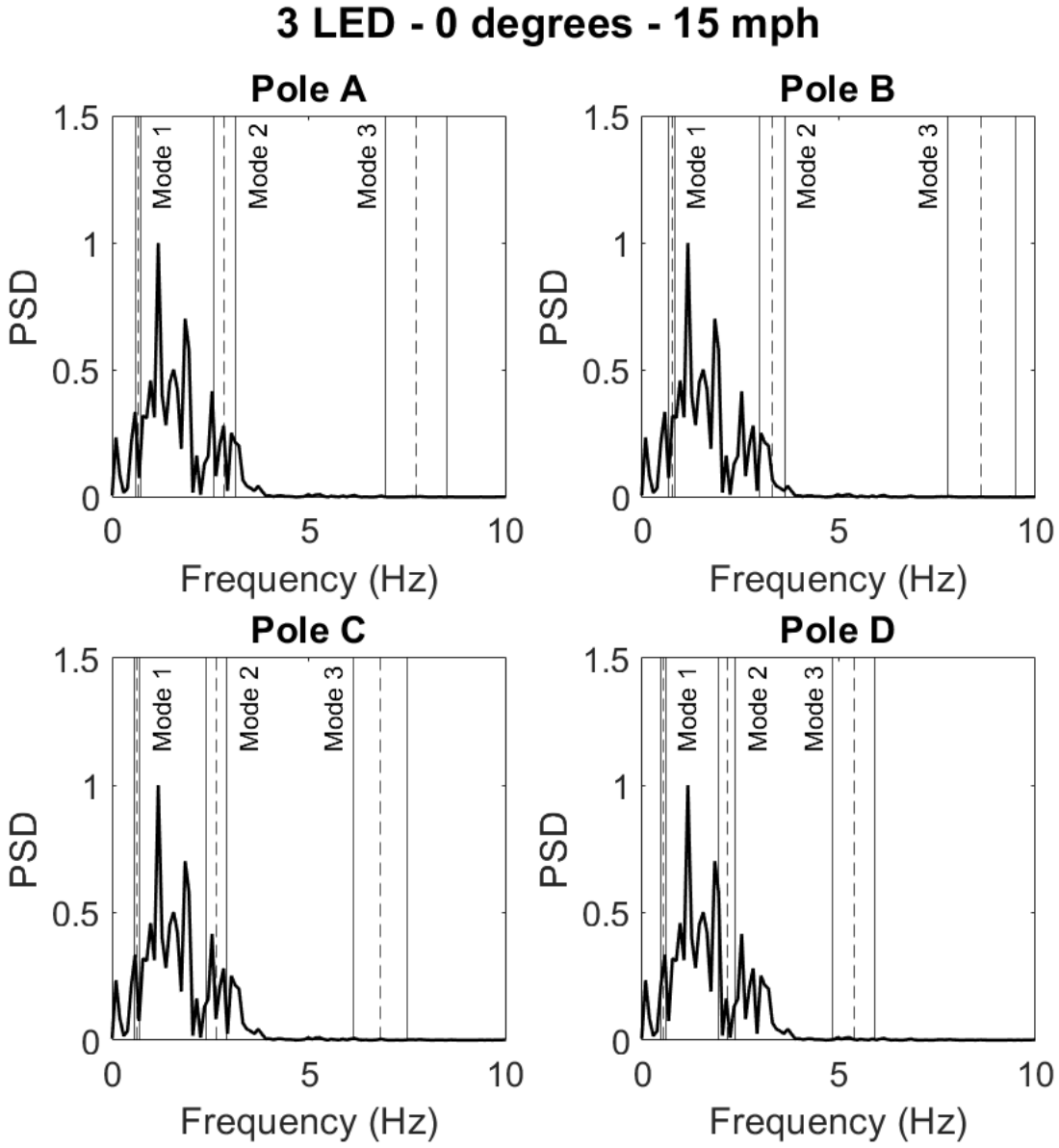

Figure B.1: PSDs for Pole A, B, C, and D for 3-LED Light Fixture Subjected to 15 mph Wind at an Angle of 0 Degrees

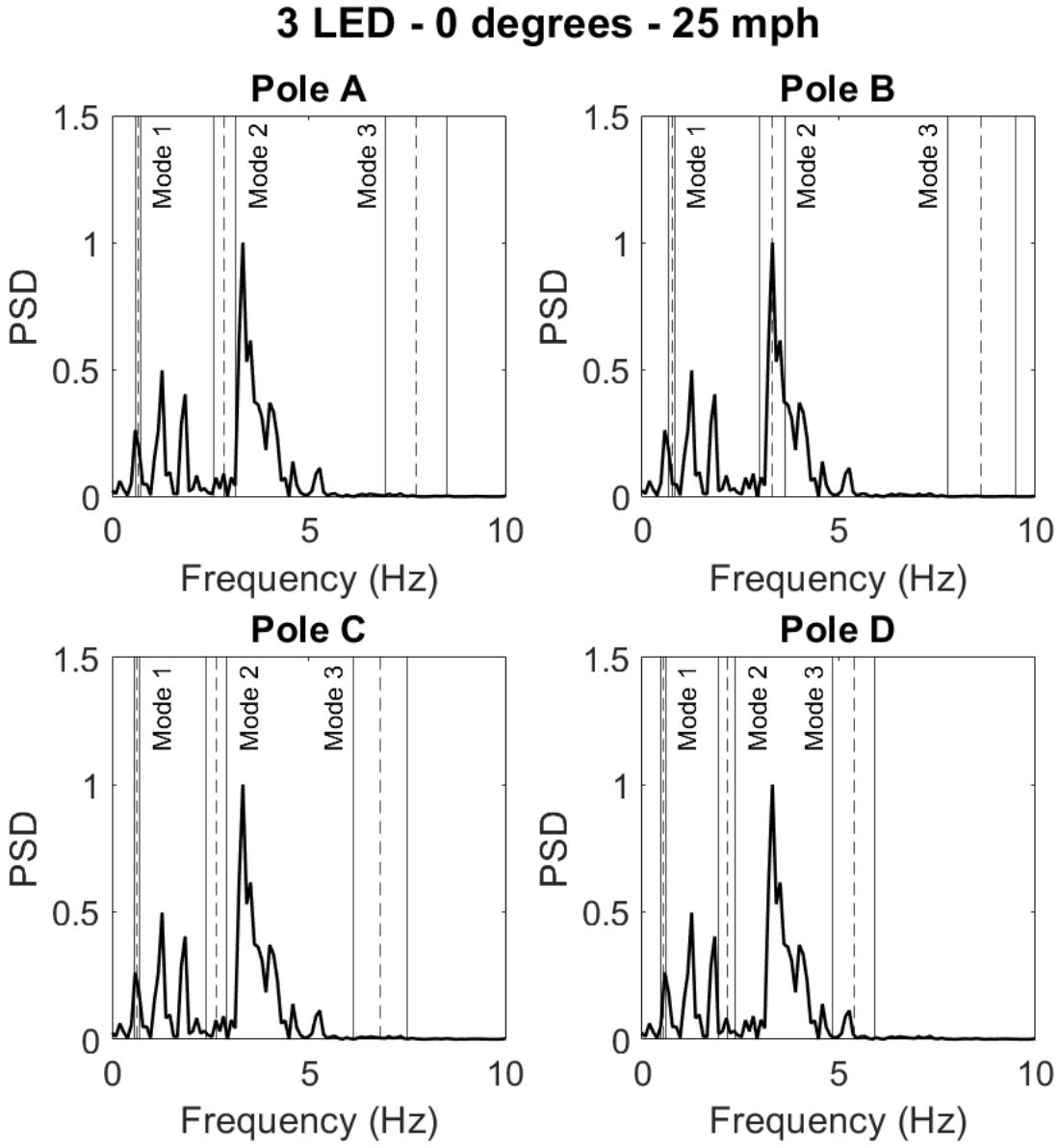

Figure B.2: PSDs for Pole A, B, C, and D for 3-LED Light Fixture Subjected to 25 mph Wind at an Angle of 0 Degrees

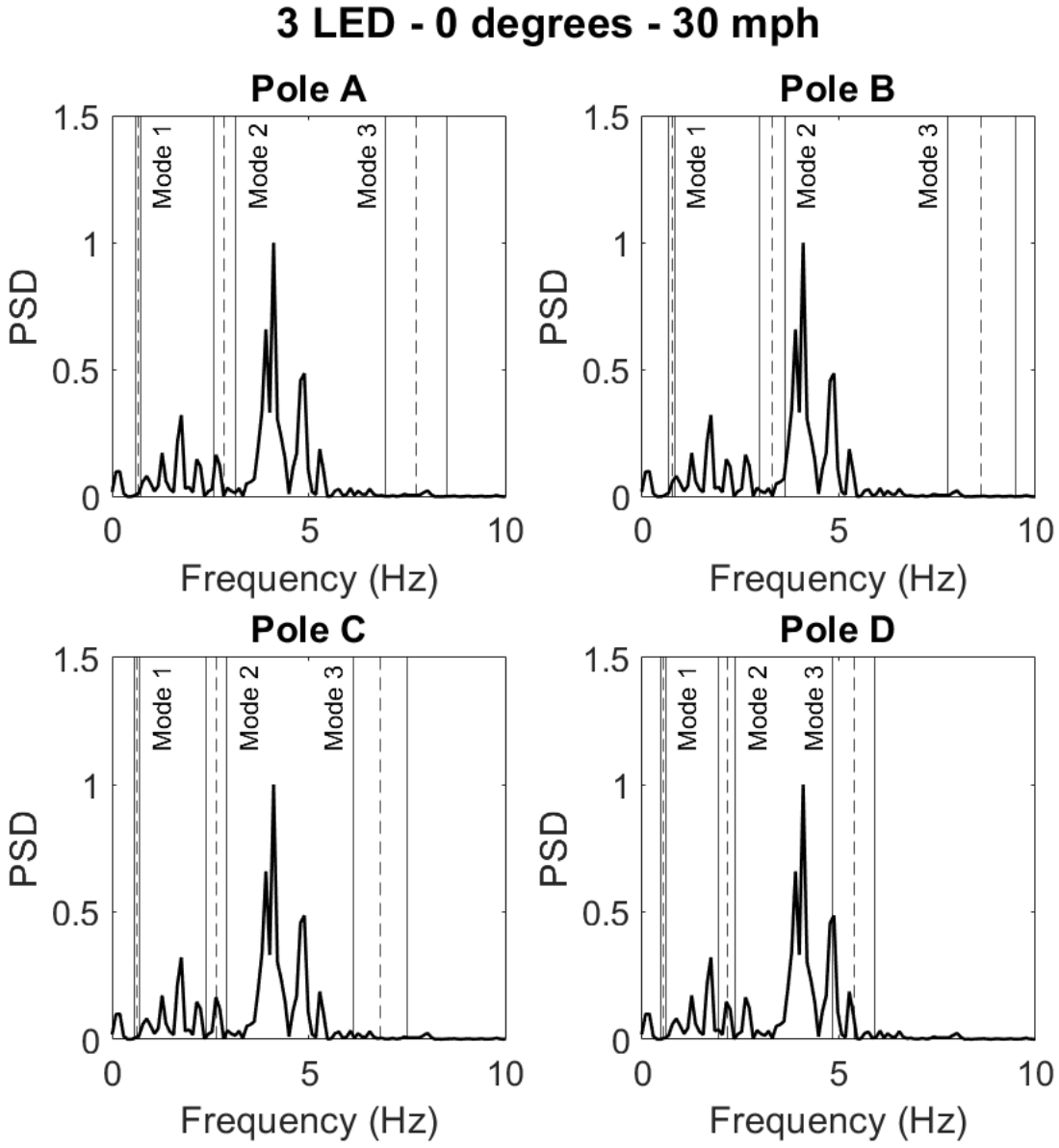

Figure B.3: PSDs for Pole A, B, C, and D for 3-LED Light Fixture Subjected to 30 mph Wind at an Angle of 0 Degrees

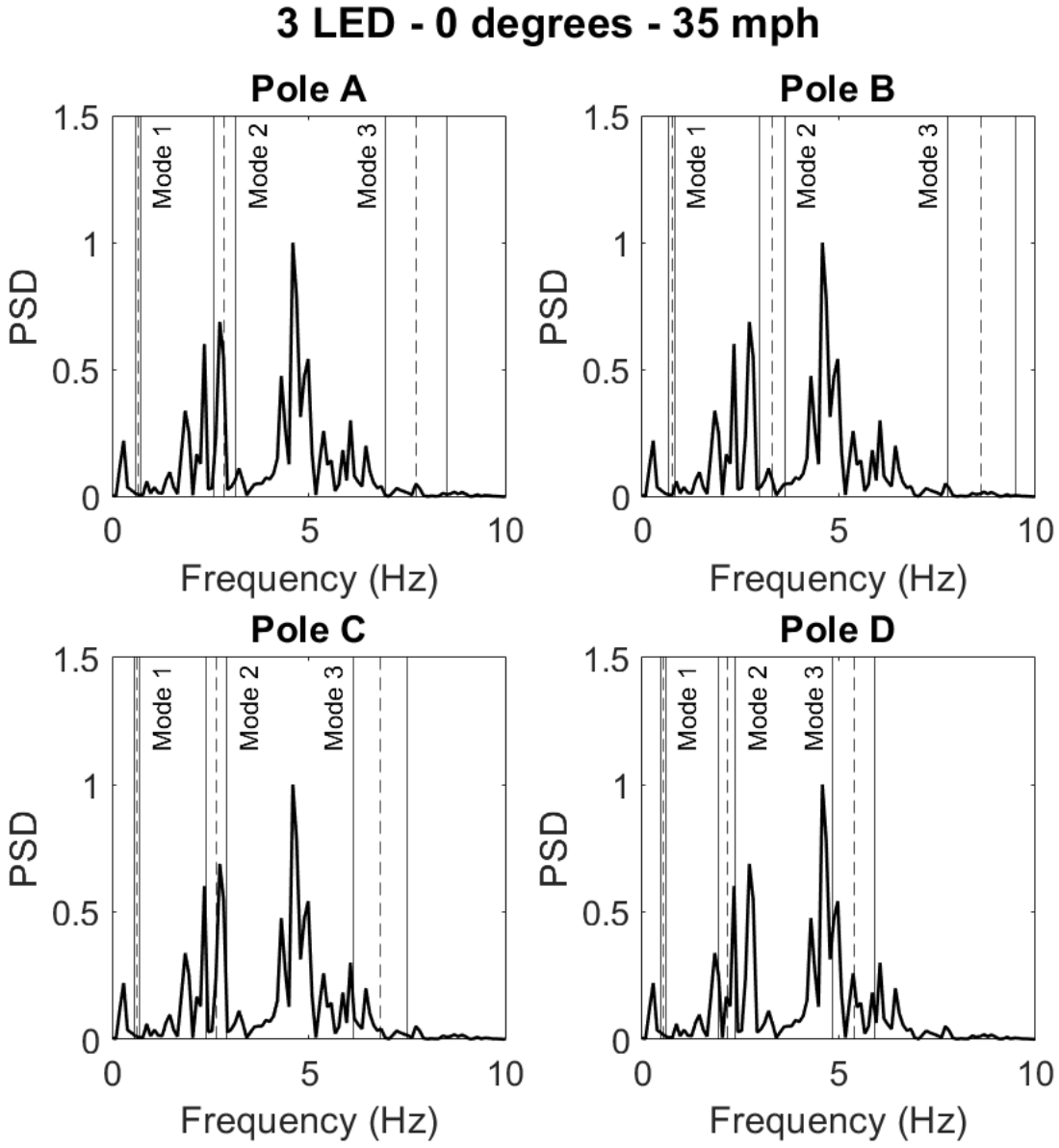

Figure B.4: PSDs for Pole A, B, C, and D for 3-LED Light Fixture Subjected to 35 mph Wind at an Angle of 0 Degrees

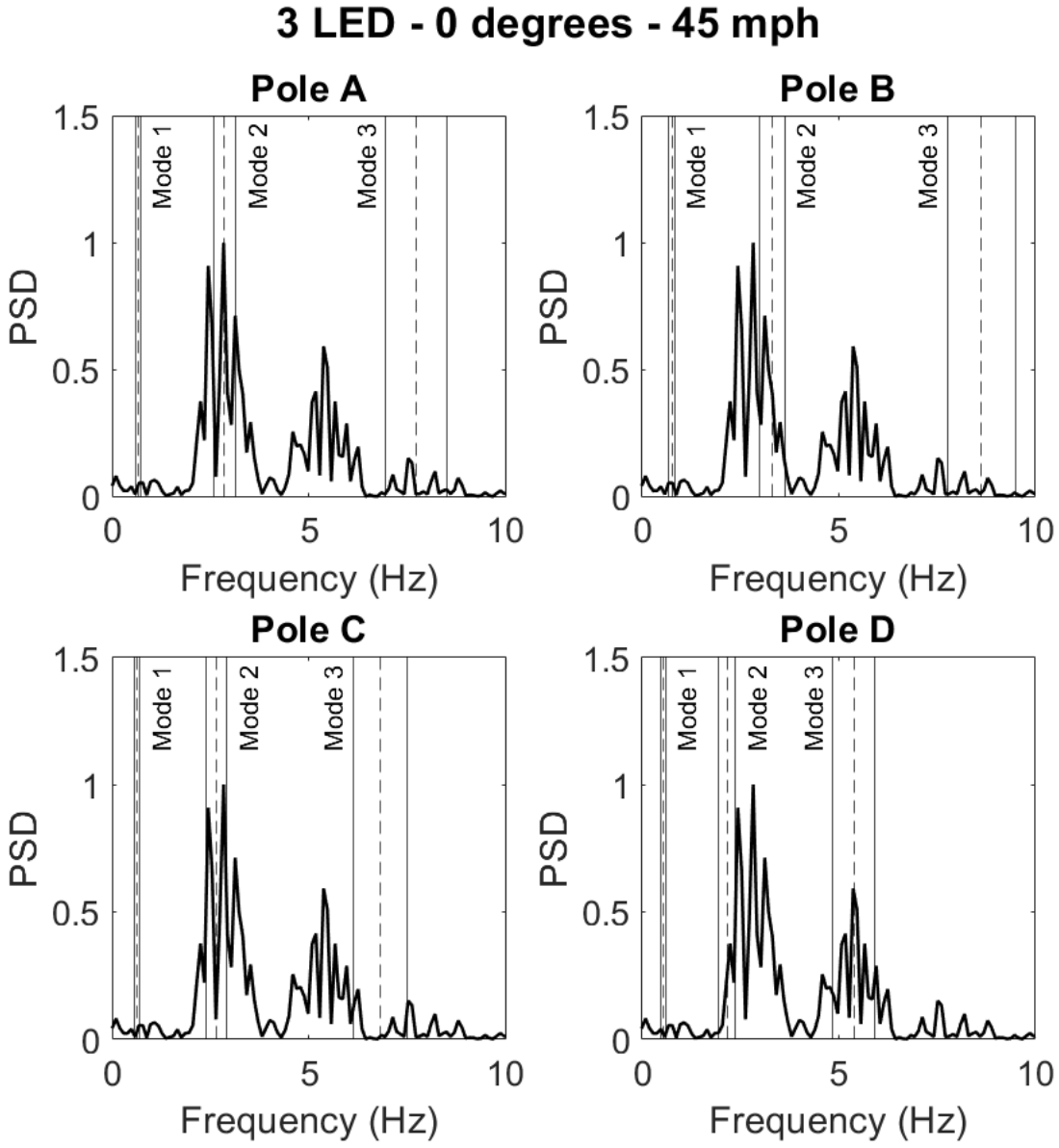

Figure B.5: PSDs for Pole A, B, C, and D for 3-LED Light Fixture Subjected to 45 mph Wind at an Angle of 0 Degrees

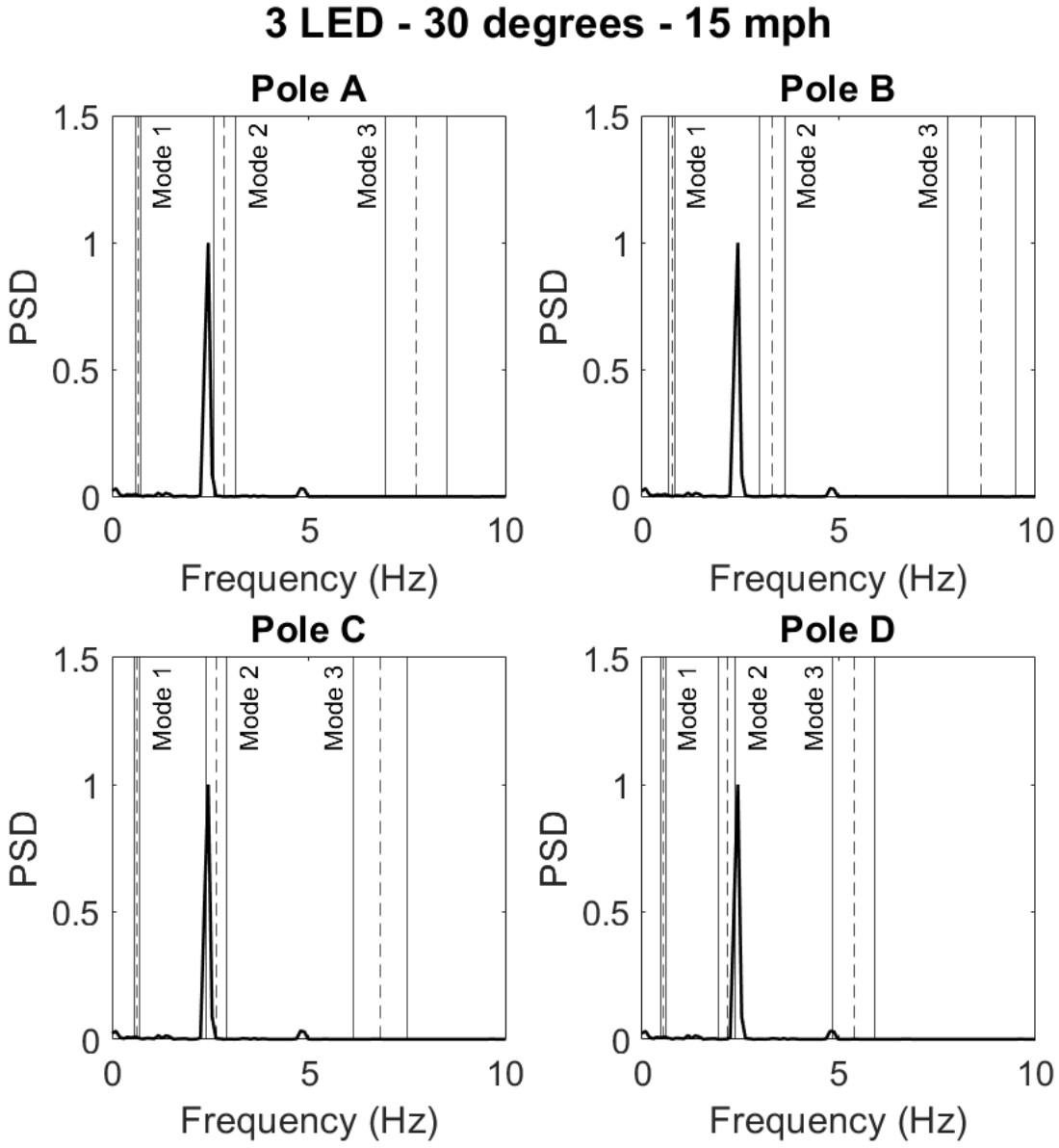

Figure B.6: PSDs for Pole A, B, C, and D for 3-LED Light Fixture Subjected to 15 mph Wind at an Angle of 30 Degrees

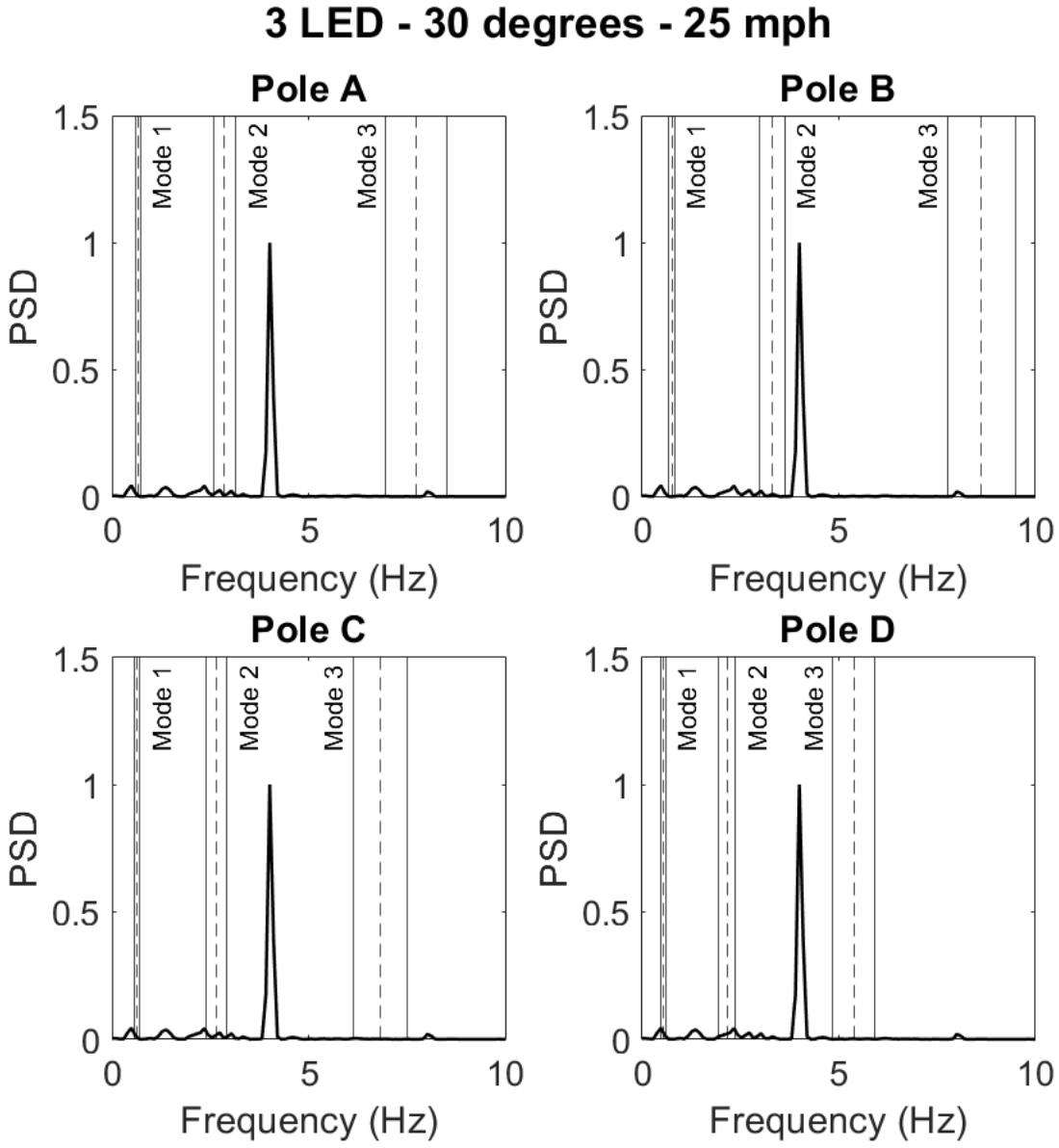

Figure B.7: PSDs for Pole A, B, C, and D for 3-LED Light Fixture Subjected to 25 mph Wind at an Angle of 30 Degrees

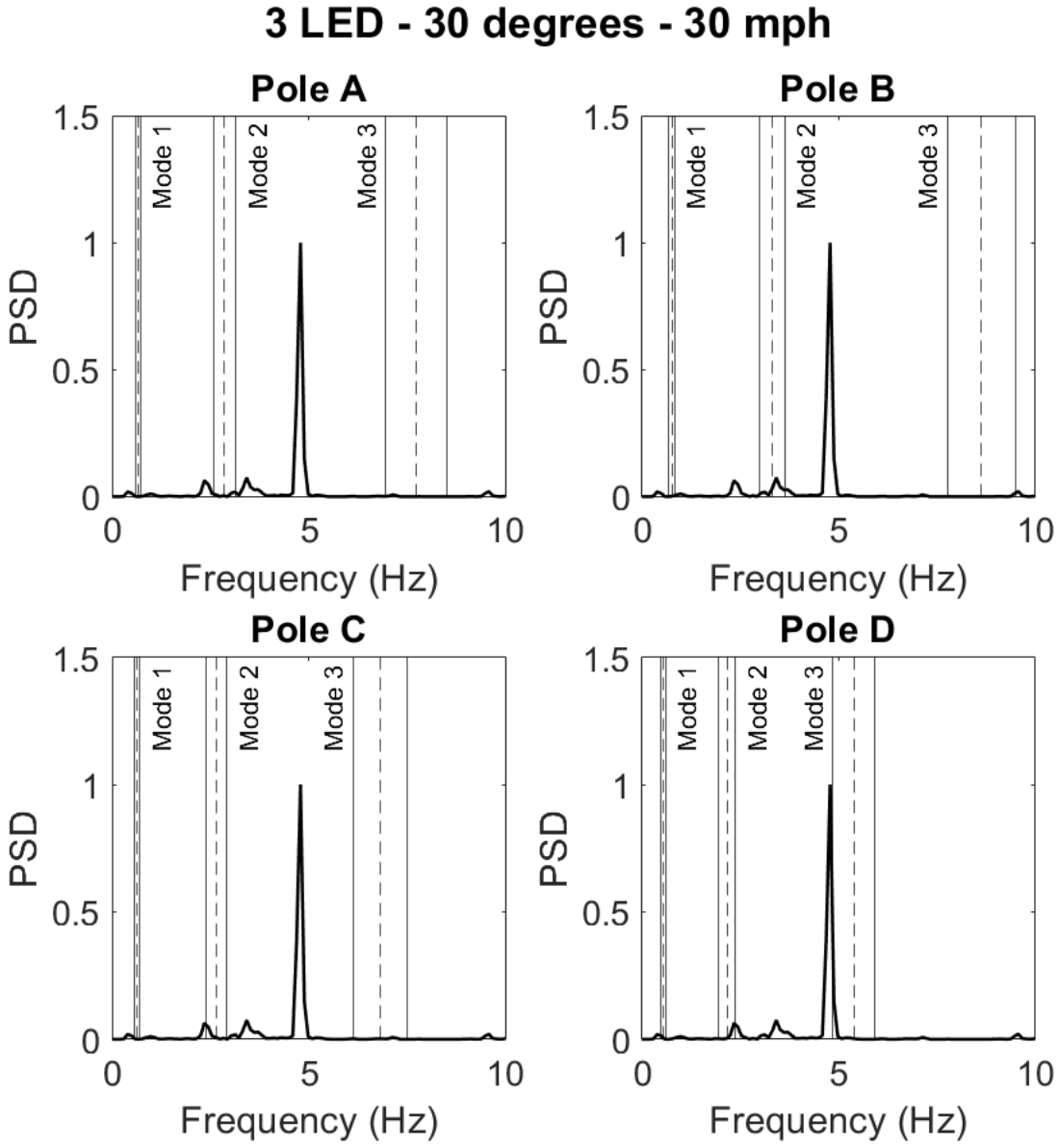

Figure B.8: PSDs for Pole A, B, C, and D for 3-LED Light Fixture Subjected to 30 mph Wind at an Angle of 30 Degrees

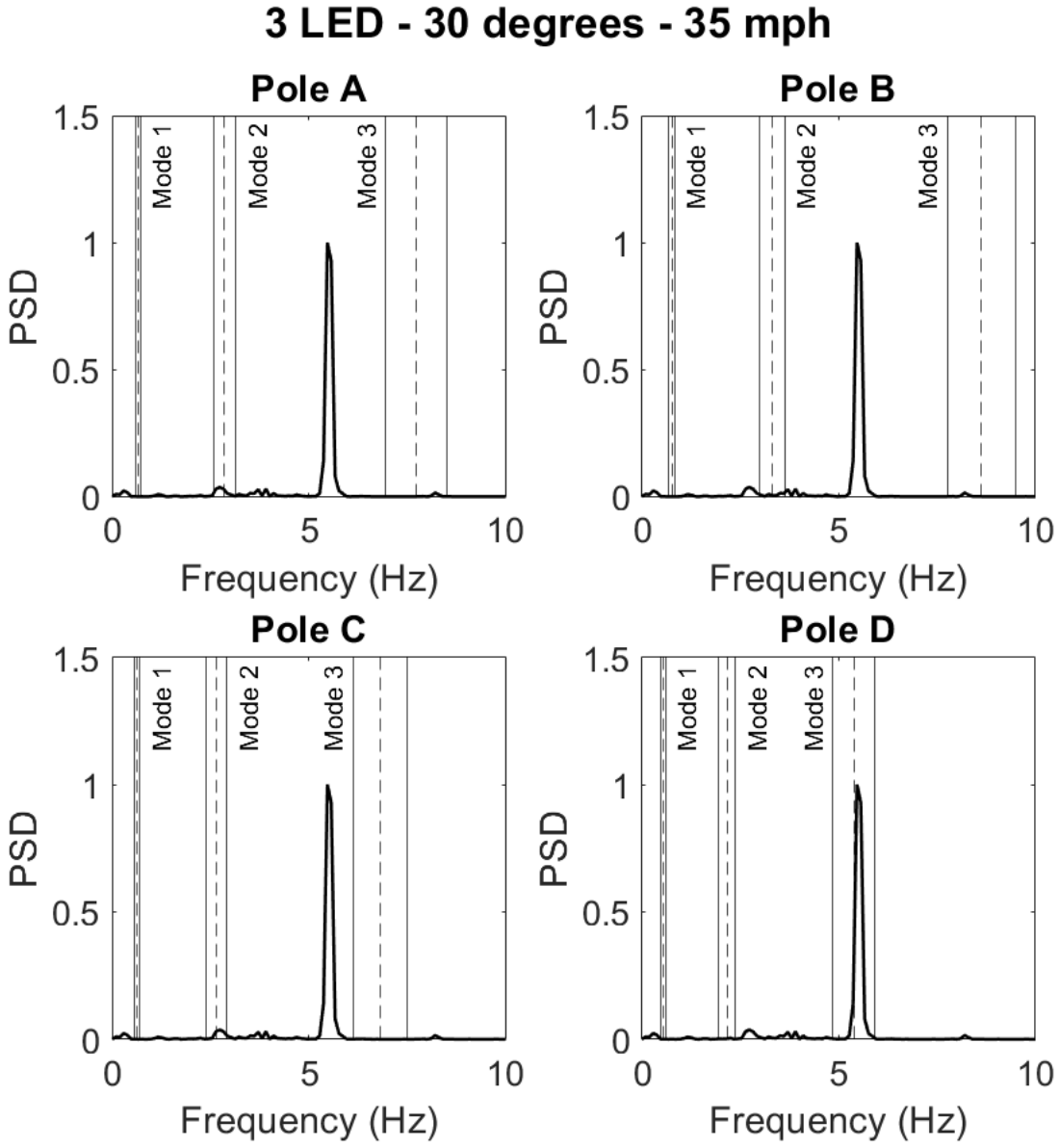

Figure B.9: PSDs for Pole A, B, C, and D for 3-LED Light Fixture Subjected to 35 mph Wind at an Angle of 30 Degrees

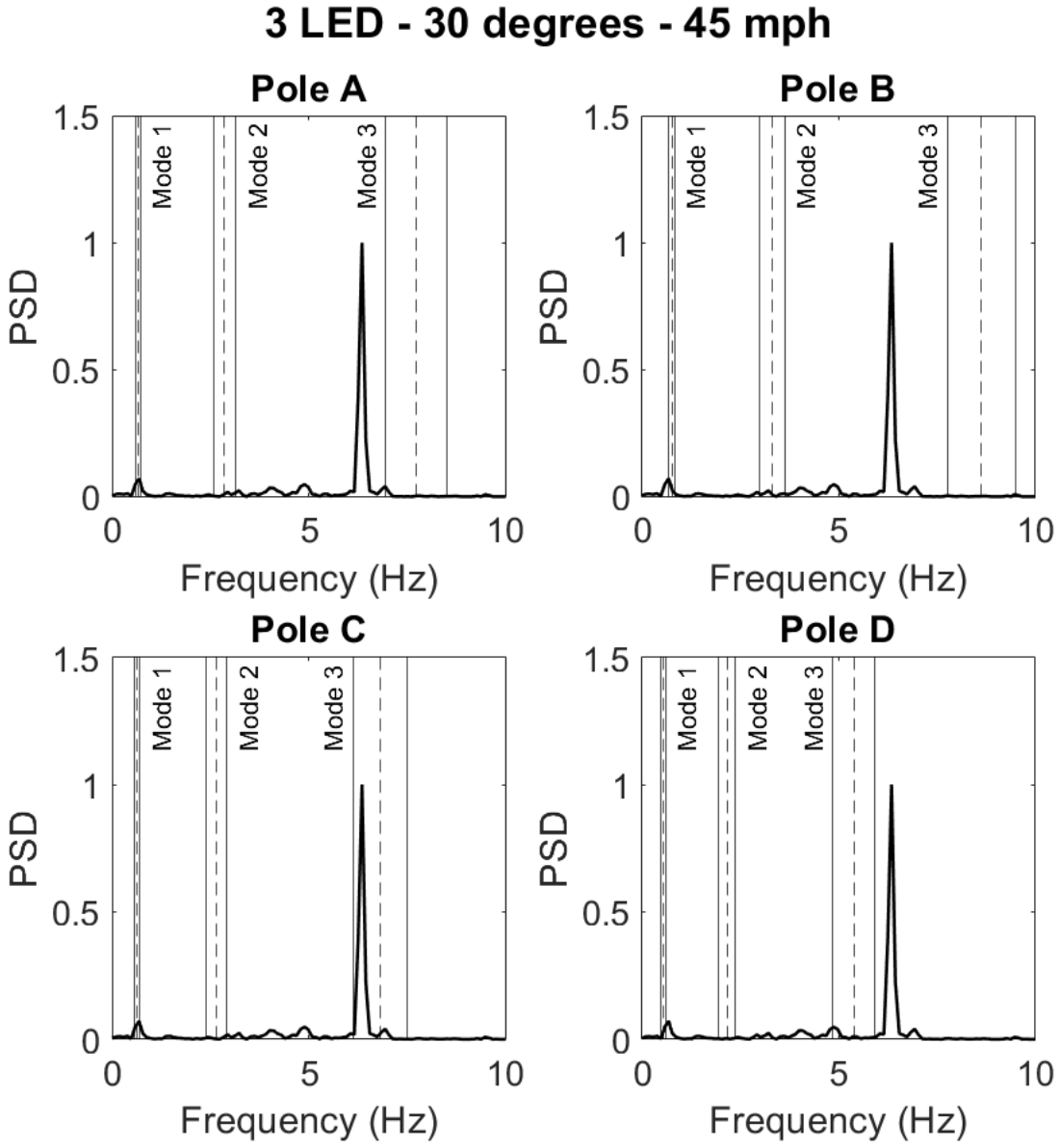

Figure B.10: PSDs for Pole A, B, C, and D for 3-LED Light Fixture Subjected to 45 mph Wind at an Angle of 30 Degrees

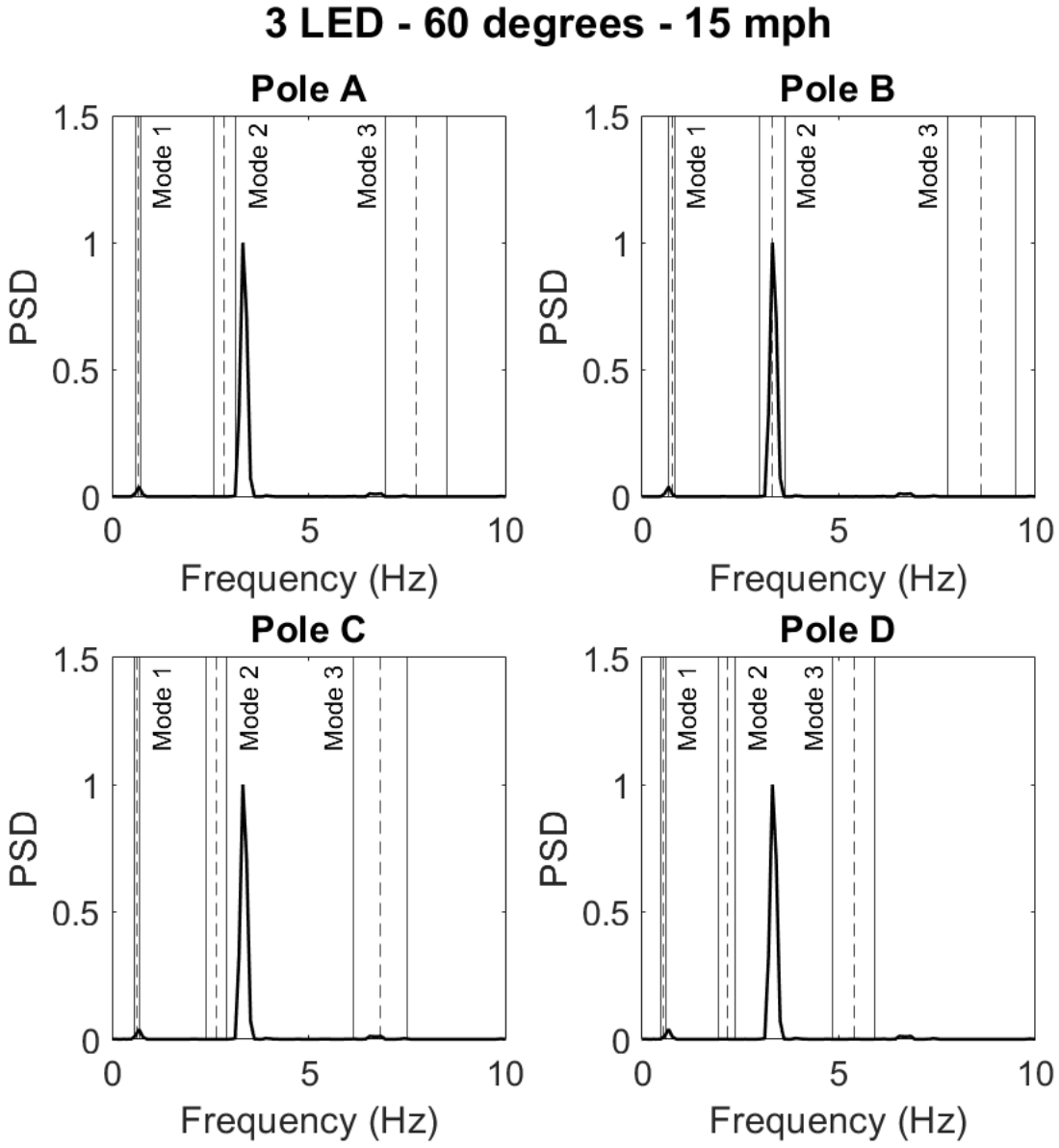

Figure B.11: PSDs for Pole A, B, C, and D for 3-LED Light Fixture Subjected to 15 mph Wind at an Angle of 60 Degrees

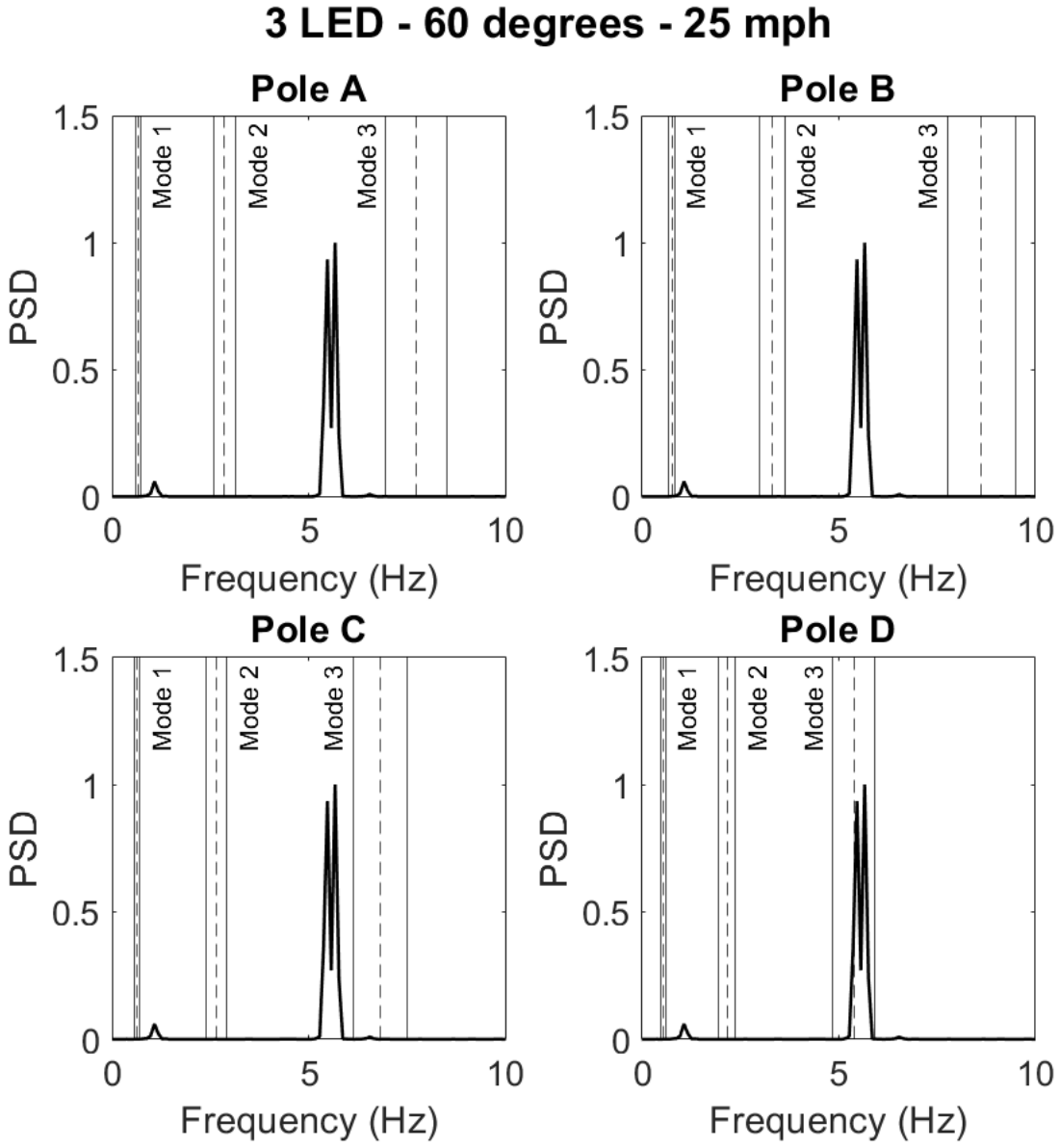

Figure B.12: PSDs for Pole A, B, C, and D for 3-LED Light Fixture Subjected to 25 mph Wind at an Angle of 60 Degrees

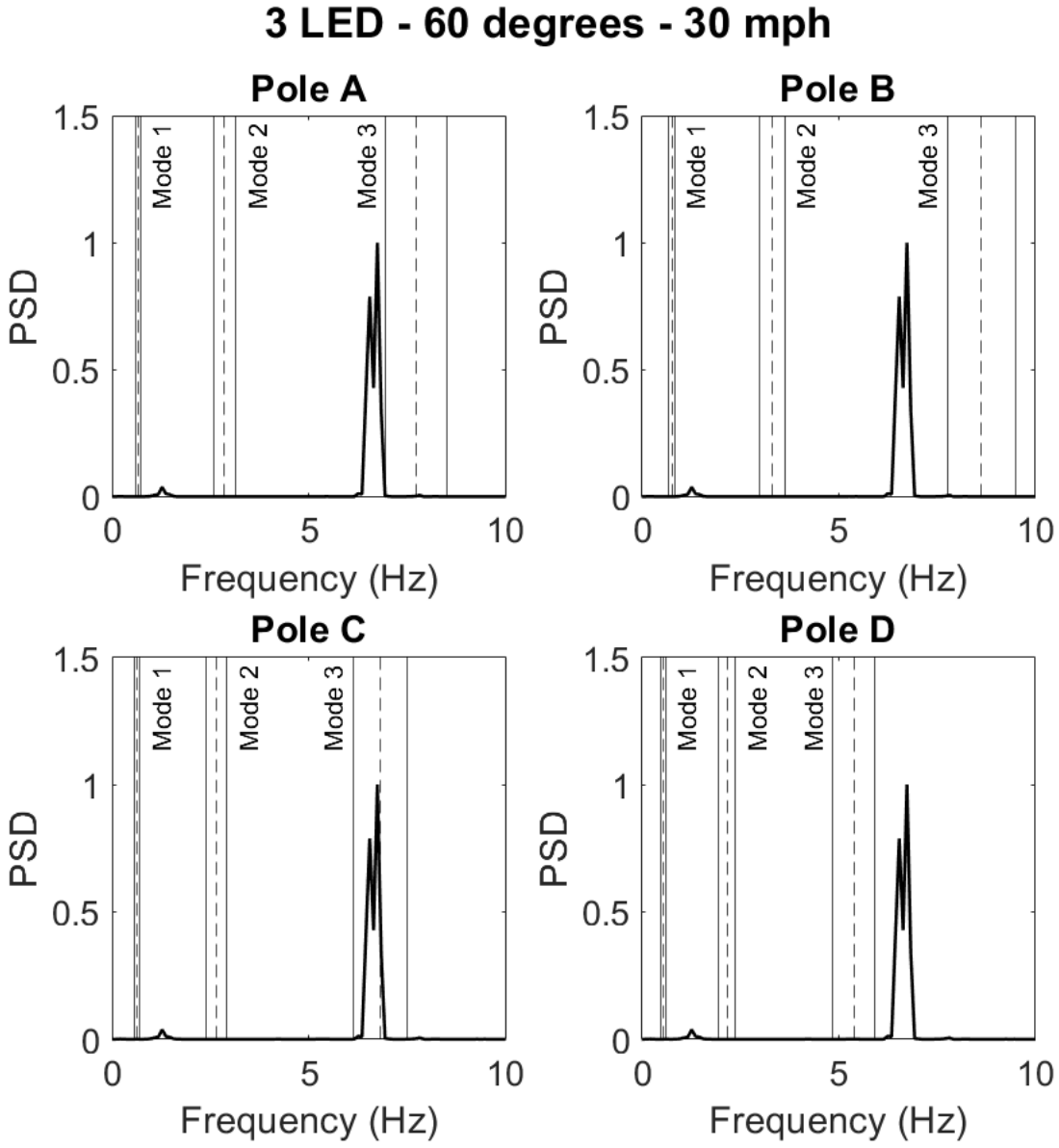

Figure B.13: PSDs for Pole A, B, C, and D for 3-LED Light Fixture Subjected to 30 mph Wind at an Angle of 60 Degrees

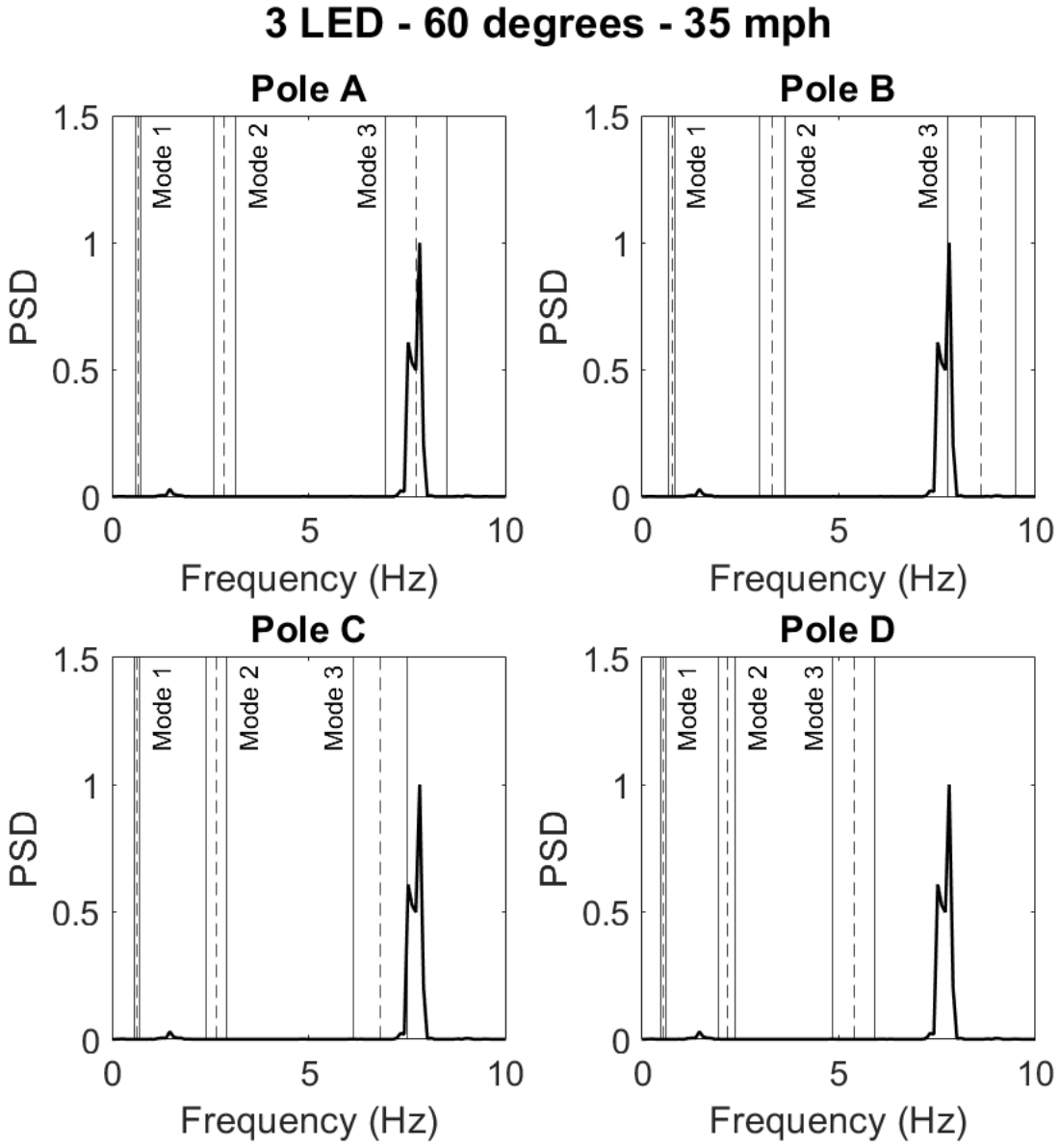

Figure B.14: PSDs for Pole A, B, C, and D for 3-LED Light Fixture Subjected to 35 mph Wind at an Angle of 60 Degrees

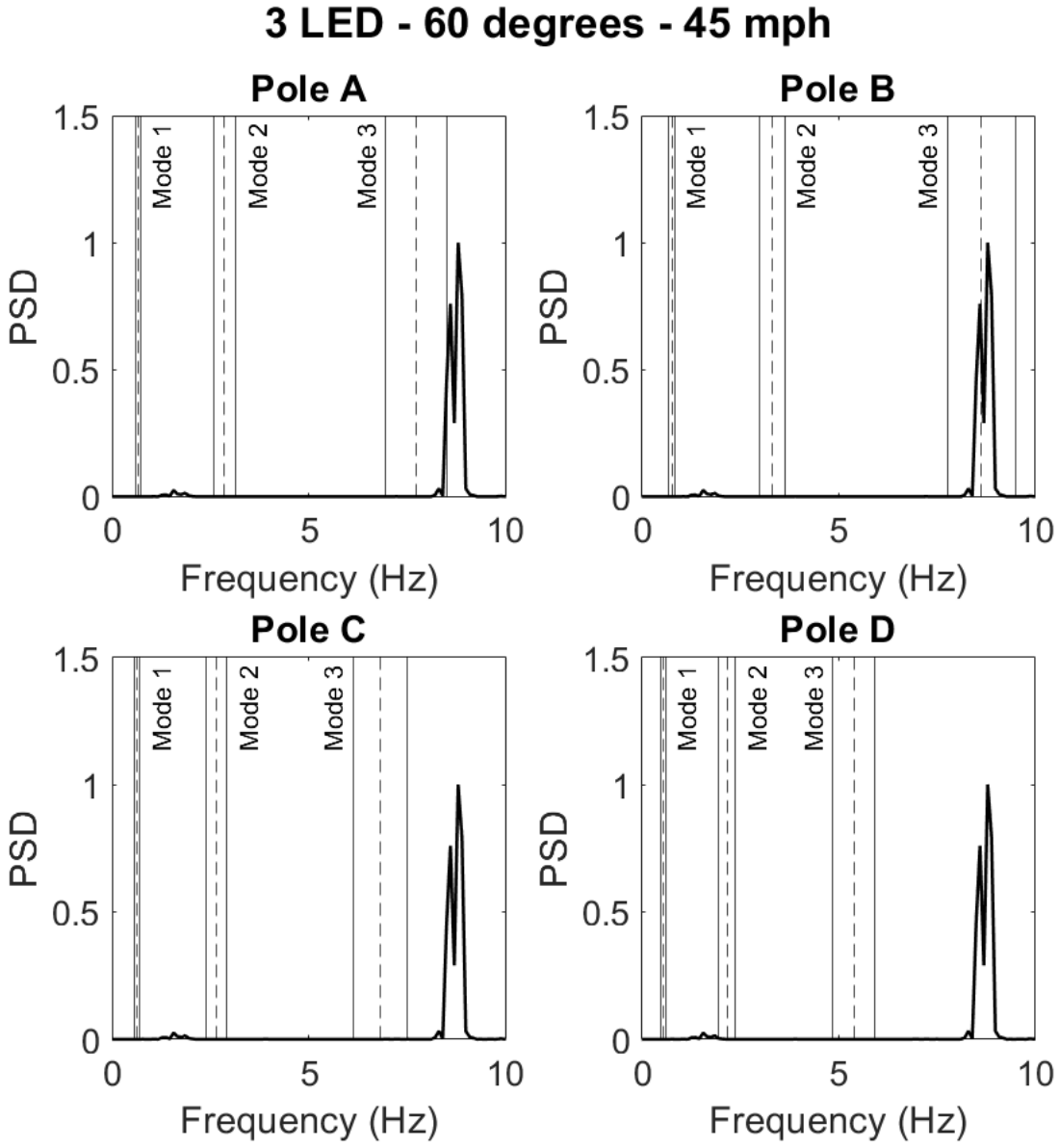

Figure B.15: PSDs for Pole A, B, C, and D for 3-LED Light Fixture Subjected to 45 mph Wind at an Angle of 60 Degrees

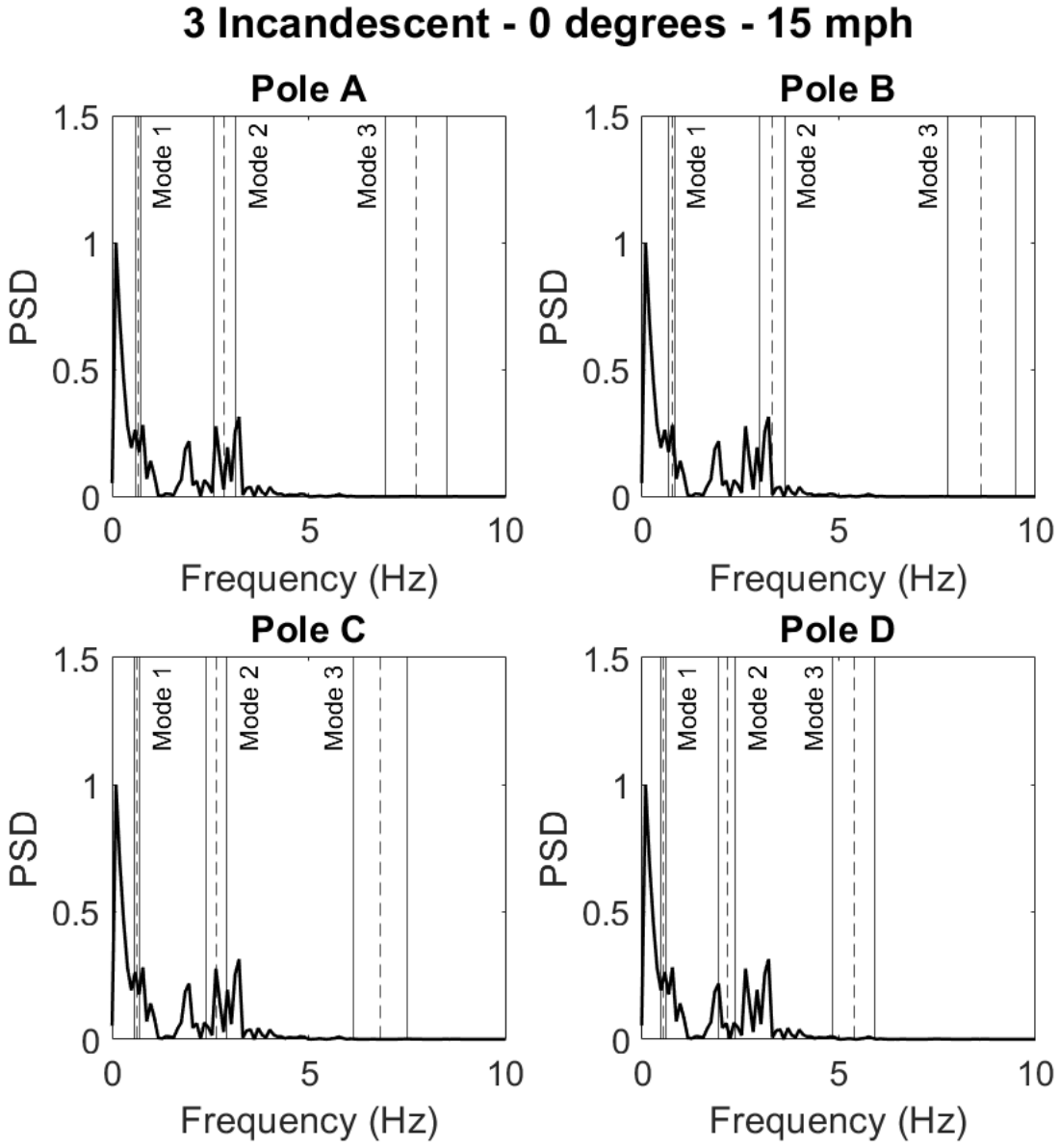

Figure B.16: PSDs for Pole A, B, C, and D for 3-Incandescent Light Fixture Subjected to 15 mph Wind at an Angle of 0 Degrees

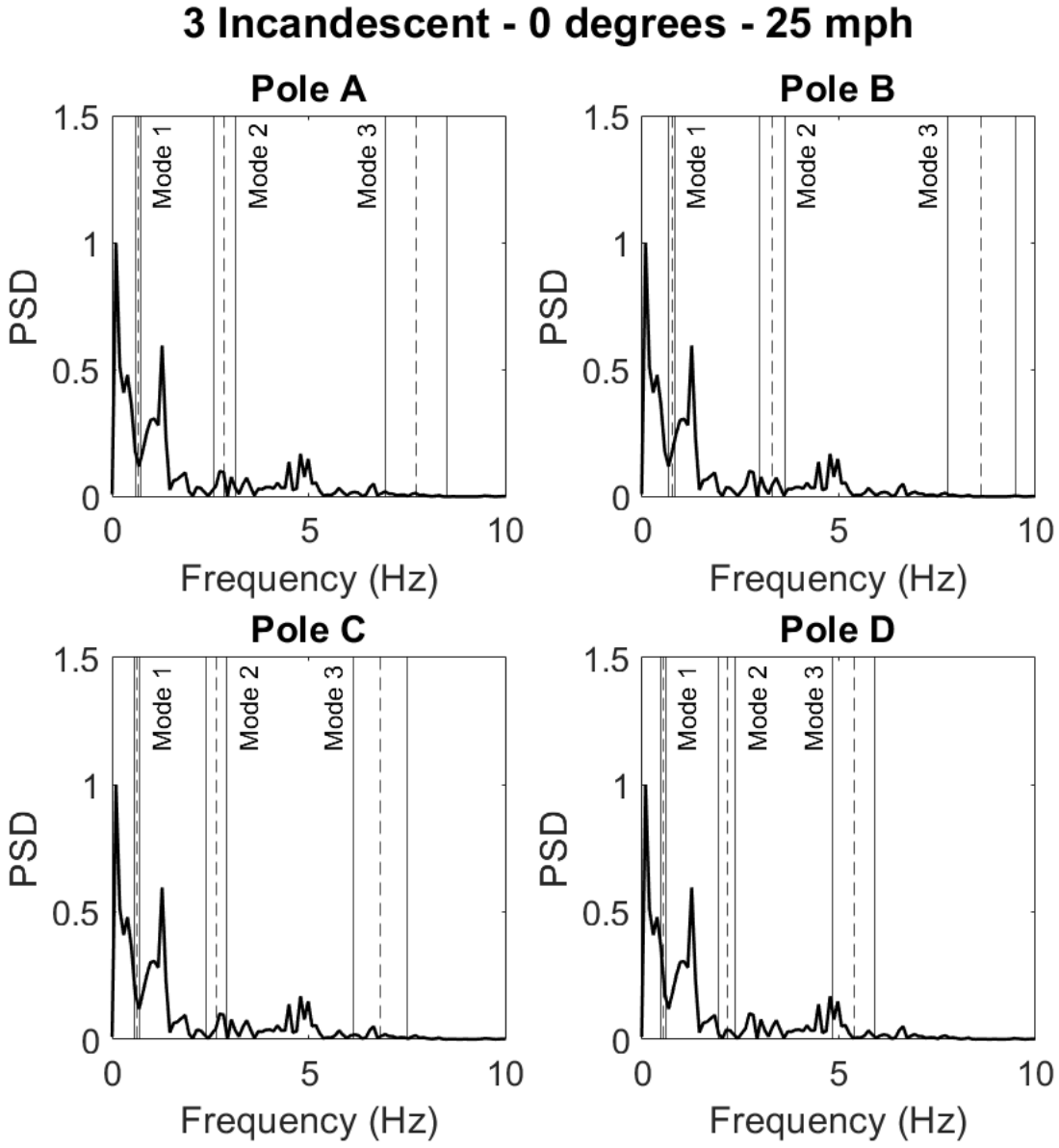

Figure B.17: PSDs for Pole A, B, C, and D for 3-Incandescent Light Fixture Subjected to 25 mph Wind at an Angle of 0 Degrees

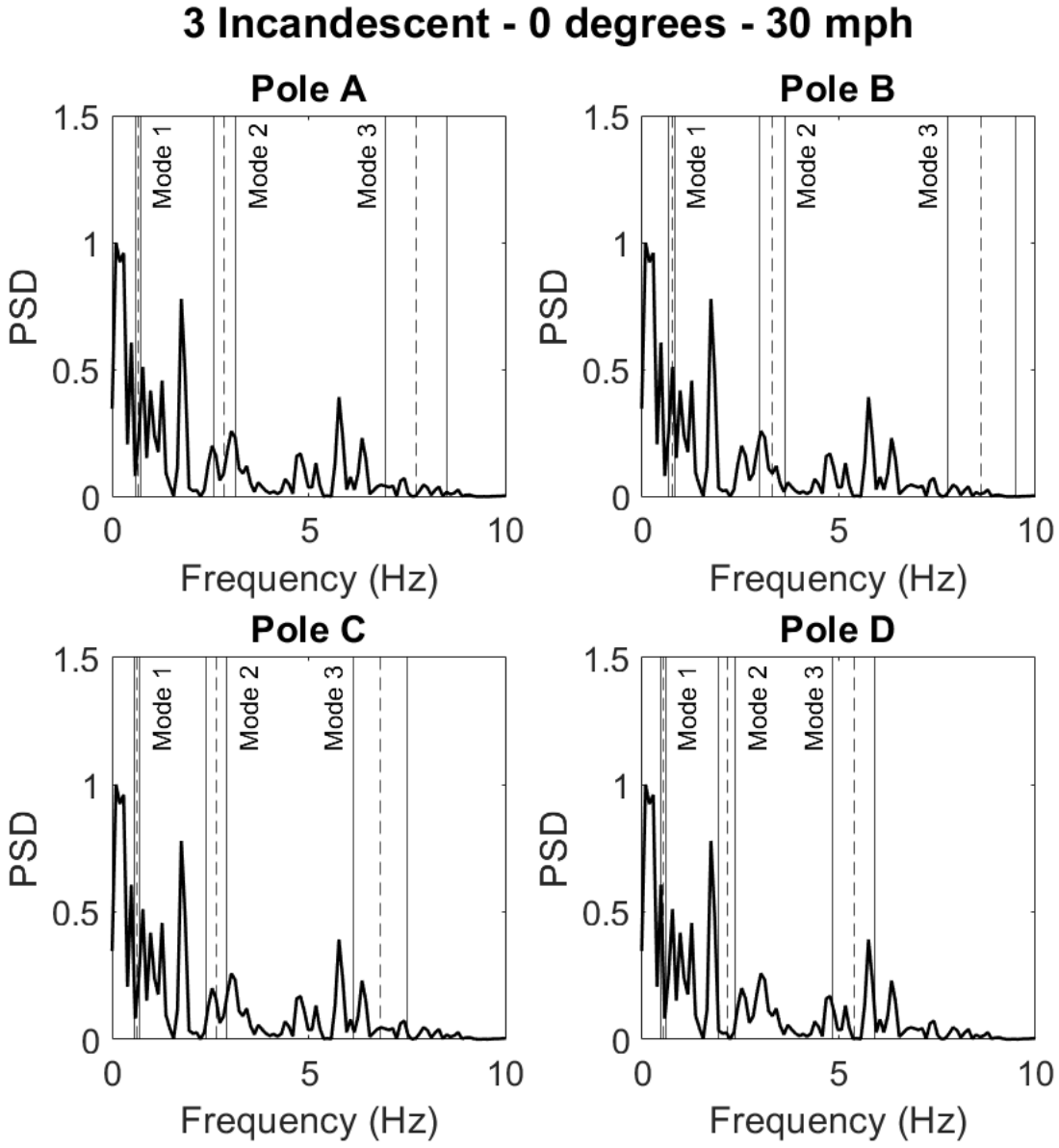

Figure B.18: PSDs for Pole A, B, C, and D for 3-Incandescent Light Fixture Subjected to 30 mph Wind at an Angle of 0 Degrees

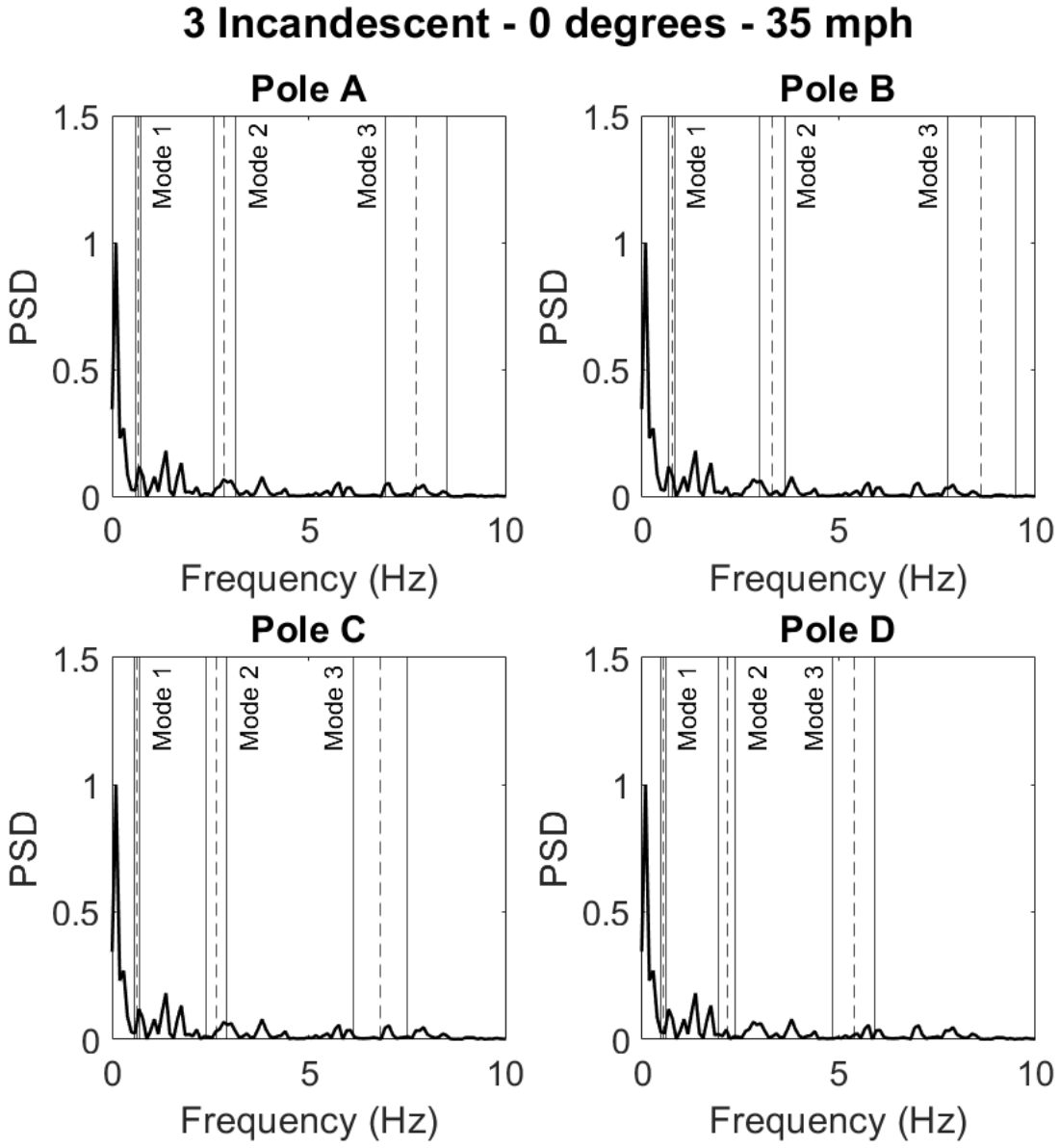

Figure B.19: PSDs for Pole A, B, C, and D for 3-Incandescent Light Fixture Subjected to 35 mph Wind at an Angle of 0 Degrees

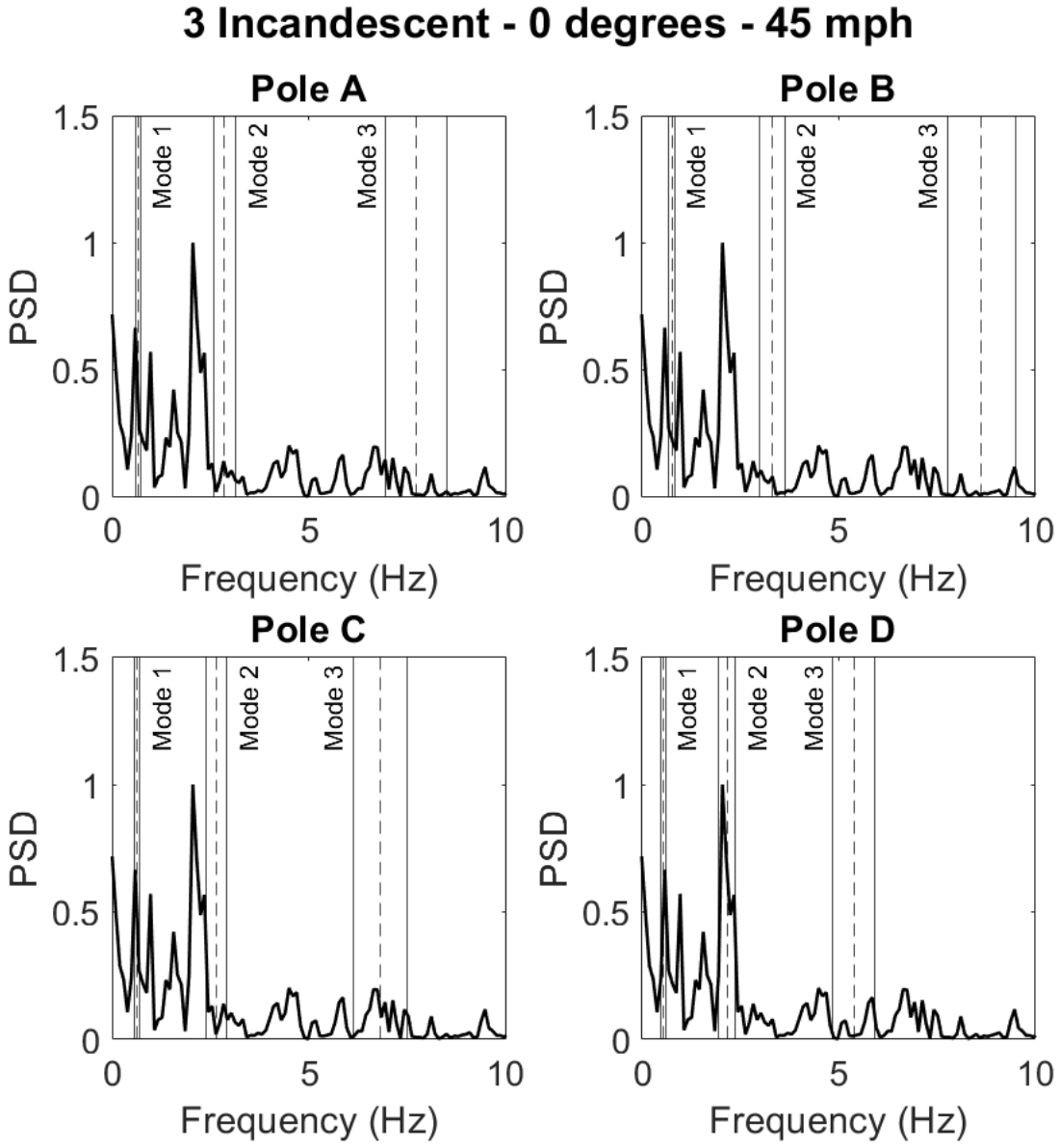

Figure B.20: PSDs for Pole A, B, C, and D for 3-Incandescent Light Fixture Subjected to 45 mph Wind at an Angle of 0 Degrees

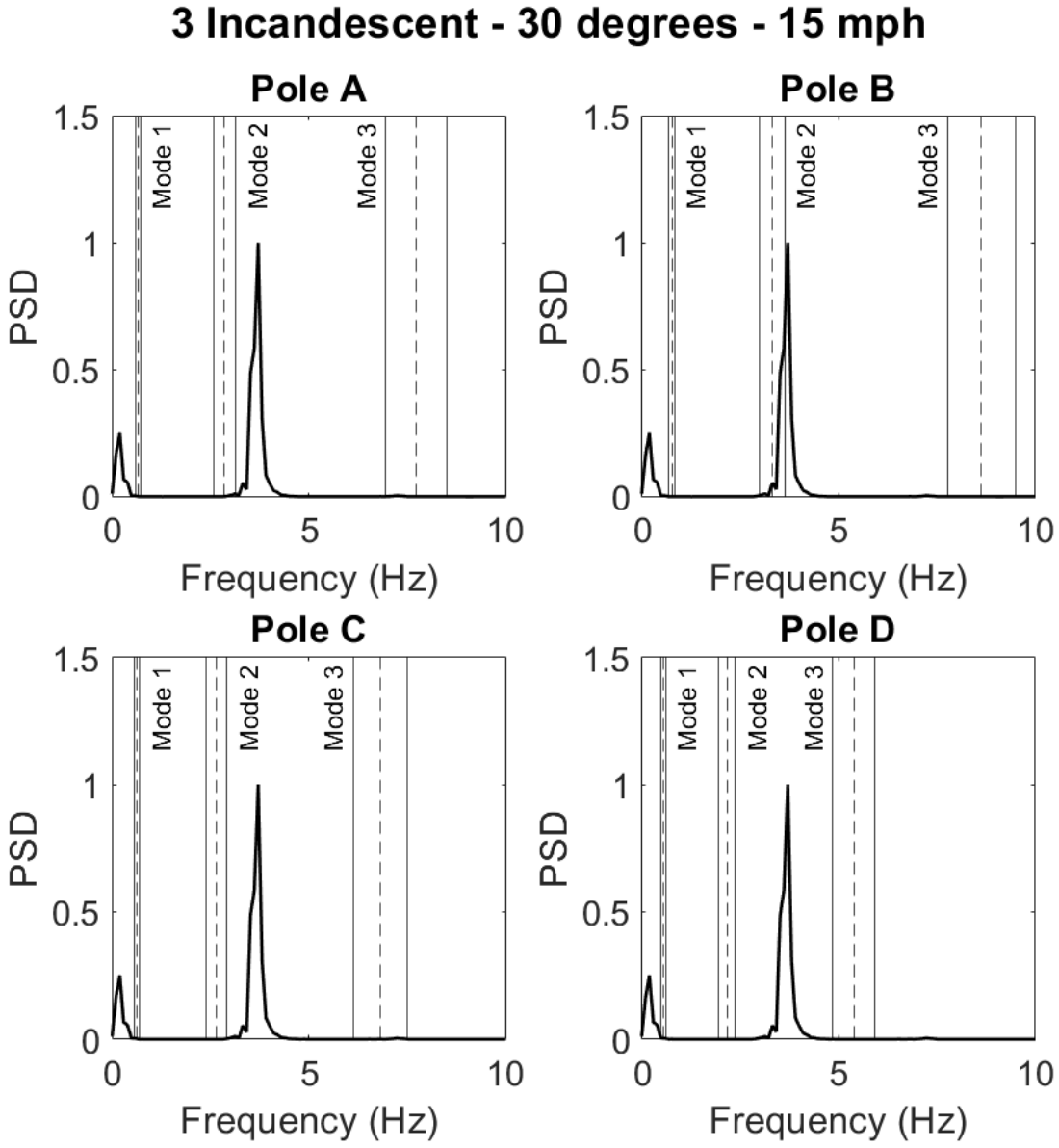

Figure B.21: PSDs for Pole A, B, C, and D for 3-Incandescent Light Fixture Subjected to 15 mph Wind at an Angle of 30 Degrees

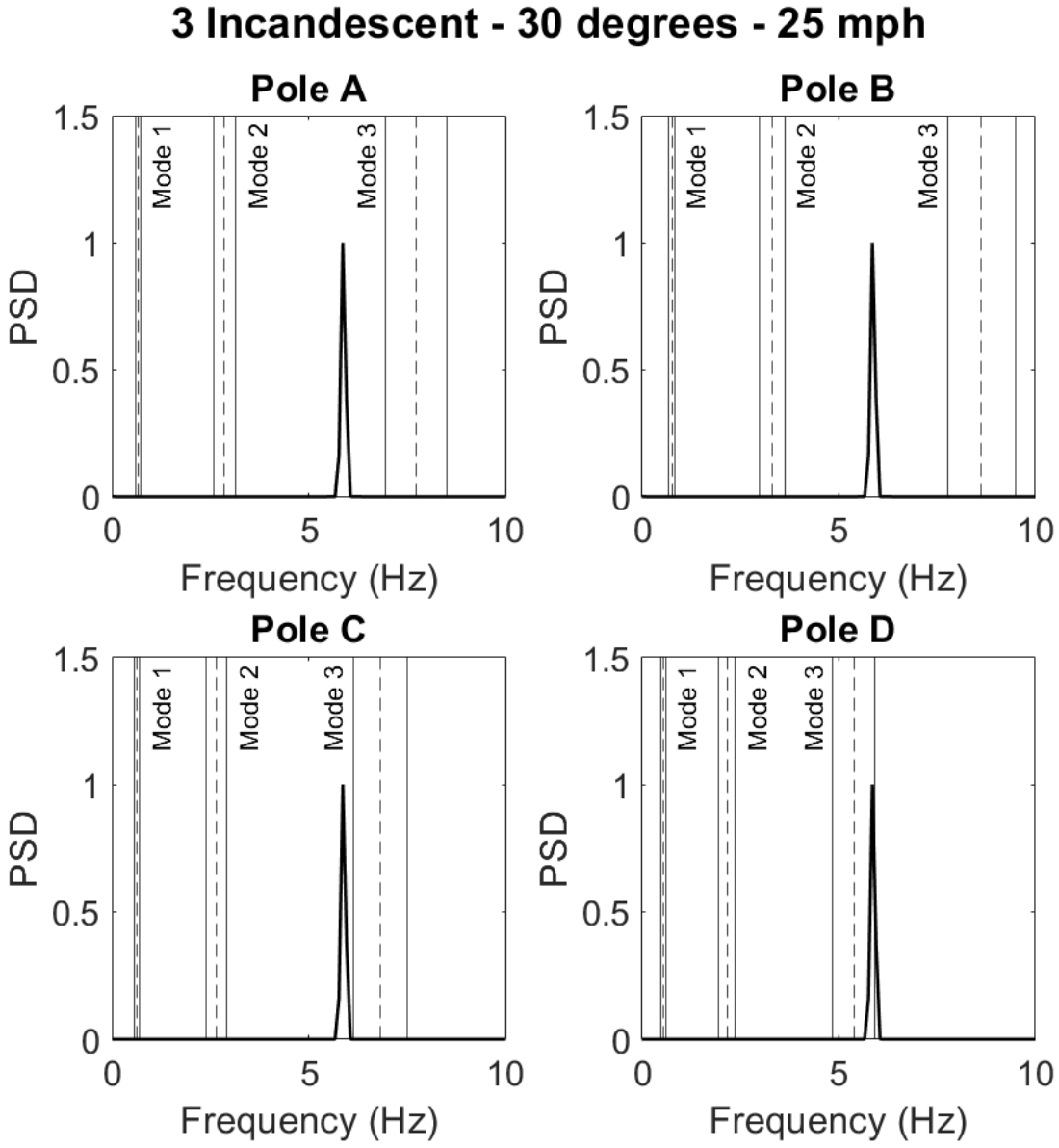

Figure B.22: PSDs for Pole A, B, C, and D for 3-Incandescent Light Fixture Subjected to 25 mph Wind at an Angle of 30 Degrees

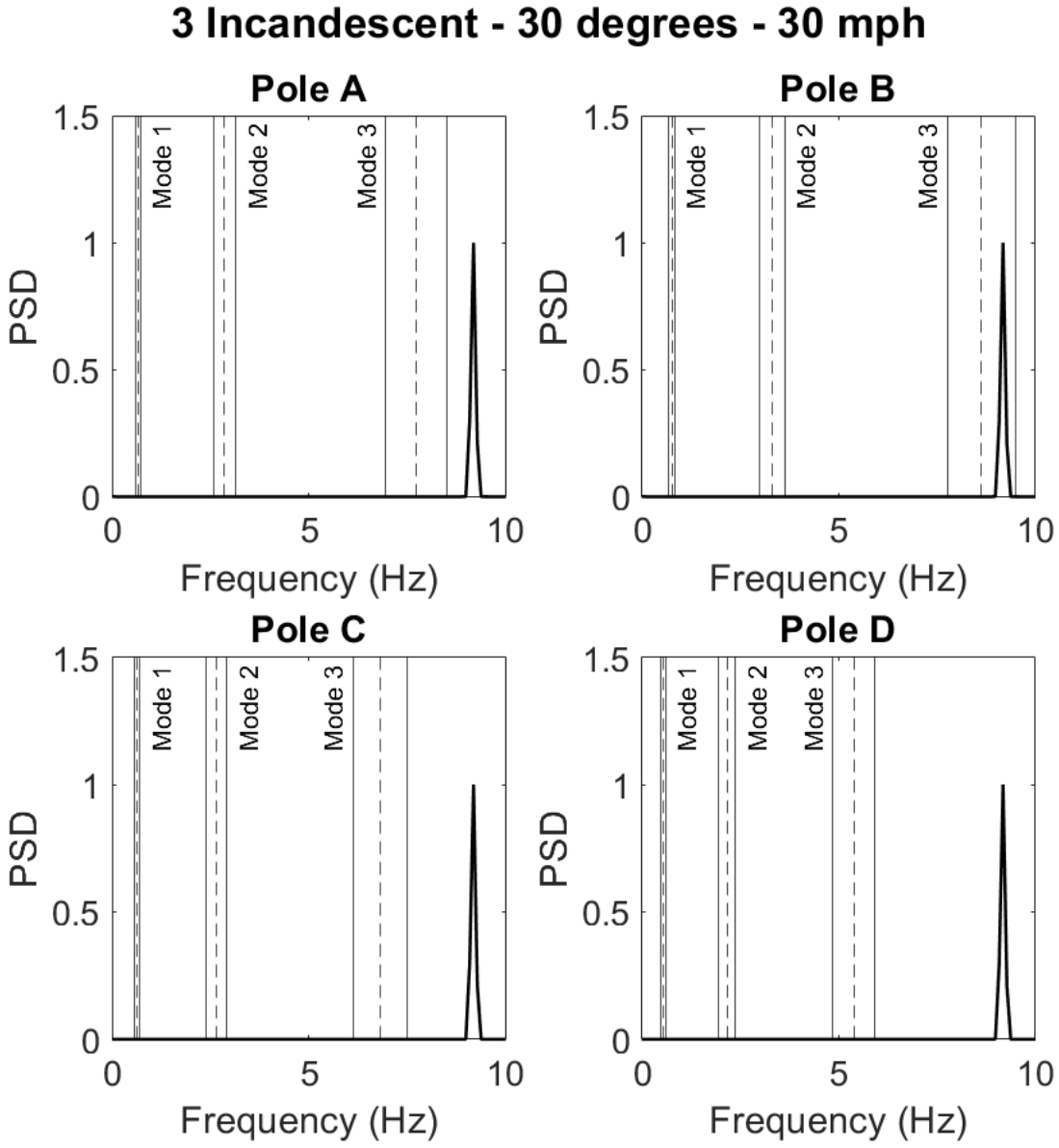

Figure B.23: PSDs for Pole A, B, C, and D for 3-Incandescent Light Fixture Subjected to 30 mph Wind at an Angle of 30 Degrees

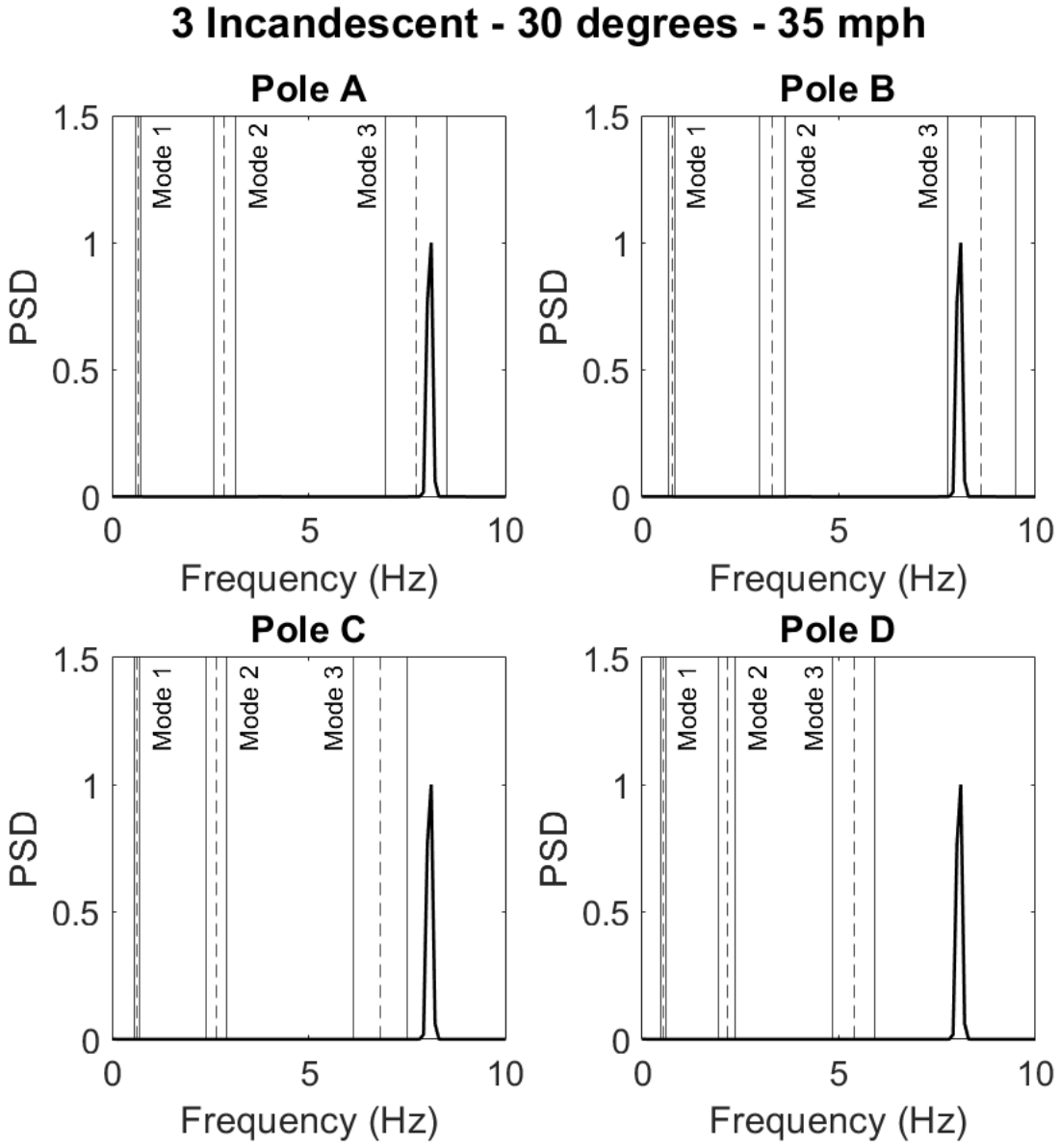

Figure B.24: PSDs for Pole A, B, C, and D for 3-Incandescent Light Fixture Subjected to 35 mph Wind at an Angle of 30 Degrees

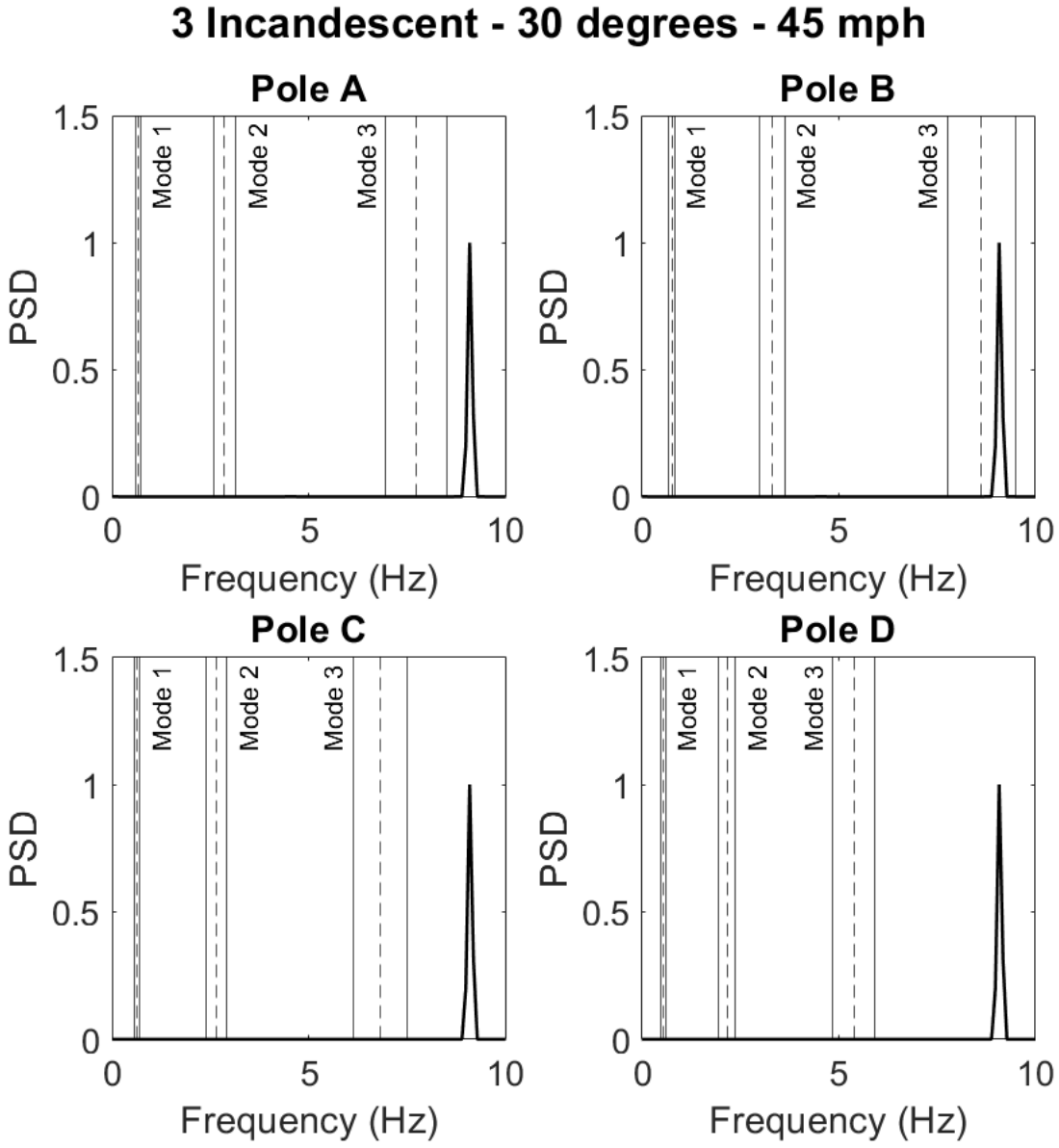

Figure B.25: PSDs for Pole A, B, C, and D for 3-Incandescent Light Fixture Subjected to 45 mph Wind at an Angle of 30 Degrees

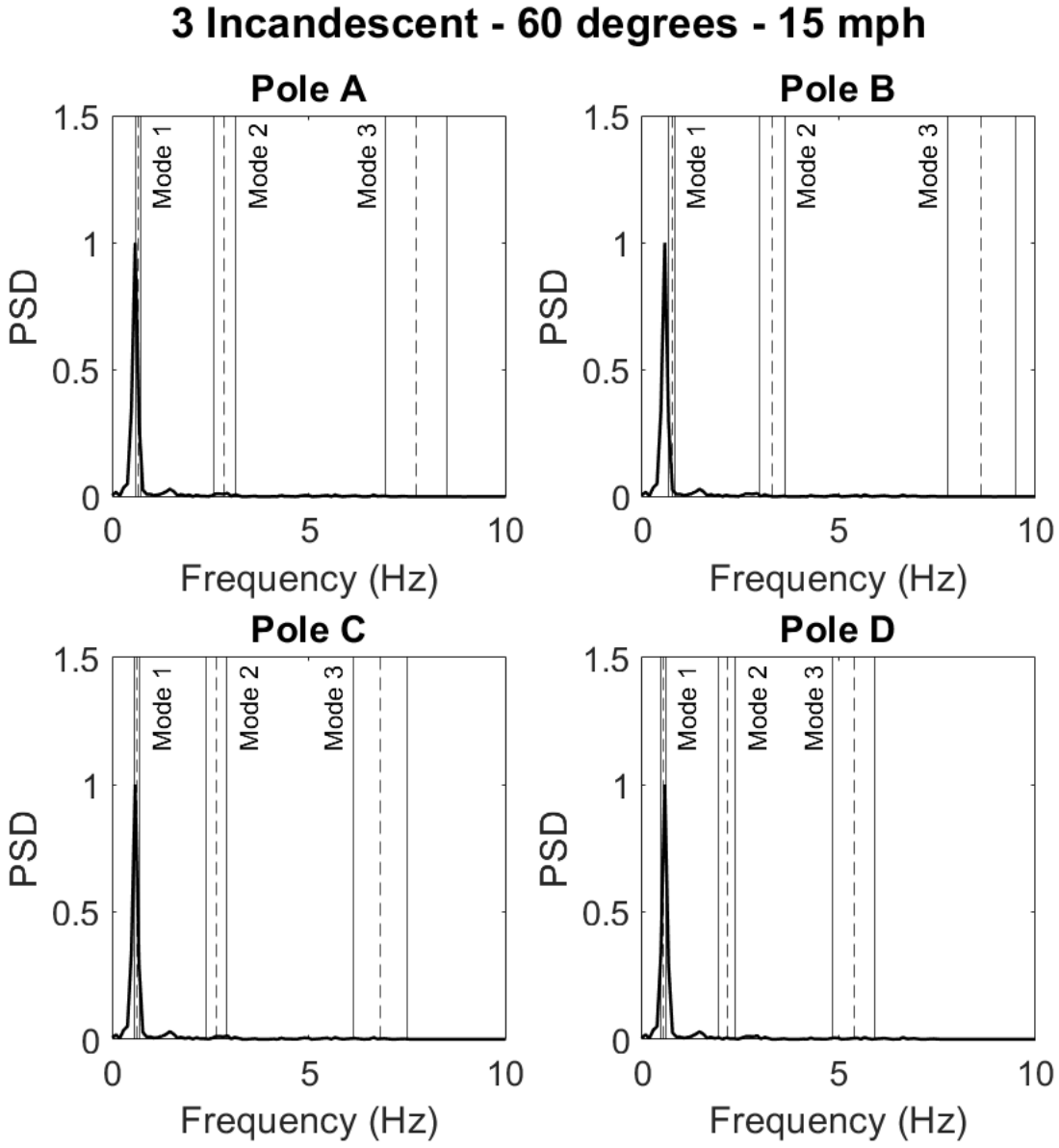

Figure B.26: PSDs for Pole A, B, C, and D for 3-Incandescent Light Fixture Subjected to 15 mph Wind at an Angle of 60 Degrees

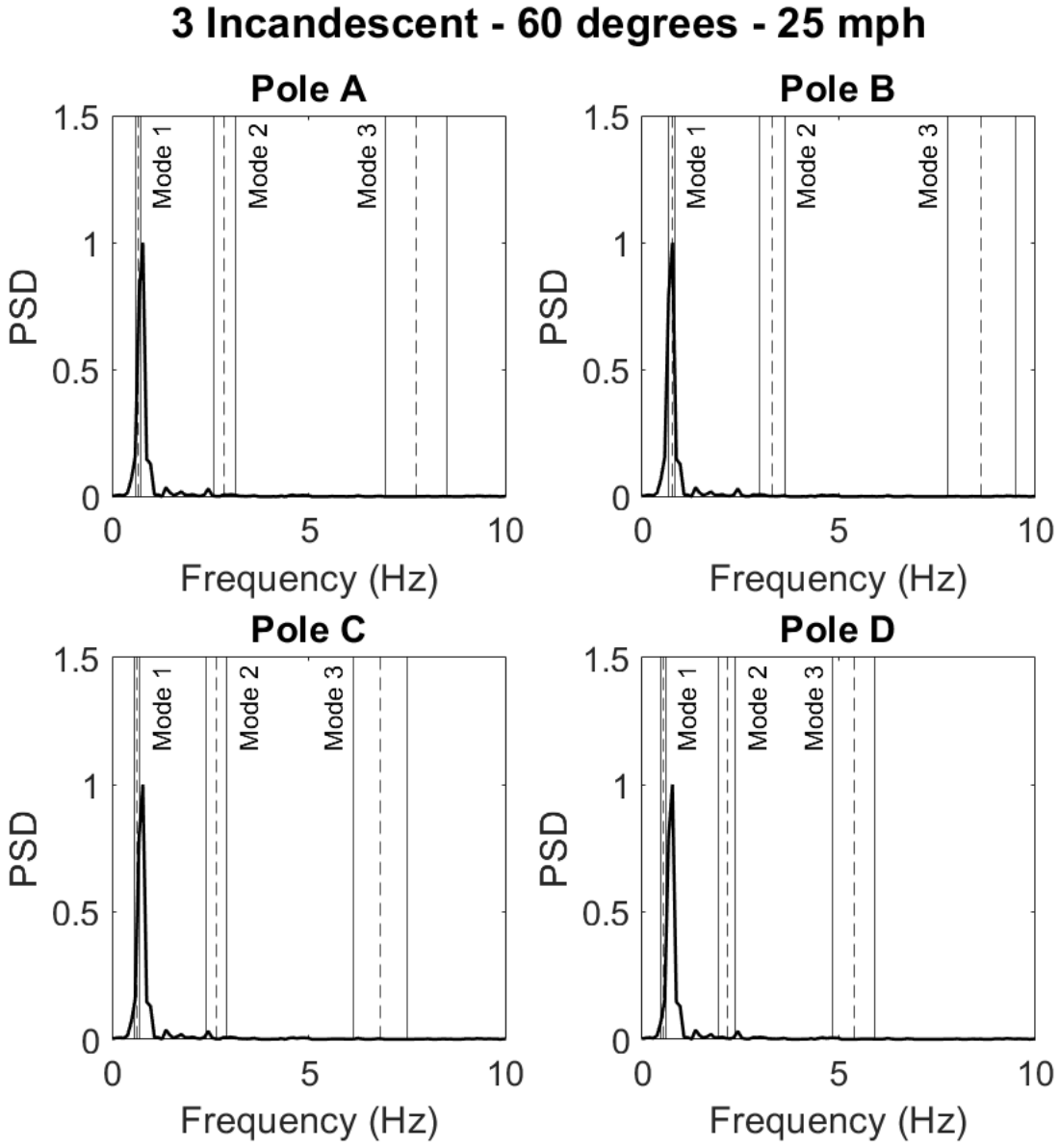

Figure B.27: PSDs for Pole A, B, C, and D for 3-Incandescent Light Fixture Subjected to 25 mph Wind at an Angle of 60 Degrees

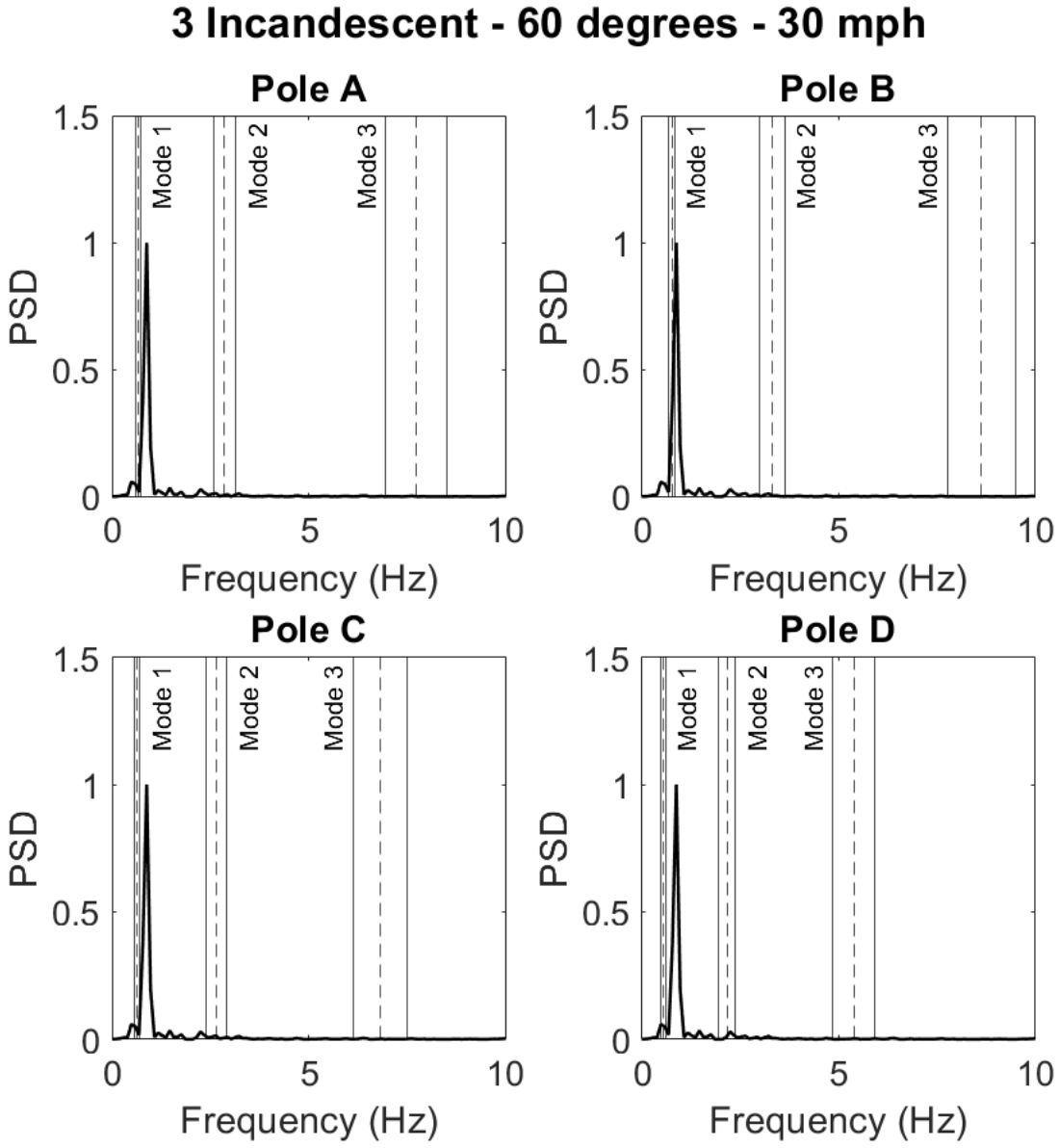

Figure B.28: PSDs for Pole A, B, C, and D for 3-Incandescent Light Fixture Subjected to 30 mph Wind at an Angle of 60 Degrees

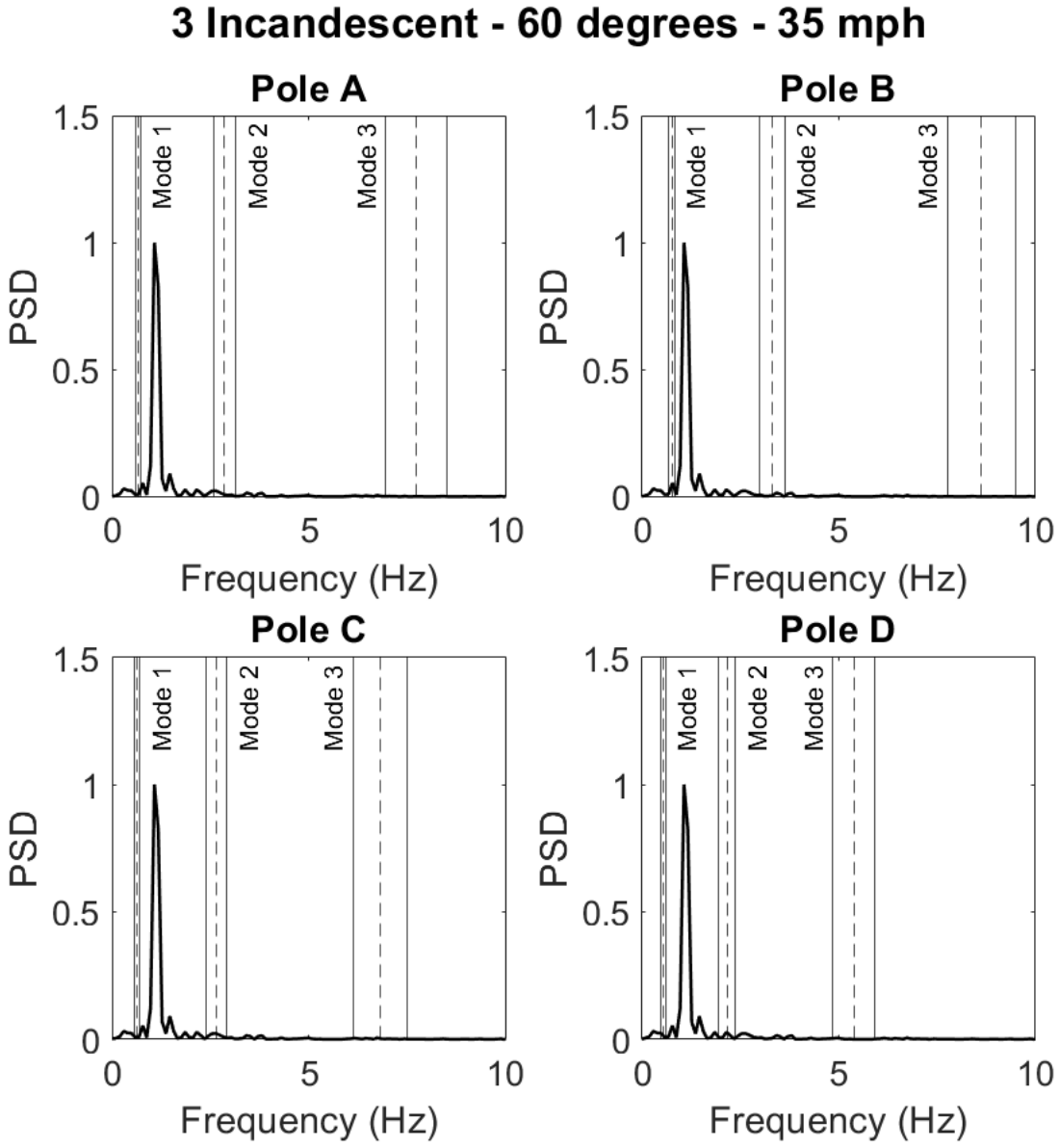

Figure B.29: PSDs for Pole A, B, C, and D for 3-Incandescent Light Fixture Subjected to 35 mph Wind at an Angle of 60 Degrees

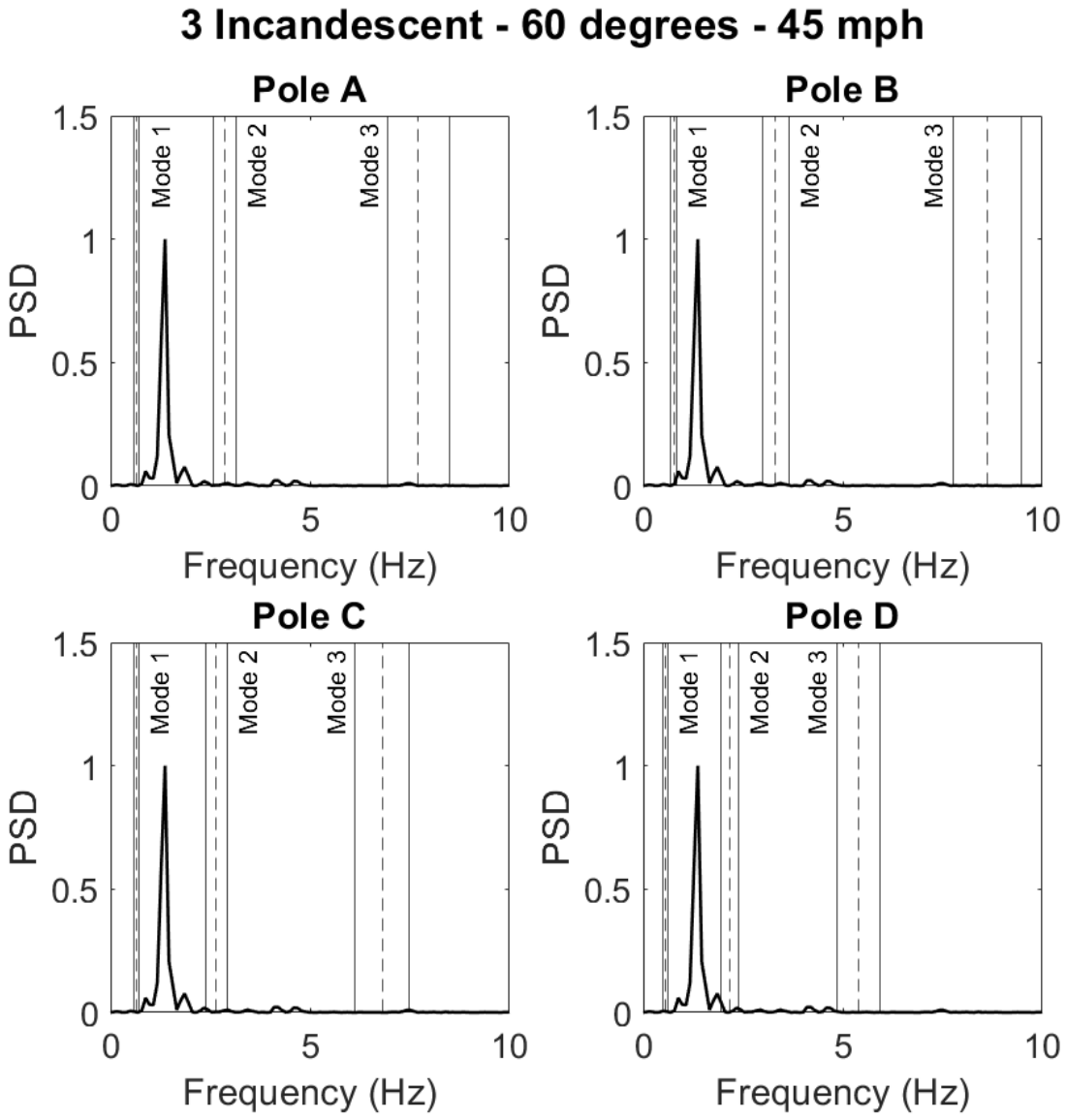

Figure B.30: PSDs for Pole A, B, C, and D for 3-Incandescent Light Fixture Subjected to 45 mph Wind at an Angle of 60 Degrees

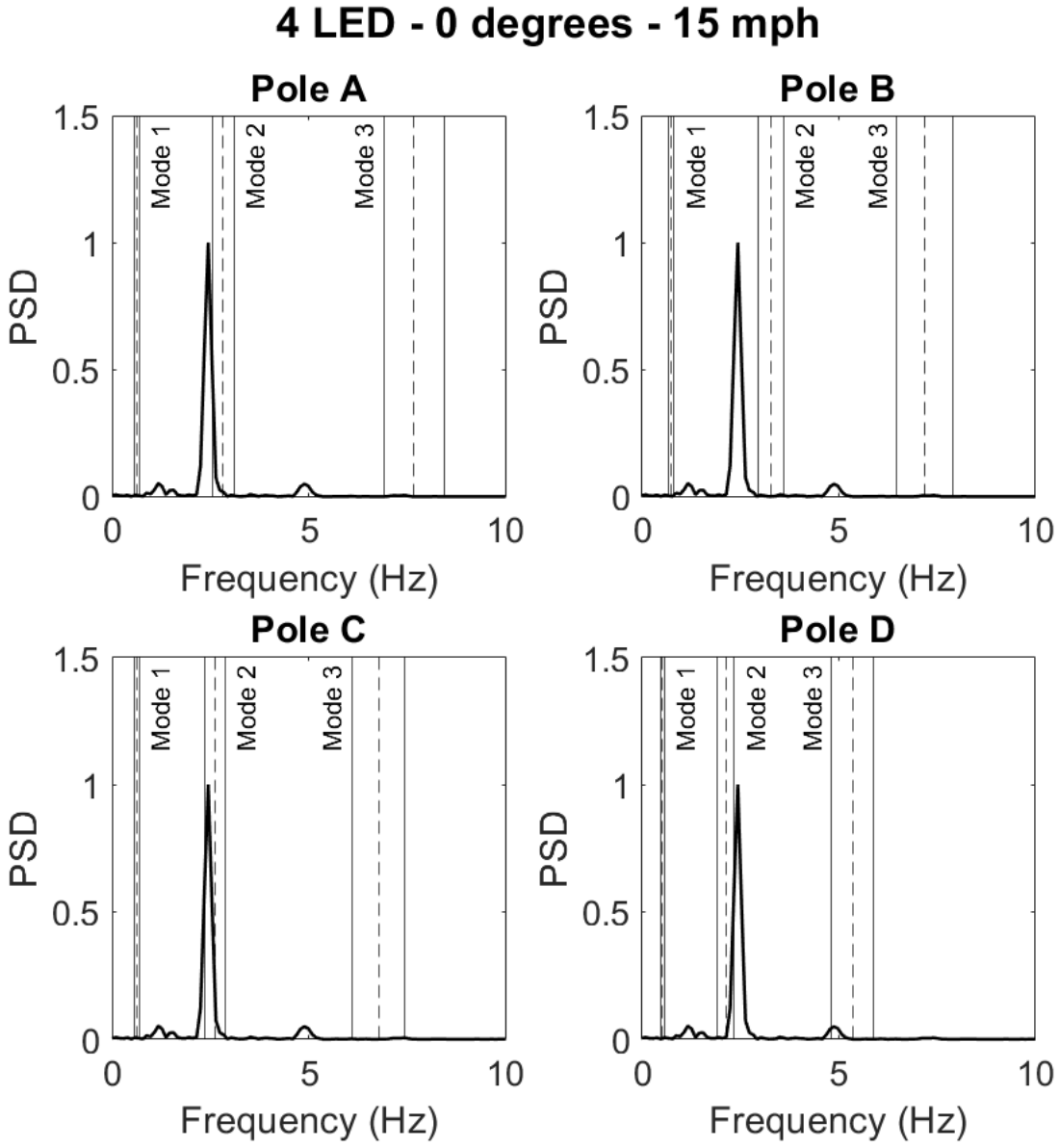

Figure B.31: PSDs for Pole A, B, C, and D for 4-LED Light Fixture Subjected to 15 mph Wind at an Angle of 0 Degrees

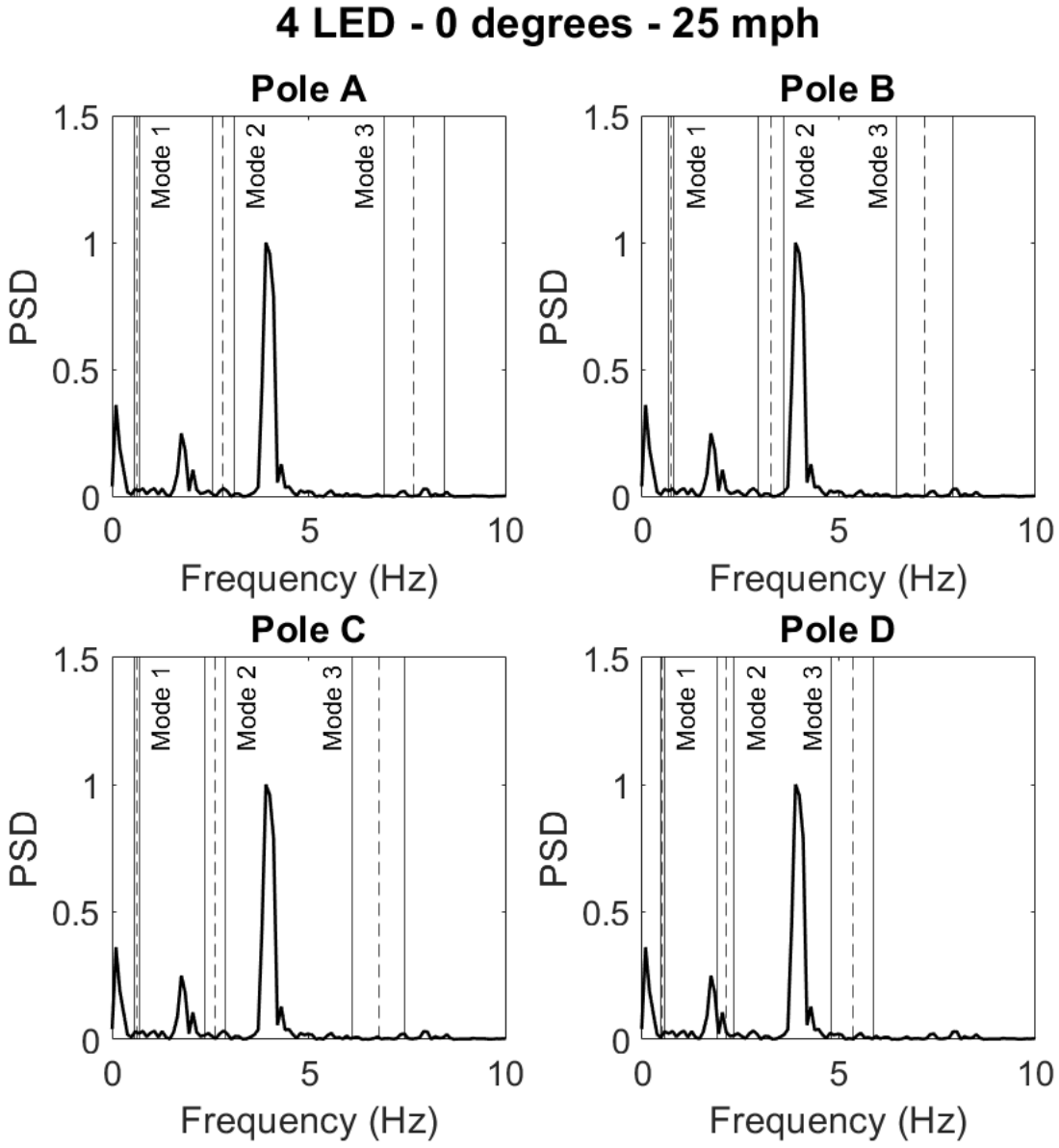

Figure B.32: PSDs for Pole A, B, C, and D for 4-LED Light Fixture Subjected to 25 mph Wind at an Angle of 0 Degrees

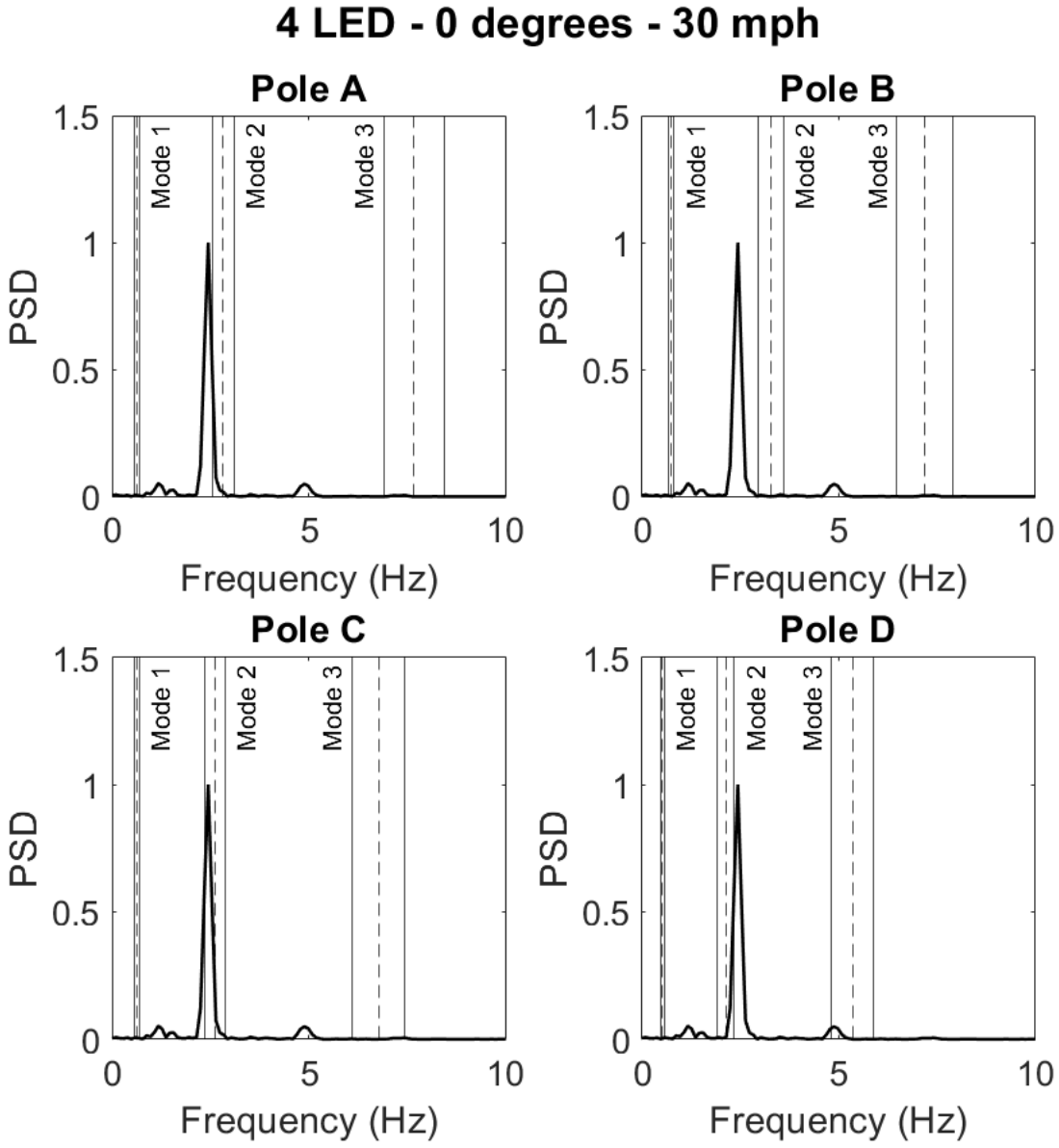

Figure B.33: PSDs for Pole A, B, C, and D for 4-LED Light Fixture Subjected to 30 mph Wind at an Angle of 0 Degrees

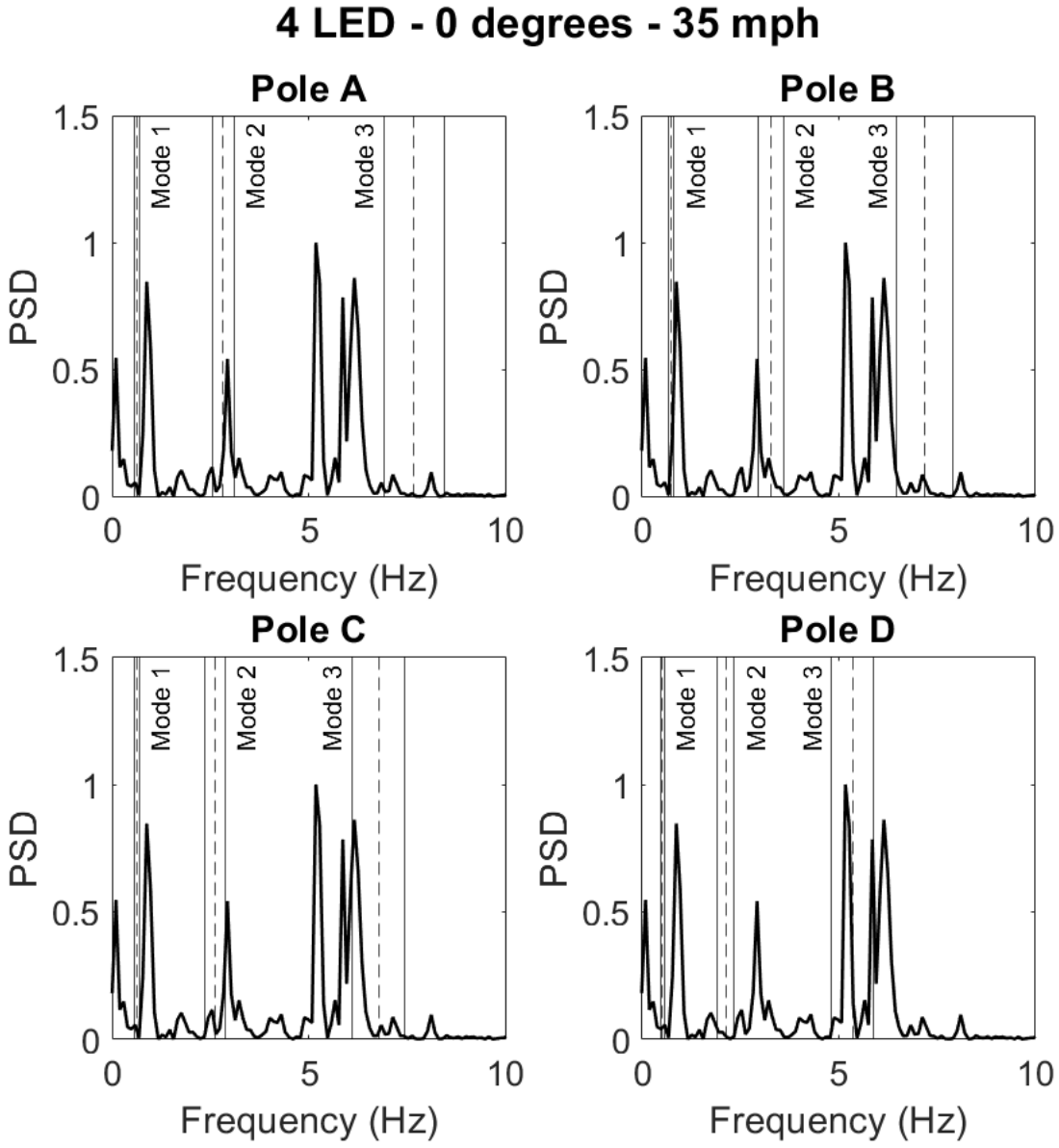

Figure B.34: PSDs for Pole A, B, C, and D for 4-LED Light Fixture Subjected to 35 mph Wind at an Angle of 0 Degrees

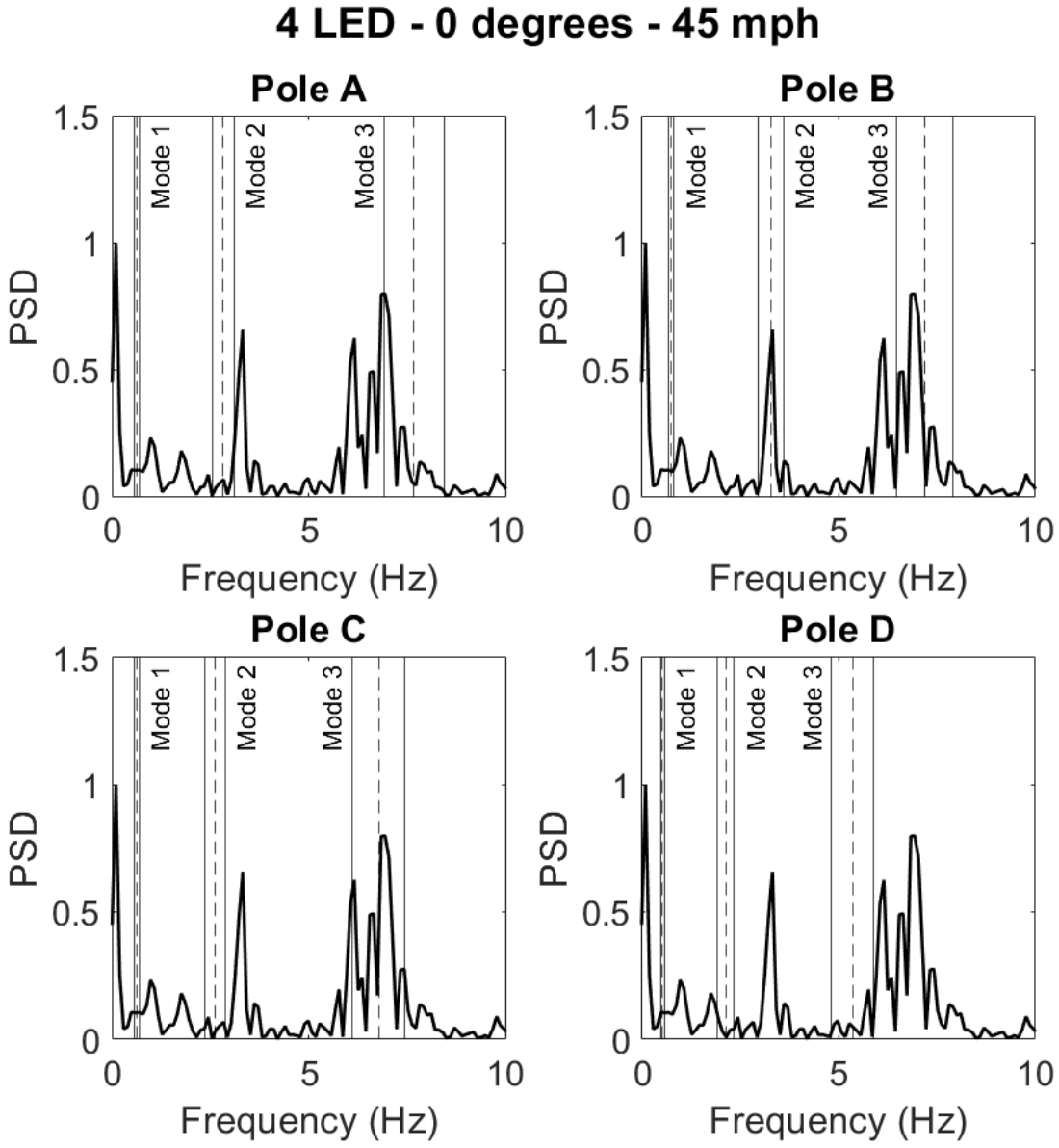

Figure B.35: PSDs for Pole A, B, C, and D for 4-LED Light Fixture Subjected to 45 mph Wind at an Angle of 0 Degrees

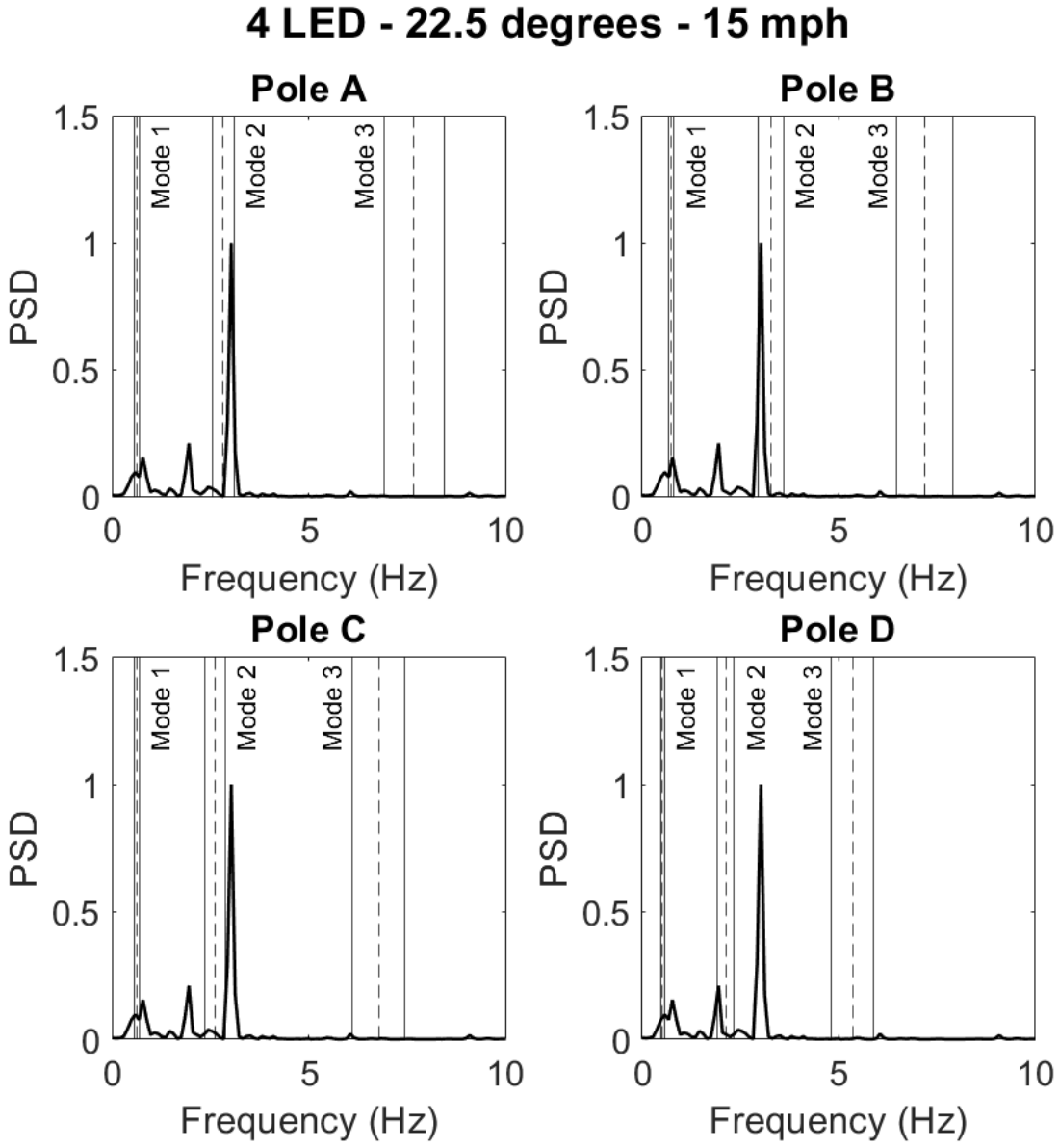

Figure B.36: PSDs for Pole A, B, C, and D for 4-LED Light Fixture Subjected to 15 mph Wind at an Angle of 22.5 Degrees

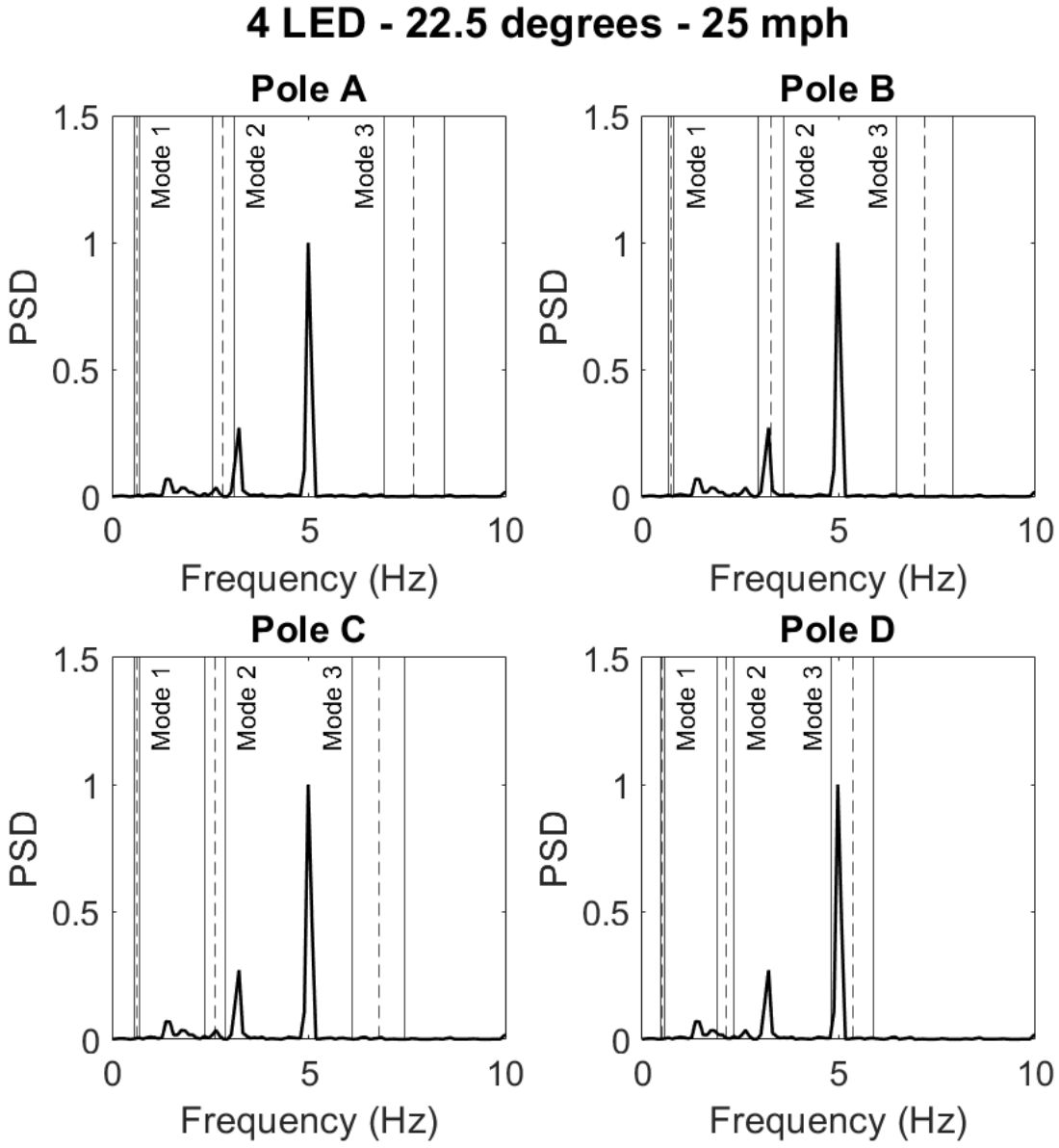

Figure B.37: PSDs for Pole A, B, C, and D for 4-LED Light Fixture Subjected to 25 mph Wind at an Angle of 22.5 Degrees

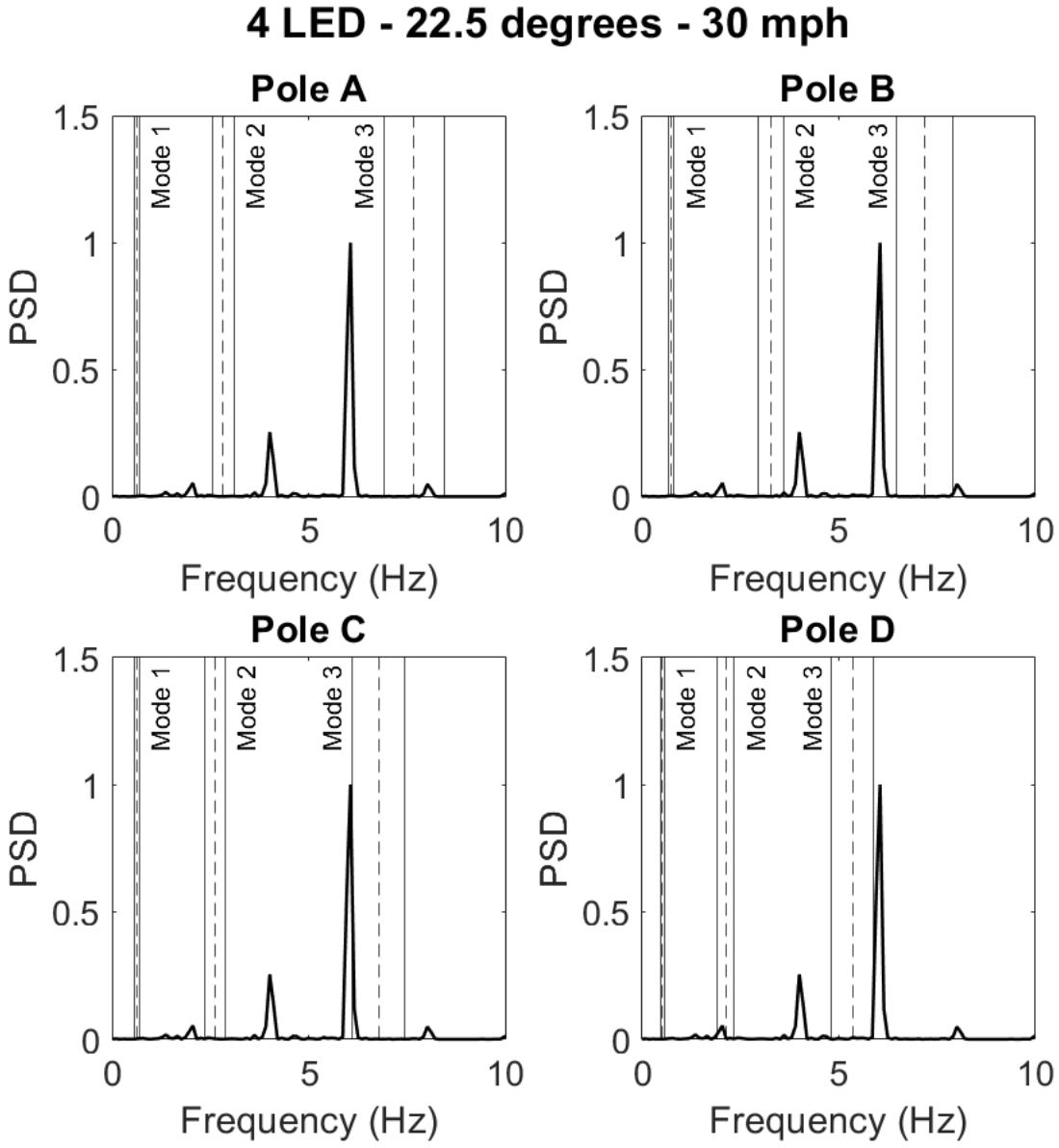

Figure B.38: PSDs for Pole A, B, C, and D for 4-LED Light Fixture Subjected to 30 mph Wind at an Angle of 22.5 Degrees

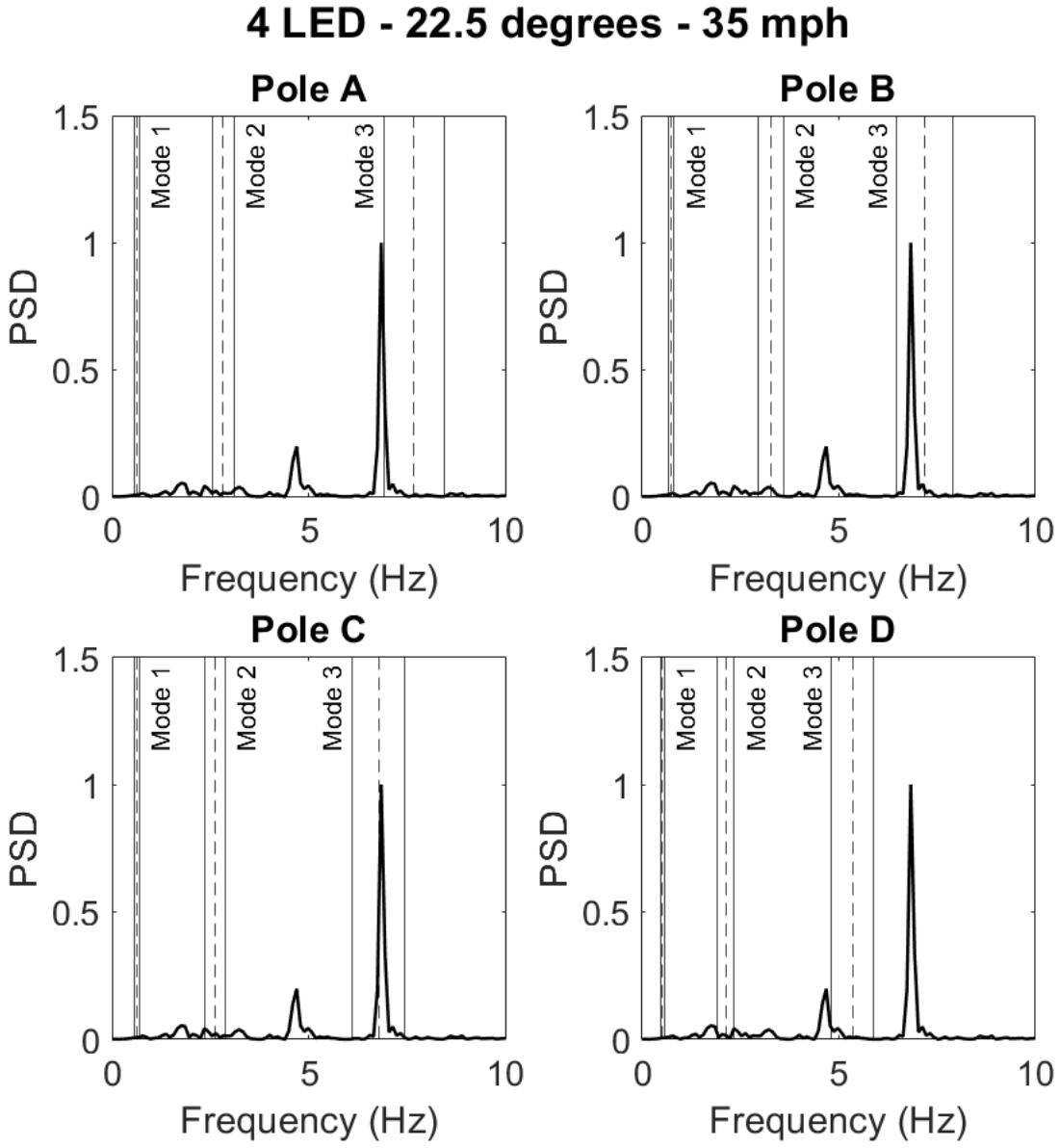

Figure B.39: PSDs for Pole A, B, C, and D for 4-LED Light Fixture Subjected to 35 mph Wind at an Angle of 22.5 Degrees

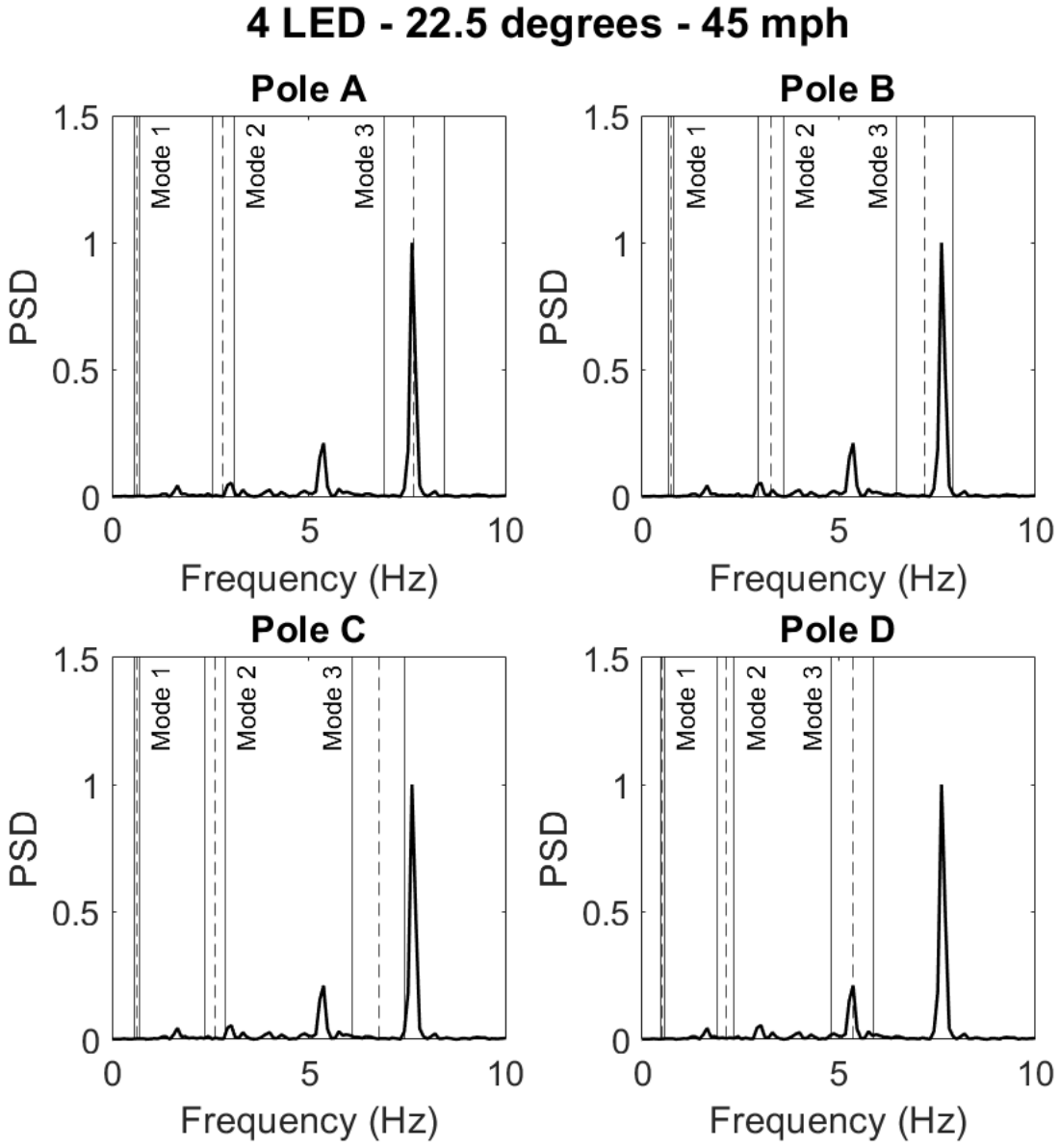

Figure B.40: PSDs for Pole A, B, C, and D for 4-LED Light Fixture Subjected to 45 mph Wind at an Angle of 22.5 Degrees

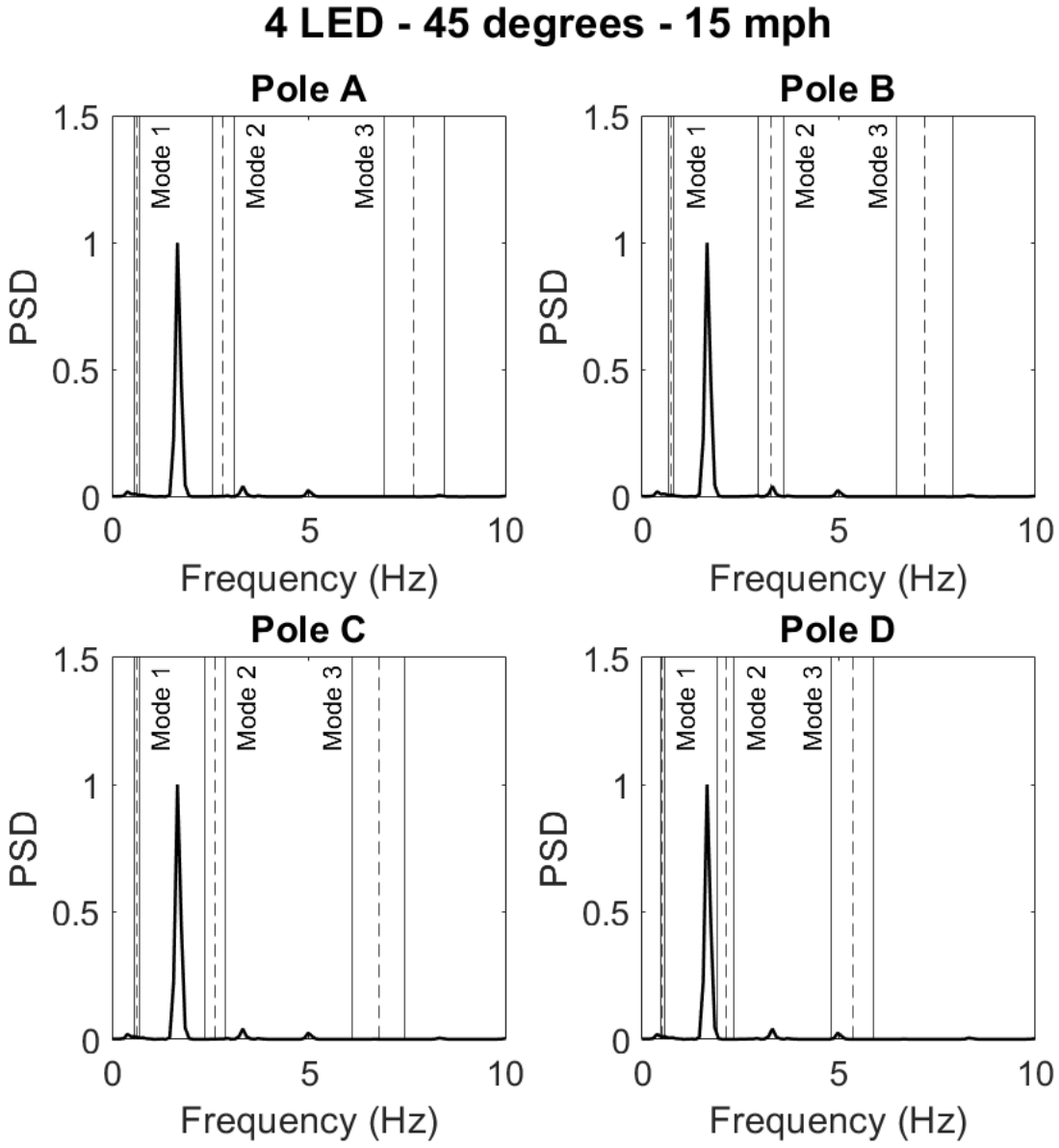

Figure B.41: PSDs for Pole A, B, C, and D for 4-LED Light Fixture Subjected to 15 mph Wind at an Angle of 45 Degrees

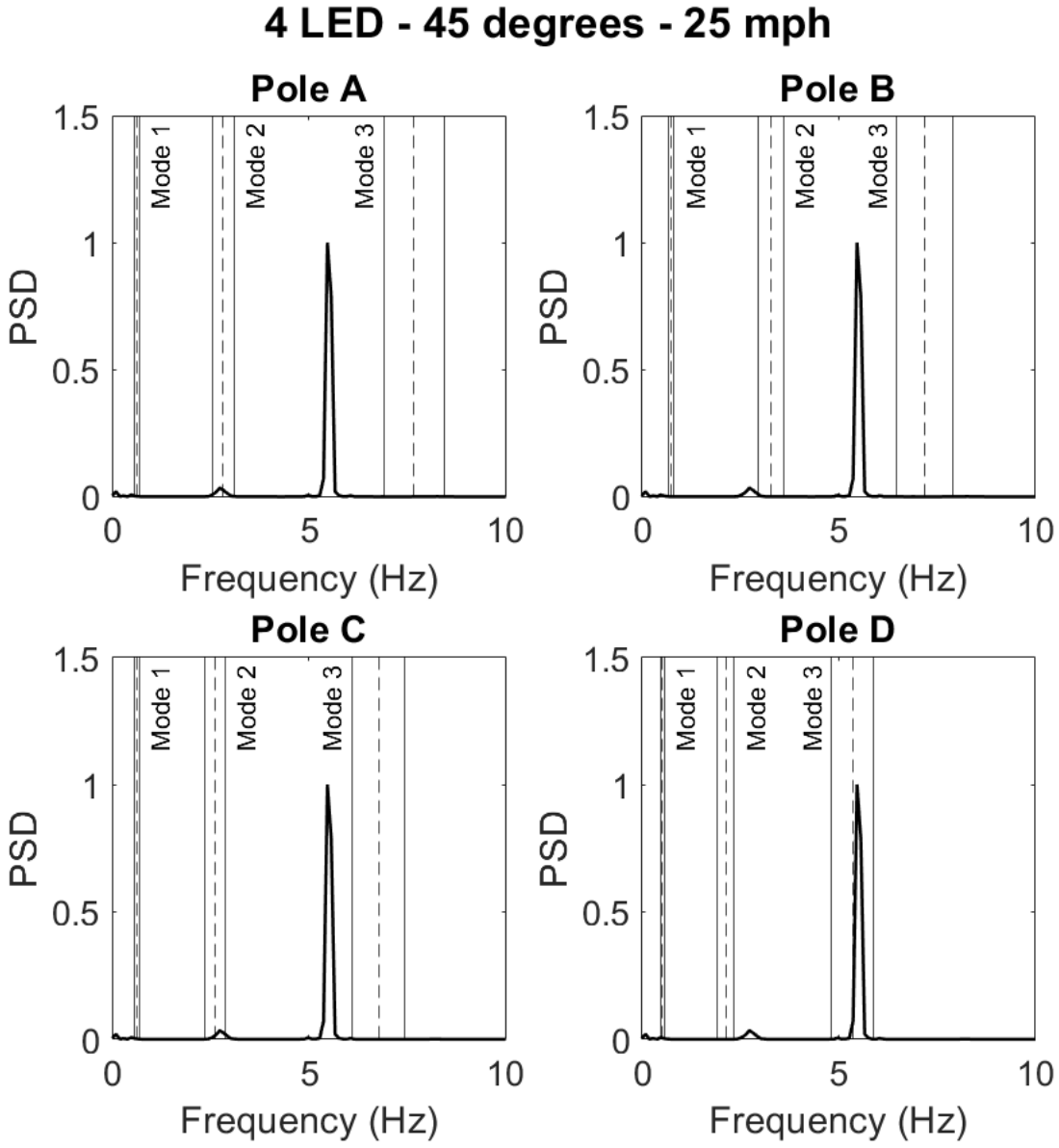

Figure B.42: PSDs for Pole A, B, C, and D for 4-LED Light Fixture Subjected to 25 mph Wind at an Angle of 45 Degrees

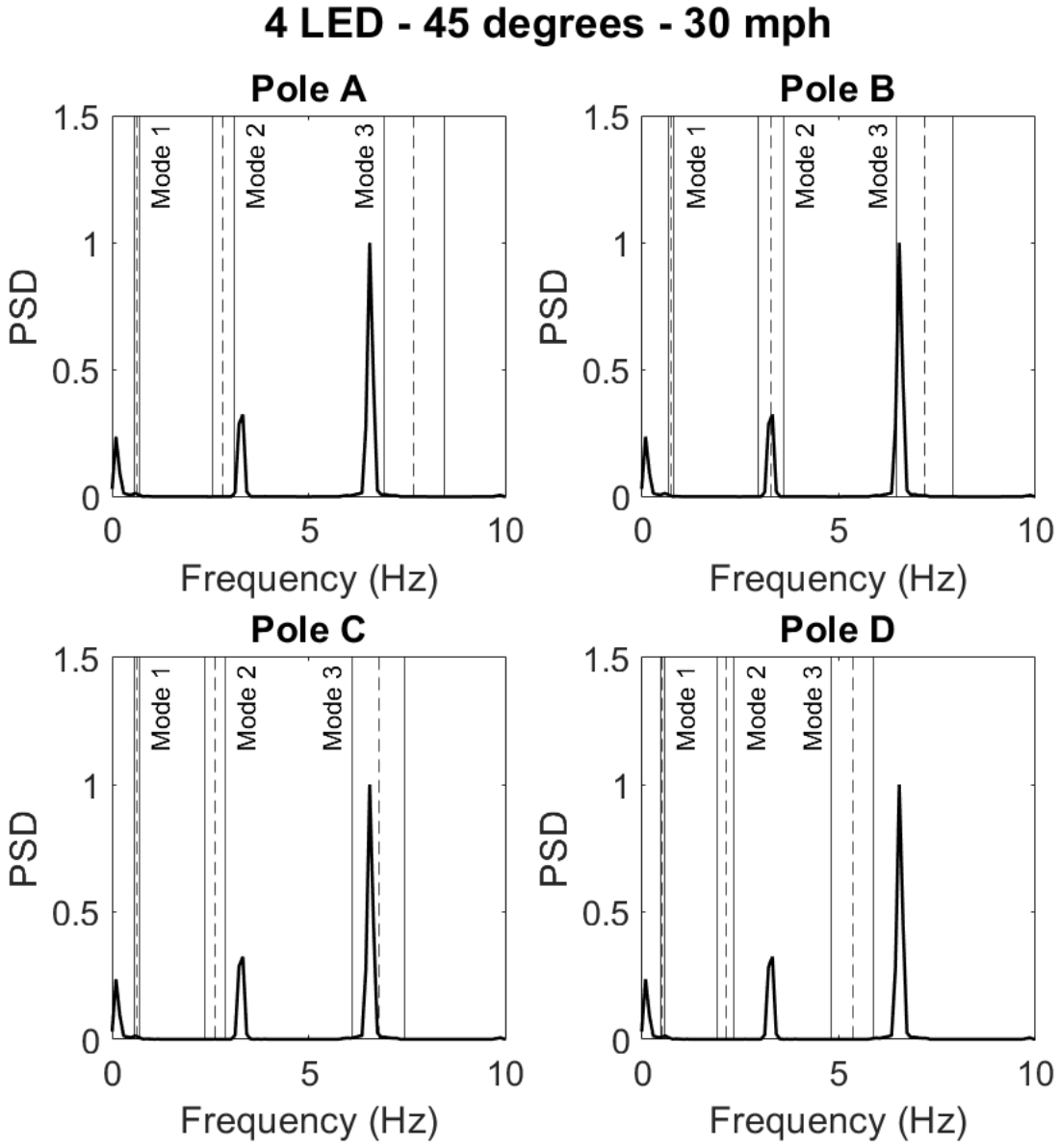

Figure B.43: PSDs for Pole A, B, C, and D for 4-LED Light Fixture Subjected to 30 mph Wind at an Angle of 45 Degrees

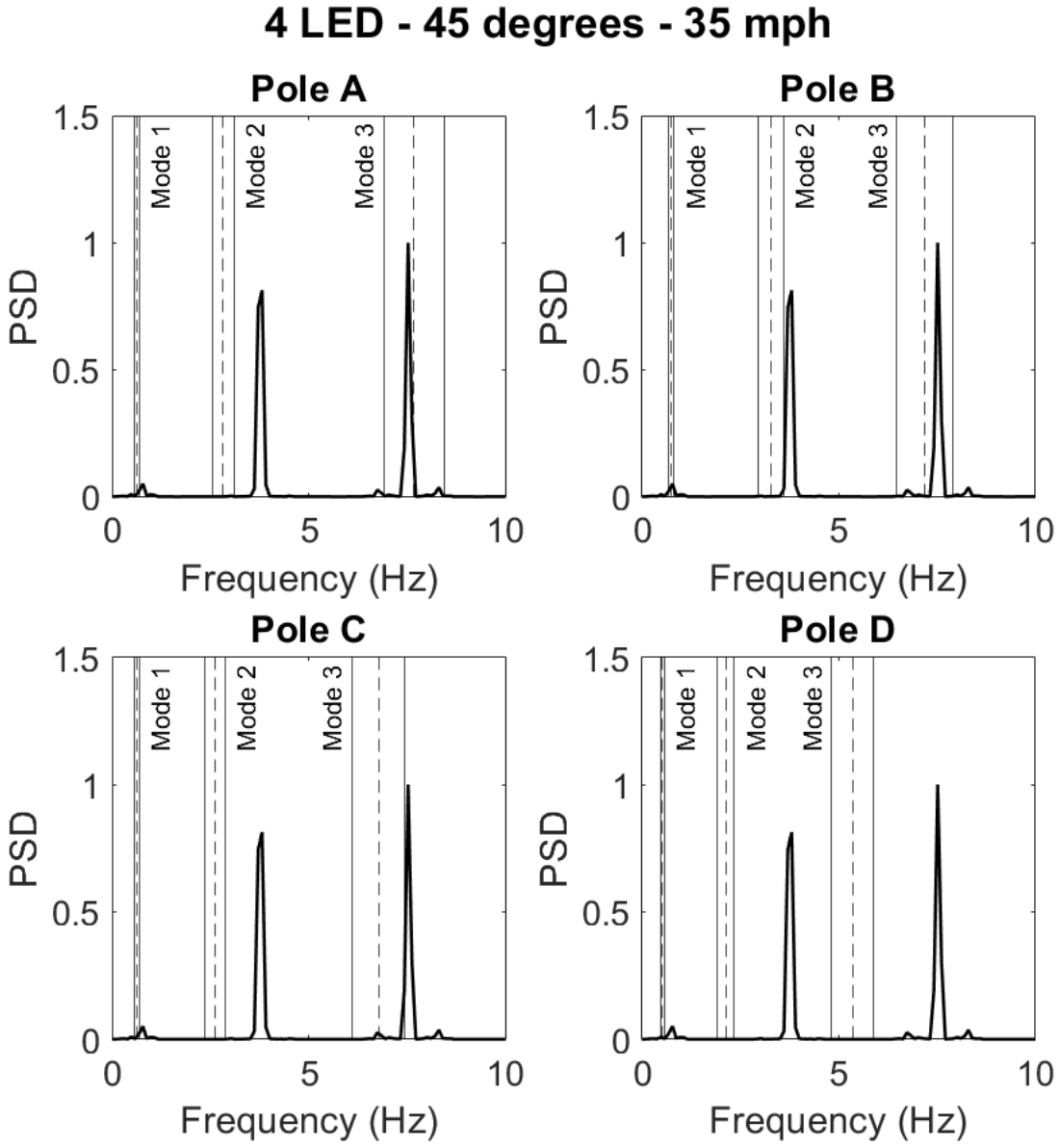

Figure B.44: PSDs for Pole A, B, C, and D for 4-LED Light Fixture Subjected to 35 mph Wind at an Angle of 45 Degrees

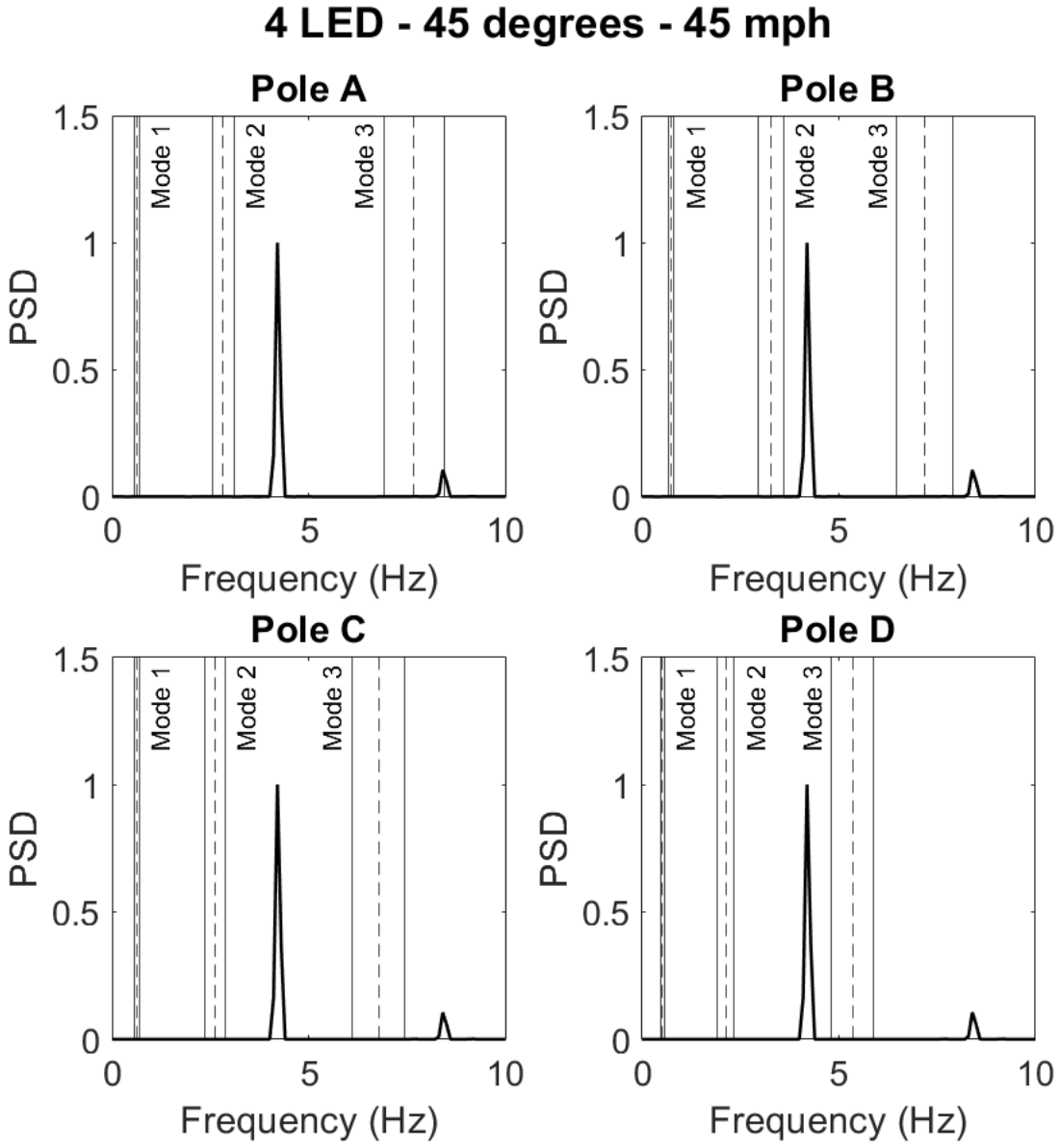

Figure B.45: PSDs for Pole A, B, C, and D for 4-LED Light Fixture Subjected to 45 mph Wind at an Angle of 45 Degrees

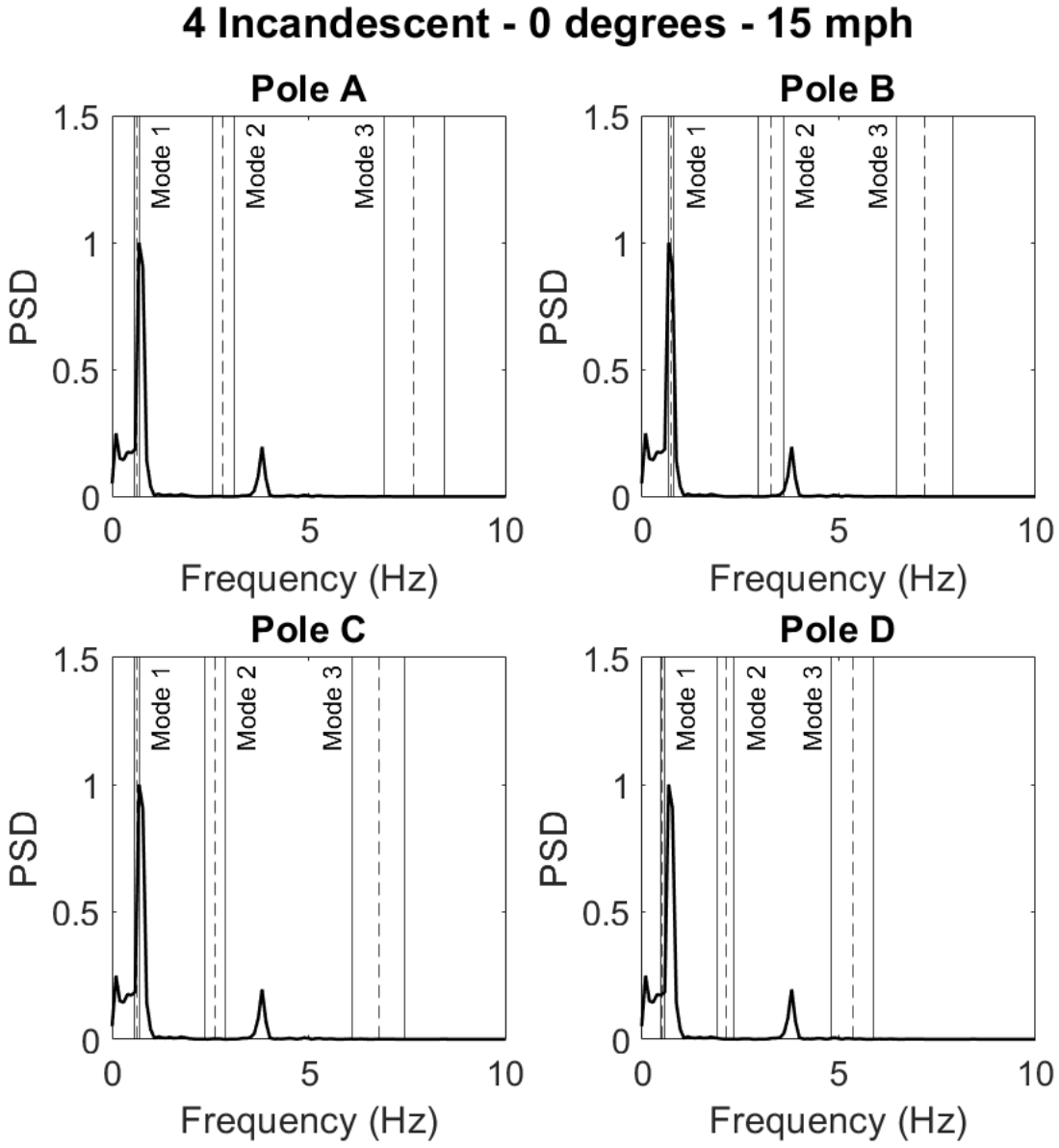

Figure B.46: PSDs for Pole A, B, C, and D for 4-Incandescent Light Fixture Subjected to 15 mph Wind at an Angle of 0 Degrees

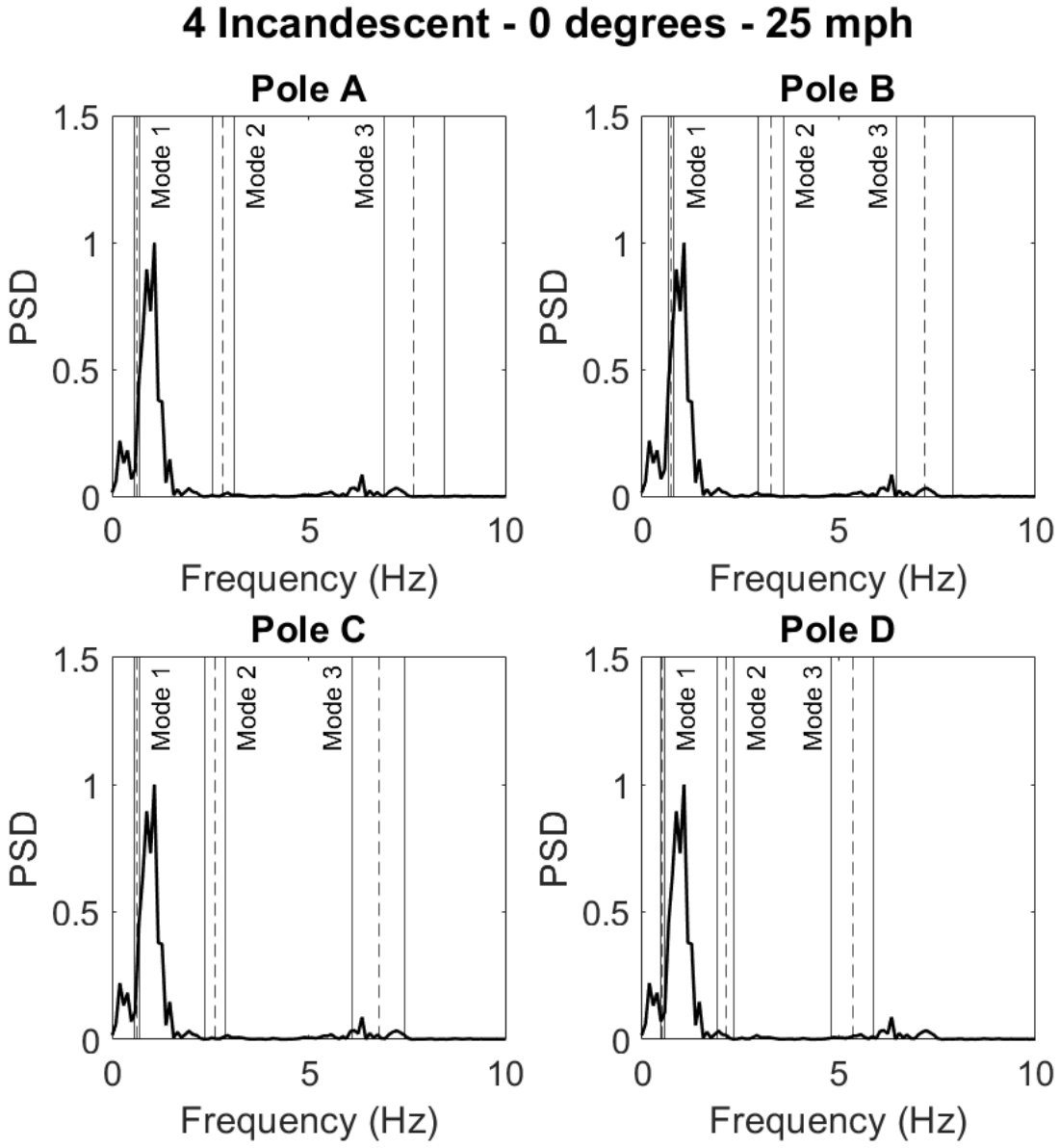

Figure B.47: PSDs for Pole A, B, C, and D for 4-Incandescent Light Fixture Subjected to 25 mph Wind at an Angle of 0 Degrees

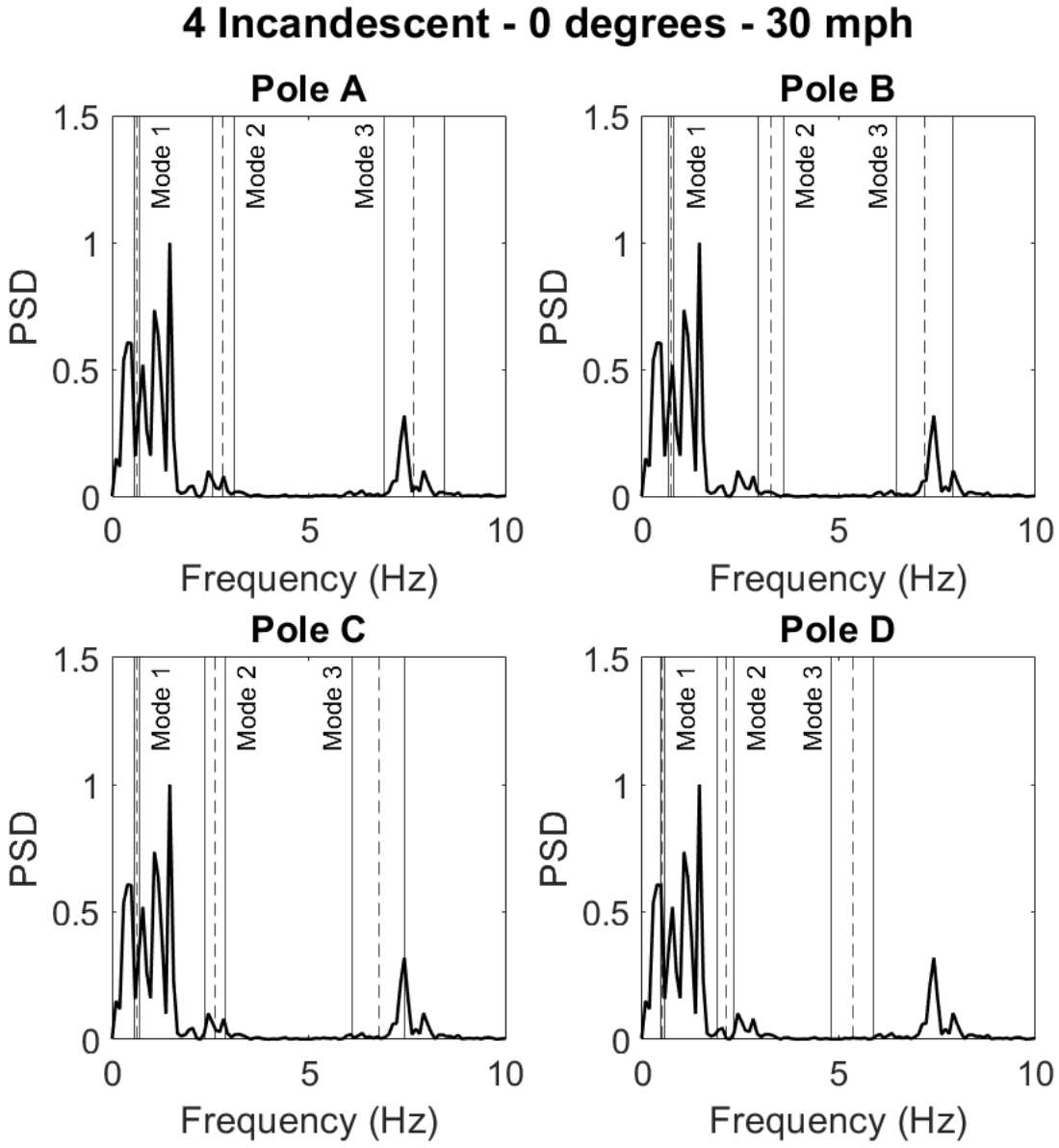

Figure B.48: PSDs for Pole A, B, C, and D for 4-Incandescent Light Fixture Subjected to 30 mph Wind at an Angle of 0 Degrees

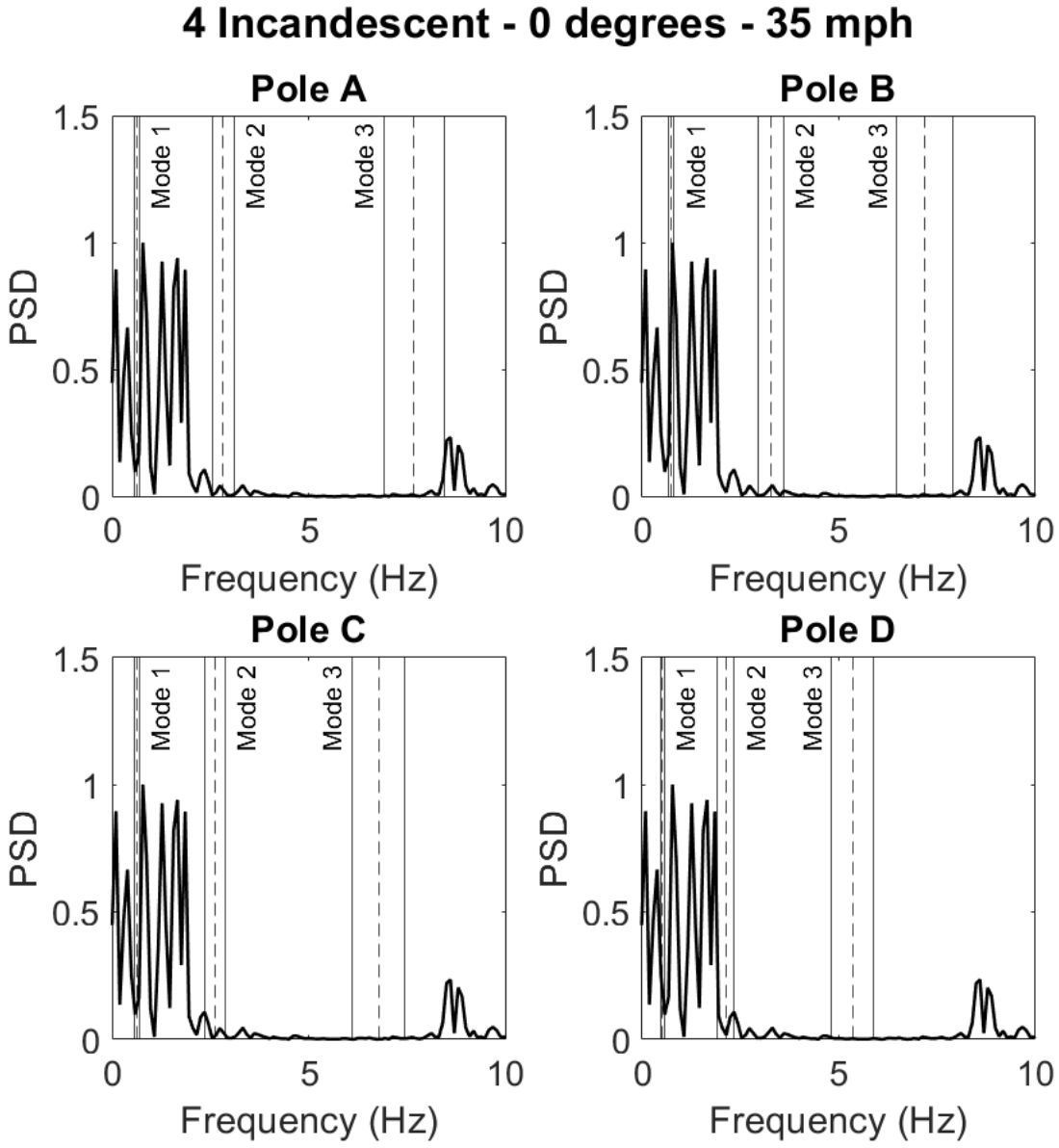

Figure B.49: PSDs for Pole A, B, C, and D for 4-Incandescent Light Fixture Subjected to 35 mph Wind at an Angle of 0 Degrees

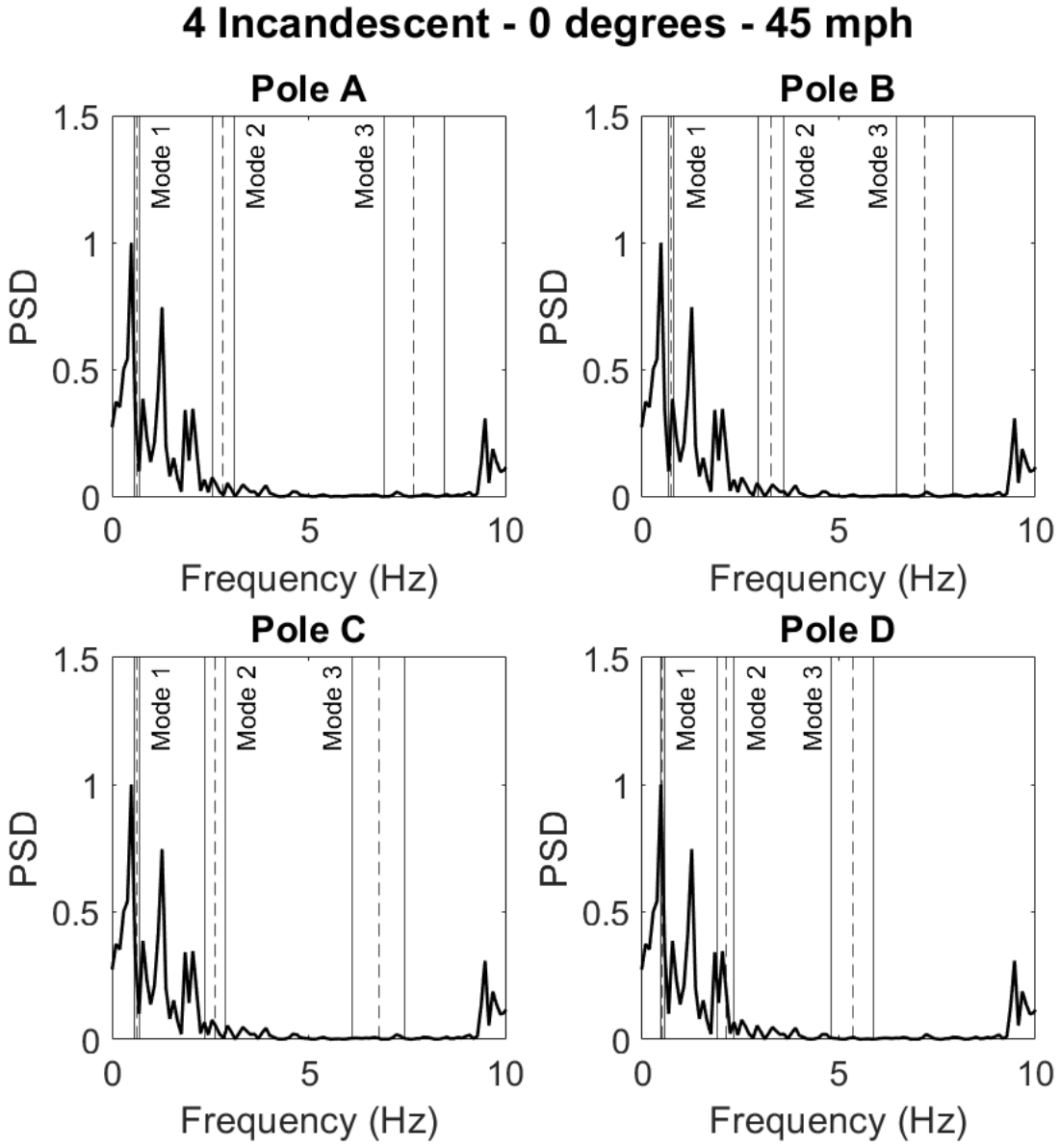

Figure B.50: PSDs for Pole A, B, C, and D for 4-Incandescent Light Fixture Subjected to 45 mph Wind at an Angle of 0 Degrees

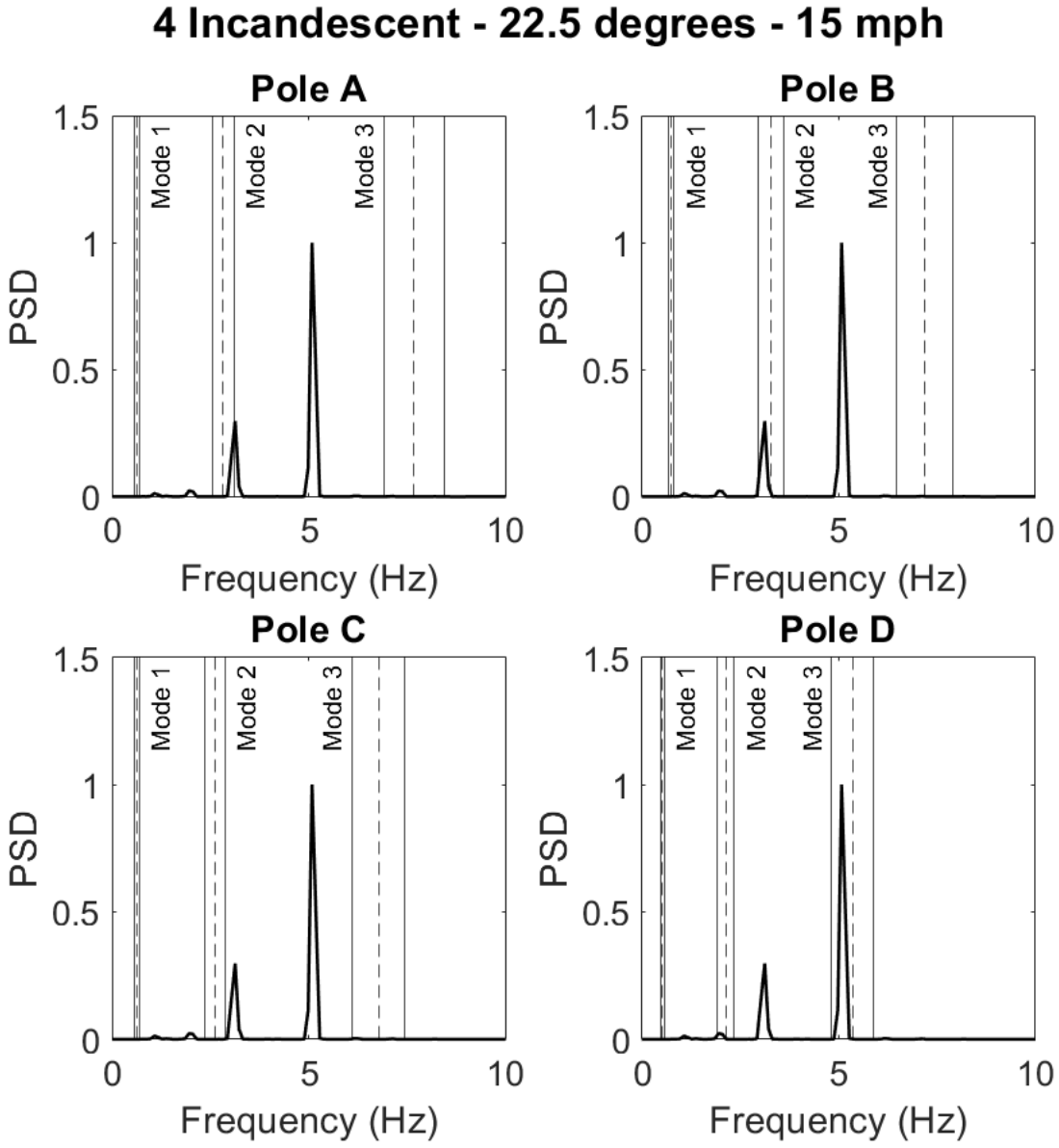

Figure B.51: PSDs for Pole A, B, C, and D for 4-Incandescent Light Fixture Subjected to 15 mph Wind at an Angle of 22.5 Degrees

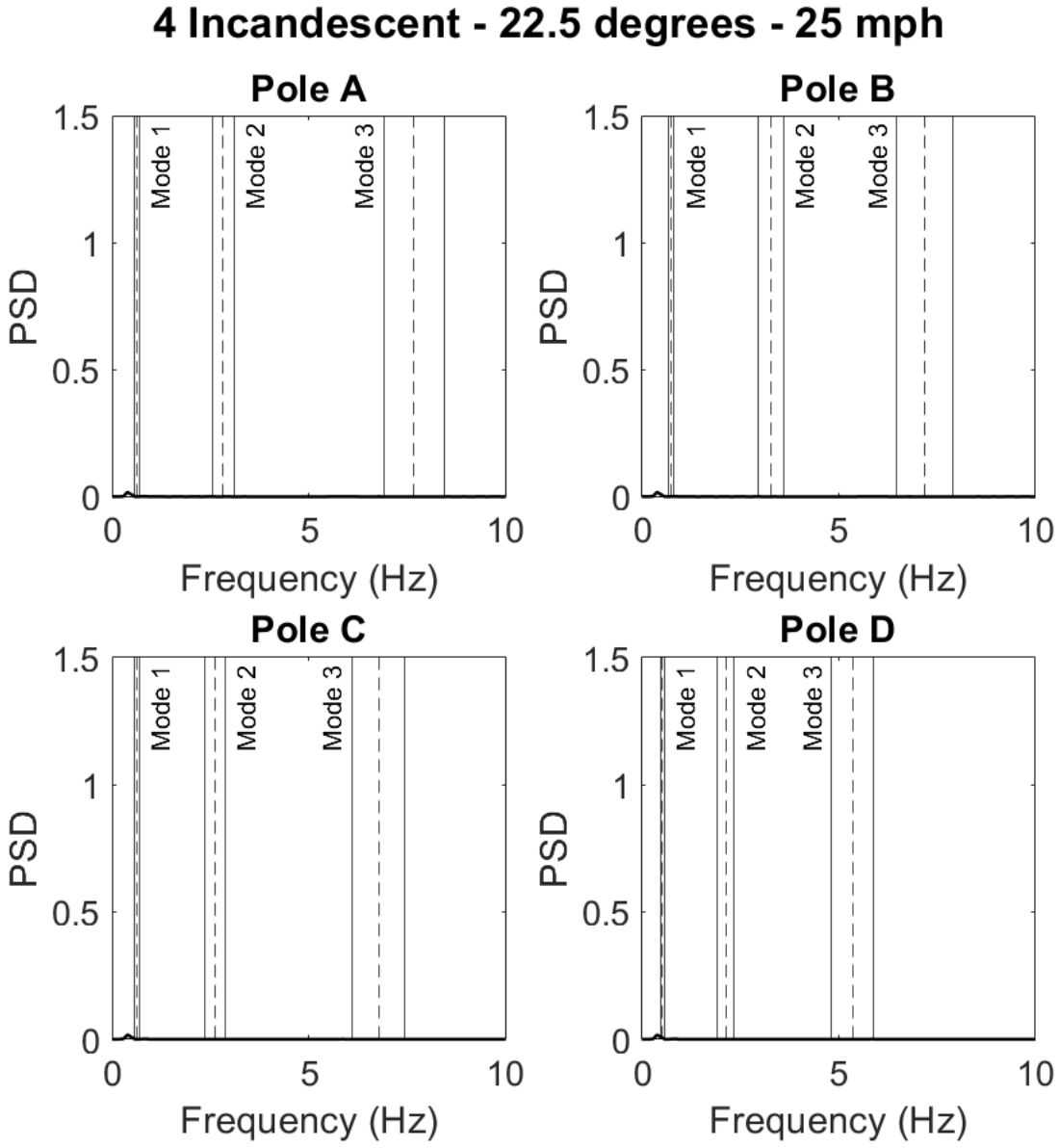

Figure B.52: PSDs for Pole A, B, C, and D for 4-Incandescent Light Fixture Subjected to 25 mph Wind at an Angle of 22.5 Degrees

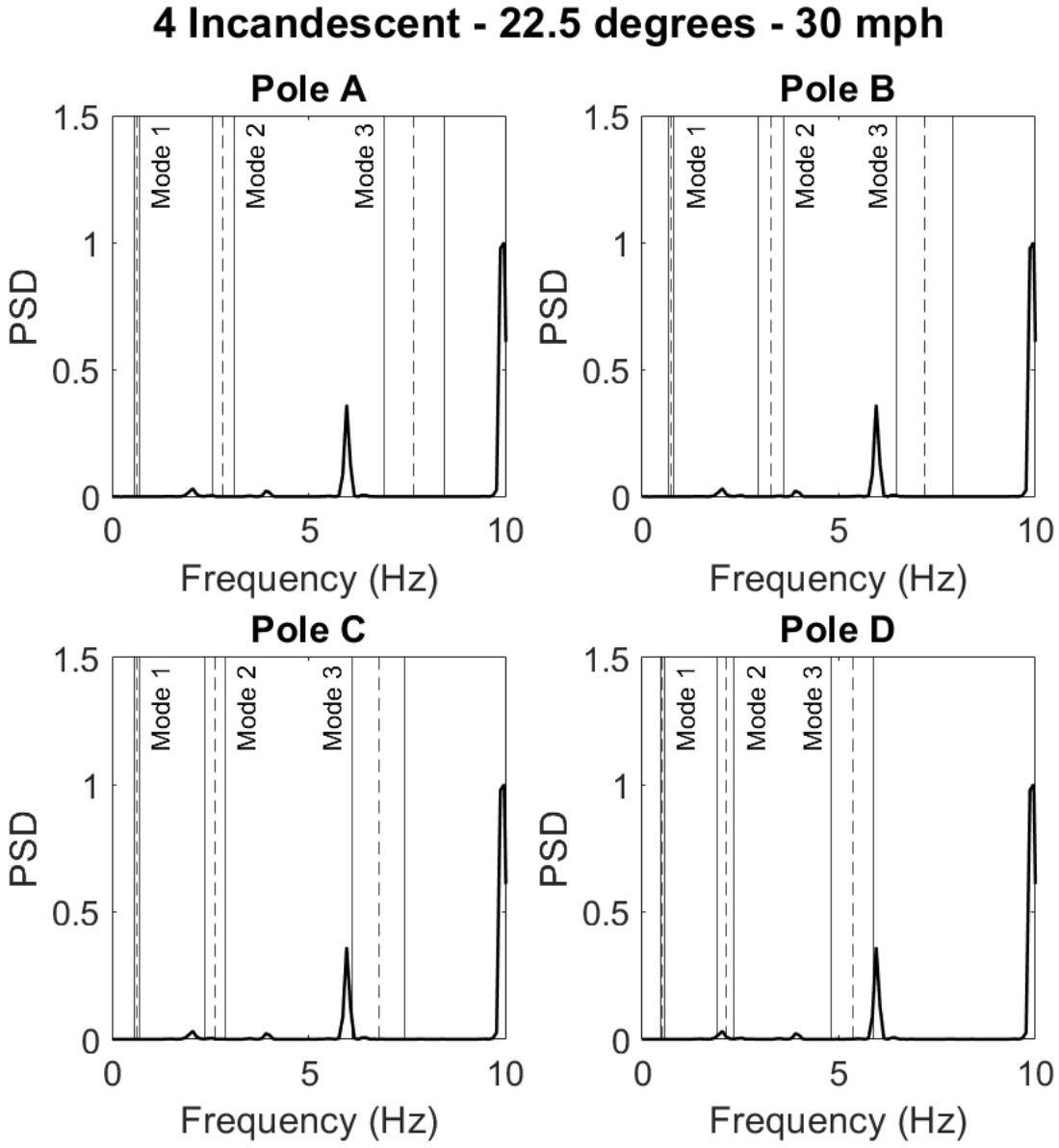

Figure B.53: PSDs for Pole A, B, C, and D for 4-Incandescent Light Fixture Subjected to 30 mph Wind at an Angle of 22.5 Degrees

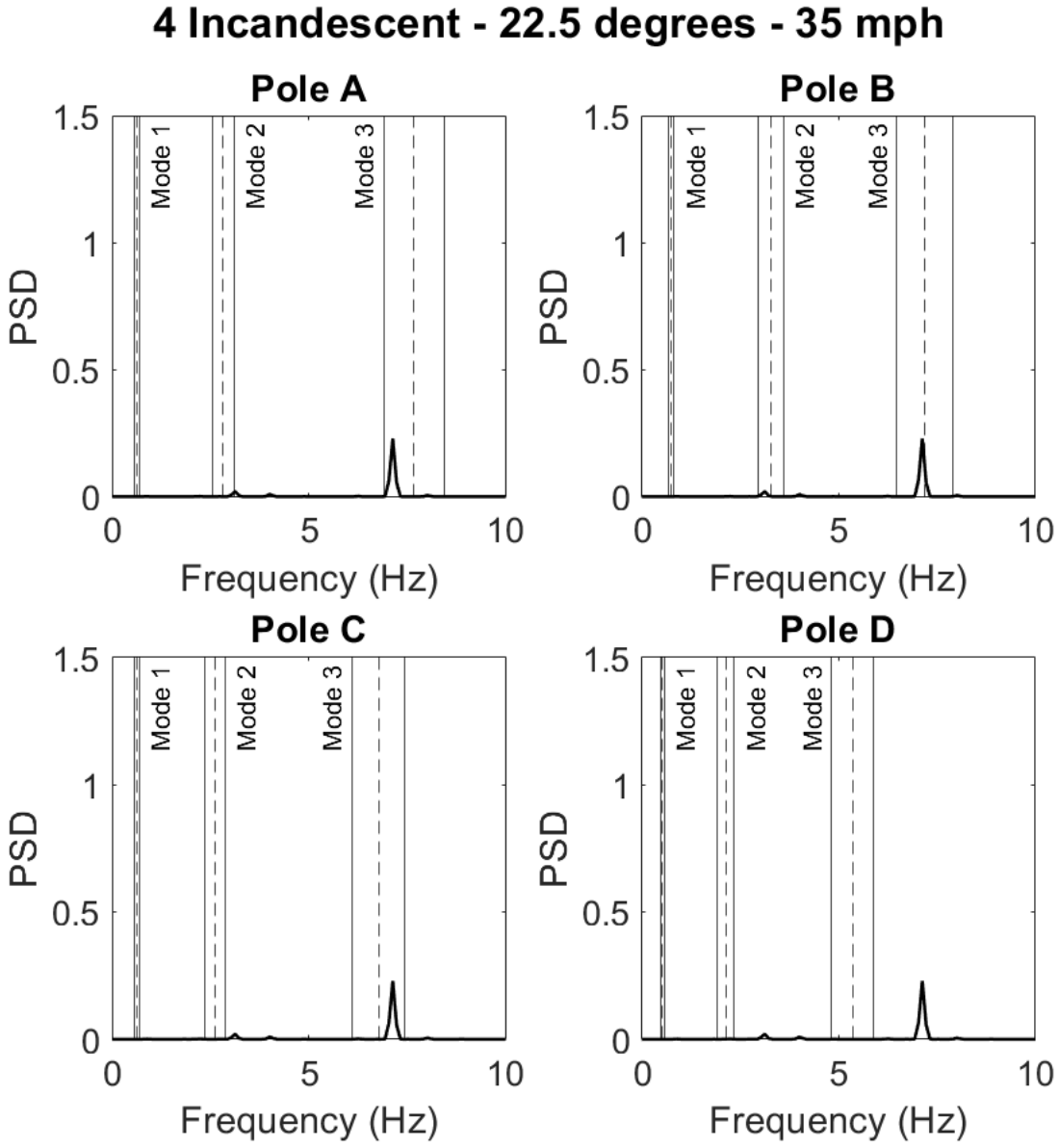

Figure B.54: PSDs for Pole A, B, C, and D for 4-Incandescent Light Fixture Subjected to 35 mph Wind at an Angle of 22.5 Degrees

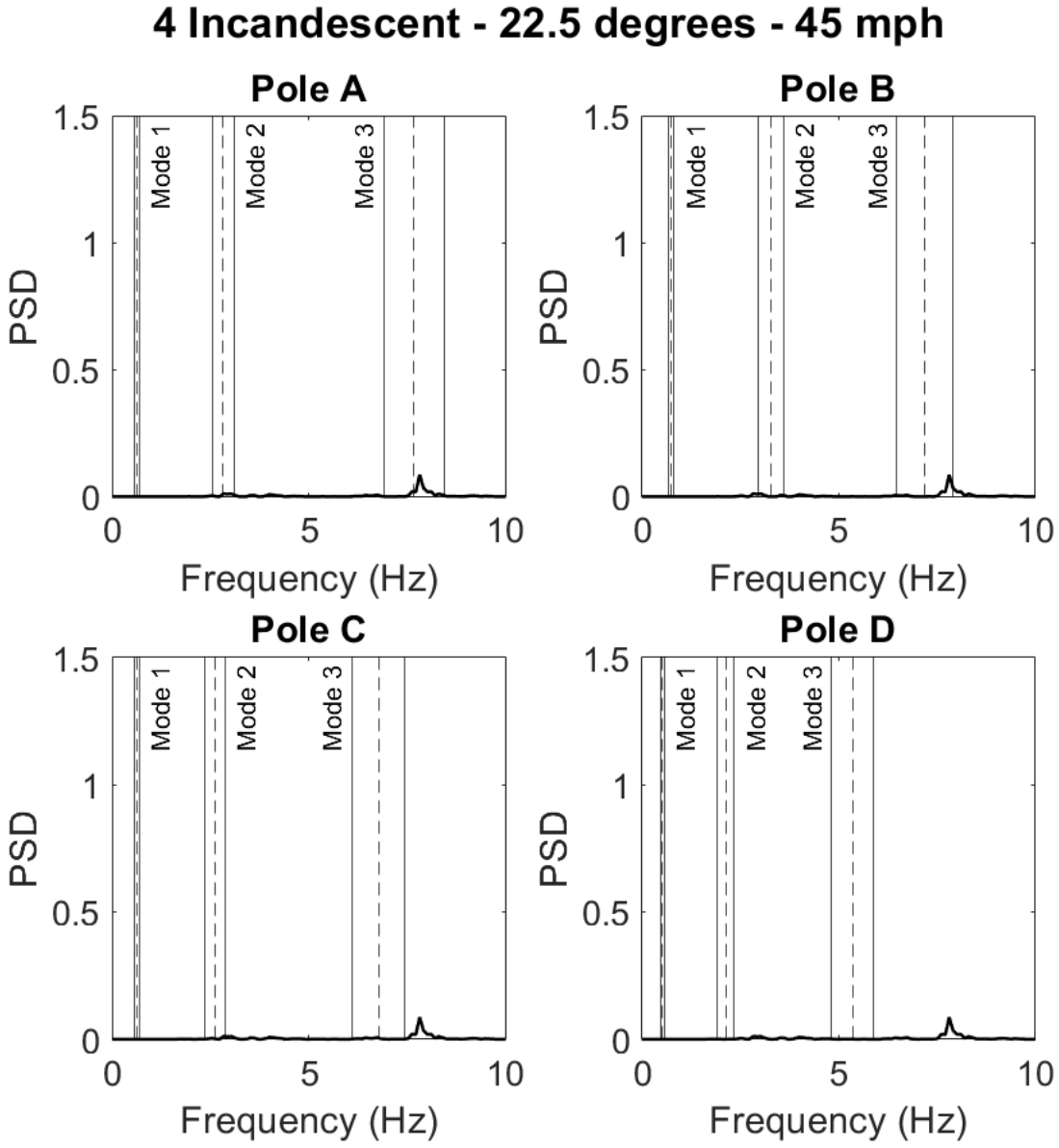

Figure B.55: PSDs for Pole A, B, C, and D for 4-Incandescent Light Fixture Subjected to 45 mph Wind at an Angle of 22.5 Degrees

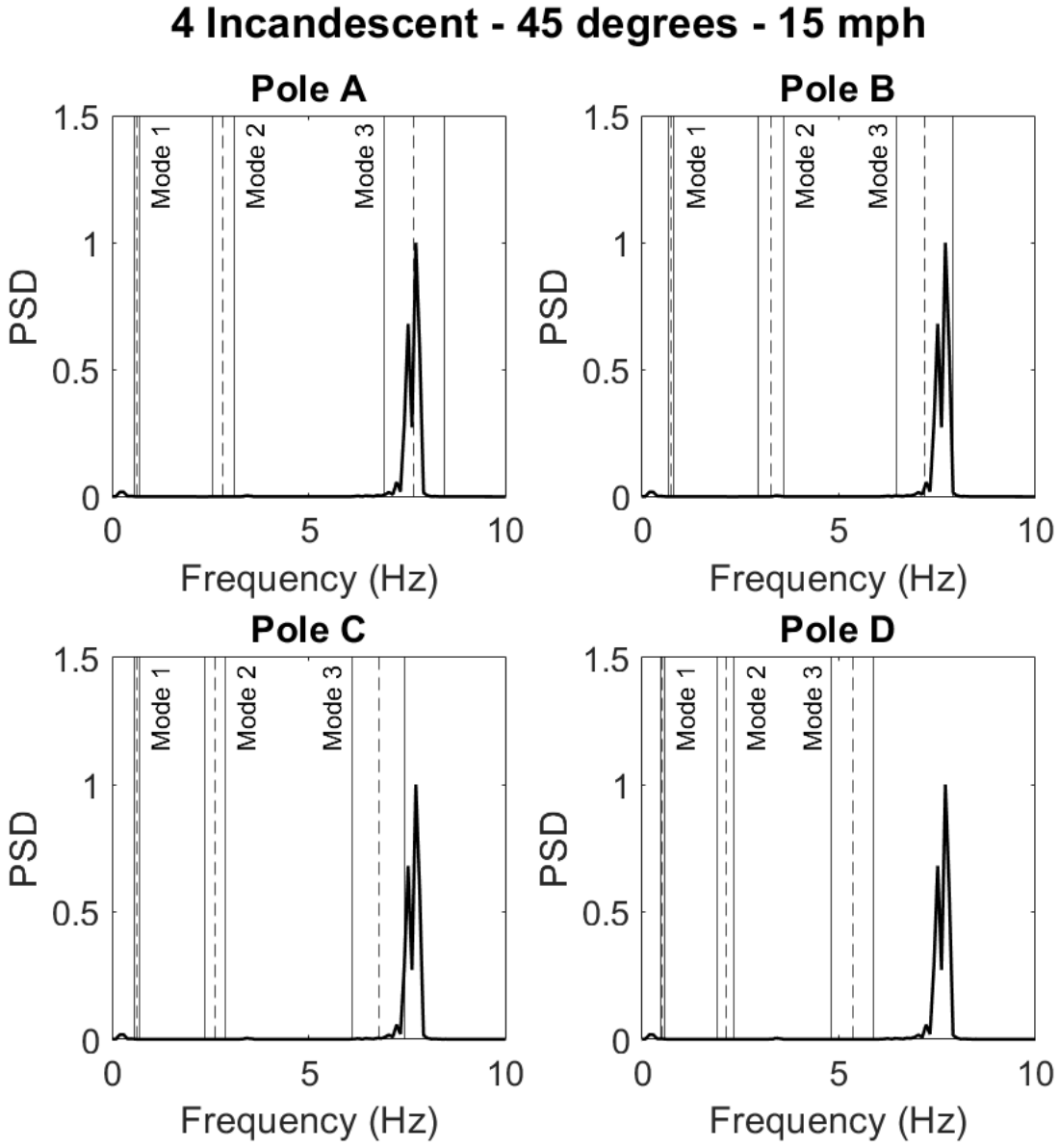

Figure B.56: PSDs for Pole A, B, C, and D for 4-Incandescent Light Fixture Subjected to 15 mph Wind at an Angle of 45 Degrees

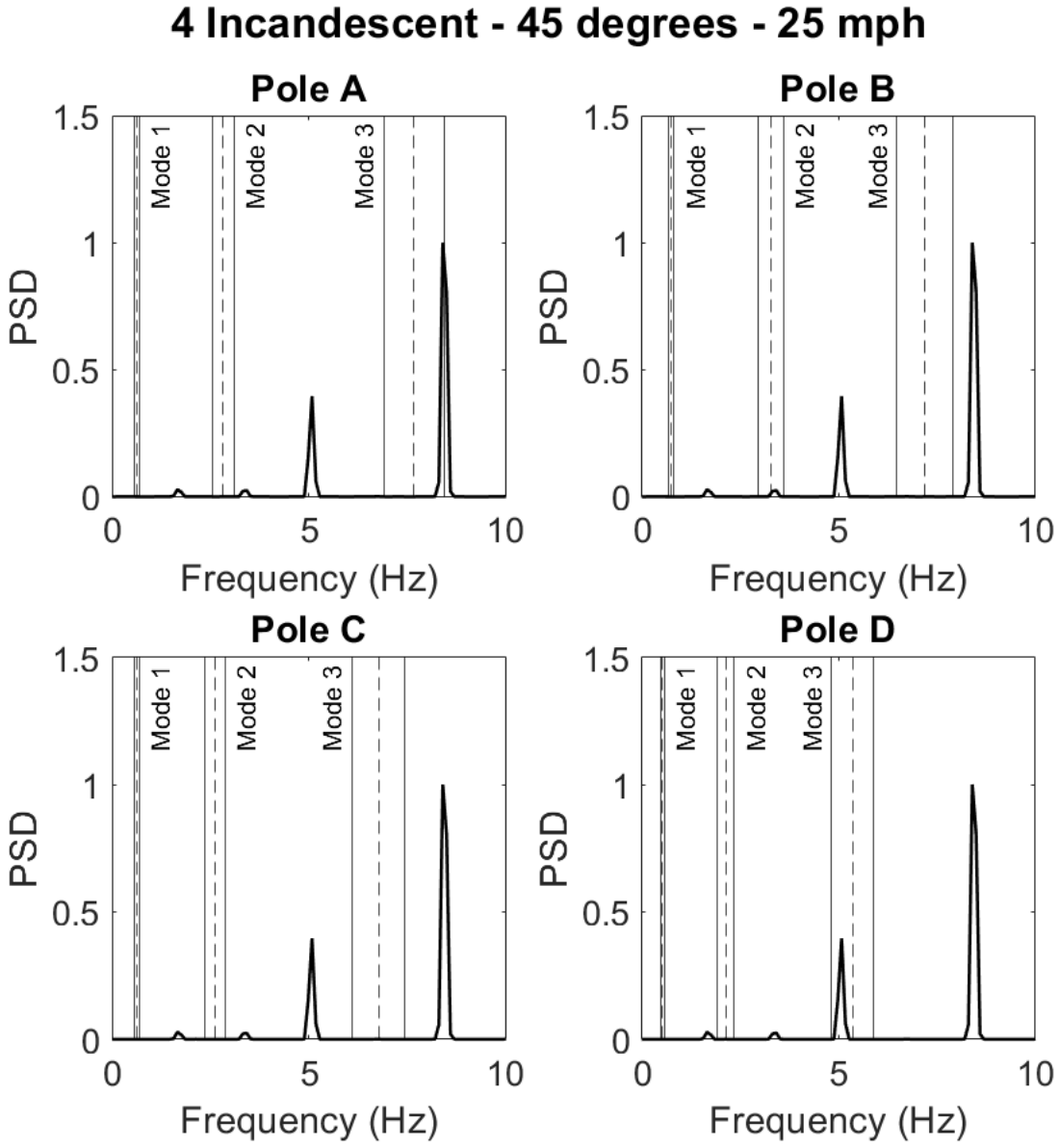

Figure B.57: PSDs for Pole A, B, C, and D for 4-Incandescent Light Fixture Subjected to 25 mph Wind at an Angle of 45 Degrees

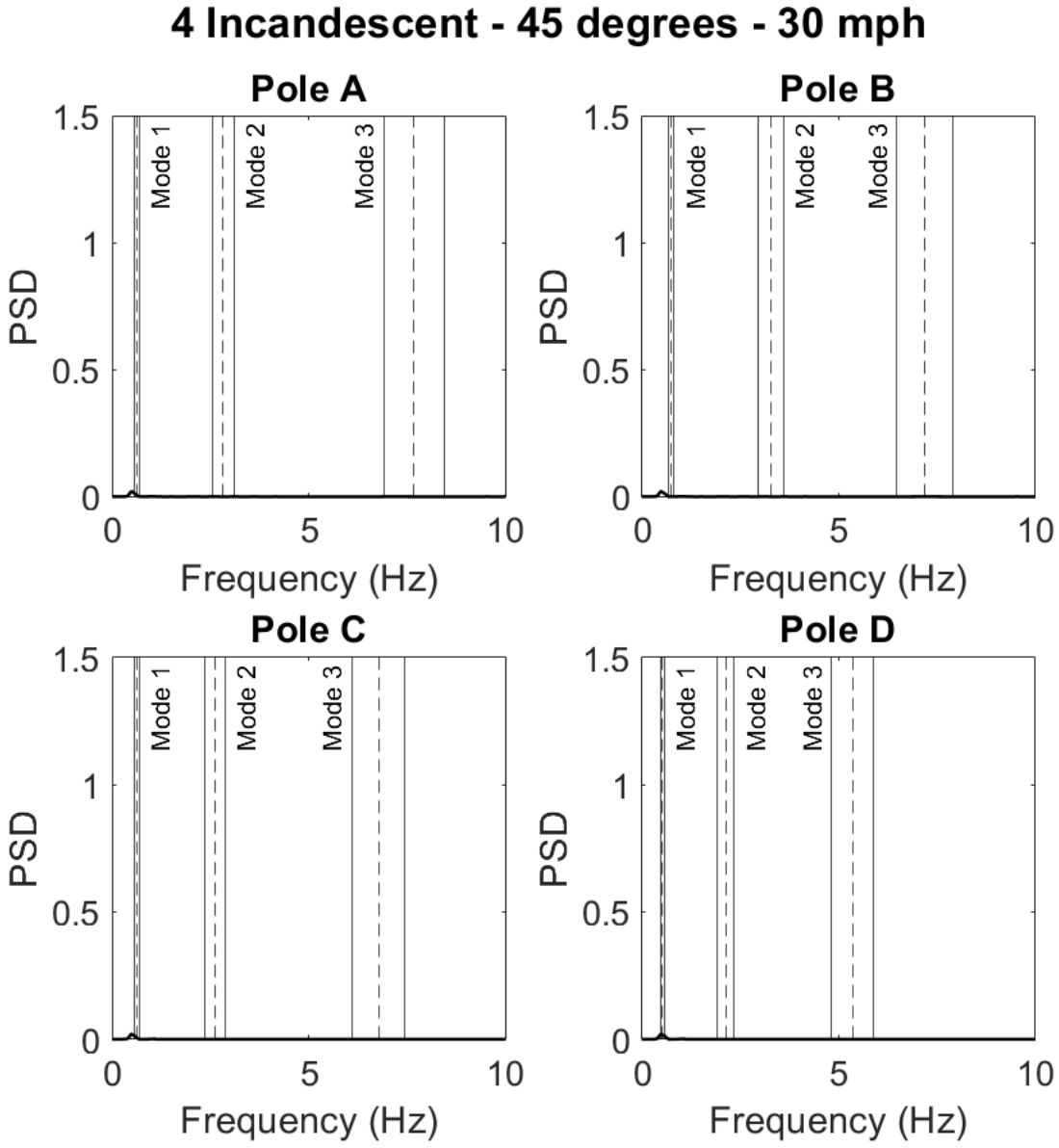

Figure B.58: PSDs for Pole A, B, C, and D for 4-Incandescent Light Fixture Subjected to 30 mph Wind at an Angle of 45 Degrees

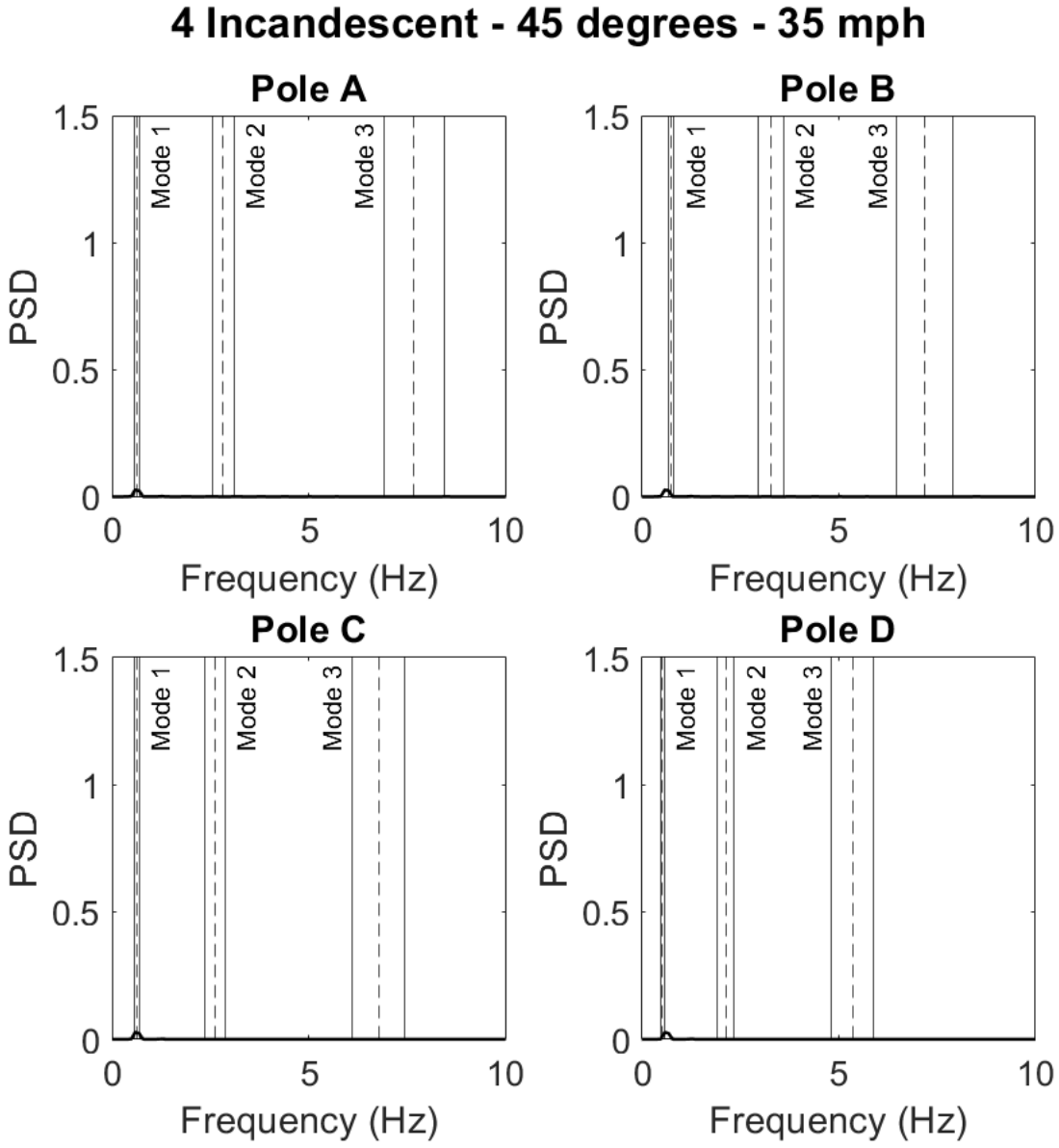

Figure B.59: PSDs for Pole A, B, C, and D for 4-Incandescent Light Fixture Subjected to 35 mph Wind at an Angle of 45 Degrees

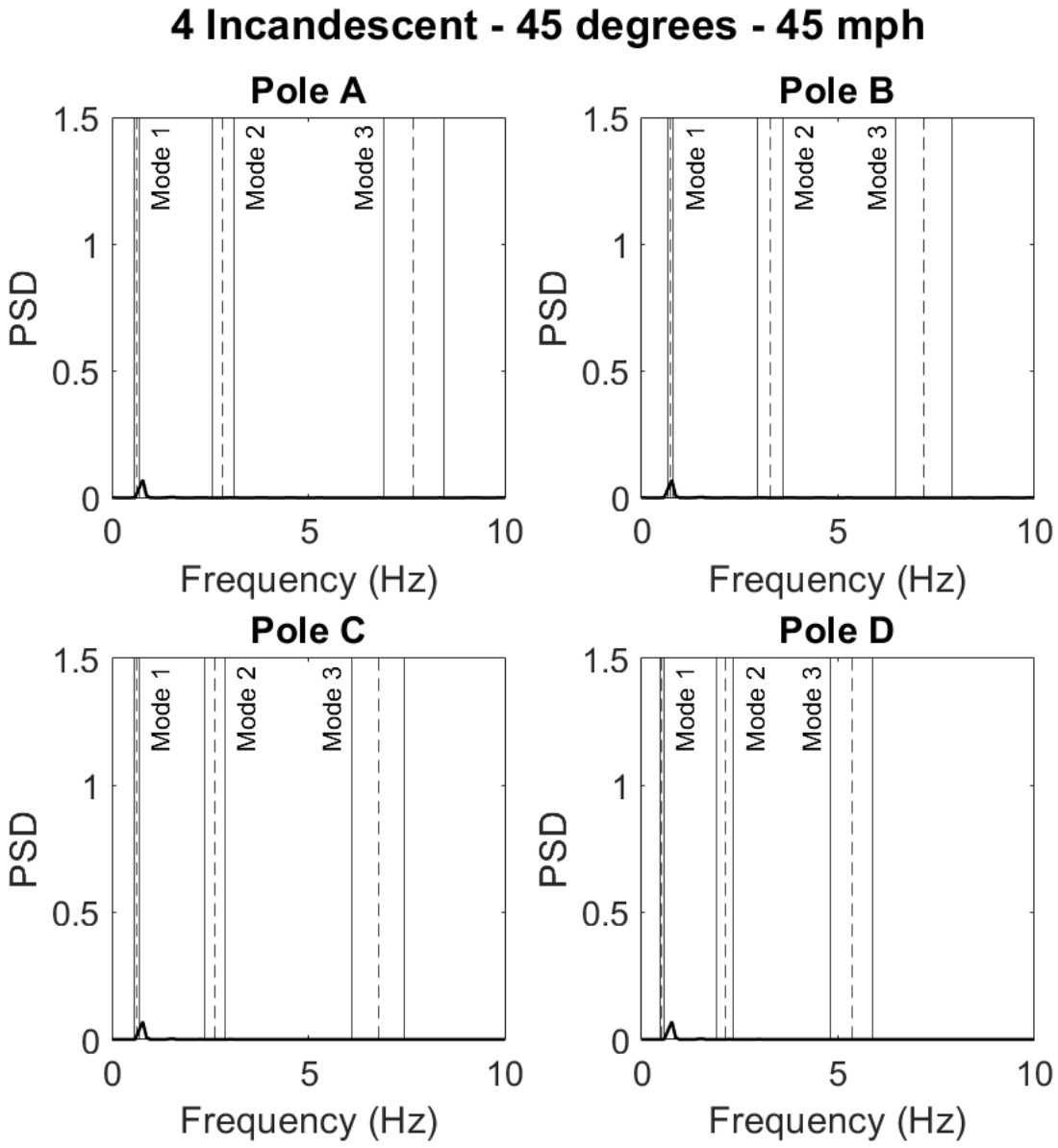

Figure B.60: PSDs for Pole A, B, C, and D for 4-Incandescent Light Fixture Subjected to 45 mph Wind at an Angle of 45 Degrees

Appendix C

C.1 Color Band Comparison Charts for Abaqus Simulations

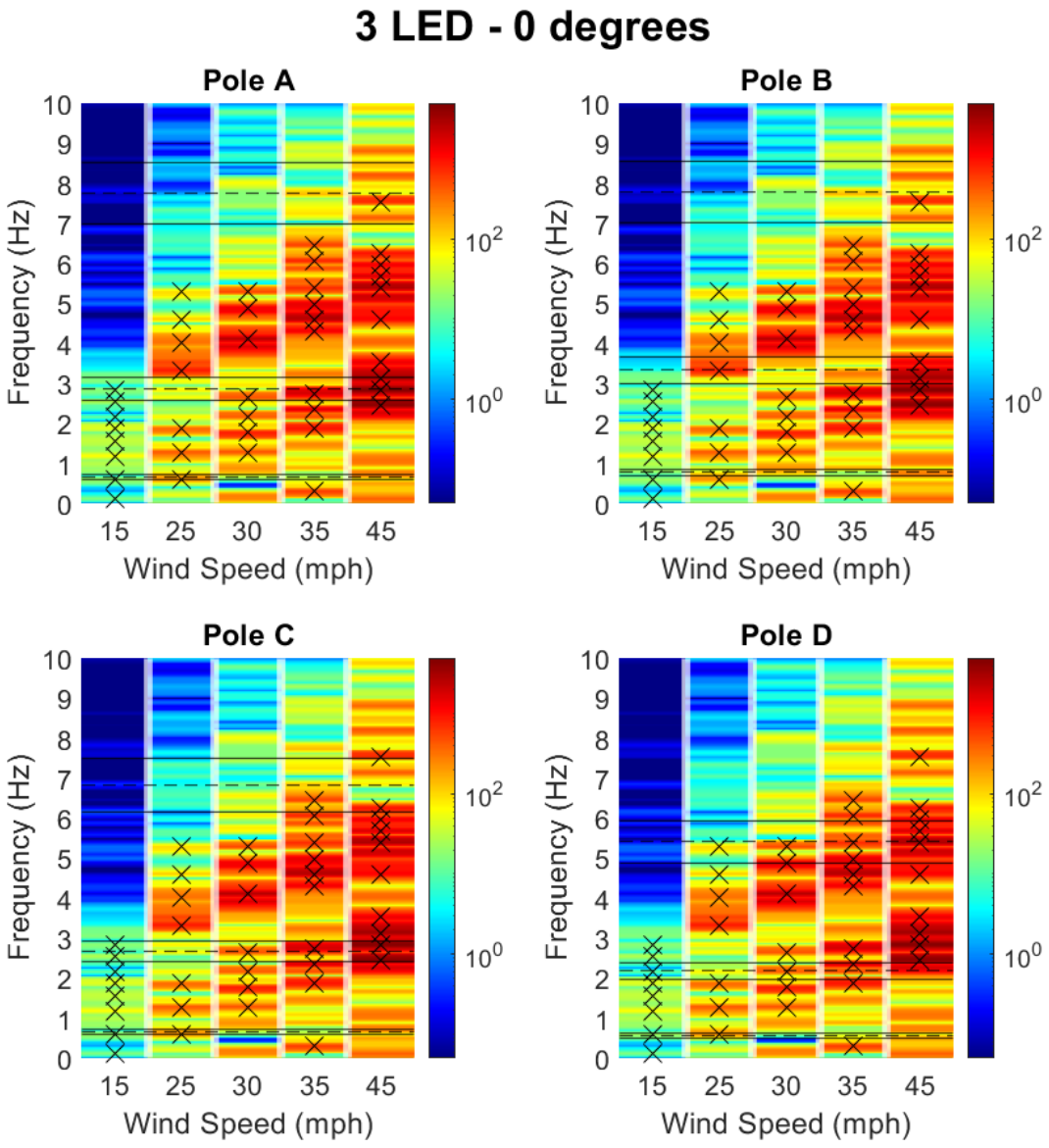

Figure C.1: Color Band Comparison Chart of PSD Curves for 3 LED Fixture Configuration Subjected to Wind at an Angle of 0 Degrees

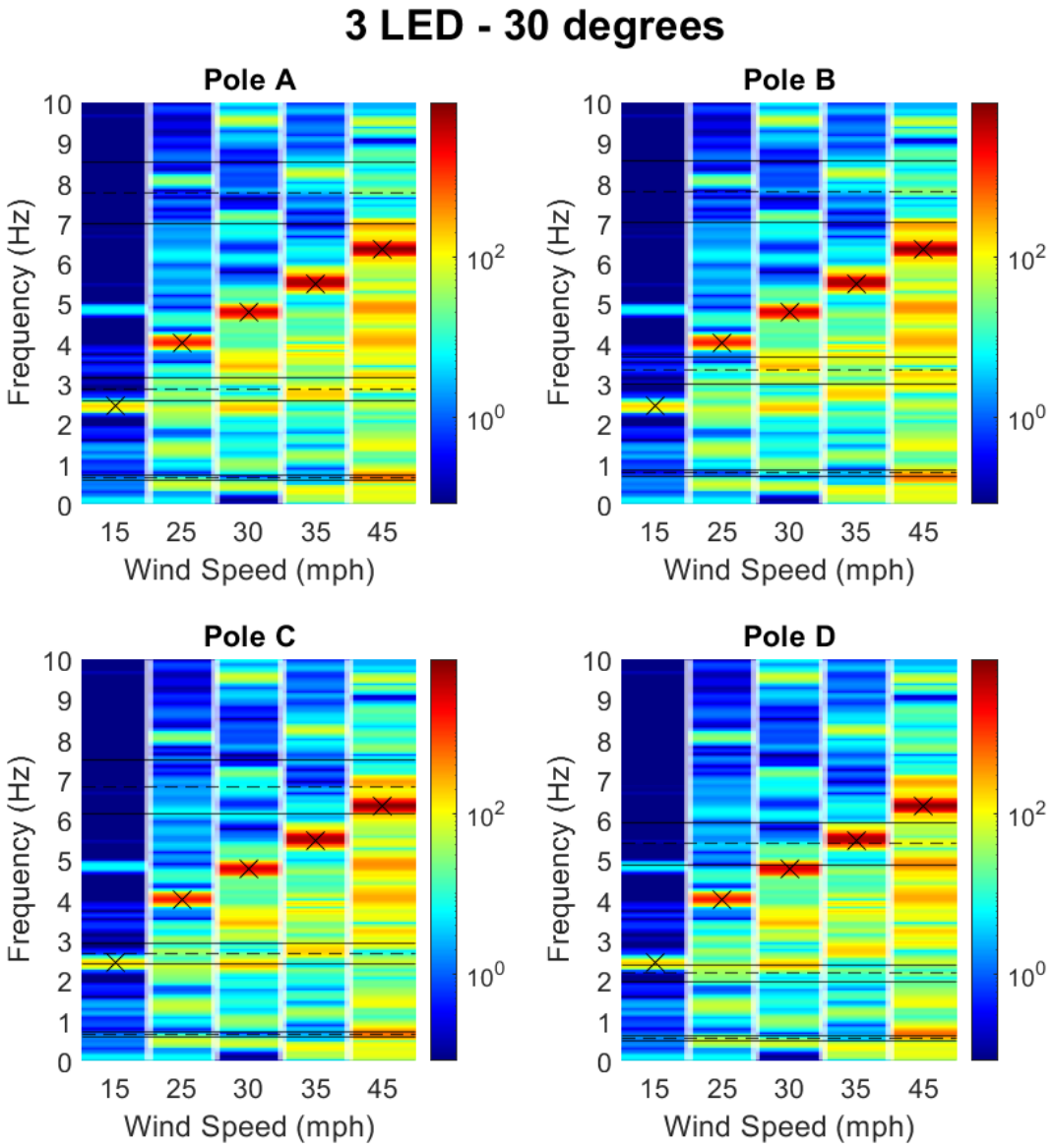

Figure C.2: Color Band Comparison Chart of PSD Curves for 3 LED Fixture Configuration Subjected to Wind at an Angle of 30 Degrees

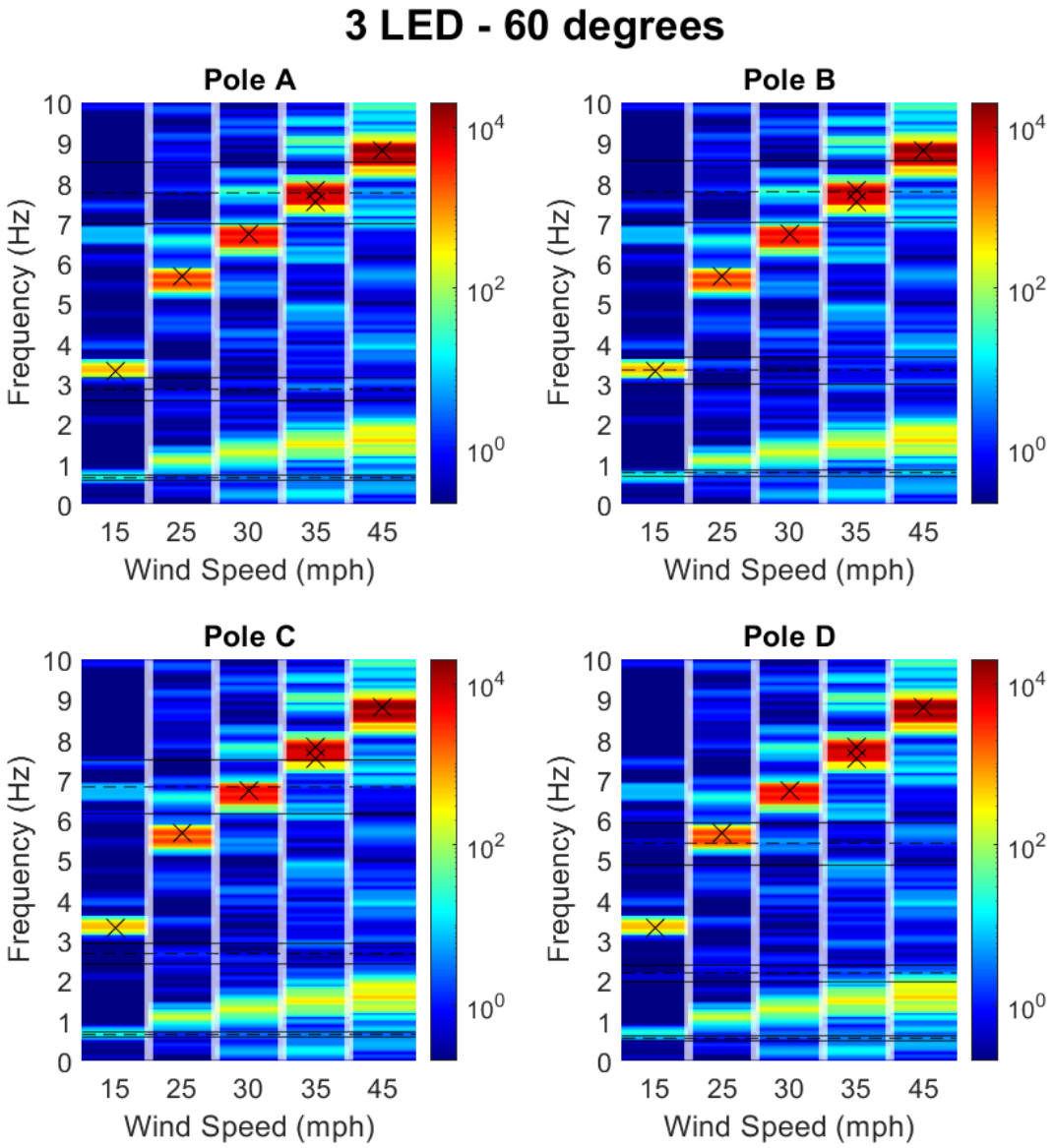

Figure C.3: Color Band Comparison Chart of PSD Curves for 3 LED Fixture Configuration Subjected to Wind at an Angle of 60 Degrees

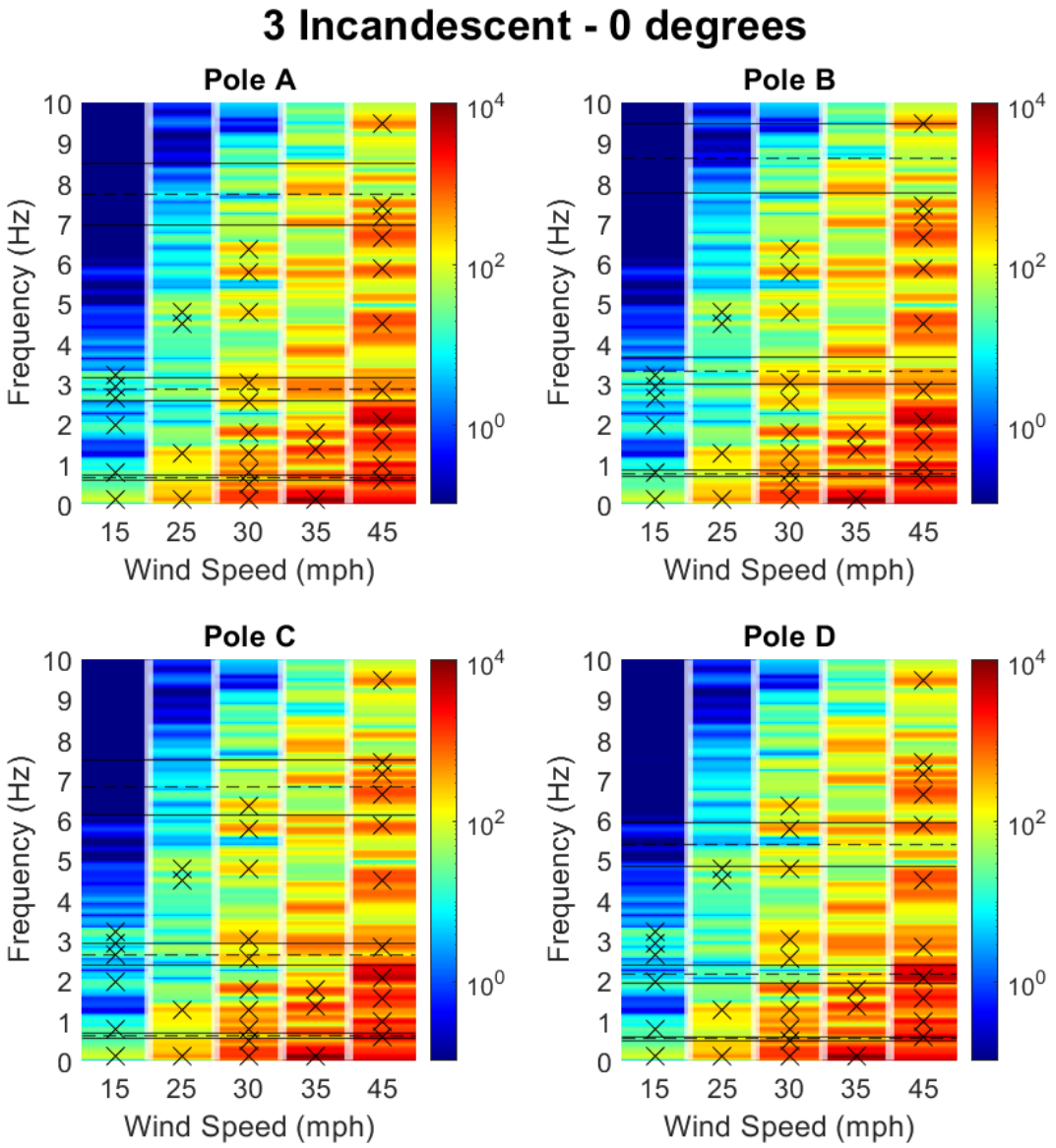

Figure C.4: Color Band Comparison Chart of PSD Curves for 3 Incandescent Fixture Configuration Subjected to Wind at an Angle of 0 Degrees

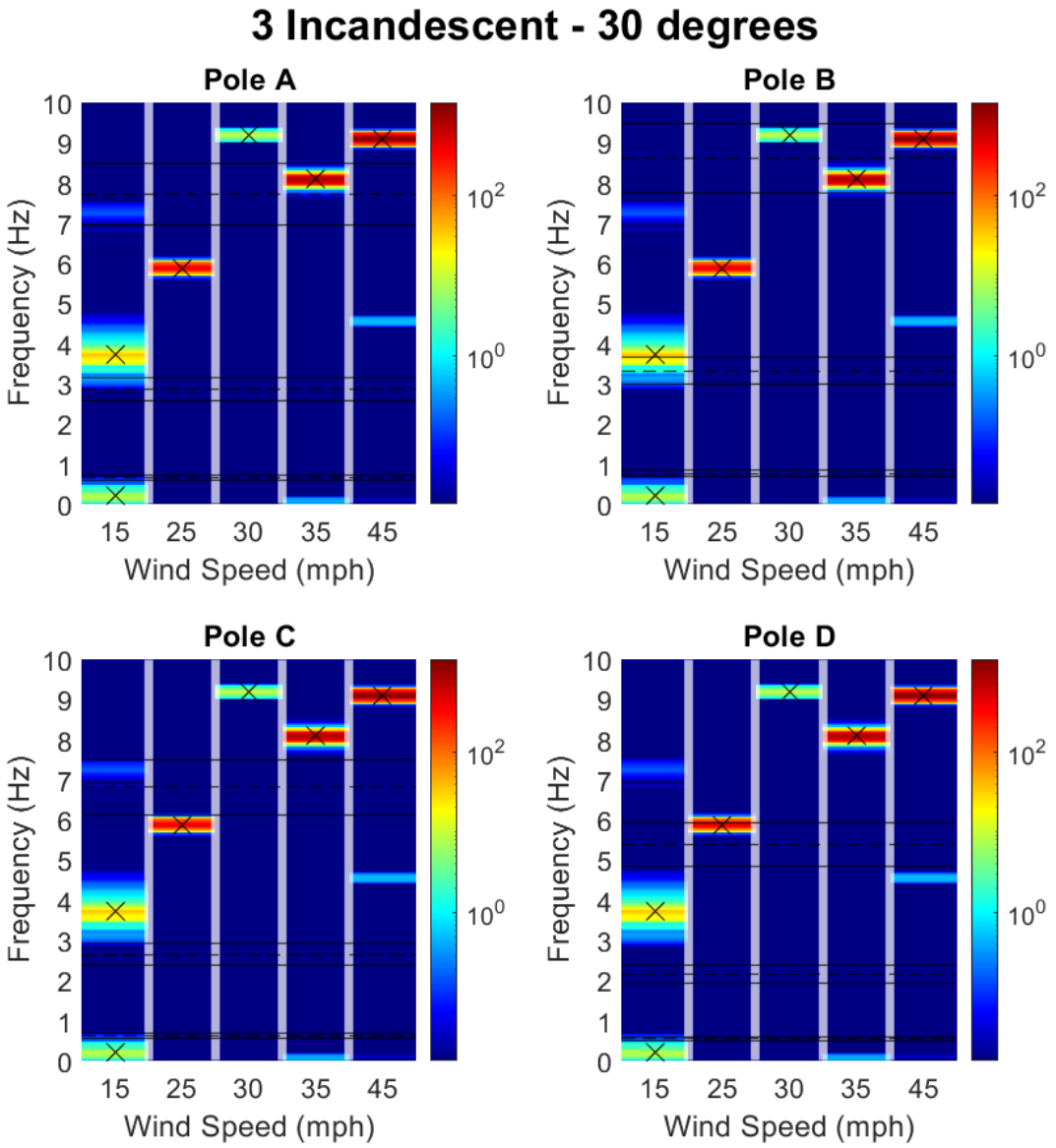

Figure C.5: Color Band Comparison Chart of PSD Curves for 3 Incandescent Fixture Configuration Subjected to Wind at an Angle of 30 Degrees

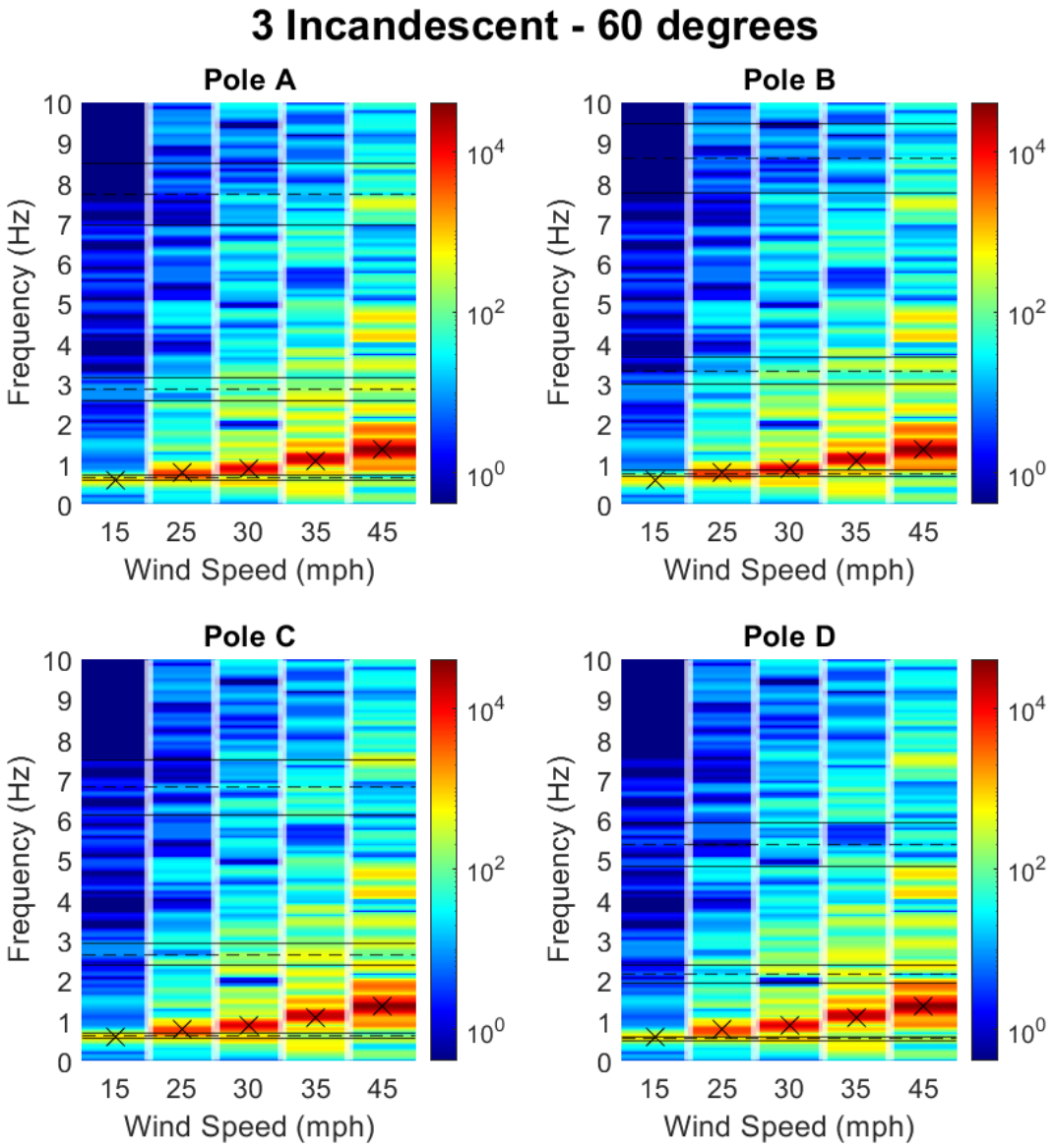

Figure C.6: Color Band Comparison Chart of PSD Curves for 3 Incandescent Fixture Configuration Subjected to Wind at an Angle of 60 Degrees

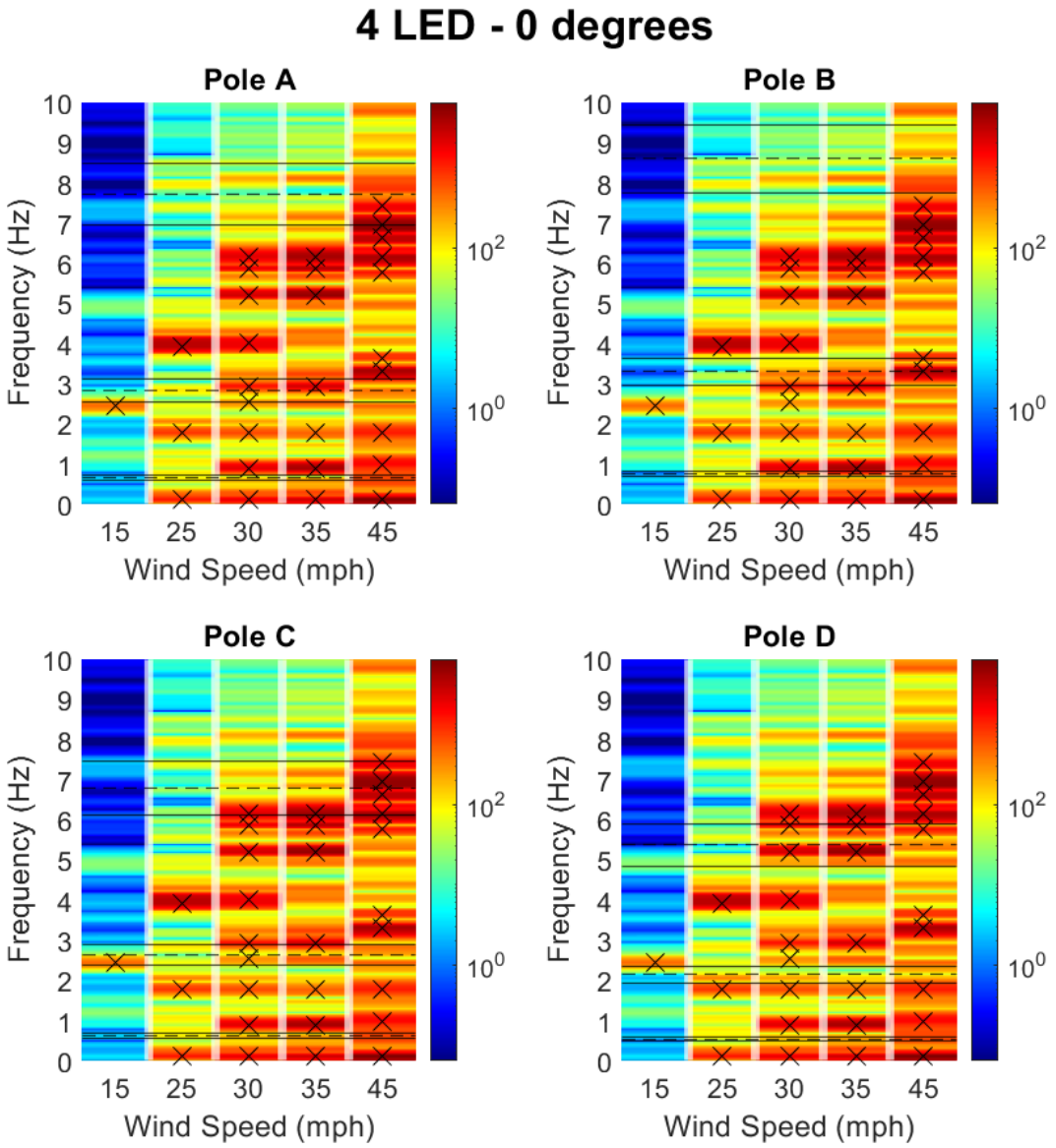

Figure C.7: Color Band Comparison Chart of PSD Curves for 4 LED Fixture Configuration Subjected to Wind at an Angle of 0 Degrees

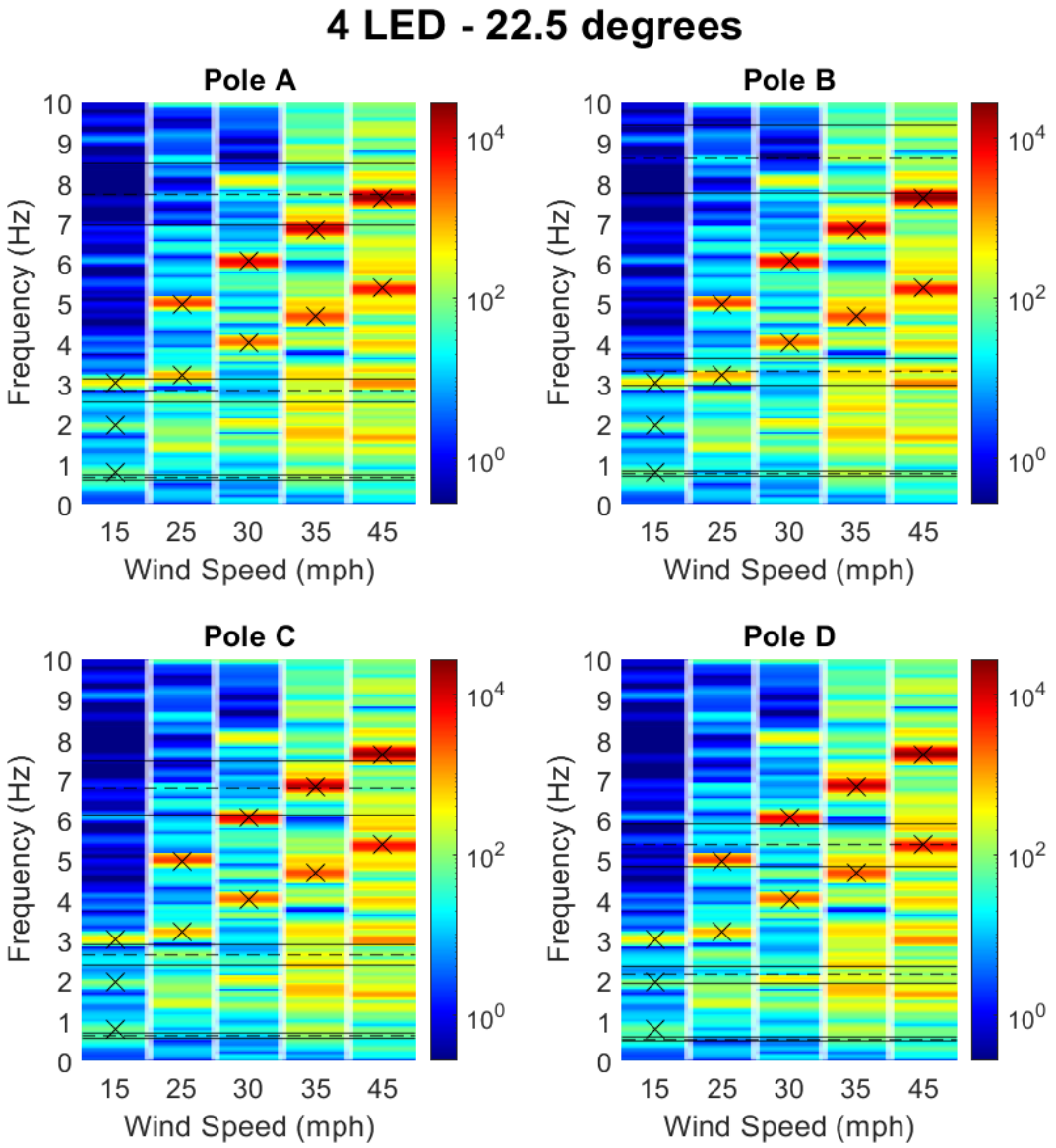

Figure C.8: Color Band Comparison Chart of PSD Curves for 4 LED Fixture Configuration Subjected to Wind at an Angle of 22.5 Degrees

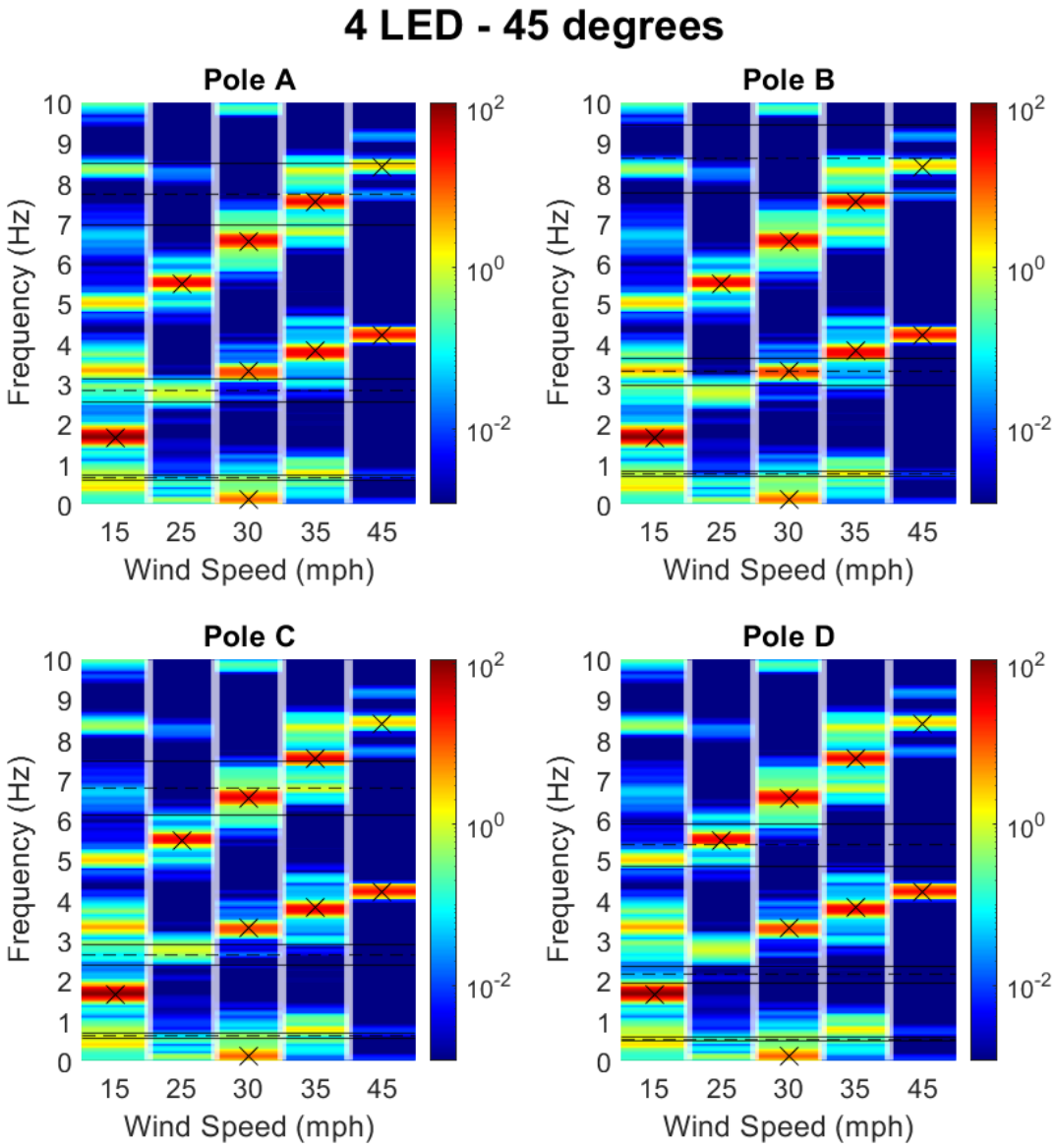

Figure C.9: Color Band Comparison Chart of PSD Curves for 4 LED Fixture Configuration Subjected to Wind at an Angle of 45 Degrees

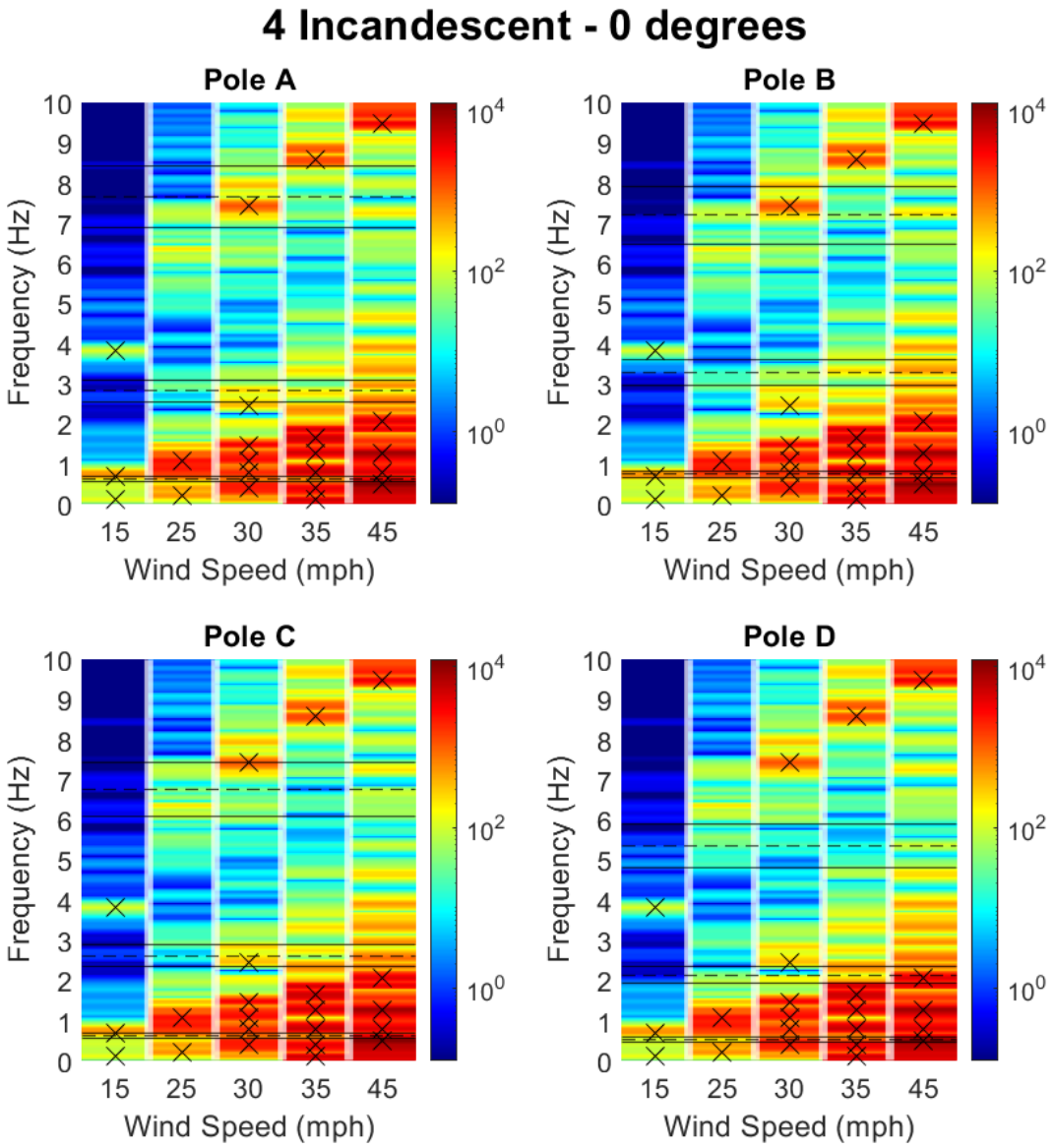

Figure C.10: Color Band Comparison Chart of PSD Curves for 4 Incandescent Fixture Configuration Subjected to Wind at an Angle of 0 Degrees

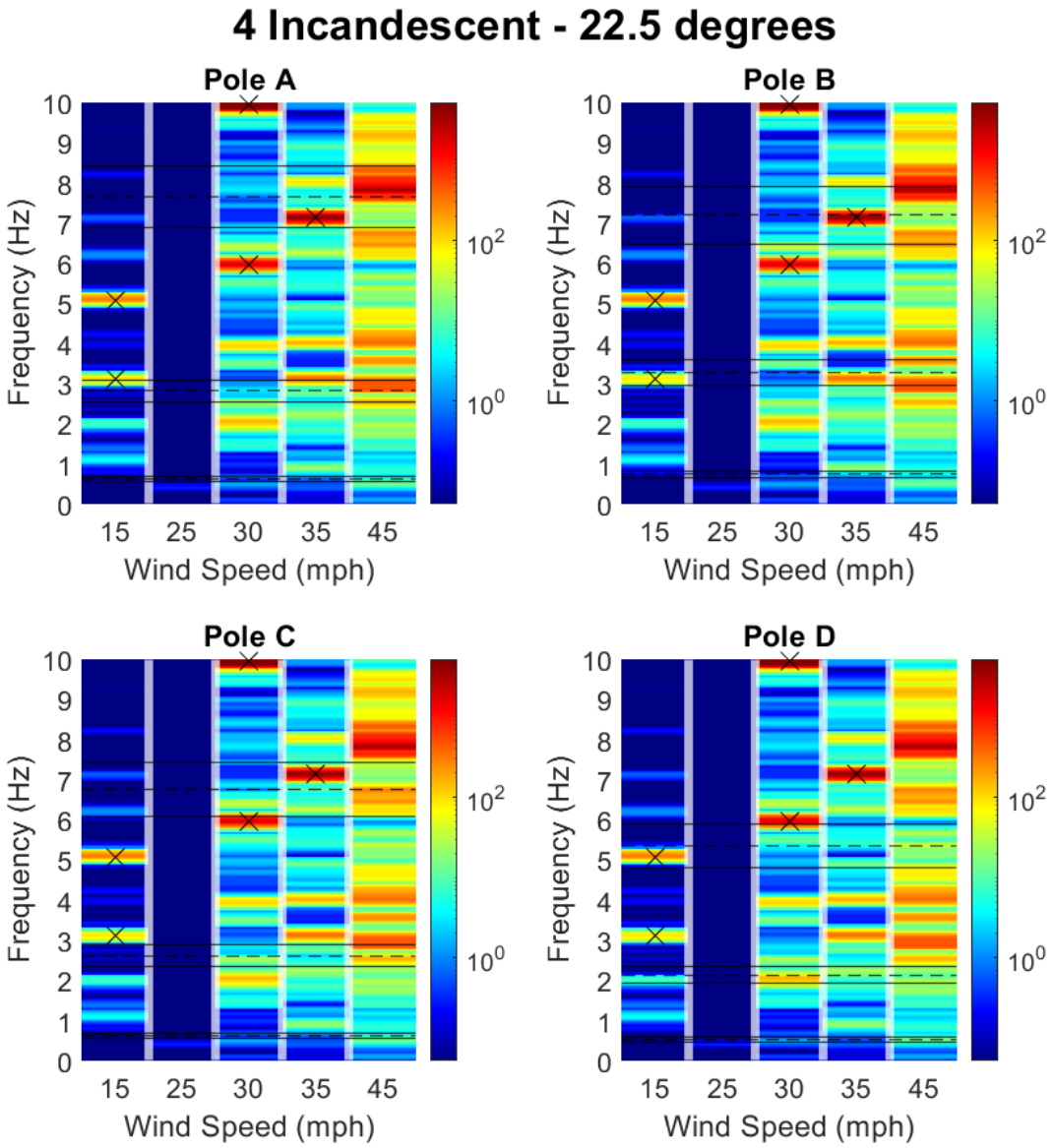

Figure C.11: Color Band Comparison Chart of PSD Curves for 4 Incandescent Fixture Configuration Subjected to Wind at an Angle of 22.5 Degrees

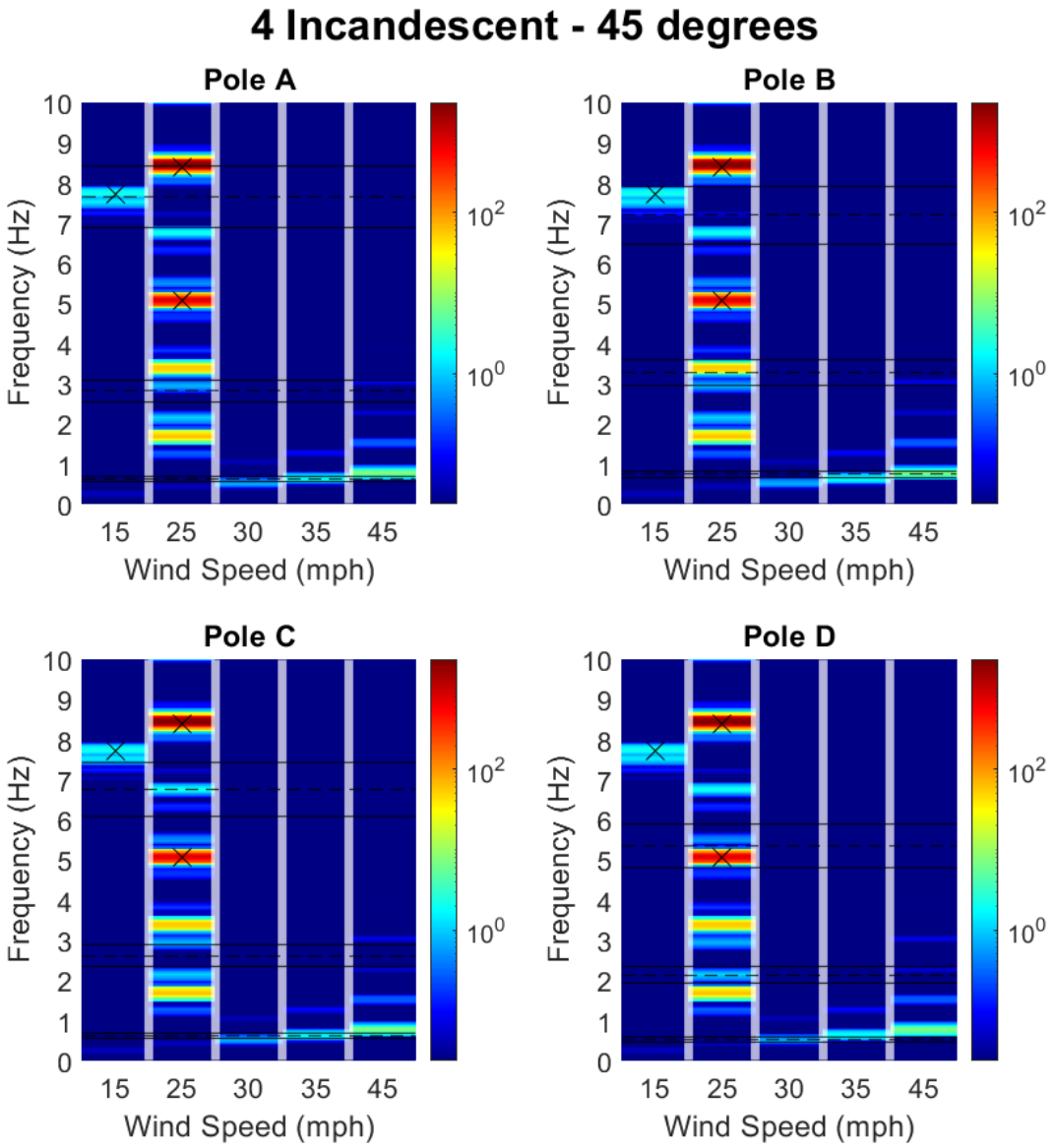

Figure C.12: Color Band Comparison Chart of PSD Curves for 4 Incandescent Fixture Configuration Subjected to Wind at an Angle of 45 Degrees

Appendix D

D.1 Bubble Comparison Charts for Abaqus Simulations

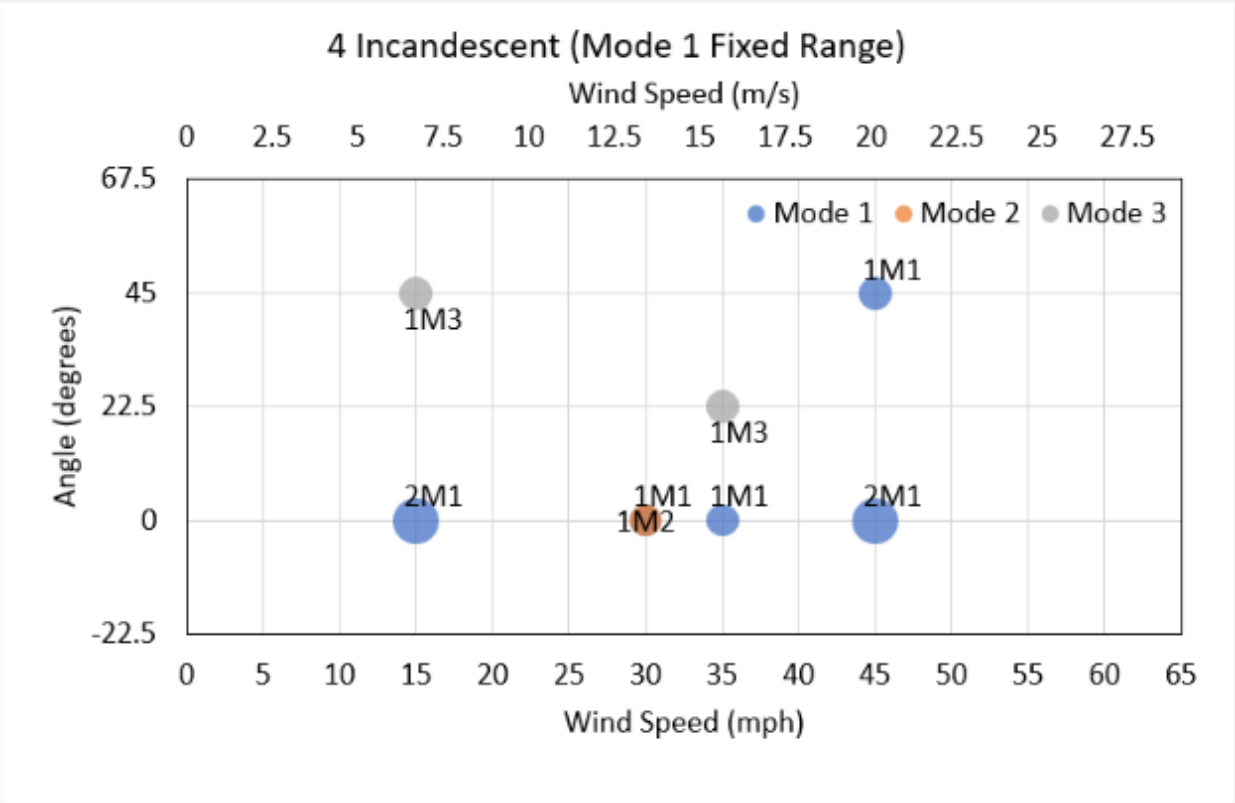

Figure D.1: Peak Hit Comparison Bubble Chart: 4 Incandescent Fixture Configuration, (Mode 1 Fixed Range)

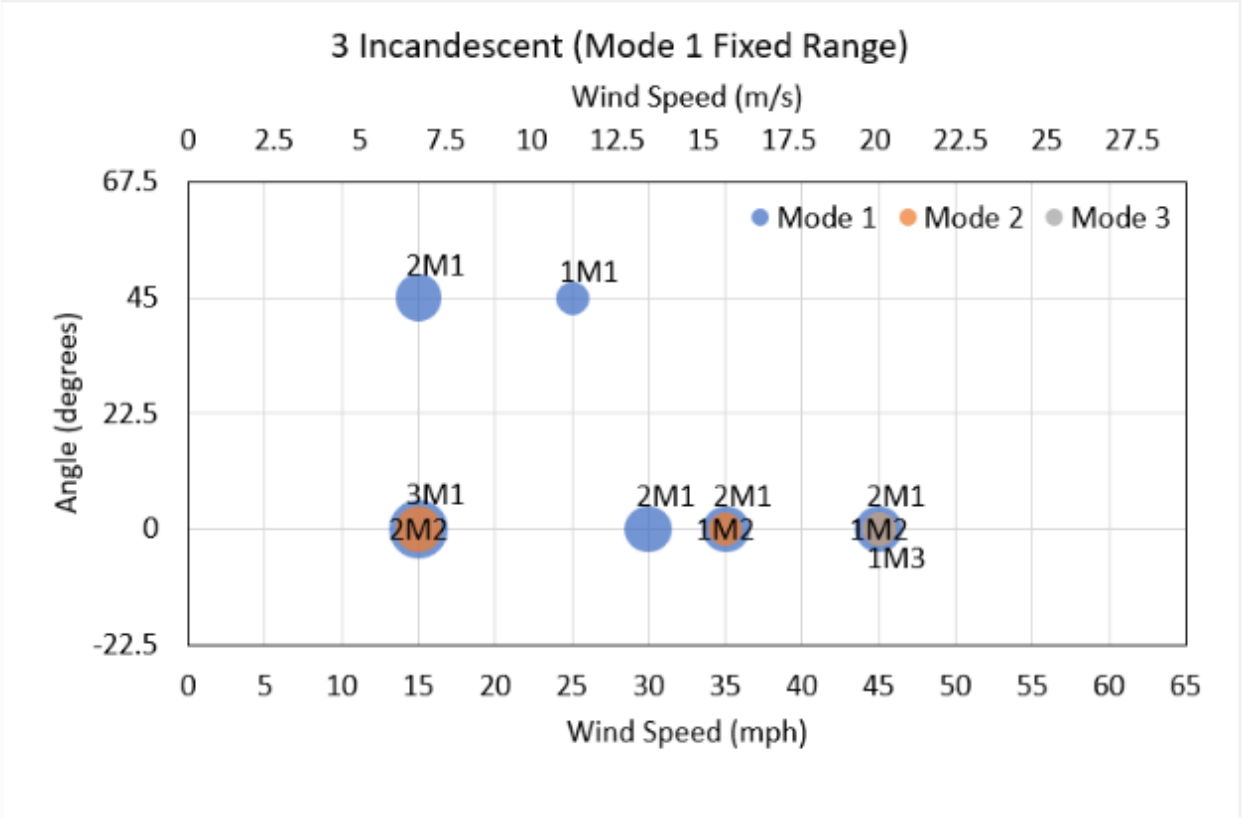

Figure D.2: Peak Hit Comparison Bubble Chart: 3 Incandescent Fixture Configuration, (Mode 1 Fixed Range)

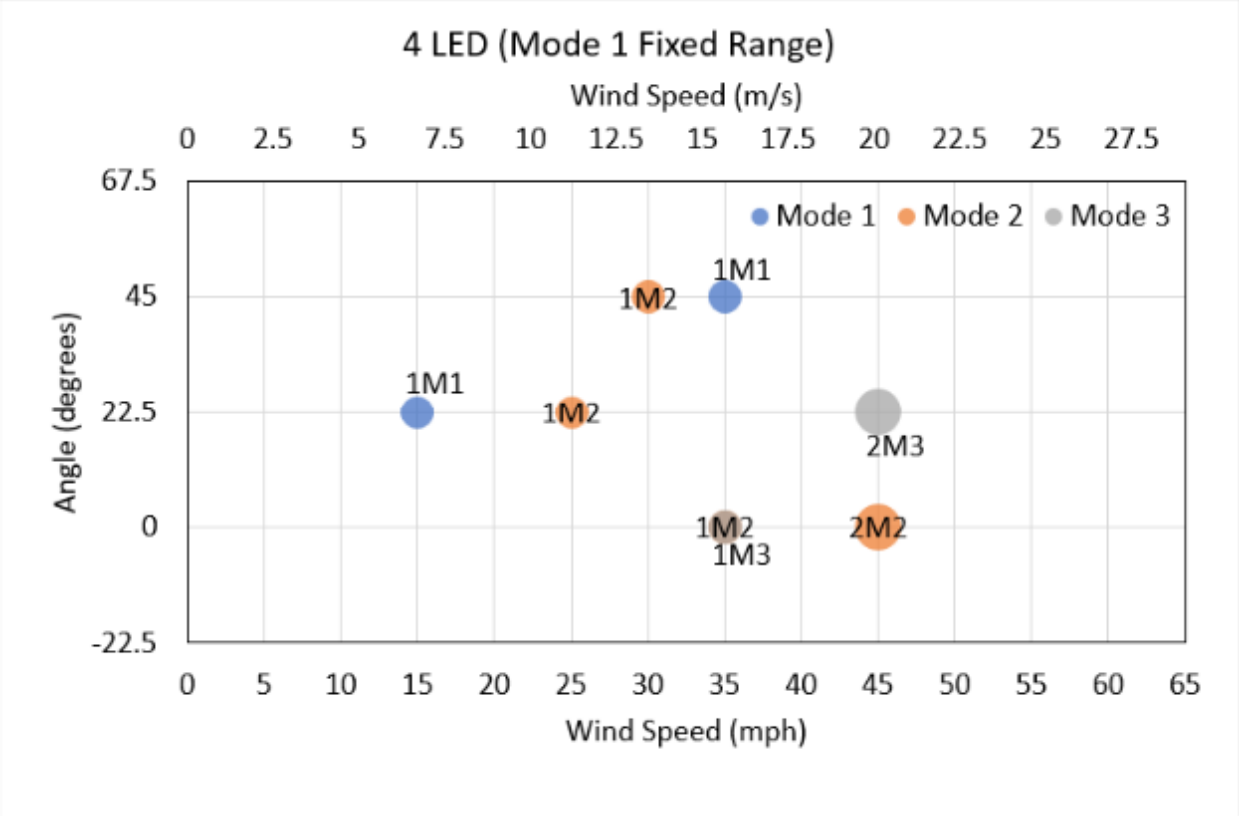

Figure D.3: Peak Hit Comparison Bubble Chart: 4 LED Fixture Configuration, (Mode 1 Fixed Range)

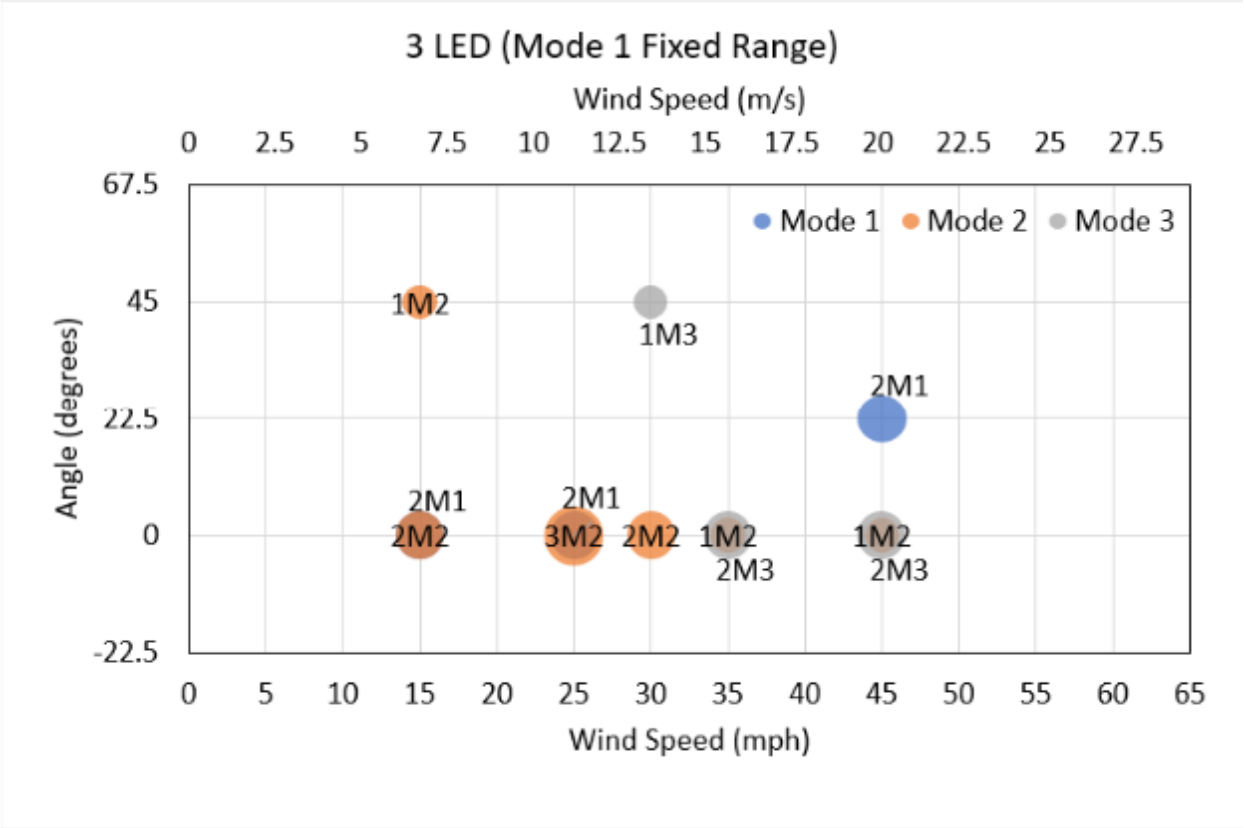

Figure D.4: Peak Hit Comparison Bubble Chart: 3 LED Fixture Configuration, (Mode 1 Fixed Range)

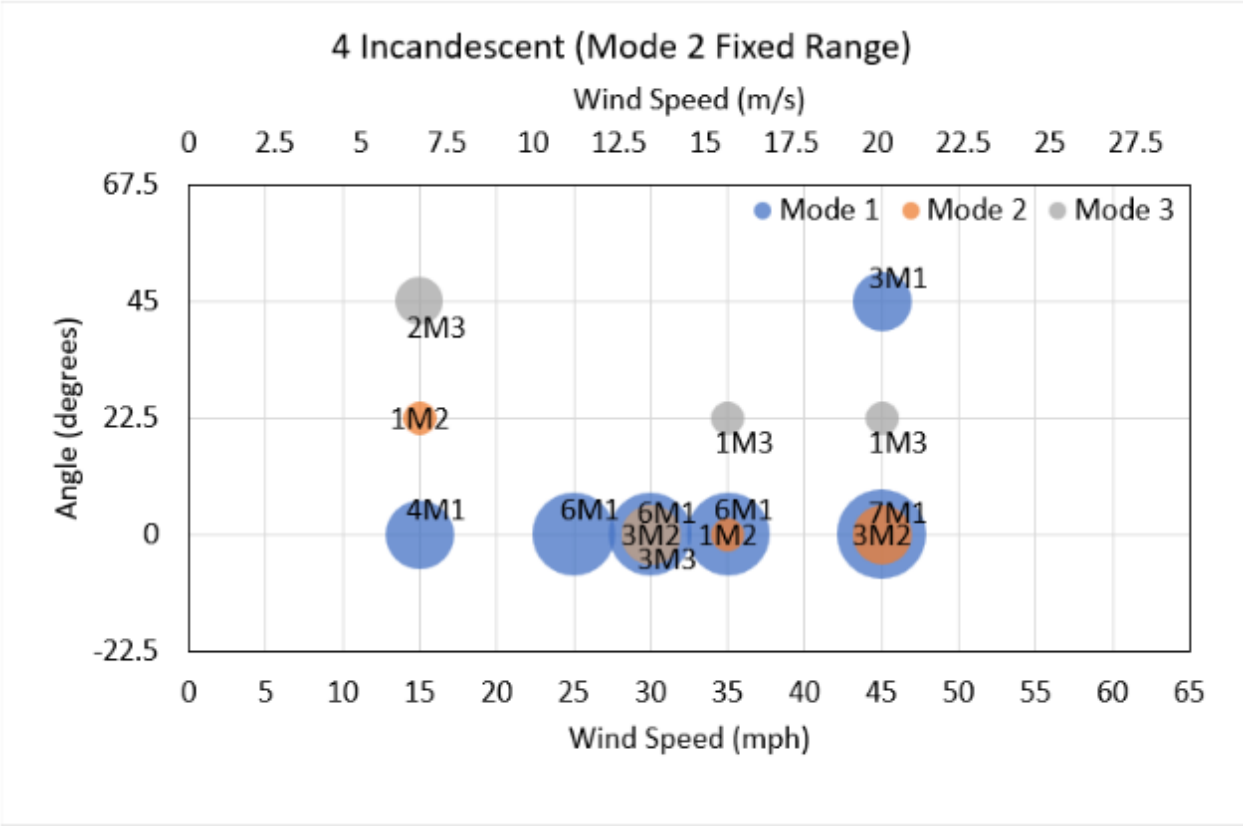

Figure D.5: Peak Hit Comparison Bubble Chart: 4 Incandescent Fixture Configuration, (Mode 2 Fixed Range)

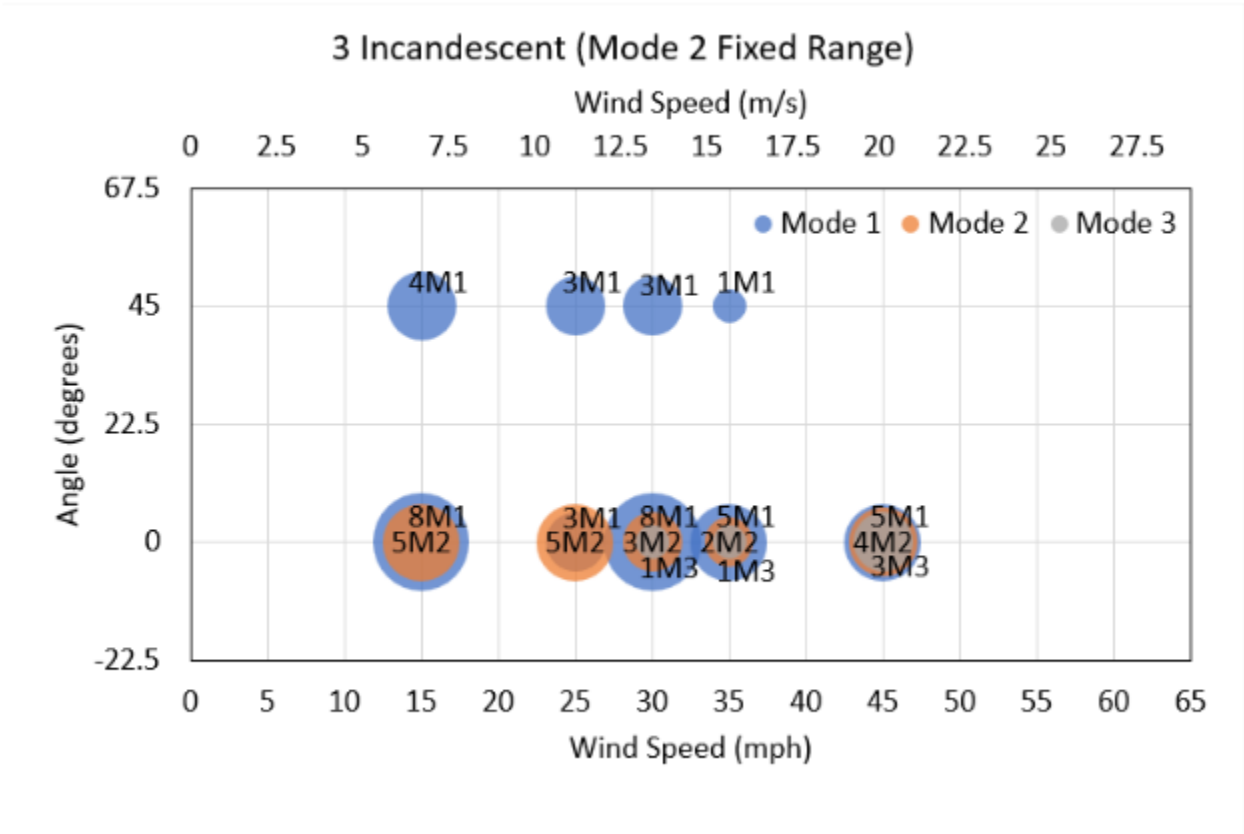

Figure D.6: Peak Hit Comparison Bubble Chart: 3 Incandescent Fixture Configuration, (Mode 2 Fixed Range)

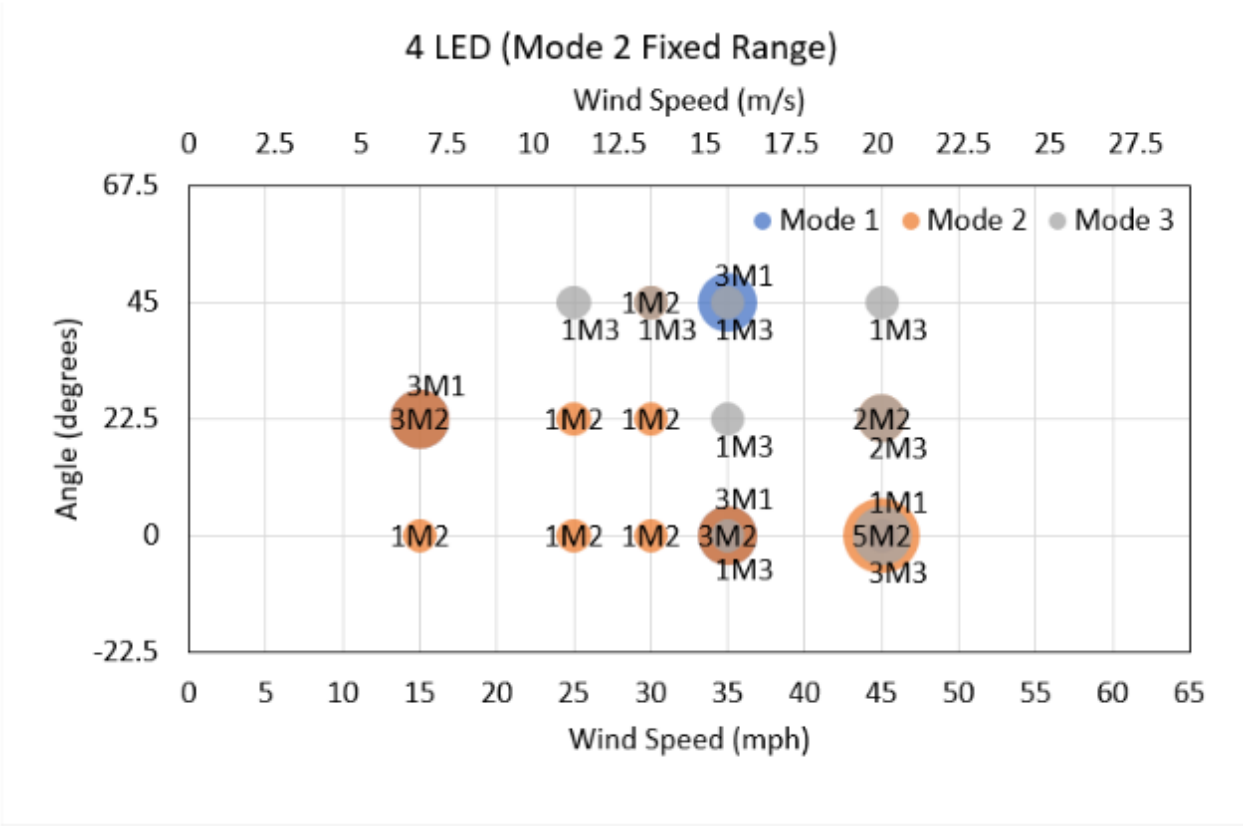

Figure D.7: Peak Hit Comparison Bubble Chart: 4 LED Fixture Configuration, (Mode 2 Fixed Range)

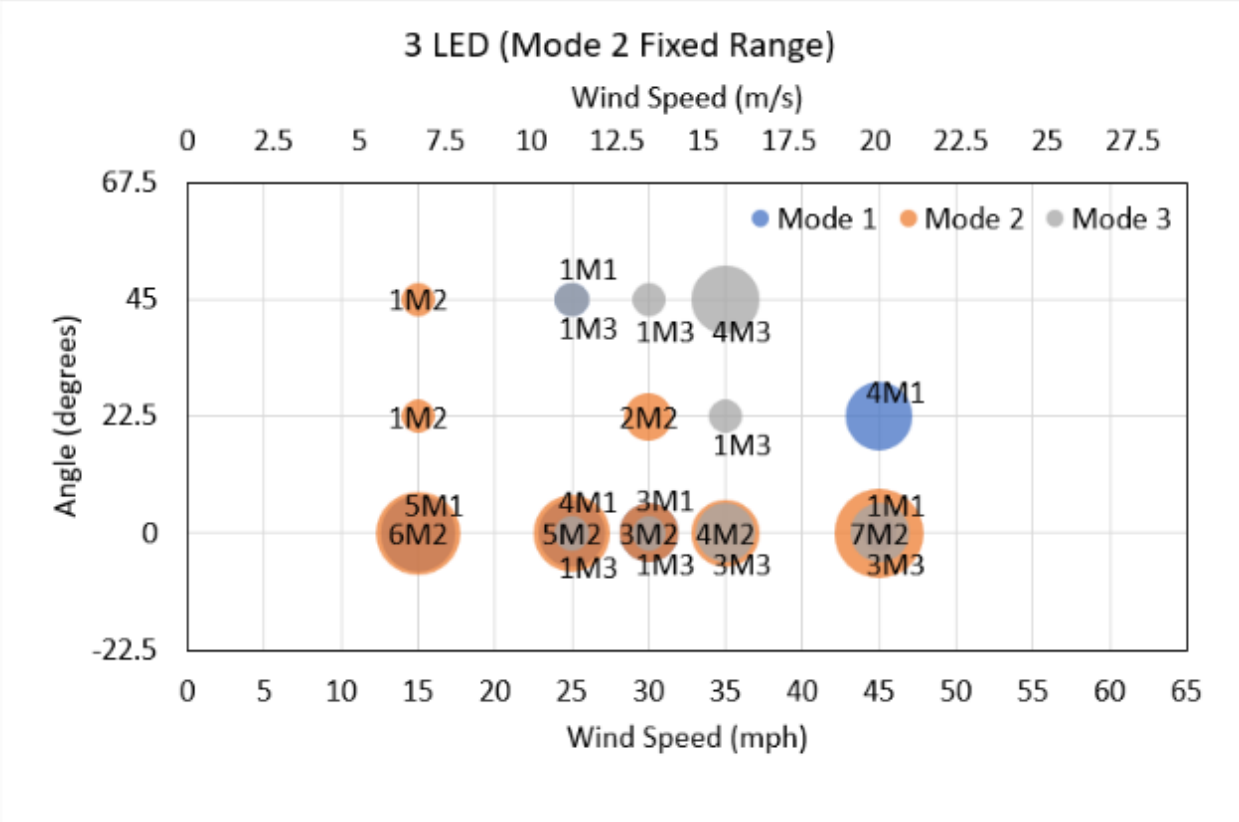

Figure D.8: Peak Hit Comparison Bubble Chart: 3 LED Fixture Configuration, (Mode 2 Fixed Range)

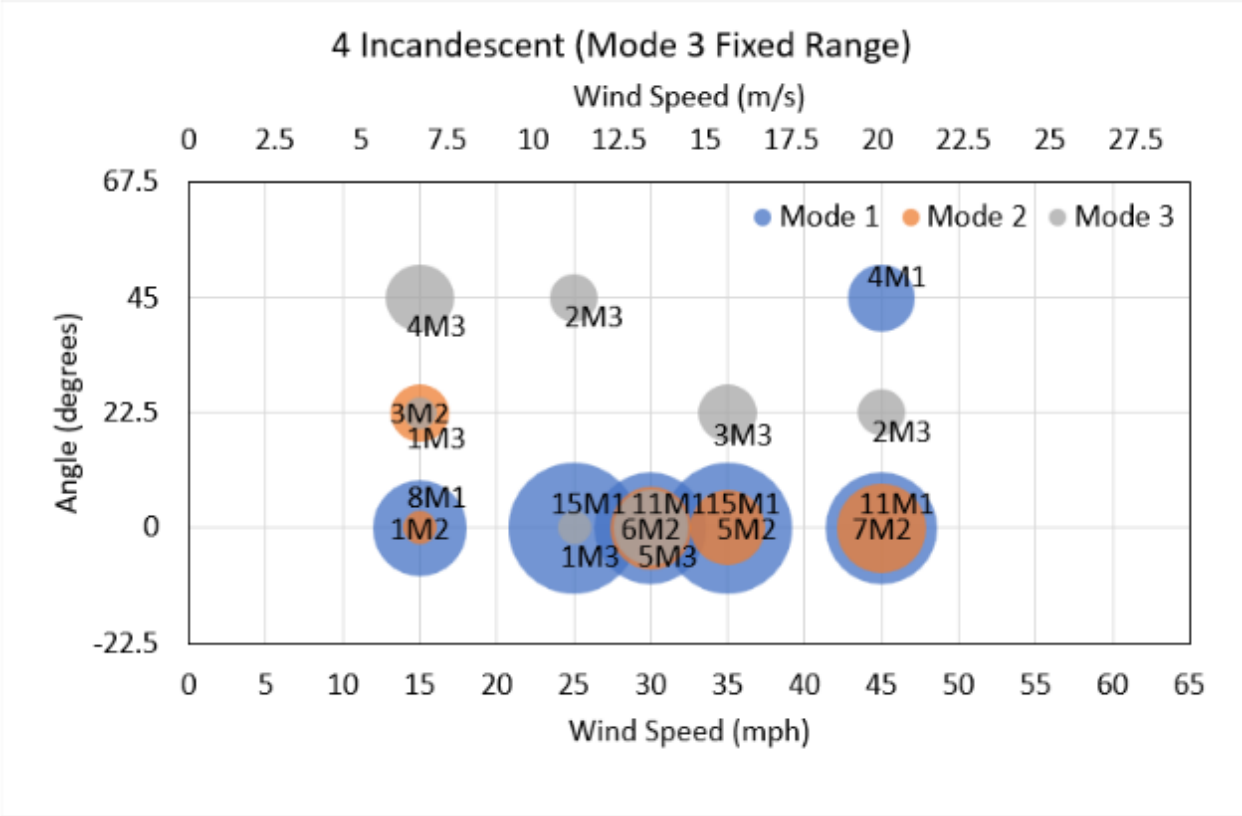

Figure D.9: Peak Hit Comparison Bubble Chart: 4 Incandescent Fixture Configuration, (Mode 3 Fixed Range)

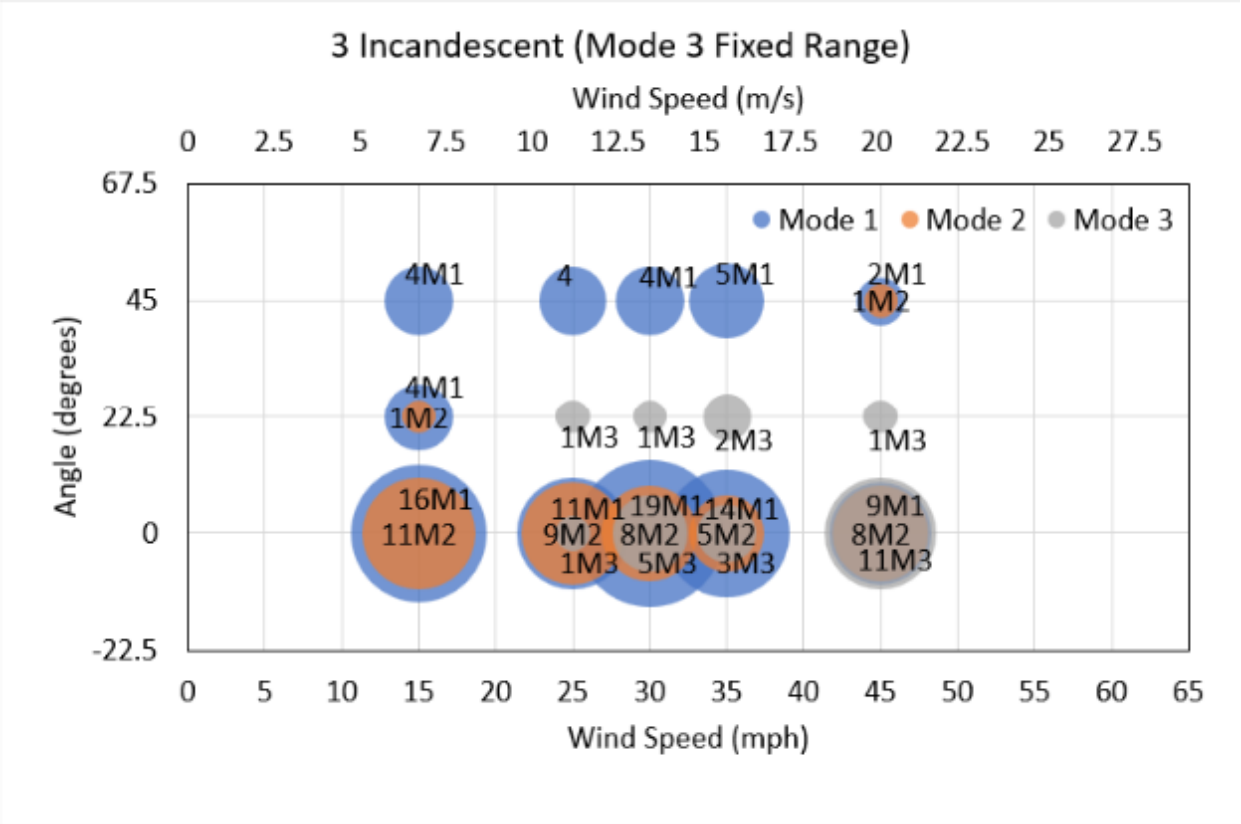

Figure D.10: Peak Hit Comparison Bubble Chart: 3 Incandescent Fixture Configuration, (Mode 3 Fixed Range)

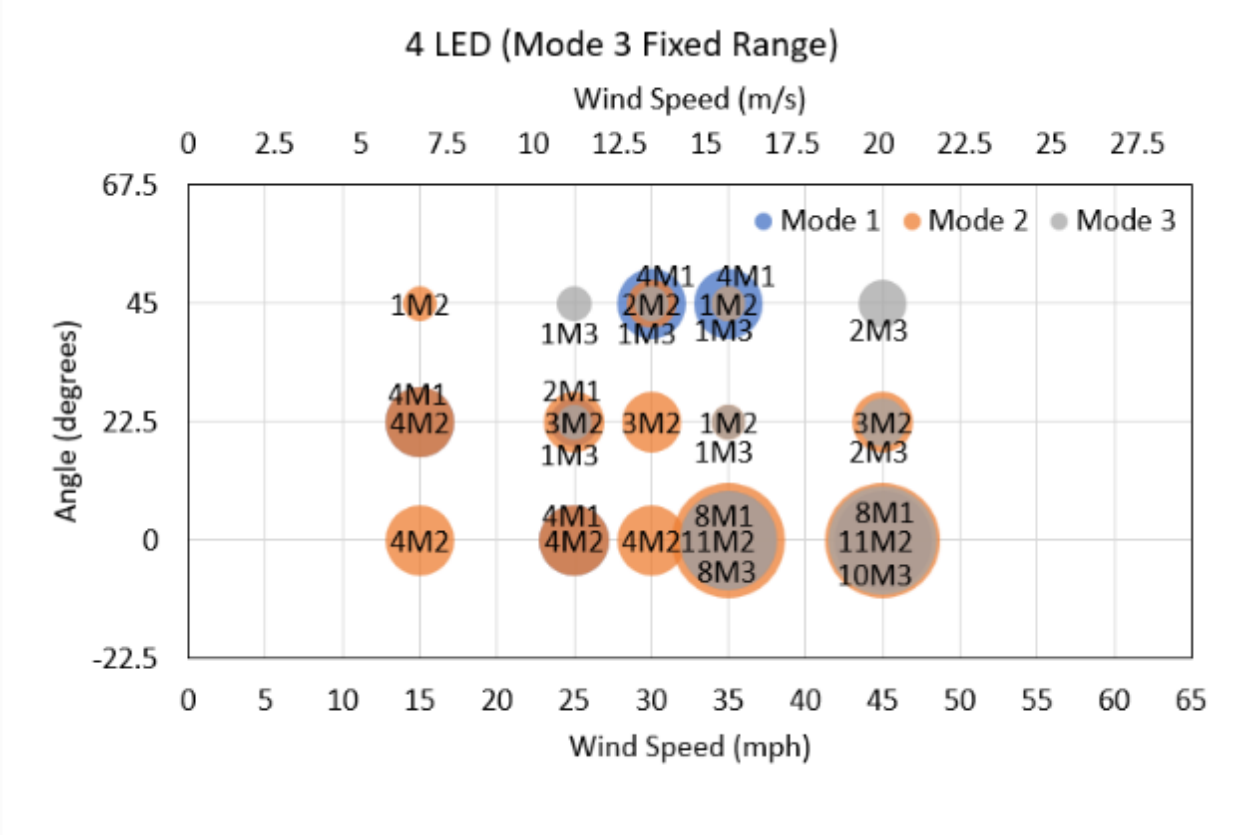

Figure D.11: Peak Hit Comparison Bubble Chart: 4 LED Fixture Configuration, (Mode 3 Fixed Range)

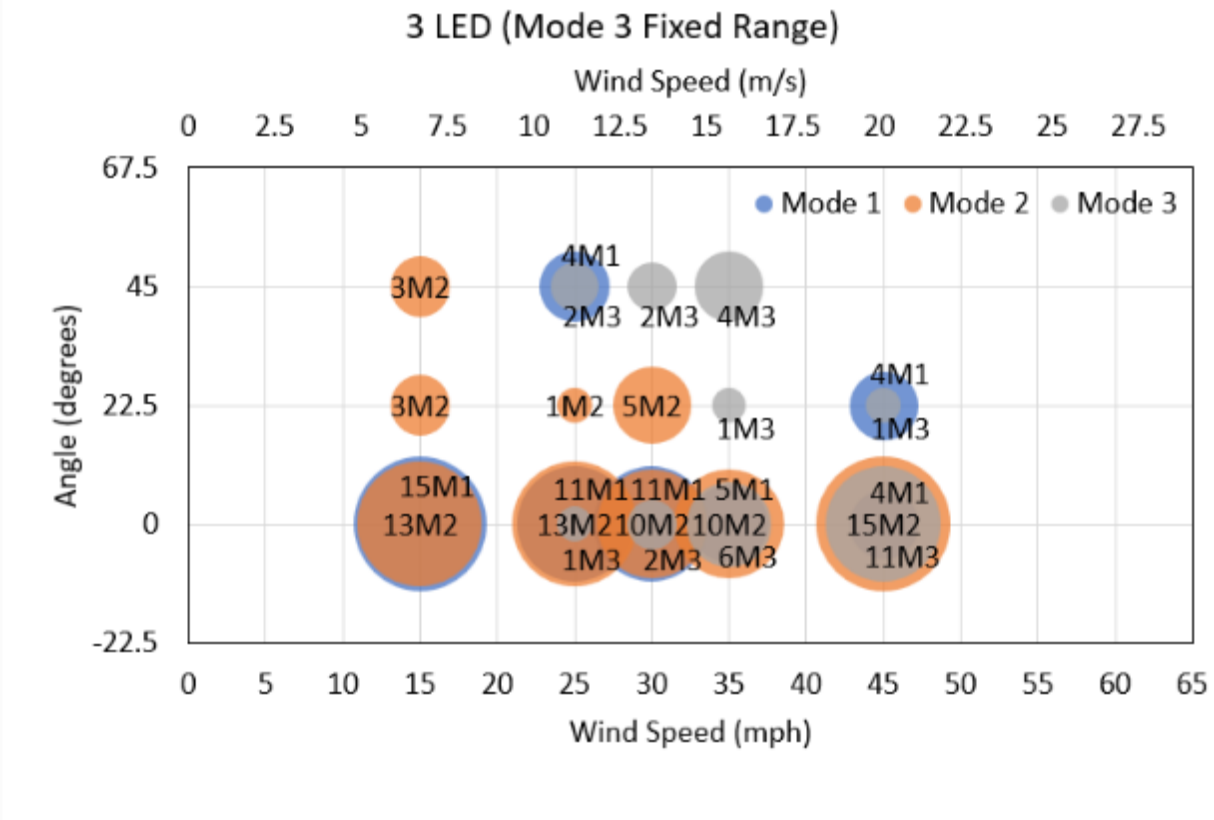

Figure D.12: Peak Hit Comparison Bubble Chart: 3 LED Fixture Configuration, (Mode 3 Fixed Range)

AD ASTRA PER ASPERA

Kansas

Department of Transportation